Crosstalk Between the Sensory Peripheral Nervous System and Atherosclerosis in Hyperlipidemic Mice

Ting Sun

München 2022

Aus dem Institut für Prophylaxe und Epidemiologie der Kreislaufkrankheiten (IPEK)
Klinikum der Ludwig-Maximilians-Universität München
Direktor: Univ.-Prof. Dr. med. Christian Weber

Crosstalk Between the Sensory Peripheral Nervous System and Atherosclerosis in Hyperlipidemic Mice

Dissertation
zum Erwerb des Doktorgrades der Naturwissenschaften
an der Medizinischen Fakultät der
Ludwig-Maximilians-Universität zu München

vorgelegt von
Ting Sun

aus

Henan, VR China

2022

Mit Genehmigung der Medizinischen Fakultät
der Universität München

Betreuerin: Univ.-Prof. Dr. rer. nat. Sabine Steffens

Zweitgutachter: Prof. Dr. rer. nat. Jürgen Bernhagen

Dekan: Prof. Dr. med. Thomas Gudermann

Tag der mündlichen Prüfung: 16. Mai 2023

Crosstalk Between the Sensory Peripheral Nervous System and Atherosclerosis in Hyperlipidemic Mice

TABLE OF CONTENTS

Zusammenfassung

Atherosklerose ist eine chronisch-progressive entzündliche Erkrankung der Arterienwand, in deren Entwicklungsstadien sowohl angeborene als auch adaptive Immunreaktionen beteiligt sind. Transient Receptor Potential Vanilloid 1- (TRPV1) exprimierende Neurone gehören zu einer Untergruppe des peripheren und zentralen Nervensystems, deren Axone ubiquitär im Körper von Säugetieren vorkommen. Es wurde gezeigt, dass TRPV1-exprimierende Neurone Entzündungsreaktionen durch die Sekretion von Neuropeptiden beeinflussen können. Die von TRPV1-exprimierenden Neurone sezernieren Neuropeptide, die die Gewebeinfiltration von Immunzellen kontrollieren. Hierdurch werden eine Vielzahl weiterer Gewebereaktionen ausgelöst. Extraneuronale Zellen wie Endothelzellen und glatte Muskelzellen können ebenfalls TRPV1 exprimieren. Die Interaktion von TRPV1 und Arterien ist nur unvollständig verstanden. Unsere früheren Daten haben gezeigt, dass es während der Progression der Atherosklerose zu einer deutlichen Axonneogenese in der Adventitia kommt, die auf Abschnitte der Aorta beschränkt ist, die atherosklerotische Plaques in der Intima aufweisen. Die Assoziation von Plaques und Axonneogenese konnte in hyperlipidämischen Mäusen und humanen Arterien nachgewisen werden. Diese Daten haben uns veranlasst, die mögliche Rolle von TRPV1 für die Progression der Atherosklerose zu untersuchen. **Methoden**: Um die möglichen molekularen Interaktionen in der Adventitia von erkrankten Mäusen zu untersuchen, wurden Genom-weite Microarray Analysen der Aorta durchgeführt; Immunfluoreszenzanalysen wurden benutzt, um selektive Neuropeptide und Immunzellen in der erkrankten Aorta und von Wurzelganglien des peripheren Nervensystems auf der Ebene der Proteine zu visualisieren; ein Immunosorbant Assay wurde benutzt, um die Gewebekonzentrationen des Neuropeptids Calcitonin Gene-related Peptide zu bestimmen; Mäuse wurden mit Resiniferatoxin behandelt, um TRPV1 pharmakologisch zu deletieren und dessen Einfluss auf die Progression der Atherosklerose zu bestimmen. **Resultate**: Atherosklerose war mit einem Anstieg der Calcitonin Gene-related Peptide-exprimierenden Nervenfasern und dessen Gewebekonzentrationen in der Adventitia erkrankter Mäuse assoziiert, führte aber zu keinen Änderungen der Neuronensubpopulationen in Hinterhornganglien. Die Hinterhornganglien von erkrankten Mäusen zeigten aber eine signifikante Infiltration von Immunzellen. In Resiniferatoxin-behandelten Mäusen zeigte sich eine signifikante Reduktion atherosklerotischer Plaques nach einem Zeitfenster von 6 Monaten. **Schlussfolgerungen**: Damit konnten wir mit Hilfe

parmakologischer Experimente zeigen, dass die Deletion von TRPV1 zu einer Reduktion der Atherosklerose führt. Experimente mit genetischen Tiermodellen, in den TRPV1 eleminiert wurde, werden zukünftig notwendig sein, ob die Pharmakotherapie von TRPV1 als eine mögliche zukunftsträchtige Therapieoption der Atherosklerose im Menschen untersucht werden sollte.

ABSTRACT

Atherosclerosis is a chronic and progressive inflammatory disorder of the arteries. Immune responses are involved in all disease stages. Transient receptor potential vanilloid 1 (TRPV1)-expressing neurons are a subset of peripheral and central nervous system sensory afferent neurons that extend free axon endings into tissues. Such axon endings are ubiquitously distributed throughout the body. It is well established that TRPV1-expressing neurons can regulate inflammation through the secretion of neuropeptides, which regulate recruitment of immune cells and other molecules involved in inflammatory tissue responses. Non-neuronal cells can also express TRPV1 including endothelial cells and vascular smooth muscle cells. However, the communication of TRPV1-expressing neurons with the aorta and atherosclerosis largely remains unknown. Our previous data have shown that the density of axons of the sensory nervous system increases in artery adventitia segments adjacent to atherosclerotic plaques of hyperlipidemic mice and human diseased arteries. These data led us to study the specific sensory innervation patterns in the aortic adventitia and delineate the potential role of TRPV1-expressing neurons during atherosclerosis progression using pharmaceutical approaches in mice. **Methods:** We used immunofluorescence analyses of sensory innervation in the adventitia and sought to identify the neuronal subpopulations and immune cells in peripheral sensory ganglia; used an enzyme immunoassay to examine calcitonin gene-related protein (CGRP) neuropeptide levels in arterial tissues; and applied microarray analyses to examine transcripts of genes that are potentially involved in neuroimmune crosstalk in the aorta adventitia. Using resiniferatoxin as a pharmaceutical drug to eliminate TRPV1 receptors in apolipoprotein E-deficient mice, we interrogated the effect of TRPV1 on atherosclerotic plaque burden. **Results:** We observed that atherosclerosis was associated with an increased density of $CGRP^+$ and $TRPV1^+$ sensory axons in the aortic adventitia and increased CGRP tissue levels in the aorta. Atherosclerosis did not alter the composition of neuron subpopulations in peripheral sensory ganglia; however, atherosclerosis was associated with increased numbers of immune cells in the soma of peripheral ganglia, with marked changes in dorsal root ganglia (DRG). Short-term (4 weeks) resiniferatoxin (RTX) treatment in adult mice did not change the plaque size in the aortic root and other segments of the aorta; yet, long-term (6 months) treatment in adult mice reduced the plaque size in both aortic root and aortic arch, and attenuated the progression of atherosclerosis. As a proof of drug efficiency, CGRP

levels were reduced after RTX treatment. **Conclusion:** Our data reveal that atherosclerosis increases innervation of TRPV1-expressing axons in the diseased aorta, and pharmacological depletion of TRPV1 reduces atherosclerosis. We conclude that a specific neuroimmune cardiovascular interface (NICI) involving atherosclerotic plaques, the adventitia, the immune system and the peripheral sensory nervous system (PSNS) regulates the progression of atherosclerosis.

ABBREVIATIONS

Apoe	Apolipoprotein E gene
ANOVA	Analysis of variance
ATLOs	Artery tertiary lymphoid organs
CLP	Common lymphoid progenitor
CMP	Common myeloid progenitor
CNS	Central nervous system
CGRP	Calcitonin gene-related peptide
DAPI	4',6-diamidino-2-phenylindole
DCs	Dendritic cells
DE	Differentially expressed
ddH_2O	Double-distilled water
DIT	Diffuse intimal thickening
DPBS	Dulbecco’s phosphate-buffered saline
DMSO	Dimethyl sulfoxide
DRG	Dorsal root ganglia
ECs	Endothelial cells
ED_{50}	Effective dose for 50% of the population
EDTA	Ethylenediaminetetraacetic acid
FACS	Fluorescence-activated cell sorting
FITC	Fluorescein isothiocyanate
GO	Gene ontology
H/E	Hematoxylin/eosin
IB4	α-D-galactosyl-binding lectin B4
LCM	Laser capture microdissection
LN	Lymph node
mRNA	Messenger RNA
NeuN	Neuron nuclei
NFM	Neurofilament medium
NG	Nodose ganglion
Ngf	Nerve growth factor
NS	Nervous system
ORO/H	Oil red O/hematoxylin

P2X3	Ligand-gated P2X receptor ion channel 3
PBS	Phosphate-buffered saline
PFA	Paraformaldehyde
PIT	Pathological intimal thickening
PNS	Peripheral nervous system
RTX	Resiniferatoxin
RT	Room temperature
SC	Spinal cord
s.c.	Subcutaneously
SEM	Standard error of the mean
SMA	Smooth muscle actin
SLOs	Secondary lymphoid organs
VSMC	Vascular smooth muscle cell
SP	Substance P
SPNS	Sensory peripheral nervous system
TCR	T cell receptor
TG	Trigeminal ganglia
TLC	Tertiary lymphoid cluster
TH	Tyrosine hydroxylase
T_H	Helper T cell
TLO	Tertiary lymphoid organ
T_{reg}	Regulatory T cell
TRPV1	Transient receptor potential vanilloid 1
wks	Weeks
WT	Wild-type

1 INTRODUCTION

1.1 Atherosclerosis

Atherosclerosis is an artery disease and the major cause of death worldwide: it constitutes the major pathology of cardiovascular diseases in multiple vital organs and can lead myocardial infarcts, stroke, peripheral artery disease, chronic renal failure, and many other clinically significant organ manifestations[1-5]. Development of atherosclerosis might start in young life in large and medium-sized arteries and appears to progress for long periods of time before becoming clinically significant[6,7]. Eventually, advanced atherosclerosis can result in plaque rupture and thrombosis and subsequently trigger tissue infarcts[3].

During the last eight decades, it has become evident that atherosclerosis is not only a chronic inflammatory disease characterized by the accumulation of lipids and fibrous elements[8], but that it is also accompanied by the continuous/persistent accumulation of several types of immune cells in arteries leading to an aberrant and uncontrollable inflammation of the entire arterial wall[9]. The disease can therefore be regarded as a non-resolving inflammatory condition of arteries[10]. Immune cells in atherosclerosis include innate immune cells such as monocyte-derived macrophages[9,11], dendritic cells (DCs)[12], and mast cells[13], and adaptive immune cells including various phenotypes of both T cells and very rarely B cells[14]. The potential contribution of these immune cells to the progression of atherosclerosis has been investigated but many fundamental issues remain unanswered.

Apolipoprotein E (*Apoe*) and low-density lipoprotein (LDL) receptor knockout mice are frequently used as genetically modified mouse models to study atherosclerosis[15,16]. In *Apoe*$^{-/-}$ mice maintained on normal chow diet, atherosclerotic lesions emerge in the aortic root at around 10 weeks (10 wks) of age as these mice are constitutively hyperlipidemic. The disease gradually progresses along the aortic tree involving the media and the adventitia[17,18]. When *Apoe*$^{-/-}$ mice are maintained on high fat diet, the extent of hyperlipidemia reaches very high levels and atherosclerotic plaques become 3-4 times larger within the same period of time compared to mice on normal chow[19]. Due to the broad applicability and the similarity to human plaques, the *Apoe*$^{-/-}$ mouse is widely used in experimental atherosclerosis.

1.1.1 Initiation and Progression of Atherosclerosis

Atherosclerosis may be associated with dysfunctions in lipid metabolism in addition to multiple other risk factors most of them resulting in arterial wall inflammation[11]. During atherosclerotic plaque initiation in hyperlipidemic mice and patients, cholesterol-rich lipoproteins are trapped within the intimal layer of the artery by extracellular matrix macromolecules. Some lipids and their protein components may undergo oxidative, enzymatic or chemical modification and this process activates both vascular smooth muscle cells (VSMCs) and endothelial cells (ECs)[11,20-22]. Activated VSMCs, because of their remarkable plasticity, undergo a phenotype switch and begin to proliferate, which makes VSMCs and VSMC-derived cells a major source of plaque cellularity and inflammation at all stages of atherosclerosis[23-27]. It has also been reported that the phenotype switch of VSMCs is reversible, at least in the early stages[23,25]. Activated ECs and VSMCs express adhesion molecules like vascular cell adhesion molecule-1, intercellular adhesion molecule 1, C-C motif-type and C-X-C motif-type chemokines[8,28,29]. These chemokines can promote the recruitment and migration of blood monocytes and lymphocytes into the intimal layer, leading to the initiation of inflammatory responses[8,21,22]. During the early stages of atherosclerosis, T cells can differentiate into T helper (T_H) cells including the pro-inflammatory T_H1 and/or few T_H2 cells and cytotoxic T cells[8]. Moreover, the immune cells secrete pro-inflammatory cytokines to amplify the local inflammatory response in the lesion which may also contribute to the generation of the plaque's fibrous cap at advanced stages of the disease[8]. However, the role of each of these cells in disease progression remains to be fully investigated as some of them also produce anti-inflammatory cytokines that are believed to be protective. There are multiple immune cell subtypes including regulatory T (T_{reg}) cells that protect the arterial wall from excessive inflammation[30]. If the inflammatory conditions are not well controlled, cycles of accumulation of monocytes, natural killer cells and other immune cells can accelerate plaque growth to contribute to the development of complicated lesions. In advanced atherosclerosis, plaques are characterized by the presence of fibrous caps and necrotic cores, the latter are sometimes calcified[22,23,25]. The fibrous cap largely contains VSMCs and associated extracellular matrix. Fibrous caps are believed to be critical in stabilizing and protecting the plaque from rupture as plaques with thin or eroded fibrous caps are most prone to rupture initiating thrombus formation[31]. Thus, VSMCs are thought to have a beneficial role in the advanced plaque by the generation of the fibrous cap[23,25,31,32]. Necrotic cores result from apoptosis of macrophages and VSMCs within extracellular lipids. Calcified areas contain macrophage/VSMCs-derived

microvesicles and debris[23,31].

1.1.2 Artery Tertiary Lymphoid Organs (ATLOs) Neogenesis in Chronic Non-resolving Inflammation and Atherosclerosis

During unresolving inflammatory tissue reactions, immune cells may form cellular aggregates termed *tertiary lymphoid organs* (TLOs) if they contain T cells and B cells[33,34]. As a chronic inflammatory disease, atherosclerosis involves all three layers of the arterial wall: The lamina intima, the lamina media, and the lamina adventitia. Intimal plaques activate and transform adjacent medial VSMCs to lymphoid tissue organizer-like cells. VSMCs in specific segments of the arterial tree - where TLOs develop - produce the lymphorganogenic chemokines C-C motif ligand 21 and C-X-C motif ligand 13 to attract and/or recruit both innate and adaptive immune cells to the inflamed adventitia. In experimental mice and human advanced plaque-burdened artery segments ATLOs have been observed[29,35], developing in the lamina adventitia adjacent to advanced plaques in the abdominal aorta of aged *Apoe*$^{-/-}$ mice. Additional locations have recently been described in mice and human diseased cardiovascular tissues including coronary arteries and multiple other arterial tree beds[33,36]. Based on the cellularities and structure, three distinctive stages of ATLOs have been proposed[29,33,36,37]: Stage I ATLOs designate small mixed T/B cell aggregates containing mostly T cells with few B cells. Stage II ATLOs feature separate T and B cell areas but no follicular DCs. Stage III contains ATLOs with separate T and B cell areas and follicular DCs in activated germinal centers (Fig. 1). In addition to immune cells, ATLOs also harbor newly formed and aberrantly structured lymph vessels, extensive neoangiogenesis, conduit networks, and high endothelial venules (HEVs)[33,37] (Fig. 1). ATLOs recruit monocytes through blood vessels, classical DCs (cDCs) through lymph vessels, and naïve T (Th0) and B cells throughh HEVs into diseased artery segments[33,37]. The recruited T and B cells become activated in the inflammatory tissue environment of the adventitia and some of them become converted into effector or memory T cells, induced T_{reg} cells, memory B cells, or plasma cells at various stages of differentiation. Given these cellular and structural characteristics and specifically the presence of activated germinal centers, Grabner et al. hypothesized that ATLOs may conduct a local T and B cell-dependent autoimmune response towards arterial wall-derived autoantigens. Nevertheless, the experimental evidence for this hypothesis remains to be demonstrated[37]. Interestingly, disruption of lymphotoxin β in VSMCs enhances atherosclerosis in aged *Apoe*$^{-/-}$ mice[33]. Recently, we demonstrated that ATLOs form neuroimmune cardiovascular interfaces (NICIs)

with the peripheral nervous system (PNS) connecting the diseased arterial wall with the brain[38]. Putting together, these data suggest that ATLOs may organize both pro- and anti-atherogenic immune responses during disease progression but there is still much to learn about their biological function.

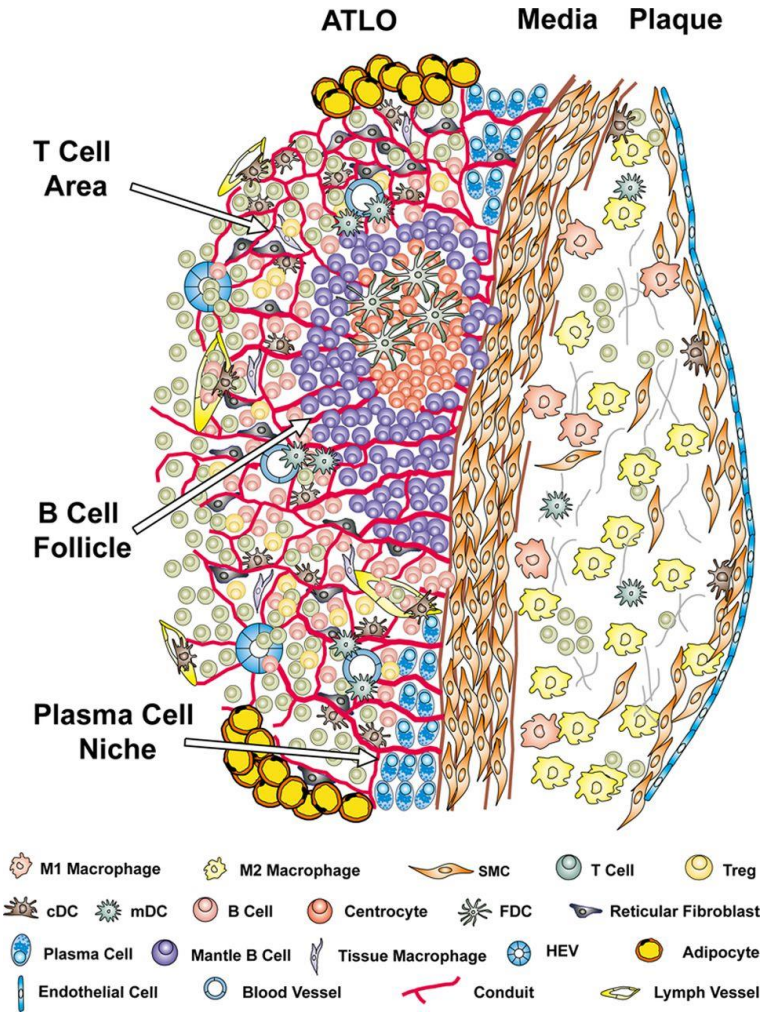

Figure 1. Schematic Choreography of the Cellularity and Structure of Advanced (Stage III) ATLOs. Well-structured ATLOs are crescent-shaped, non-encapsulated lymphoid aggregates that resemble lymph nodes (LNs) in both cellularity and structure. Advanced ATLOs are characterize by separate T cell areas, B cell follicles including follicular dendritic cells (FDCs) and plasma cell niches containing blood vessels, lymph vessels, HEVs and conduits. (Figure adapted from ref. [33])

1.2 The Nervous System (NS)

The NS coordinates the whole organism through detecting or transmitting signals from or to different parts of the body. The NS is anatomically classified into the central NS (CNS) and the PNS. In vertebrates (Fig. 2), the CNS comprises the brain and the spinal cord (SC)[39]

while the PNS includes the autonomic NS and the somatic NS[40,41]. The somatic NS is responsible to the control of voluntary body movements through skeletal muscles (Fig. 2). The autonomic NS is associated with involuntary physiologic processes of the internal organs (Fig. 2), including heart rate, blood pressure, respiration, digestion, and sexual arousal. It is further subdivided into the sympathetic, parasympathetic and enteric NS[41-44]. The sympathetic NS responds to the “fight or flight” mechanisms through increasing the heart rate, blood pressure, glycogenolysis but also controls gastrointestinal peristalsis. The parasympathetic NS responds to the “rest and digest” mechanisms through decreasing the heart rate, blood pressure but also regulating digestion. The enteric NS contains its own neural circuits and functions fully independently from the CNS[45-47]. However, the gut is also innervated by sympathetic efferent fibers arising from the spinal cord, parasympathetic efferent fibers from the brainstem, and afferent neurons from the dorsal root ganglia (DRG) and nodose ganglia (NG)[45,48]. In addition, the enteric sensory neurons can also project to the prevertebral ganglia, including the celiac ganglia and mesenteric ganglia[45,47,48] (Fig. 3).

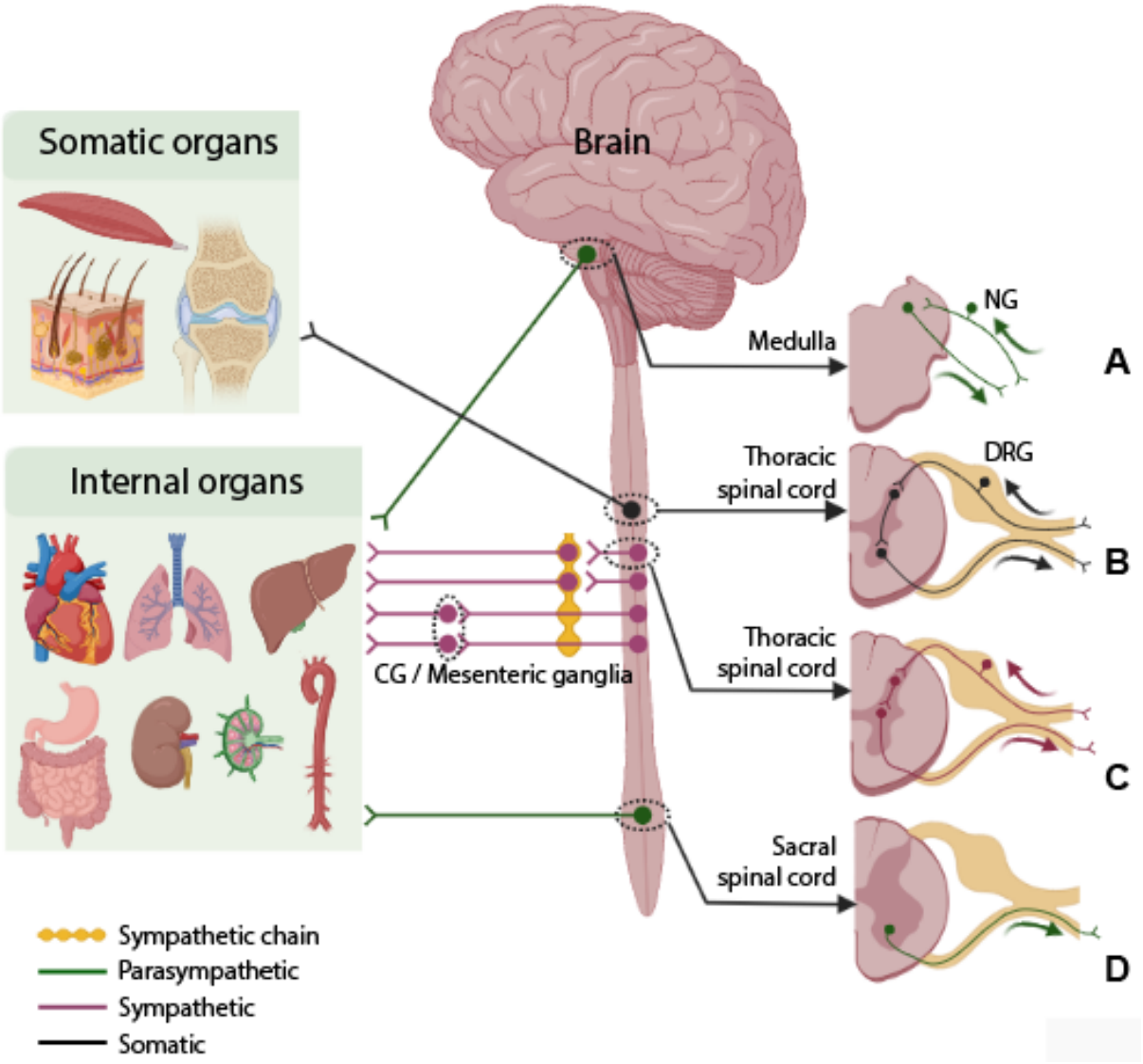

Figure 2. The Somatic, Parasympathetic, and Sympathetic NS. The schematic shows somatic fibers connected to skeletal muscle, skin, and bone (upper left and B). It also depicts somatic, parasympathetic and sympathetic inputs to internal organs (bottom left); for simplicity, only the connection to one side is shown. Preganglionic parasympathetic fibers are predominantly derived from the brainstem, which receive the signals from the NG afferent neurons (A). Preganglionic parasympathetic fibers originate in the ventral horn of the sacral spinal cord (D). Most preganglionic parasympathetic fibers form synapses with ganglia near the target organ. Preganglionic sympathetic fibers emerge from the gray matter of the thoracic or lumbar spine, which receive the signals from DRGs (C), then interact with the ganglia of the sympathetic chain or the prevertebral ganglia, including the celiac ganglia and mesenteric ganglia. NG: nodose ganglia. DRG: dorsal root ganglia. CG: celiac ganglia. (Figure created with BioRender.com)

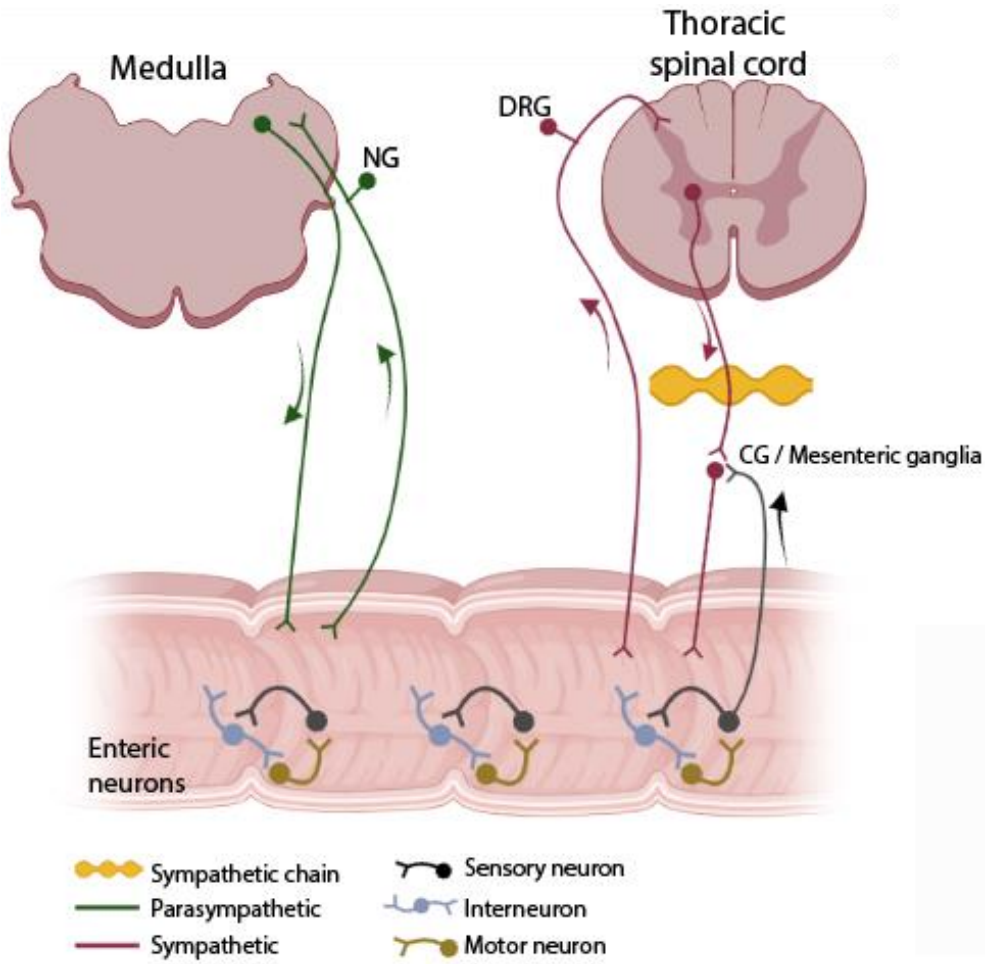

Figure 3. The Enteric NS and Its Major Neural Pathways with Spinal Cord and Brain. The enteric NS has its own neurons, including sensory neurons, motor neurons, and interneurons. These neurons are capable of generating reflex responses independently from the CNS (bottom). But it is also affected by the efferent innervation, including the parasympathetic pathway arising from the brainstem and the sympathetic pathway arising from the spinal cord. The afferent innervations include vagus neurons arising from the NG and the spinal afferent neurons arising from the DRGs. The enteric sensory neurons can also synapse on the prevertebral ganglia like CG or mesenteric ganglia. NG: nodose ganglia. DRG: dorsal root ganglia. CG: celiac ganglia. (Figure created with BioRender.com)

1.2.1 Organization of the SPNS

The sensory PNS consists of all the sensory nerves that innervate the peripheral tissues or organs, which can detect the internal and external changes and which sense potentially harmful circumstances[49,50]. Neuronal cell bodies of the SPNS, except the gastrointestinal tract, are mainly located in trigeminal ganglia (TG), NG, and DRG[44,51,52]. Sensory neurons whose cell bodies reside in the TG are bipolar neurons which have two axons extending from the cell body (Fig. 4 A). One axon is termed the peripheral axon and mainly innervates

the head. A second axon is termed the central axon and projects to the brain or SC. Sensory neurons arising from both the DRGs and NGs are pseudounipolar neurons which have one axon from the cell body but then split into two branches to the periphery and the CNS (Fig. 4). NG sensory neurons mainly innervate the visceral organs and project to the brain. DRG neurons mainly innervate the trunk of the body and the visceral organs through the long sprouting peripheral-terminals to sense the internal and external environment and convert noxious or non-noxious signals to action potentials at the peripheral terminals. The central axons of DRG neurons target the multiple laminae of the SC via the dorsal root and synapse with the interneurons and the second-order neurons in SC. The peripheral-terminal signals are finally projected to the medulla, mesencephalon and thalamus of the brain to complete the connection between the PNS and the CNS[53-55] or to the skeletal muscle and the visceral organs to complete a reflex arc[56]. Based on anatomical and functional criteria, the SPNS can be categorized into three main groups[55,57-59]: Aα and Aβ fibers, Aδ fibers, and C fibers. The Aα and Aβ sensory fibers are heavily myelinated and with the medium- to large diameter axons conduct rapidly transmitted signals (Fig. 5 A) mainly responding to proprioception and innocuous mechanical stimuli applied to skin, muscle and joints. The Aδ sensory fibers are lightly myelinated with a medium-diameter conducting rapid signals to mediate the initial type of pain (acute and sharp pain) (Fig. 5 B). The C fibers are unmyelinated and are small-diameter axons which conduct slow signals to mediate a second type of pain (diffuse and dull pain) (Fig. 5 C)[49,57]. The Aδ fibers are further divided into two main classes based on electrophysiological studies[57]. Type I with high heat thresholds (~53°C) are insensitive to capsaicin which constitutes a major chili pepper ingredient. Both type II Aδ and C fibers have lower heat thresholds (~43°C)[60] and are polymodal to respond to multiple noxious stimuli including mechanical, thermal and chemical stimuli (including capsaicin)[55,57].

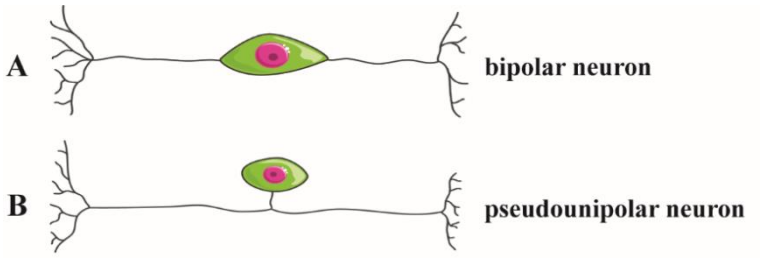

Figure 4. Two Main Types of Primary Peripheral Sensory Neurons Can be Distinguished. The primary peripheral sensory neurons mainly include two types of neurons: bipolar neurons and pseudounipolar neurons (green: cytoplasm; red: nuclei). (A) The bipolar neuron has two axons extending from its cell body into two

directions. (B) The pseudounipolar neuron has one axon from its cell body but splits into two branches forming a “T” shape.

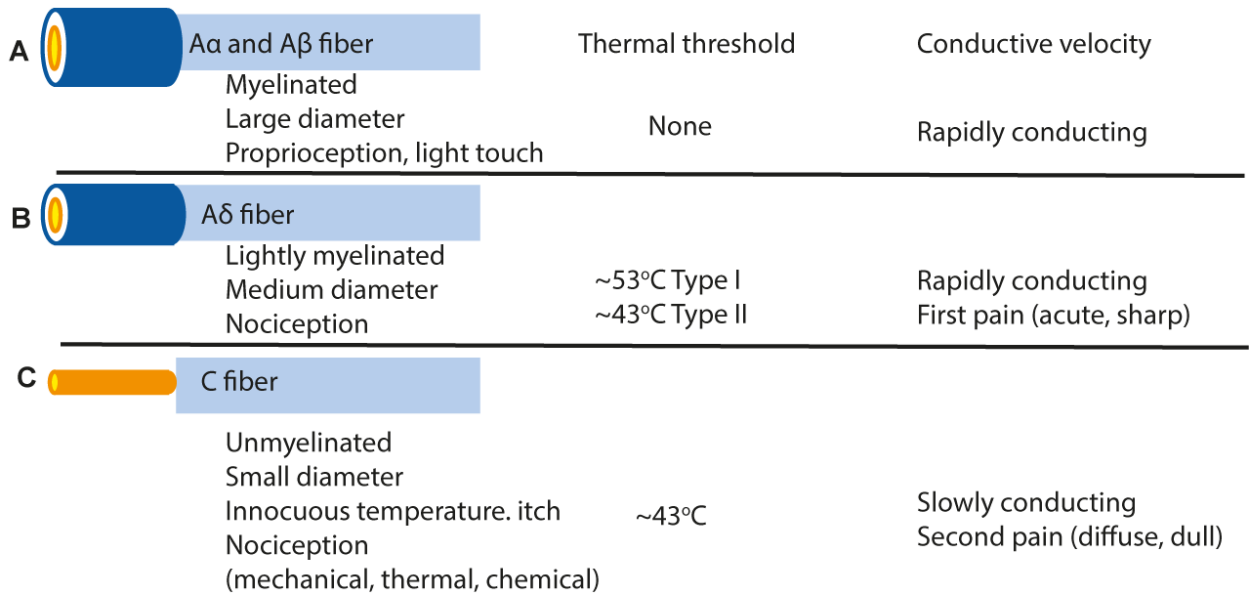

Figure 5. Three Main Types of Primary Peripheral Sensory Axons. The primary peripheral sensory neurons are classified into three subgroups based on their functionality and morphologic heterogeneity: (A) the large to medium diameter heavy myelinated Aα and Aβ fibers which mediate rapid conduction and are involved in the proprioception and light touch. (B) medium diameter slightly myelinated Aδ fibers which mediate somewhat slower but still rapid conduction and sense temperature and first pain. (C) small-diameter unmyelinated C fibers which mediate slow conduction and sense temperature and second pain. Blue: Schwann cell; white ring: myelin sheath; yellow ring: axon. (Figure adapted from ref [57]).

1.2.2 Transient Receptor Potential Vanilloid 1 (TRPV1)-expressing Sensory Neurons

Mammalian TRP proteins are ion channels that form six transmembrane domains. They are cation-permeable, which mediate the flux of cations into the cytoplasm and raise intracellular Ca^{2+} and Na^{+} concentrations. Cation influx depolarizes the cell and action potentials are generated. The TRPV1 channel belongs to the TRPV family. It is the first identified member among all TRPV channels and was discovered by David Julius in 1997[61], who was bestowed 2021 Nobel Prize in Physiology or Medicine together with Ardem Patapoutian for the contribution to the discovery of TRP channels. TRPV1 was subsequently characterized as the specific receptor of capsaicin, an active component of chili peppers. TRPV channels represent one of the seven subfamilies of TRP ion channels which participate in a broad range of sensory pathways and play important roles in the detection

and transduction of internal and external nociceptive stimuli[62,63], including subtypes TRPV1-6[62-66]. But only TRPV1-4 are activated by heat[53,65], while TRP ankyrin 1 and TRP melastatin 8 mediate cold sensation in mice[53,55,60,67,68]. To date, TRPV1 is the best studied member among the TRPV family. It is abundantly expressed in the soma, peripheral free nerve endings, central-terminals, and axons of the peripheral primary sensory neurons[49,55]. Based on their neuroanatomy, the TRPV1-expressing sensory neurons contain mainly two groups: type II Aδ and C sensory neurons[69,70] (Fig. 6). In the SC, different populations of primary sensory neurons project at different regions of the dorsal horn. The TRPV1-expressing Aδ sensory neurons target superficial dorsal horn laminae II[58,59]. The TRPV1-expressing C sensory neurons target laminae I and II[58,59]. About 10% of C fibers only sense harmless thermal information, the majority of C fibers are polymodal and respond to all forms of noxious stimulation including mechanical, thermal and chemical stimuli[55,57,59]. The nociceptive C sensory neurons are further divided into two categories based on the content of peptides and neurotransmitters: the peptidergic and nonpeptidergic sensory neurons[59] (Fig. 6). The peptidergic subsets target laminae I and outer II, which co-express neuropeptides including substance P (SP) and/or calcitonin gene-related peptide (CGRP) and participate in the regulation of physiological functions or pathological processes through the release of neuropeptides[58,59,71] (described in section 1.3). The nonpeptidergic subsets target inner laminae II, which selectively bind to the α-D-galactosyl-binding lectin isolectin B4 (IB4), and express ATP-gated ion channel ligand-gated P2X receptor ion channels 3 (P2X3) purinergic receptors[58,59,71]. Both groups of C fibers respond to similar types of noxious stimulation and express TRPV1.

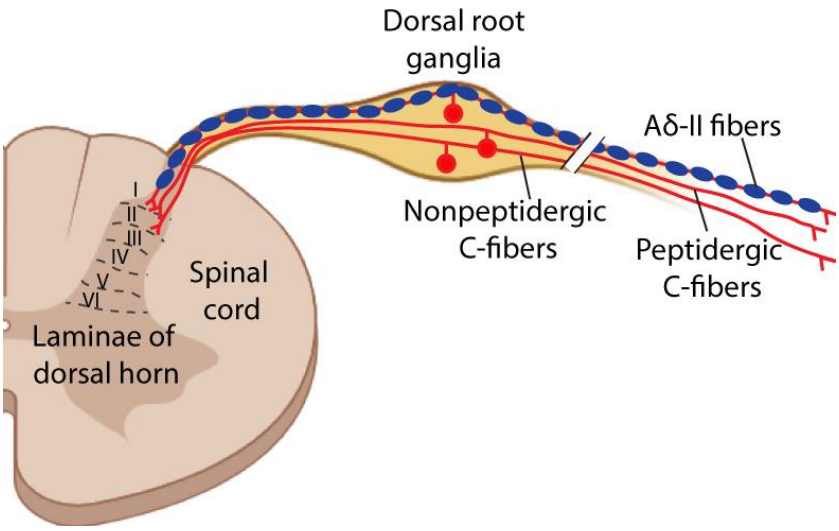

Figure 6. Anatomy of TRPV1 Sensory Neurons. The schematic shows the projection of three subtypes of TRPV1-expressing neurons in the SC via the dorsal horn. The thinly myelinated type II Aδ sensory neurons target laminae I, the peptidergic unmyelinated C sensory neurons target laminae I and outer laminae II, the nonpeptidergic unmyelinated C sensory neurons target inner laminae II. (Figure adapted from refs [55,58,59])

1.2.3 Activation of TRPV1

As a member of the TRP family, TRPV1 exhibits the prototypic family properties including six transmembrane domains and cation-permeability (Fig. 7). TRPV1 can be activated by a wide array of endogenous and exogenous physical and chemical stimuli that are divided into three categories: receptor-induced activation, ligand-induced activation, and direct activation[63,65,72]. Receptor-induced activation refers to the activation by phospholipase C of receptor tyrosine kinases and G protein-coupled receptors [73]. Ligand-induced activation refers to the binding of small organic molecules (like cytokines[57,74] and capsaicin[65,72]), inorganic ions (like protons[75]), lipids or products of inflammatory lipid metabolism[74]. Direct activation mainly includes mechanical and thermal stimuli (noxious heat > 43°C)[71] (Fig. 5 B and C). Ligand-induced activation is involved in the actions of capsaicin or the pharmaceutical resiniferatoxin (RTX).

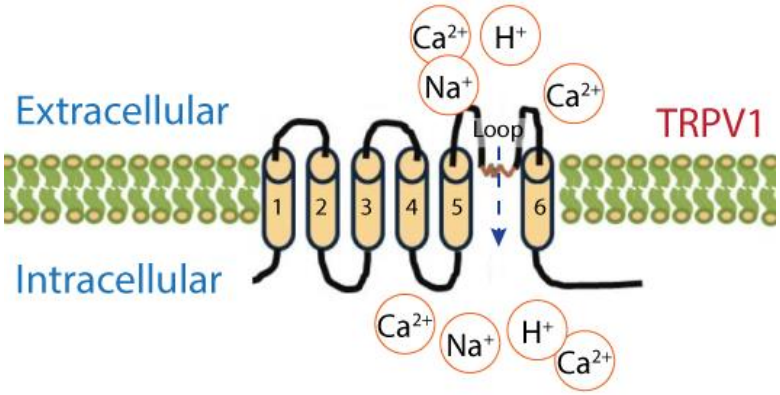

Figure 7. Activation of TRPV1. The schematic shows the structure of the TRPV1 channel with six transmenbrane domains and a hydrophobic loop between the fifth and sixth transmembrane domains. Blue dashed arrow indicates the influx of cations from the extracellular to intracellular milieu when TRPV1 gets activated. (Figure adapted from ref [72])

Capsaicin was first isolated in 1846 by Thresh[72]. The chemical structure was only determined 1919 by Nelson. Its complete synthesis was achieved in 1930 by Spath and Darling[76,77]. As a highly selective exogenous agonist of TRPV1, capsaicin contains an aromatic ring (vanillyl group), an amide group and a hydrophobic side chain (fatty acid

chain)[62,78] (Fig. 8). TRPV1 can also be targeted by RTX, a phorbol ester extracted from the stimulating ingredients of Moroccan cactus, with a much higher affinity than capsaicin[79,80]. RTX, as a functional analog of capsaicin, contains three similar regions: an aromatic ring, an ester bond, and a polyring group[62] (Fig. 8). Both capsaicin and RTX have been broadly studied and used in the pharmacological and biochemical characterization of TRPV1. Capsaicin/RTX activates TRPV1 in a dose-dependent manner, leading to a multitude of effects on TRPV1 and the related signal transduction cascades[81,82]. When administrated with a threshold concentration, capsaicin/RTX can activate the TRPV1 channel and allow cation influx to convert the chemical stimuli to neuronal/electrical signals or action potential. But when administrated with a repeated and overdose concentration, capsaicin/RTX can cause TRPV1 depletion (as described in more detail below).

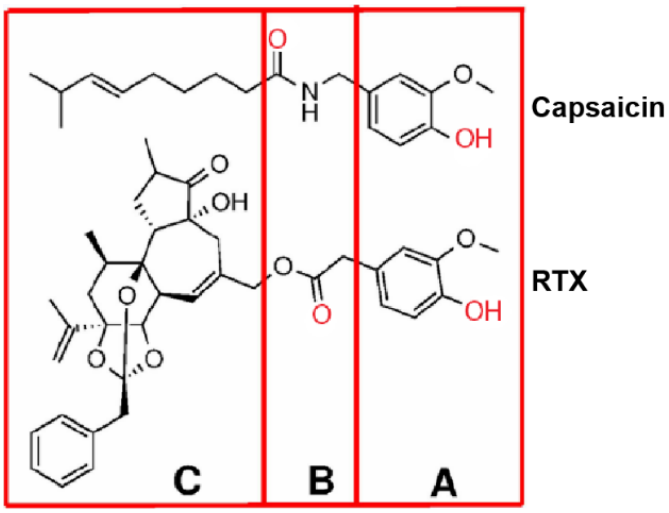

Figure 8. Chemical Structures of Capsaicin and RTX. Three similar structural regions between capsaicin and RTX are defined as (A) the aromatic ring, (B) the amide/ester bond, and (C) the hydrophobic side chain or polyring group. The atoms forming hydrogen bonds with TRPV1 are highlighted in red. (Figure adapted from refs [62,79])

1.2.4 Depletion of TRPV1

Sensory neurons expressing TRPV1 have been shown to innervate a wide variety of tissues and organs and are involved in different diseases[63,74,83-86]. To date, chemical and genetically mediated TRPV1 depletion has been most broadly used to explore its potential role in different diseases.

Capsaicin and RTX are commonly used for chemical depletion. There are three main

mechanisms that contribute to the TRPV1 depletion by over-dose capsaicin/RTX[87-89]: (1) Decreased receptor sensitivity through sustained Ca^{2+} influx from activated TRPV1 channels; (2) blocked voltage-gated Na^{+} channels operating by repeated TRPV1 activation and continuos cation influx; and (3) swelling and excessive Ca^{2+} influx due to mitochondrial membrane depolarization, which leads to impaired function and destruction of nerve-terminals, as well as destruction of cell bodies in DRGs, i.e. neuronal death. Therefore, chemical treatments can elicit a variety of effects, including desensitization. Chemically treated animals have been reported to display long-lasting (~5 wks), but reversible, decreased responses to noxious-heat and chemical irritants in different experimental conditions[90-93]. Noxious-heat responses include reaction latency to the hot plate test or the tail-flick test at 52° C. Chemical irritant responses include the corneal reflexes to 1% NH_4OH or 0.1% capsaicin[90,91,94]. Immunofluorescence (IF) data revealed that chemical depletion caused the loss of TRPV1 channels/proteins in the cell bodies in both DRGs and NGs, and in the corresponding nerve terminals in both the periphery and the SC[92,95,96]. More importantly, chemical depletion also resulted in the loss of TRPV1-expressing peptidergic ($CGRP^{+}$) and non-peptidergic ($IB4^{+}$) sensory neuron subtypes[92,93,97], indicating death of TRPV1-expressing neurons. In NG, terminal deoxynucleotidyl transferase dUTP nick end labeling $(TUNEL)^{+}$ neuronal nuclei and a decrease in total neuron number confirmed neuronal death after chemical depletion[93]. Therefore, the chemical depletion is also referred as chemical denervation in the literature[92,96]. To date, capsaicin and RTX are the most commonly used chemicals for depletion of TRPV1-expressing neurons. However, RTX is more broadly used than capsaicin because of its unique spectrum of pharmacological actions. When administered subcutaneously (s.c.), the ED_{50} for RTX is 3×10^{-7} g/kg compared to 2×10^{-3} g/kg for capsaicin, indicating a higher affinity of RTX for TRPV1 vs capsaicin[79]. An important information for the current thesis is that mice show a better tolerance to RTX compared to capsaicin: e.g. RTX treatment does not induce lethal pulmonary edema like capsaicin[80].

In addition to chemical depletion, genetic ablation of TRPV1 sensory neurons was reported in 2000 through the generation of TRPV1 knockout (*Trpv1*$^{-/-}$) mice. *Trpv1*$^{-/-}$ mice completely lose the TRPV1 immunoreactivity in DRG or at the nerve terminals in the periphery and the SC similar to chemical treatment, but the knockout genotype was not associated with changes in the number of SP^{+} peptidergic and $IB4^{+}$ non-peptidergic neuronal cell bodies in DRGs and the axon terminals in the SC[92,98]. These results suggested that the sensory

neurons that are predicted to express TRPV1 are viable in the knockout mice after genetic ablation unlike chemical treatment which is associated with an elusive number of neuron deletion. Moreover, *Trpv1*$^{-/-}$ animals show indistinguishable general appearance, gross anatomy, body temperature, locomotion, or overt behavior compared to WT animals[99]. *Trpv1*$^{-/-}$ mice show robust deficits in the response to the TRPV1 agonist (capsaicin/RTX) and pain-related behavior (like noxious heat), while the reactions to mechanical stimuli remain unaffected[98]. These mice show a reduced overall metabolism and age-dependent weight gain of around 15% but are resistant to a diet-induced weight gain[100,101]. Interestingly, *Trpv1* knockout mice have an extended life span of an average of 100 days, probably because of enhanced oxygen consumption and insulin sensitivity[102].

1.3 Neuro-immune Interactions between the SPNS and the Immune System

Research during the last decades has broadened our insight into the interface between the NS and the immune system[43]. Neuroimmunology is an emerging field in medical research with major implications to develop novel pharmacological targets to treat a large variety of clinically important human diseases[103-105]. Neuronal pathways are implicated in physiological regulators of immune function and inflammation. Many innate and adaptive immune cells express receptors for neurotransmitters and neuropeptides[106-108] (like CGRP and SP), which can be directly regulated by the NS in their recruitment, activation and function locally or primary and secondary lymphoid tissues[105,106,109-112]. Also, neuronal function can be altered in particular conditions by inflammation and immune dysregulation. Sensory neurons can also express receptors for cytokines, lipids and other inflammation-related molecules released by both innate and adaptive immune cells[113-115]. Therefore, sensory neurons can be modified through the interaction with immune cells directly or by binding molecules during the immune response[74,116-118]. Both the interaction and the functional cooperation between the NS and the immune system is essential to homeostasis and survival.

TRPV1-expressing sensory neurons can sense both physical and chemical stimuli and participate in the regulation of physiological function or the pathological process through the release of neuropeptides, including CGRP and SP[105,119,120]. The dense sensory innervation network in peripheral tissues/organs allows for rapid local and systemic modulation of

immunity. The modulation includes the recruitment, homing, activation and maturation of innate immune cells like macrophages, DCs and mast cells[106,121]. Moreover; TRPV1 is involved in adaptive immune responses including those in which T lymphocytes and their subtypes such as T_H1, T_H2, T_H17, and T_{reg} cells are involved. Some of these responses are mediated by CGRP or SP[122-125]. In general, the regulation of TRPV1$^+$ sensory neurons on the immune response has a dichotomic nature as it may affect the localization, severity, duration, and type of inflammation taking place to promote or suppress inflammation[115,126-129]. The experimental approaches used to study the interaction of TRPV1$^+$ sensory neurons and the immune system are - among others – the use of agonist activation, pharmaceutically and/or genetically altered *Trpv1* deficient mice, neurotransmitter antagonists, and/or inhibitors of neurotransmitter-containing vesicles[83,92,95,96,130-134].

1.3.1 Neuro-immune Interactions in Host Defense

The SPNS innervates whole organs and tissues and controls the response to peripheral alterations in immune homeostasis to defend against infection and injury caused by the invasion of pathogens. Sensory neurons can directly sense pathogens and rapidly communicate with the tissue resident or recruited immune cells in inflammation. A main group of these neuro-immune interaction-mediating sensory neurons are the specialized TRPV1-expressing neurons, which innervate some of the major barrier tissues, including the lung, the skin, and the gastrointestinal tract[54,135-137].

In *S. Aureus*-induced pain, the Nav1.8$^+$ TRPV1$^+$ sensory neurons are activated directly by interaction with bacteria through sensing pore-forming toxin α-hemolysin and N-formylated peptides. Activated neurons act directly on macrophages to reduce tumor necrosis factor-α production, thereby suppressing the recruitment of neutrophils and monocytes to the locally infected tissue through the release of the neuropeptide CGRP[138]. The reduced recruitment of neutrophils to infected tissue caused by activated TRPV1-expressing neurons is also apparent during *S. Pyogenes* infection[111]. Treatment with CGRP antagonist, botulinum neurotoxin A (BoNT/A), that inhibits its release, successfully blocked neuro-immune interactions, thereby improving host defense against bacterial infection[111]. During *C. Albicans*-induced cutaneous candidiasis[139], optogenetically activated TRPV1 sensory neurons drove the production of interleukin-23 by CD301b$^+$ dermal DCs. This process is mediated by the neuropeptide CGRP, which is also critical for the production of interleukin-17 by dermal γδ T cells, leading to enhanced host defense from C. Albicans.

The respiratory tract is also densely innervated by TRPV1$^+$ free nerve endings. In *S. Aureus* induced lung infection, cytokine induction and the CD11b$^+$Ly6G$^+$ neutrophil recruitment into the lung was increased by chemical ablation of TRPV1$^+$ sensory neurons and CGRP antagonist-mediated blockade of neuro-immune communication, leading to suppressed protective immunity. To distinguish TRPV1$^+$ sensory neurons from the TRPV1 channel itself, the authors also used *Trpv1*$^{-/-}$ mice. It turned out that the TRPV1$^+$ sensory neurons but not the TRPV1 channel are relevant for the pulmonary host defense.

The gastrointestinal tract is constantly exposed to microbial stimuli and TRPV1 sensory neurons are major gut-innervating neurons which sense disturbances in the gastrointestinal tract. During Salmonella infection in the intestine through intestinal microfold cells within Peyer's patches, DRG TRPV1 sensory neurons but not the vagal TRPV1 neurons, suppress the infection via CGRP to attenuate Salmonella invasion through reducing the density of microfold cells[96]. Moreover, TRPV1 sensory neurons reduce the invasion and colonization through maintaining the level of segmented filamentous bacteria in the small intestine.

Putting together, TRPV1 sensory neurons play critical roles in the host defense against several pathogens at epithelial barriers and the immune response in general. The impact of TRPV1 sensory neurons on the host defense depends on the type of pathogens involved, the affected tissue and the type of immune response involved. Chemical or genetic treatment of TRPV1 sensory neurons and inhibition of specific neuropeptides or their optogenetic activation indicate multiple mechanisms where the research area may develop in the future.

1.3.2 Neuro-immune Interactions in Inflammation

Sensory neurons themselves are also regulated by the immune system through direct or indirect interaction with immune cells. Some indirect interactions are mediated via receptor tyrosine kinases, G protein-coupled receptors, cytokines, growth factors and neuropeptides[105]. When a tissue gets injured, inflammation occurs, and this results in the local secretion of inflammatory mediators and the recruitment of both innate and adaptive immune cells including mast cells, macrophages, neutrophils, and T cells[140,141]. The local immune response finally creates an inflammatory environment. In this environment, the activated immune cells can release molecular mediators including cytokines, nerve growth

factor, serotonin and histamine, which bind to their corresponding receptors expressed on the surface of TRPV1$^+$ sensory neurons. These include a number of cytokine receptors, TRPV1, P2X receptors, tropomyosin receptor kinase A and G protein-coupled receptors, resulting in the change of neuronal thresholds leading to depolarization at locally and enhancing electric activity of nerve conductance[52,57,72,142].

During imiquimod-induced ear inflammation, TRPV1$^+$NaV1.8$^+$ sensory neurons have been reported to be integral for the production of interleukin-23 by dermal DCs and γδT17 cells and the recruitment of CD11b$^+$Ly6C^{hi} monocytes and CD11b$^+$Ly6G^{hi} neutrophils into the imiquimod-induced inflammatory ear[95]. Regarding functional roles of TRPV1$^+$ sensory neurons in cancer cell proliferation, survival and migration was also reported to be associated with anti-inflammatory and anticancer effects[83,132-134].

1.3.3 Neuro-immune Interactions in Cardiovascular Diseases

Although the effects of peripheral sensory neurons on diseases are widely recognized in cancer[143,144], rheumatoid arthritis[145], pain[146,147], and inflammation[119,124,126,148] of different organs or tissues like skin, lung, gut and brain, the neuro-immune crosstalk in atherosclerosis is drawing more and more attentions recently. In our group, the existence of CGRP$^+$ sensory nerves at both the thoracic and abdominal aorta adventitia in aged WT mice has been documented[38]. Morphometric analyses revealed a higher density of CGRP$^+$ fibers in the adventitia of abdominal aorta with plaque and even higher in ATLO-containing segments of aged *Apoe*$^{-/-}$ mice *vs*. aged WT mice. Both sensory neurons of the DRGs and TGs innervate the aorta but the mechanisms underlying increased sensory fiber density remains unclear. The pseudorabies virus (PRV) in virus tracing studies was injected into the abdominal aorta adventitia to trace sensory neurons that innervate the abdominal aorta and ATLOs in aged *Apoe*$^{-/-}$ mice. We found sensory neurons in the thoracic 6th -13th DRGs connecting to the abdominal aorta adventitia[38].

TRPV1$^+$ sensory neurons also impact the cardiovascular system. Blockade of TRPV1$^+$ neurons has been reported to promote increased blood pressure in hypertension through several routes. In blood vessels, knockout or blockade of TRPV1 channels reduced vasodilation in mouse arteries by inhibiting the release of CGRP[149]. In the kidney, TRPV1$^+$ sensory neurons increased natriuretic and diuretic effects via neuropeptides, thereby reducing high salt-induced blood pressure in rats.[150,151]. In the bladder, *Trpv1*$^{-/-}$ mice

exhibited higher frequencies of low-amplitude, non-voiding bladder contractions because of the loss of ATP release[152]. In a model of spontaneous hypertension[153], further elevation of blood pressure was prevented in 8-week-old rats when epidural application of RTX specifically depleted T1-T4 DRGs. However, this did not occur when depletion of the L2-L5 DRGs was performed, suggesting segmental differences in the function of DRG neurons. Furthermore, in 16-week-old rats, depletion of the T1-T4 DRGs only lowered blood pressure but did not prevent further increases, suggesting a modifiable role of DRGs neurons in disease progression. However, as mentioned above, the characteristics of aortic innervation and their role in the progression of atherosclerosis remain unclear. On the other hand, the effect of atherosclerosis on aortic innervation and on inflammatory infiltration in their distal ganglia remains to be determined. The potential involvement of these neurons in atherosclerosis progression is therefore of major interest and their study is central to this thesis.

1.4 TRPV1 in the CNS

TRPV1 is also expressed in the microglia and astrocytes of rodent brains[154]. But the expression of TRPV1 in neuronal cells in brain is controversial. TRPV1 expression in brain neuronal cells is reported in restricted regions (like hippocampus[155]) and at low-level expression[156] or only under particular situations, like neuropathic pain[154]. However, the functional role of TRPV1 in brain has been confirmed. It is reported that $TRPV1^{+}$ microglia in the anterior cingulate cortex controls microglia activation and the release or uptake of neurotransmitters in neurons, as well as the intrinsic electrical properties and synaptic strength of $TRPV1^{+}$ neuronal cells in neuropathic pain[154]. The intracerebroventricular administration of the TRPV1 agonists also revealed the role of TRPV1 in thermoregulation-associated brain regions[157]: It has been reported that *Trpv1*$^{-/-}$ can ablate its expression in brain[154,158]. But it is difficult for peripheral administration of capsaicin or RTX to function in brain since several fold-higher doses and longer time treatments are needed to cross the blood-brain barrier and affect brain function[157,159]. A caveat of pharmacological treatments of mice is the interpretation of the results as it is difficult to identify the target tissues.

1.5 Aim of the Project

As a chronic inflammatory disease, atherosclerosis is mainly involved in large and medium-sized arteries and – as pointed out above - immune responses participate in all stages of

atherosclerosis. Since TRPV1$^+$ sensory neurons are reported to participate in the inflammatory response in different diseases and since we also find increased sensory fiber density in the adventitia of abdominal aorta burdened with plaques, clarification of a potential impact of TRPV1$^+$ sensory neurons on atherosclerosis is the major aim of this thesis. To reveal the potential functional role of TRPV1 sensory neurons on atherosclerosis, we asked the following specific questions:

1) What are the characteristics of the sensory neuronal innervation in the adventitia of atherosclerotic aorta segments?
2) Does atherosclerosis affect neuronal cellularity and immune cell infiltration in peripheral sensory ganglia?
3) Does the pharmacological interference with TRPV1$^+$ sensory neurons affect the process of atherosclerosis?

To answer these questions, we set the plans as below:

1) Delineate patterns of sensory axons innervation in the adventitia of adult aortic root and aged abdominal aorta of WT and *Apoe*$^{-/-}$ mice respectively.
2) Quantify the distribution of neuronal subpopulations, and immune cell infiltration in peripheral sensory ganglia including DRGs and NGs in both adult and aged WT and *Apoe*$^{-/-}$ mice.
3) Investigate the potential role of TRPV1 sensory neurons in modulating the progression of atherosclerosis.

2 MATERIALS AND METHODS

2.1 Materials

2.1.1 Mice

WT C57BL/6J and B6.129P2-*Apoe*tm1Unc/J (002052) mice were obtained from the Jackson Laboratories and housed in the animal facility of the University Hospital of Munich. Animals were housed in a specific pathogen-free environment on a 12-hour light/dark cycle and fed standard rodent chow (Altromin, Germany) and water ad libitum. All animal experiments were performed in strict adherence to local governmental and institutional animal care regulations (Gz.: 55.2-1-54-2532-6-2014, Regierung Oberbayern München).

2.1.2 Reagents, Buffers and Equipment

The following tables contain the list of reagents, buffers and equipment used in the experiment.

Table 1: Reagents and Materials

Reagents	Company	Catalogue NO.	Storage
Phosphate-buffered saline (PBS)	Sigma	P4417-100TAB	4ºC
Dulbecco's phosphate-buffered saline (DPBS)	Gibco	14190-094	4ºC
Ethylenediaminetetraacetic acid (EDTA)	Roth	8040.1	RT
Sucrose	Sigma-Aldrich	90M003524V	RT
Oil red O (ORO)	Romeis	S378	RT
Sudan-IV	Sigma	198102	RT
Hematoxylin	Dako	S2020	RT
Giemsa	Merck	192040100	RT
Alizarin Red S	ROTH	0348.2	RT
10% bovine serum albumin	Aurion	70411/1	4ºC
10% fetal calf serum (FCS)	Lonza	DE14-801F	-20 ºC
Goat serum			4ºC
Acetone	Merck	K40718714	RT
Isopropanol	Merck	K40615718	RT
Methanol	Roth	Sorte420	RT
Ethanol abs.	VWR	18k144019	RT
Xylene	Fisher Chemical	x/0250/17	RT

Paraformaldehyde (PFA)	Sigma-Aldrich	P-6148	RT
Tissue Tec	Sakura	0827400006	RT
Fluromount G	DAKO	S3023	4ºC
Aqueous mounting medium G	DAKO	S3025	4ºC
Eosin	ROTH	X883.1	RT
Sirius red	Waldeck	1A-280	RT
Roti-Histokit II	ROTH	T160.1	RT
Dimethyl sulfoxide (DMSO)	PanReac AppliChem	A3672 0100	RT
Tween 80	Sigma Aldrich	P1754	RT
Ammoniaque 30%	ROTH	CP17.1	RT
NaCl 0.9%	BRAUN	6726174.00.00	RT
Triton X-100	ROTH	3051.1	RT
Acetic acid	Roth	3738.4	RT
96 Well Polystyrene Plate	Corning	Costar 9018	RT
EDTA-coated tubes	Sarstedt	41.1504.005	RT
O.C.T. Compound	Tissue-Tek	25608-922/924/916	RT

Table 2: Buffers

Solution	**Composition**	**Storage**
1 X PBS	137 mM NaCl, 2.7 mM KCl, 10 mM Na_2HPO_4, 1.76 mM KH_2PO_4, pH 7.2-7.4	4ºC
4% PFA	40 g paraformaldehyde in PBS (1000 ml final), pH 7.2-7.4	4ºC
0.2 mol/L PB buffer	2.3 g Na_2HPO_4, 0.6 g $NaH_2PO_4.2H_2O$ in 100 ml double-distilled water (ddH_2O), pH 7.2-7.4	RT
20% Sucrose	20.0 g sucrose in a mixture of 50 ml ddH_2O and 50 ml 0.2 M PB buffer	RT
30% Sucrose	30.0 g sucrose in a mixture of 50 ml ddH_2O and 50 ml 0.2 M PB buffer	RT
20% EDTA	20.0 g EDTA in a mixture of 100 ml ddH_2O, pH 7.2-7.4	RT
50 mM EDTA	1.46 g EDTA in a mixture of 100 ml ddH_2O, pH 8.0	RT
Oil Red O stock	0.5 g Oil red O in 100 ml isopropanol	RT
Sudan-IV stock	0.5 g Sudan-IV in a mixture of 35 ml ethanol, 50 ml acetone, and 20 ml water	RT
Picro-Sirius red solution	0.1% (w/v) Sirius red powder dissolved in picric acid	RT
0.5% acidified water	5 ml Glacil acetic acid in 1000 ml ddH_2O	RT
Alizarin Red S working solution	2 g Alizarin Red S in 100 ml ddH_2O, PH 4.1-4.3	RT

4% Triton X-100	4 ml Triton X-100 in 100 ml ddH_2O, pH 7.2-7.4	4°C
0.5% Triton X-100	0.5 ml Triton X-100 in 100 ml ddH_2O, pH 7.2-7.4	4°C
4% Acetic acid	4 ml acetic acid (abs.) in 100 ml ddH_2O	4°C
Fluorescence-activated cell sorting (FACS) buffer	DPBS with 2% fetal calf serum	4°C
Ammonium-Chloride-Potassium (ACK) lysis buffer	0.15 mM NH_4Cl, 1 mM $KHCO_3$, 0.1 mM Na_2EDTA, pH 7.3	RT
PBS (10x)	80 g NaCl, 2 g KCl, 27 g $Na_2HPO_4 \cdot 7H_2O$, 2.4 g KH_2PO_4 in ddH_2O (1000 ml final), PH 7.2-7.4	RT
PBS (1x)	Dilute PBS (10x) in 10 times with ddH_2O	RT
PFA-sucrose solution	50 g sucrose into 1000 ml 4% (w/v) PFA in ddH_2O	RT

Table 3: Equipment

Name	**Company**	**Model/Type**
Dissection stereomicroscope	Leica Microsystems	Stemi 2000
Light microcope	Leica Microsystems	DM LB
Fluorescence microscope	Leica Microsystems	DM 6000 B
Confocal laser scanning microscope	Leica Microsystems	True Confocal Scanner (TCS)-SP8
Cryostat microtome	Leica Biosystems	Leica RM2235
Centrifuge	Eppendorf	Centrifuge5415 R
	Thermo Scientific	Heraeus®Multifuge®3S-R
Dissecting pan black wax	Thermo Scientific	S17432
Minutien black anodized pins	Thermo Scientific	26002-15
Complete blood cell counter	Scil Vet abc	scil animal care company GmbH
Microplate Reader	Tecan	Spectra Fluor Plus
Flow cytometer	BD	Canto-II
Thunder upright microscope	Leica Microsystems	DM6 B
Balance	Ohaus	Analytical Plus
Hematology analyzer	Scil Animal Care	ScilVet ABC
pH-meter	WTW	InoLab level 1
Ultrapure purification	Millipore	Milli-Q Plus ultrapure purification
-80°C freezer	C7736CD	Miele
Hot plate controller	Leica	KL 1500H

2.1.3 Antibodies for Immunofluorescence Microscopy and Flow Cytometry

Primary and secondary antibodies used to define SPNS neurons and immune cells by immunofluorescence staining are listed in the following tables.

Table 4: List of Primary Antibodies

Antibody	Clone or reference	Cell/ structure	Host	Dilution	Company
Anti-neurofilament medium 200	N4142	Pan-neuronal	Goat	1:500	Sigma
Anti-neurofilament heavy	AB5539	Pan-neuronal	Goat	1:500	Sigma
Anti-neurofilament medium (NFM)	AB5735	Pan-neuronal	Chicken	1:500	Millipore
Anti-neurofilament light	ab134460	Pan-neuronal	Chicken	1:500	Abcam
Anti-TRPV1	AGP-118	Vanilloid receptor 1	Guinea pig	1:500	Alomone labs
Anti-TRPV1	ACC-030	Vanilloid receptor 1	Rabbit	1:500	Alomone labs
Anti-CGRP	ab36001	Peptidergic neuron	Goat	1:500	Abcam
Antbi-IB4 biotin conjugate	L2140	Non- peptidergic neuron	Bandeiraea simplicifolia	1:500	Sigma
Anti-P2X3	APR-016	Non- peptidergic neuron	Rabbit	1:500	Alomone labs
Anti-TH	AB152	Type C low-threshold mechanoreceptors	Rabbit	1:500	Millipore
Anti-NeuN Alexa Fluor®488 conjugated	MAB377X	Neuronal cell body	Mouse	1:200	Millipore
Anti-CD68	FA-11	Macrophage or monocyte	Rat	1:100	Serotec
Anti-CD3e	145-2C11	Pan-T cell	Hamster	1:500	BD
Anti-B220	RA3-6B2	Pan-B cell	Rat	1:200	BD
Anti-SMA-fluoresceinisothiocyanate (FITC)	1A4	Smooth muscle cell	Mouse	1:300	ThermoFisher

Table 5: List of Secondary Antibodies

Antibody	Host	Format	Dilution	Company
Anti-rabbit IgG	Goat	Alexa 488	1:200	Invitrogen
	Donkey	Cy3; Cy5	1:300	Dianova
	Goat	Cy3; Cy5	1:300	Dianova
Anti-rat IgG	Donkey	Cy3; Cy5	1:300	Dianova
Anti-A. Hamster IgG	Goat	Cy3; Cy5	1:300	Dianova

Anti-chicken IgY	Donkey	Cy3; Cy5	1:300	Dianova
Anti-FITC IgG	Mouse	Cy3	1:300	Dianova

Table 6: List of Flow Cytometry Antibodies

Antibody	Clone	Format	Dilution	Company
Fixable viability dye	-	APC	1:200	eBioscience
Anti-CD45	30-F11	Percp-Cy5.5	1:200	eBioscience
		APC-cy7	1:200	eBioscience
Anti- T cell receptor β (TCRβ)	H57-597	BV605	1:200	eBioscience
Anti- CD4	GK1.5	PE-Cy7	1:200	eBioscience
Anti-CD8α	53-6.7	V450	1:200	eBioscience
Anti-B220	RA3-6B2	V500	1:200	eBioscience
Anti-CD11b	M1/70	APC	1:200	eBioscience
Anti-CD11b	M1/70	BV711	1:200	Biolegend
Anti-CD11c	N418	FITC	1:200	eBioscience
		BUV395	1:200	eBioscience
Anti-Foxp3	FJK-16s	PE	1:200	eBioscience
Anti- CD44	IM7	APC-Cy7	1:200	eBioscience
Anti- CD62L	MEL-14	FITC	1:200	eBioscience
Anti- CD69	H1.2F3	PE	1:200	BD
Anti- CD16/32	93	PE	1:500	Biolegend
Anti-c-kit	2B8	PE-Cy7	1:500	Biolegend
Anti-MHC-II	M5/114.15.2	PE-Cy7	1:200	Biolegend
Anti-SiglecH	551	Percp-Cy5.5	1:200	Biolegend
Anti-CD86	GL1	BV421	1:200	Biolegend
Anti-CD103	2E-7	BV605	1:200	Biolegend
Anti-F4/80	BM8	FITC	1:200	Biolegend
Anti-Ly6G	560600	APC-Cy7	1:200	BD
Anti-CD206	C068C2	PE	1:200	Biolegend

2.2 Methods

2.2.1 Capsaicin Treatment

Mice were randomly divided into two groups for vehicle and capsaicin treatment,

respectively. Capsaicin (Sigma, M2080) was dissolved in absolute ethanol and further diluted in normal saline to get a stock solution of 6.25 g/l in saline with 10% (v/v) tween 80. Prior to each capsaicin injection, mice were deprived of the drinking water for 3 hours and supplied with 90% oxygen for 2 hours after injection to reduce the mortality caused by pulmonary edema[160]. Mice were anesthetized with ketamine/xylene just before the injection to avoid severe local stimulation caused by capsaicin injection and injected s.c. in the flank on 3 consecutive days with 25 mg/kg (day 0), 50 mg/kg (day 1), and 50 mg/kg (day 2)[161] (Fig 38. A). Mice were kept on a 37°C warming plate for at least 1 hour after capsaicin injection to keep the body core temperature.

2.2.2 RTX Treatment

For short-term RTX treatment, male *Apoe*$^{-/-}$ mice at the age of approximately 28 wks were used. Mice were randomly divided into two groups for vehicle and RTX treatment, respectively. RTX (Alomone labs, R-400) was dissolved with absolute DMSO and further diluted in PBS to a stock solution containing 2% (v/v) DMSO with 0.15% (v/v) tween 80[92]. Each time before the injection, mice were deprived of the drinking water for 3 hours to reduce the mortality caused by pulmonary edema[160]. Mice were anesthetized with ketamine/xylene just before the injection to avoid severe local stimulation caused by RTX injection. Mice were s.c. injected in the flank on continuous days with three increasing doses of RTX (30, 70, and 100 μg/kg) [92] (Fig 39. A). In case of local skin inflammation, three injections were applied at different positions, including the neck, the left and right abdomen. The vehicle group was given the same dose of vehicle (2% (v/v) DMSO with 0.15 (v/v) % Tween 80 in PBS). After the injection, the body temperature was maintained by keeping the mice on a 37°C warming plate for 3hours until the recovery from anesthesia. Then, mice were rested for 4 wks and sacrificed at 32 wks for short-term RTX treatment.

For long-term RTX treatment, male *Apoe*$^{-/-}$ mice aged at 8 wks were used. Mice were randomly divided into two groups for vehicle and RTX treatment, respectively. Mice were given flank injections on consecutive days with three increasing doses as described in the short-term treatment protocol. Then, the mice were given the repeated injection one time every 4 wks with 100 μg/kg RTX or the same volume of vehicle (Fig 43. A). Before the injection, mice were deprived of the drinking water for 3 hours and anesthetized with ketamine/xylene just before the injection to avoid severe local irritation caused by RTX injection. Two days before each repeated injection time point, blood was collected via the

tail vein for cholesterol measurement. In addition, a behavior test was done 24 hours after each repeated injection to determine the effectiveness of the long-term RTX injection. After the last injection, mice were rested for 4 wks and sacrificed at around 32 wks.

2.2.3 Behavioral Tests

For behavioral method, experimentor was blinded to the treatment condition. The behavior tests were done 24 hours after the last injection for the short-term treatment, and also 24 hours after each repeated injection for the long-term treatment. To measure the sensitivity to noxious irritation, eye-wiping tests for corneal reflex was done by giving a small drop (20 µl) amount of a 1% (w/v) NH_4OH solution in saline into the right eye and subsequently placing the mice into a transparent box for oberservation[90,161]. The number of eye-wipes with the ipsilateral forelimb during 30s was counted. To measure the sensitivity to noxious heat, hot plate test for thermal sensitivity was done by putting the mice on the hot plate (52° C). Latency to hindpaw lifting, licking or flinching was counted, and ended at a maximum of 60s[92].

2.2.4 Cholesterol Test

For cholesterol analysis, blood was taken via heart puncture on the sacrifice day for short-term treatment from control and treated groups. For long-term treatment, blood was taken 2 days before every repeated injection thorough the tail vein. Approximately 4 drops of blood were collected into an EDTA blood collection tube and centrifuged at 300g × 10 min to separate the plasma. Total cholesterol concentration was measured with a commercial cholesterol kit[162]. The plasma was diluted 3 times with 0.9% NaCl before mixing with the reaction regent. The standard calibrator (160 mg/dl) was serially diluted with 0.9% (w/v) NaCl to 10 mg/dl for the standard curve. Five µl of diluted sample plasma or standards or blank control (0,9% NaCl) was loaded into a 96-well plate in duplicates. Subsequently, 200 µl reaction regent was added per well and gently mixed on a shaker. The plate was incubated at room temperature (RT) for 30 min. Then, the absorbance was measured by a multi-well plate reader (SpectraFluor Plus, Tecan) at 450 nm. The cholesterol concentration was calculated as mg/ml plasma based on the standard curve.

2.2.5 CGRP Enzyme Immunoassay (EIA)

To determine the CGRP concentration in aortic tissues, the ascending arteries of WT and *Apoe*$^{-/-}$ mice aged 32 wks (considered as adult mice), the abdominal aorta between renal

arteries of WT and *Apoe*$^{-/-}$ mice aged around 76 wks (aged mice) and abdominal aortas of *Apoe*$^{-/-}$ mice aged around 76 wks without plaque was collected (negative control). All samples were frozen in liquid nitrogen and stored at -80°C until further use. Samples were prepared for CGRP measurement following the manufacturer's instructions of the CGRP EIA kit (Cayman Chemical;Cay589001) as reported[92,96,111]. The concentration was adjusted to 1 mg tissue per 4 ml acid. The measurement was performed using a multi-well plate reader (SpectraFluor Plus, Tecan) at 405 nm every 15 min up to how long ? to identify the optimal measurement time point. The CGRP concentration was reported as pg/ml.

2.2.6 In Situ Detection of Apoptotic Cells

To detect apoptosis in atherosclerotic plaques, cryosections of the aortic root were collected from both control and RTX-treated mice and stained in situ using the cell death detection Kit (Roche, 12156792910) through a TUNEL reaction according to the manufacturer's instructions. Then, the slides were incubated for 1 hour with DAPI, rinsed in PBS 3 times for 5 min and mounted in PBS for subsequent fluorescence microscopic analysis.

2.2.7 Tissue Preparation, Embedding, and Sectioning

Mice were anesthetized with ketamine/xylene. Blood samples were taken by cardiac puncture for flow cytometry. The vasculature was then perfused with 10 ml 0.5 mM EDTA in PBS, 20 ml ice-cold PBS and 20 ml FACS buffer through left ventricular puncture. After the perfusion, the spleen, liver and lung was collected. Small tissues including LNs, DRGs and aorta were dissected under the stereomicroscope.

For aortic root sectioning, the aorta was removed at cutting point A from the level above the coronary artery near the atria at the base of heart (Fig. 9 A). The heart was cut into two parts at the cutting point B which is plane parallel to the atria (Fig. 9 A). Aortic root was embedded upright in the tissue block and gently squeezed to remove air bubbles inside the heart chamber. Tissue blocks were frozen on dry ice and kept at -80°C. The tissue was cryosectioned in the direction as the red arrow indicated. Serial 10 µm-thick cross-sections were collected on slides from the appearance of the aortic sinus until the fibrous ring was completely disappeared. The sections were kept at -80°C for future use.

For frozen aorta sections, the whole aorta with adjacent adipose tissue was isolated from the level above the coronary artery near the atria, onto the level below the iliac bifurcation

of the abdominal aorta. Then the aorta was separated into 4 parts[163] as indicated in Fig. 10: thorax-I - from the level of coronary artery, to the level of 7th rib that included the short ascending aorta, aortic arch with innominate artery, the right subclavian, the right common carotid, the left carotid, and the left subclavian arteries, and long descending thoracic aorta; thorax-II - from the level of 7th rib to the diaphragm level; abdomen-I - below the diaphragm to the middle of the abdominal aorta containing the celiac, the superior mesenteric, the right and left renal arteries; and abdomen-II - from the middle of the abdominal aorta to below the level of iliac bifurcation including the inferior mesenteric, and the common iliac arteries at the iliac bifurcation. The 4 parts were embedded into tissue block in the direction as indicated in Fig. 10. Tissue blocks were frozen on dry ice and kept at -80°C. The tissue was sectioned in the direction as red arrow indicated. Serial 10 µm-thick cross-sections were collected for future use.

For DRG, the whole spine was isolated from surrounded muscle, adipose tissue and connected organs. The last rib was kept for the identification of last pair of thoracic DRGs (T13 DRGs) which located in the intervertebral foramen under the last rib (Fig. 11 A and B). The spine was opened thorough the vertebrae adjacent to the SC which was slightly removed afterwards to expose the DRGs (Fig. 11 A). Thoracic DRGs were defined starting from T13 DRGs. Then T12, T11, T10 up to T1 DRGs were defined in the direction as indicated in Fig. 11 A (black arrow). Thoracic DRGs were divided into upper (T1-5) and lower (T6-13) segments. They were slightly pulled out with short axons using angled fine forceps and collected into two tubes filled with 4% PFA. DRGs were fixed with 4% PFA for 4 hours, then transferred to PBS solution for 1 hour to remove the PFA, followed by dehydration with 20% and 30% sucrose solution overnight (Fig. 11 C), then embedded into tissue block with Tissue Tec and stored at -80°C. DRGs were cryosectioned with serial 12 µm-thick cross-sections. All sections were collected and kept at -80°C until future use. The DRG area for quantification was defined as indicated in Fig. 11 D (red dashed line). NGs were treated in the same way as DRGs.

For DRG associated tertiary lymphoid clusters (DRG-TLCs), the whole spine was isolated from surrounded muscle, adipose tissue and connected organs. The last rib was kept for the identification of last pair of thoracic DRGs (T13 DRGs) which located in the intervertebral foramen under the last rib (Fig. 11 A). The spine was divided into the 3 parts: cervical and throracic T1-5 spine, throracic T6-13 spine, and lumbar spine. The three parts were

decalcified in 20% EDTA solution for one week with shaking at 4°C. The EDTA solution was changed twice a week until the spine was soft and peliable. Then the spine was washed three times with PBS, embededed into the tissue block, and kept at -80°C until future use.

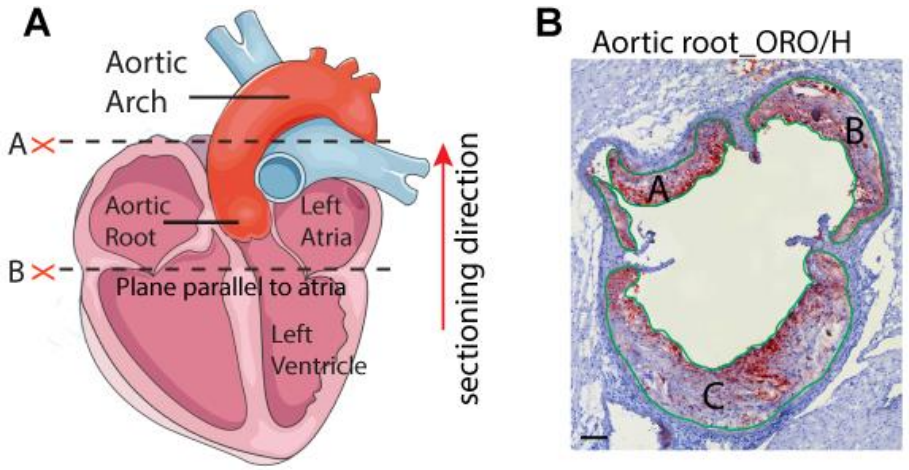

Figure 9. Schematic Presentation of the Heart. The schematic presentation (A) shows the structure of the heart including aortic arch, the atria, the ventricle. The two cutting points are marked with A at the base of heart and B plane parallel to the atria. The red arrow indicates the sectioning direction. (B) shows the morphometry of an Oil Red O/hematoxylin stained frozen cross-section of the aortic root. The plaque area between the three valves is marked as A, B and C (green line). Scale bar: 100 µm.

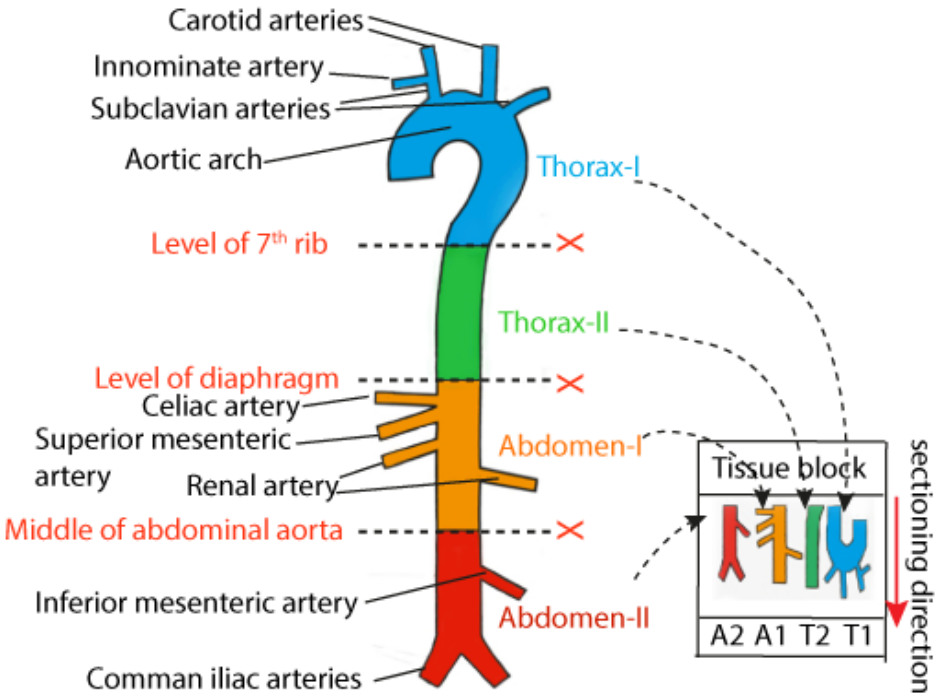

Figure 10. Schematic Presentation of the Aortic Tree. The schematic presentation includes the aortic arch,

the thoracic aorta, abdominal aorta and the main artery branches. The aorta is divided into 4 parts: thorax-I (T1), thorax-II (T2), abdomen-I (A1), abdomen-II (A2). The 3 cut points is marked with level of 7th rib, level of diaphragm, middle of abdominal aorta. The embedding direction in tissue block as indicated on the left. The red arrow indicates the section direction. (Figure adapted from refs [163])

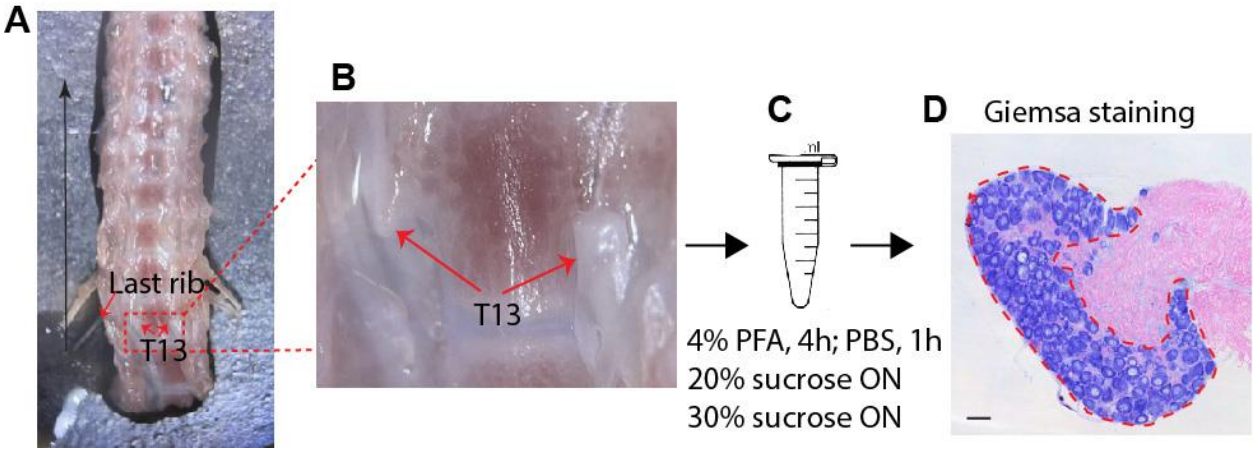

Figure 11. Schematic Presentation of DRG Preparation. The schematic presentation shows (A) the opened spine without SC, (A, B, red arrow) last rib and the last pair of thoracic DRGs-T13 DRGs. (A) Black arrow indicated the direction for thoracic DRGs identification. (C) shows the fixation of DRGs with 4% PFA for 4 h, 1 h PBS to remove PFA, followed with 20% and 30% sucrose solution ON for dehydration. (D) shows the Giemsa stained DRG frozen section. Red dashed line circles the DRG area for quantification. Scale bar: 50 µm. ON: overnight.

2.2.8 *En-face* Staining and Quantification in Atherosclerosis

For aorta *en-face* whole mount staining, the whole aorta was isolated as published before[163], all the perivascular adipose tissue was completely removed with fine scissors and forceps under the dissection microscope. The important branches including innominate artery, carotid artery and left subclavian artery of aortic arch were kept and other small branches were removed for better process afterwards. The whole aorta was fixed in 4% PFA for 1-2 hours for slight fixation, then the entire aorta was longitudinally split to expose the intimal surface following the sequence and direction indicated in Fig. 12 A. The aorta was gently pined to a flat black wax plate in a Y-shape as indicated in Fig. 12 B and fixed overnight (≥12h) with a 5% sucrose solution in 4% PFA at 4°C. The next day, the aorta was rinsed with PBS 3 x 10 min and 70% ethanol for 5 min. A Sudan-IV working solution was prepared one day before by completely dissolving 1 g Sudan-IV in a mixture of 100 ml acetone, 70 ml ethanol, and 30 ml distilled water. The whole aorta was immersed in Sudan-IV working solution for 10 min, washed twice in 70% ethanol and further rinsed in distilled water prior to imaging.

To determine the percentage of atherosclerotic lesion in aortic arch, thoracic aorta, abdominal aorta, images were taken with a digital camera (DSLR-a580, Sony) with a scale bar. All the analysis was manually quantified using Java-based image processing software Image J as indicated in Fig. 13 A and C. Aortic arch area was defined as the segment spanning from the aortic root to 3 mm below the subclavian artery branch; the thoracic aorta area as the segment from the level of the aortic arch up to the diaphragm; and the abdominal aorta area as the segment from the diaphragm until to iliac bifurcation . The atherosclerotic lesion area was determined as Sudan-IV positive area with intense red spots. All positive spots were double-checked under the microscope to avoid false results caused by unremoved adipose tissue from the adventitia (Fig. 12 C)[163]. All the selected areas were saved to the 'ROI Manager' for further analysis. The atherosclerotic lesion area was quantified as the percentage of Sudan-IV positive area per aortic vessel surface in the aortic arch, thoracic aorta and abdominal aorta segments. The total atherosclerotic lesion area was quantified as the sum of all analyzed aorta segments.

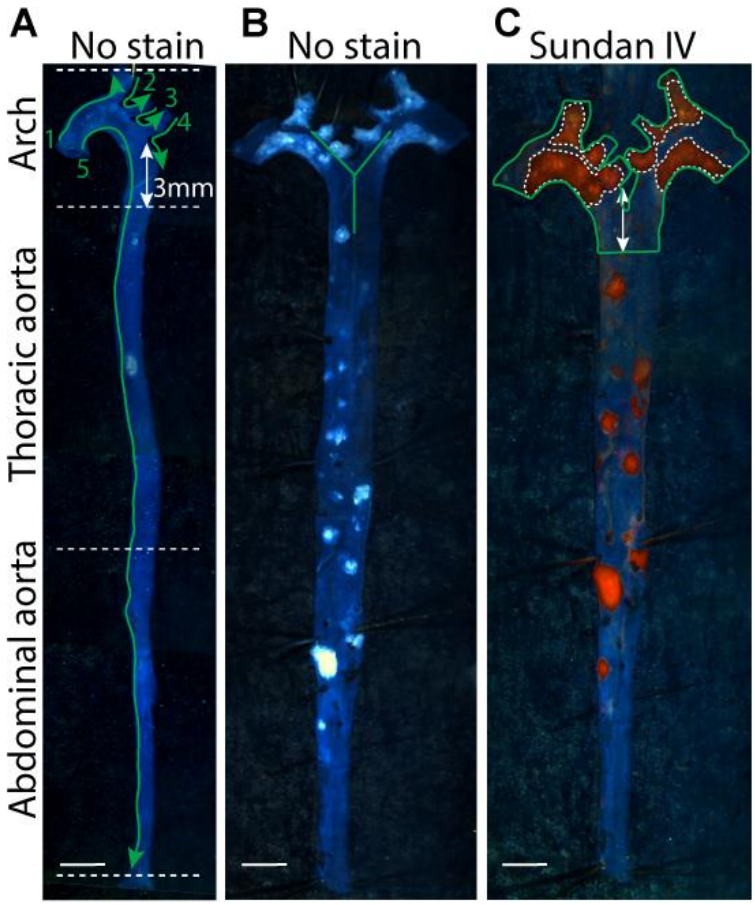

Figure 12. Dissection and Atherosclerosis Lesion Analysis of Whole Aorta. (**A**) shows the whole aorta including aortic arch, thoracic aorta, abdominal aorta after the removal of all the perivascular adipose tissue. (1) Open the aorta through the outer curve of innominate artery, (2) from innominate artery to left common carotid artery, (3) left common carotid artery to from left subclavian artery, (4) a short cut along the outer curve of left subclavian artery, (5) a longuinal cut along the inner curve of aorta. Double-arrow indicates the 3mm distance under left subclavian artery. (**B**) shows the pined Y-shape aorta before *en-face* staining. (**C**) shows the pined aorta after Sudan-IV staining. The aortic arch area is circled with green line based on the 3mm distance (double-arrow). Sudan-IV positive plaque area in aortic arch is circled with white dashed line. Scale bar: 0.2 cm. (Figure adapted from ref [163])

2.2.9 Histology

In all the histologic staining of aortic root and aorta, every 10th serial section was selected. Oil Red O/Hematoxylin (ORO/H) staining was used for plaque size analysis: sections were fixed with 4% PFA for 10 min, followed by 10 min wash in PBS, then stained with Oil Red O working solution for 10 min, briefly washed in 60% isopropanol, followed by 6 min staining with hematoxylin, and rinsed thoroughly in tap water (pH > 7) for 10 min for bluing. The sections were mounted with an aqueous Faramount Mounting Medium. Hematoxylin/Eosin (HE) staining was applied for the analysis of necrotic core and fibrous cap: sections were fixed with 4% PFA for 10 min, rinsed with PBS for 10 min, followed by 6 min staining with hematoxylin, and rinsed thoroughly in tap water (pH > 7) for 10 min, then stained with eosin working solution for 10 min and rinsed with absolute ethanol for 30 seconds. The sections were air-dried and mounted with Roti-Histokit II. Sirius Red staining was used for collagen analysis: sections were fixed with 4% PFA for 5 min, rinsed with PBS for 10 min, then stained with Sirius-red solution for 1h, then washed twice with 0.5% acidified water, three times with 100% Ethanol, and twice with 100% Xylene. The sections were air-dried and mounted with Roti-Histokit II.

In all the histologic staining of DRGs, every 10th serial section was selected. Giemsa staining was used for mast cell analysis: sections were fixed with 100% methanol for 10 min, air dried for 15 min, then stained with Giemsa solution for 30 min, and rinsed thoroughly in tap water (pH > 7) for 20 min. Then sections were air dried for 15 min and mounted with Roti-Histokit II.

All images were taken with a bright field microscope (Leica DM6000B, Leica Microsystems) or a Thunder microscope (Leica DM6 B, Leica Microsystems). All images were taken with a

10x objective.

2.2.10 Immunofluorescence Staining

Frozen sections were quickly thawed on a hot plate at 37˚C for one minute and then air dried for 30 min. Freshly embedded sections were fixed with 4% PFA or with 4% PFA-acetone combination, then rehydrated with PBS at RT for 10 min. 4% PFA-sucrose pretreated sections (as described in 2.2.7) were directly rehydrated with PBS at RT for 10 min and blocked for 60 min and incubated with primary antibody for overnight (>10 hours). For the membrane protein antibodies, sections were blocked with 2.5% bovine serum albumin in PBS; for intranuclear and intracelluar protein antibodies, sections were blocked with 2.5% bovine serum albumin 5% NES in triton X-100 in PBS for blocking and permeabilization. Primary antibodies were diluted in the same solution with blocking solution and incubated for overnight. The information for each primary antibody is listed in table 4. Then primary antibody was removed. Slides were washed with PBS 5 min/3 times and incubated with secondary antibody and DAPI diluted in 2.5% bovine serum albumin in PBS for 1 hour. For neuronal cells staining, NeuN was added into the secondary antibody for the neuronal nuclei staining. The information for each secondary antibody is listed in table 5. Following 3 times washing in PBS for 5 min, slides were mounted in Flouromount-G mounting media and kept at 4°C until imaging. For negative controls, the immunostaining procedure was routinely used but without antibodies in the primary antibody incubation solution.

2.2.11 Image Analysis and Processing

image processing was performed with ImageJ (NIH, USA). For immunofluorescence stained images, only brightness and contrast adjustion were applied to the whole frame, and no particular part of the frame was modified in any way. For the area selection, all the procedures were saved as ROI for the experiment record. For automatic neuronal cell counting, analyzed particles were used with threshold setting and watershed separation and the procedures were saved as Macro for the further application and experiment record.

2.2.12 Morphometry

2.2.12.1 Morphometry of Atherosclerosis Lesion in Aortic Root and Aorta

For the atherosclerotic lesion in aortic root, every 10th serial aortic root cross section was

selected for ORO/H staining. Image were taken under 10X objective. The plaque area of each valve was manually encircled by ImageJ and recorded as valve A, valve B and valve C (Fig. 9 B). Usually, the plaque area of first section is too small to quantify, so the first section for analysis was at a distance of 100 μm from the aortic sinus. For the plaque area of one valve, such as valve A, every 10th serial section was recorded as valve A1, A2, A3 and so on. Accordingly, the plaque area for valve B was recorded as B1, B2, B3 and so on. So was valve C. The plaque area was analyzed in two ways: total area and distance area. The total area was the average area of $SUM_{valve\ A}$+ $SUM_{valve\ B}$ + $SUM_{valve\ C}$. The distance area at 100 μm was defined as the average area of (valve A1) + (valve B1)+ (valve C1), 200 μm was defined as the average area of (valve A2) + (valve B2)+ (valve C2), and so on.

For the atherosclerotic lesion analysis in aorta, the sections between renal arteries from abdomen-I (Fig. 10) were selected for ORO/H staining. The images were taken under 10X objective of LEICA DFC9000 GT. ImageJ was used to manually encircle the lumen border, the internal elastic lamina (IEL) and the external elastic lamina (EEL) of arterial media (Fig. 13). The intima area was measured by subtracting IEL area from lumen area and media area by subtracting EEL area from IEL area. The plaque size was calculated as ration of the intima area versus media area: Equation: intima/media ratio = intima area (IEL-lumen area)/ media area (EEL-IEL area)[163].

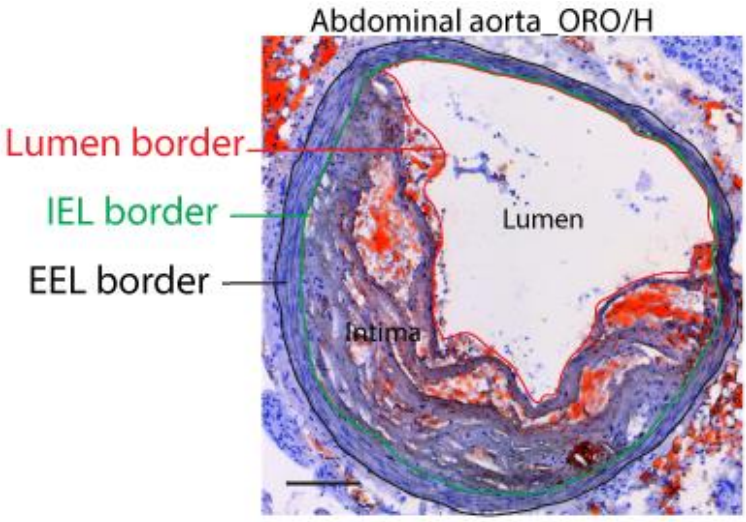

Figure 13. Atherosclerosis Lesion Analysis of Aorta. Schematic presentation shows the border of lumen area, internal elastic lamina (IEL) and external elastic lamina (EEL) area for morphometric analysis of ORO/H -stained abdominal aorta. (Figure adapted from ref [163])

2.2.12.2 Morphometry of Axon Density

Every 10th section from aortic root and/or aorta was selected for the axon density analysis. The *Apoe*$^{-/-}$ no plaque, *Apoe*$^{-/-}$ with plaque with or without ATLO are sections from different segments of aortic root or aorta of one mouse. Images were taken by confocal (True Confocal Scanner-SP8, Leica Microsystems) or Thunder microscope (Leica DM6 B, Leica Microsystems) under 20X objective. The number of specific subpopulations of fibers was calculated manually through ImageJ according to length (≥5 μm). Axon density was quantified as the number of axons within the aortic adventitia.

2.2.12.3 Morphometry of Neuronal Cells and Immune Cells in Peripheral Ganglia

For quantification of neuronal cells, every 10th DRG and/or NG sections were stained with neuronal markers TRPV1, CGRP, IB4 and TH. NeuN was co-stained as a neuronal nuclei marker. The number of each neuronal subpopulation was quantified automatically by imageJ, except for IB4^{+} neurons which were done manually. Neuronal cells were quantified as a percentage of the number of subpopulations versus the number of NeuN^{+} cells.

For immune cell infiltration, every 10th DRG and/or NG section was stained with macrophages (CD68), T cells (CD3e), and mast cells (Giemsa stain). Macrophage density was quantified as a percentage of macrophage area in the DRG area. The density of T cells and mast cells was quantified as the number per DRG area (per mm^2).

All DRG and/or NG sections were obtained from 4-7 adult or aged WT and *Apoe*$^{-/-}$ mice. A minimum of 10 sections from T1-5 and T6-13 DRGs were used per mouse, and 6-8 NG sections were used per mouse.

2.2.13 Lesion Stages

As shown in Fig. 14[23,31], plaques were classified into 3 stages according to the progression of atherosclerosis. Intimal xanthomas or fatty streaks represent an accumulation of foam cells without a fibrous cap and a necrotic core. Intimal xanthomas do not always progess into the next stage and are considered regressive[23]. Early pathological intimal thickening (PIT) contains a lipid pool, a thick or thin fibrous cap, but without a necrotic core. Advanced PIT can progress to fibroatheroma which is charcacterized with a fibrous cap, a necrotic core, and large calcification granules. Intimal xanthoma and PIT are classified as early

atherosclerosis. Fibroatheroma is classified as advanced atherosclerosis.

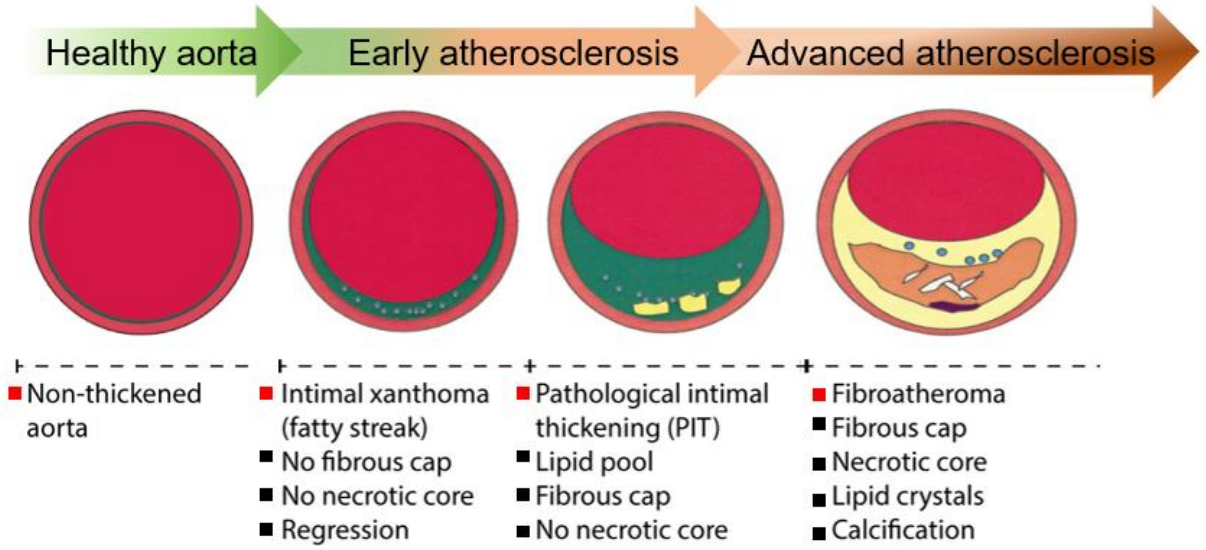

Figure 14. Progression of Atherosclerosis. Schematic presentation shows the lesion characteristics of atherosclerosis. Early atherosclerosis is in the progression from intimal xanthomas to early PIT. Advanced atherosclerosis is in the progression from advanced PIT to fibroatheroma. Intimal xanthoma is regressive and has no fibrous cap and necrotic core; early PIT contains a lipid pool and a fibrous cap but no necrotic core; advanced PIT and fibroatheroma contain both a fibrous cap and a necrotic core, as well as lipid crystals and calcified granules. (Figure adapted from refs [23,31])

2.2.14 Flow Cytometry

2.2.14.1 Preparation of Single Cell Suspensions of Blood and Spleen

Blood was collected by cardiac puncture with a 1 ml syringe, immediately transferred to a 15 ml Falcon tube containing 5 ml ice-cold EDTA, and shaken gently upside down to avoid blood clotting. The blood was centrifuged at 400 g/5 min and the supernatant was carefully discarded. The pellet was resuspended in 8 ml ACK lysis buffer and incubated at RT for 5 min to lyse red blood cells. An additional 5 ml FACS buffer was added to stop the lysis. The sample was centrifuged at 400 g/5 min at 4°C. The supernatant was carefully discarded. The pellet was resuspended with 200 µl ice-cold FACS buffer and transferred to 96-well plate for staining.

Spleen was collected into a 1.5 ml Eppendorf tube and cut into small pieces with fine Bonn scissors. The sample was transferred to a 70 µm cell strainer placed on a 50 ml falcon tube and mashed softly with a syringe-piston. The cell suspension was flushed into the 50 ml tube by intermittent addition of FACS buffer, then centrifuged at 400 g/5 min and the

supernatant was carefully discarded. The pellet was resuspended in 8 ml ACK lysis buffer and incubated for 5 min at RT to lyse red blood cells. An additional 5 ml FACS buffer was added and centrifuged at 400 g/5 min at 4°C. The supernatant was carefully discarded and the pellet was resuspended again with 5 ml ice-cold FACS buffer. The cell suspension solution was filtered into a 15 ml falcon tube with 50 µm strainer and centrifuged again. The pellet was resuspended in 1 ml FACS buffer and 200 µl was transferred to 96-well plate for staining.

2.2.14.2 Preparation of single cell suspensions of LNs

LNs were collected into 1.5 ml Eppendorf tubes containing FACS buffer and cut into small pieces with fine Bonn scissors. The sample was transferred to a 70 µm cell strainer placed on a 50 ml falcon tube and softly mashed with a syringe-piston. The cell suspension was flushed into the 50 ml tube by intermittent addition of FACS buffer and centrifuged at 400 g/5 min. The supernatant was carefully discarded. The pellet was resuspended with 200 µl ice-cold FACS buffer and transferred to 96-well plate for staining.

2.2.14.3 Preparation of single cell suspensions of bone marrow

Two femurs were isolated from the distal metaphysis and the connected muscle. Both sides of the femurs were cut and placed the left parts into an 1.5 ml Eppendorf tube. The bone marrow was collected by centrifuging at 5000rpm/5 min at 4°C. The sample was resuspended with 1 ml ice-cold FACS buffer and an aliquote of 150 µl transferred to a 96-well plate for staining.

2.2.14.4 Antibody staining for FACS

The 96-well plate was centrifuged at 400 g/5 min. The supernatant was carefully discarded. The pellet was resuspended with 100 µl fixable viability dye solution (1:1000, in DPBS) for 20 min to stain dead cells. 200 µl FACS buffer was added to each well to and the plate was centrifuged twice at 400 g/5 min. The pellet was resuspended with 60 µl Fc blocker CD16/32 (1:200, in FACS buffer) and incubated for 10 min. Then 60 µl antibody cocktail (in FACS buffer) was added and incubated for another 30 min in the dark for the extracellular staining. After incubation, 200 µl FACS buffer was added added to each well. The plate was centrifuged at 400 g/5 min twice and the supernatant was carefully discarded. The pellet was resuspended with 200 µl freshly prepared fixation/permeabilization working solution (1 part fixation/permeabilization concentrate buffer was mixed with 3 parts fixation/

permeabilization dilute buffer), incubated for 40 min at 4°C, then centrifuged at 400 g/5 min. The supernatant was carefully discarded. The pellet was resuspendd with 200 µl permeabilization buffer (which was prepared from 10× permeabilization buffer stock diluted in sterile water) and centrifuged at 400 g/5 min. The supernatant was carefully discarded. The pellet was resuspended with 60 µl anti-mouse Foxp3 solution (1:200, in FACS buffer) and incubated for 50 min for the intracellular staining. The plate was centrifuged and washed twice with FACS buffer. Finally, the pellet was resuspended with 250 µl FACS buffer and transferred to FACS tubes for FACS analysis.

Single cells from blood and LNs were divided into two groups. Single cells from spleen were divided into three groups. One group was stained for lymphoid cells with antibodies against CD45, B220, TCRβ, CD4, CD8, Foxp3, CD44, CD62L. Lymphoid cell populations were defined as follows: B cells ($CD45^+TCR\beta^-B220^+$), CD4 T cells ($CD45^+TCR\beta^+B220^-CD8^-CD4^+$), CD8 T cells ($CD45^+TCR\beta^+B220^-CD8^+CD4^-$), T_{reg} cells ($CD45^+TCR\beta^+B220^-CD8^-CD4^+Foxp3^+$), naïve T cells ($CD45^+TCR\beta^+B220^-CD8^-CD4^+CD44^-CD62L^+$), effector memory T cells ($CD45^+TCR\beta^+B220^-CD8^-CD4^+CD44^+CD62L^-$), central memory T cells ($CD45^+TCR\beta^+B220^-CD8^-CD4^+CD44^+CD62L^+$).

One group was stained for myeloid cells with antibodies against CD45, CD11c, CD11b, F4/80, MHC-II, SiglecH, CD86, CD206, CD103. Myeloid cell populations were defined as follows[29,164-166]: plasmacytoid DCs ($CD45^+CD11c^+$MHC-$II^+SiglecH^+$), mature DCs ($CD45^+CD11c^+$MHC-$II^+SiglecH^-CD86^+$), DC1s ($CD45^+CD11c^+$MHC-$II^+SiglecH^-CD86^-CD103^+CD11b^-$), DC2s ($CD45^+CD11c^+$MHC-$II^+SiglecH^-CD86^-CD103^-CD11b^+$), macrophages ($CD45^+CD11b^+F4/80^+$), M1-like proinflammatory macrophages ($CD45^+CD11b^+F4/80^+CD86^+CD206^-$), M2-like anti-inflammatory marcophages ($CD45^+CD11b^+F4/80^+CD86^-CD206^+$).

Bone marrow and one group of splenocytes were stained for progenitors with antibodies against TER-119, Gr1, B220, CD3, CD11b, CD150, CD34, CD48, CD16/32, c-kit, Sca1. Hematopoietic cell populations were defined as follows: LSK ($Lin^-c\text{-}Kit^+Sca\text{-}1^+$), common myeloid progenitor ($Lin^-c\text{-}kit^+sca\text{-}1^-CD34^+CD16/32^-$), myeloid progenitor cells ($Lin^-c\text{-}kit^+sca\text{-}1^-$), hematopoietic stem cells ($Lin^-c\text{-}kit^+Sca\text{-}1^+CD48^-CD150^+$), granulocyte-monocyte progenitor cells ($Lin^-c\text{-}kit^+Sca\text{-}1^-CD34^+CD16/32^+$), and common lymphoid progenitors ($Lin^-c\text{-}kit^{low}Sca\text{-}1^{low}CD127^+$).

Splenocytes and compensation beads (Thermo Fisher) were used as single staining controls for lymphoid cells and myeloid cells; bone marrow and compensation beads (Thermo Fisher) were used as single staining controls for myeloid progenitor cells. Counting beads were added prior to running the samples for calculating the absolute cell numbers of single cell suspensions.

2.2.15 Laser capture microdissection (LCM) and microarray analyses

Aorta tissue messenger RNA (mRNA) microarray analyses were performed as previously reported with minor modifications[37,167]. Total aortas of 3 WT and 3 *Apoe*$^{-/-}$ mice aged at 6, 32, and 78 wks and LCM-derived arterial wall compartments of 3 WT adventitia and 4 *Apoe*$^{-/-}$ without plaque and 4 ATLO at 78 weeks were extracted. In this thesis, the CEL files were freshly analyzed for SPNS-related genes, including neuron projection, axon guidance, sensory perception and ion channel activity. Arrays were scaled to trimmed mean of 200. All further steps were performed using R and Bioconductor. A correction procedure was performed to correct media effects in LCM experiments on adventitia (RME ≤ 0.666). Genes with low expression or without variability between 2 groups were filtered and removed before statistical analysis. Statictic analyze was done under a one-way analysis of variance (ANOVA) with Benjamini and Hochberg correction for multiple testing ($P \leq 0.05$). The resulting total lists of differentially expressed (DE) probe sets ($P \leq 0.05$) were used for derived lists of GO terms.

2.2.16 Statistical Analyses

All data were expressed as means per mouse ± standard error of the mean (mean ± SEM). Statistical differences were analyzed with two-sided unpaired Student's t-test or one-way ANOVA using GraphPad Prism 9 (GraphPad Software, San Diego). Welch's correction for Student's t-test and Bonferroni's post-hoc correction for ANOVA were applied. $P < 0.05$ were regarded as statistically significant.

3 RESULTS

3.1 Association of Atherosclerosis with the SPNS in Adult Mice

Previous data from our group demonstrated that the arterial wall of aged WT mice is innervated by nerve fibers derived from the sympathetic perivascular ganglia and sensory DRGs[38]. NF200$^+$ axons including CGRP-expressing sensory axons were present in the aged aorta adventitia, but not in the aorta media. In advanced atherosclerosis, NF200$^+$ axon density significantly increased in ATLOs of aged *Apoe*$^{-/-}$ mice compared to WT mice and a significant fraction of the NF200$^+$ axons were CGRP$^+$ sensory axons. These findings indicated a potential crosstalk between the SPNS and diseased artery segments.

3.1.1 Association of Atherosclerosis with Sensory Innervation in Aortic Root

To reveal the sensory innervation patterns in adult mice, every 10th serial aortic root sections from ~ 32 wks old WT and *Apoe*$^{-/-}$ mice were analyzed using neurofilament medium (NFM) as pan-neuronal marker, TRPV1 as nociceptive sensory neuron maker and CGRP as peptidergic sensory neuron marker as described in Methods.

In the adventitia of aortic root, TRPV1$^+$ axon density tended to be 2-fold higher in adult *Apoe*$^{-/-}$ mice without adjacent plaques (197.0 ± 70.88, Fig. 15 B) compared to WT mice (89.00 ± 38.18, Fig. 15 A) but these measurements did not reach significance. However, they were strikingly (> 8-fold) higher when the aortic root was burdened with heavy plaques (714.3 ± 95.41, Fig. 15 C). CGRP$^+$ axon density in aorta segments of *Apoe*$^{-/-}$ mice without adjacent plaques (56.67 ± 40.04, Fig. 16 B) was close to WT mice (94.75 ± 21.88, Fig. 16 A) without reaching significance. However, when the aortic root was burdened with plaque, the density was significantly higher (> 8-fold, 490.40 ± 36.42, Fig. 16 C) compared to WT mice. These data indicated that atherosclerosis affects the SPNS and triggers highly localized axon sprouting events of sensory neurons in the adventitia of adult aortic root.

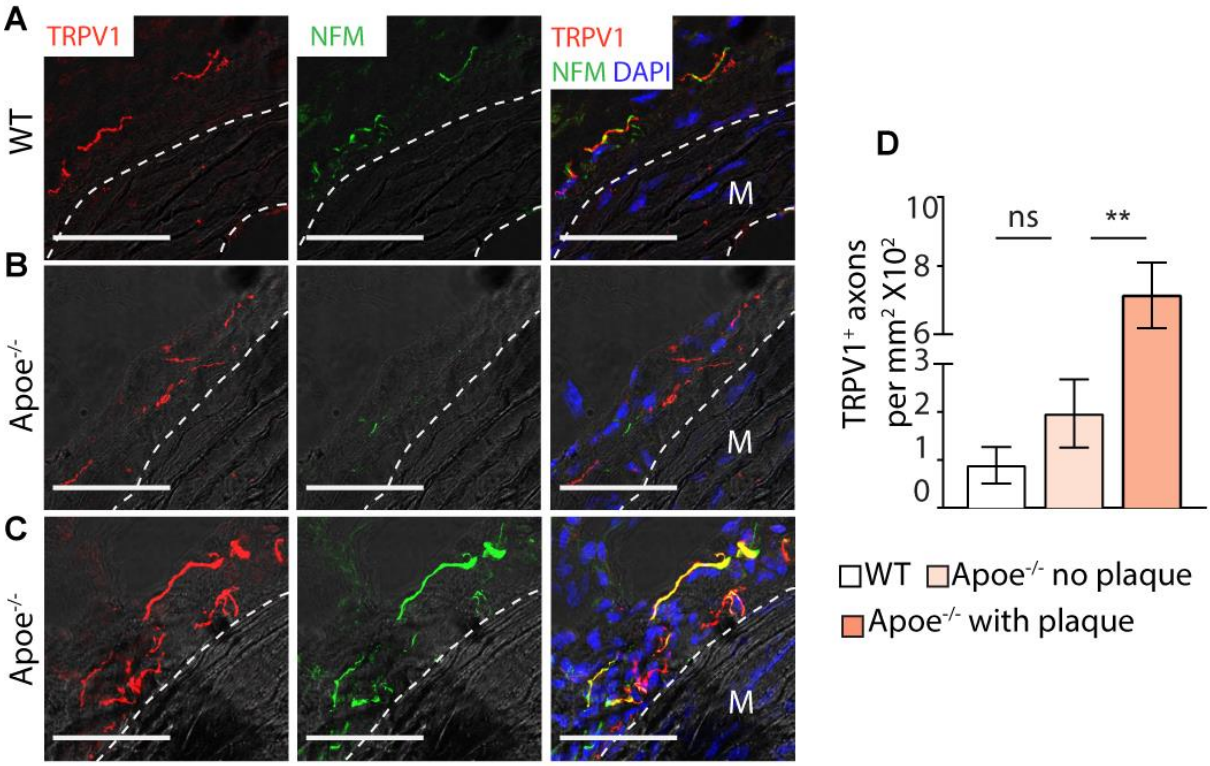

Figure 15. TRPV1-expressing Sensory Axons in the Aortic Root of Adult WT and *Apoe*$^{-/-}$ Mice. Representative confocal images for TRPV1^{+} axons (red) in the adventitia of aortic roots from adult WT mice (A), *Apoe*$^{-/-}$ aortic segments without plaque (B), *Apoe*$^{-/-}$ aortic segments with plaque (C). The media (M) is marked by dashed lines. (D) Axon density was quantified as the number of TRPV1^{+} axons (> 5 μm in length) from the adventitia area (per mm^2). WT = 3, *Apoe*$^{-/-}$ aortic segments without plaque = 3, *Apoe*$^{-/-}$ aortic segments with plaque = 6. A minimum of 3 sections per mouse were used for the analyses. Ordinary one-way ANOVA; data represent means per mouse ± SEM; ns, not significant. **P < 0.01. M: media. Scale bar: 50 μm.

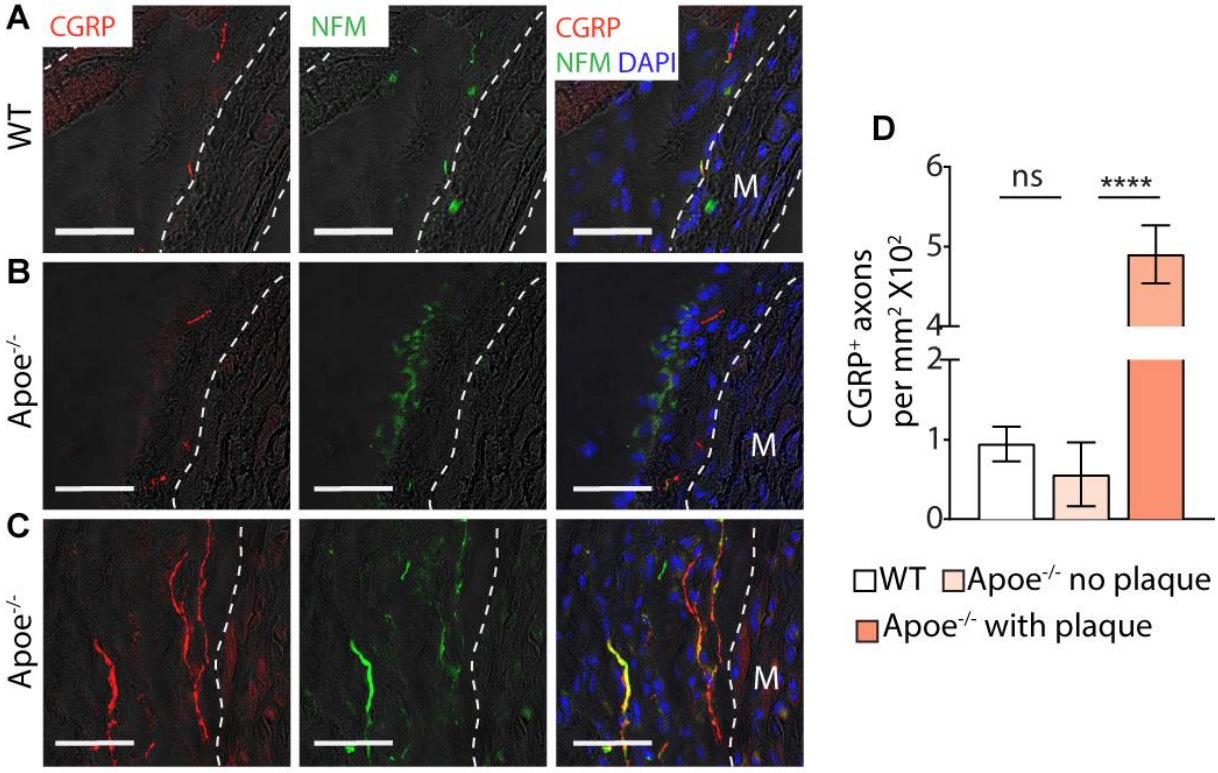

Figure 16. CGRP Sensory Axons in the Adventitia of the Aortic Root in Adult WT and *Apoe*$^{-/-}$ Mice. Representative confocal images for CGRP axons (red) in the adventitia of aortic roots from adult WT mice (A), *Apoe*$^{-/-}$ aortic segments without plaque (B), *Apoe*$^{-/-}$ aortic segments with plaque (C). The media (M) is marked by dashed lines. (D) Axon density was quantified as the number of CGRP^{+} axons (> 5 μm) of the adventitia area (per mm^2). WT = 3, *Apoe*$^{-/-}$ segments without plaque = 3, *Apoe*$^{-/-}$ segments without plaque = 6. A minimum of 3 sections per mouse were used for the analyses. . Ordinary one-way ANOVA; data represent means per mouse ± SEM; ns, not significant. ****P < 0.0001. Scale bar: 50 μm.

3.1.2 Neuronal Subpopulations of Peripheral Sensory Ganglia in Atherosclerosis

Since we have found increased density of TRPV1^{+} and CGRP^{+} sensory axons in the adventitia of the aortic root in adult *Apoe*$^{-/-}$ mice versus WT mice, we asked whether atherosclerosis is associated with alterations of the number of specific sensory neuronal sutypes in the peripheral sensory ganglia. To answer this question, the NG and thoracic DRGs were collected from both WT and *Apoe*$^{-/-}$ mice at 32-34 wks as described in Methods. DRGs were divided into an upper segment T1-5 and a lower segment T6-13. The ganglia were sectioned at a thickness of 12 μm for IF staining. TRPV1 antibody were used as a nociceptive sensory neuron marker (Fig. 17 and 18 A), CGRP antibody as a peptidergic sensory neuron marker (Fig. 17 and 18 B), IB4 antibody as a non-peptidergic sensory neuron marker (Fig. 17 and 18 C), tyrosine hydroxylase (TH) antibody as a type C low-threshold mechanoreceptor marker (Fig. 17 and 18 D), NeuN as a pan-neuronal marker and

DAPI to stain nuclei. For quantification of specific neurons, data were expressed as the percentage of marker-positive cells versus $NeuN^+$ cells. A minimum of 10 sections per mouse for DRGs and 5 sections per mouse for NGs were used for the quantification of each subpopulation.

In the DRGs of WT or *Apoe*$^{-/-}$ mice, there was no significant difference in the distribution of neuronal subpopulations between the upper and the lower segments (Fig. 17). We also did not observe significant differences between WT and *Apoe*$^{-/-}$ mice in the same segments. In NG, we also did not find significant differences between WT and *Apoe*$^{-/-}$ mice (Fig. 18). The increased density of $TRPV1^+$ and $CGRP^+$ sensory nerve axons despite unchanged distribution of neuronal subpopulations suggested that atherosclerosis affects the-terminals and localized sprouting events of sensory neurons in the adventitia of aortic root but not the distribution of neuronal cell bodies in DRGs and NGs.

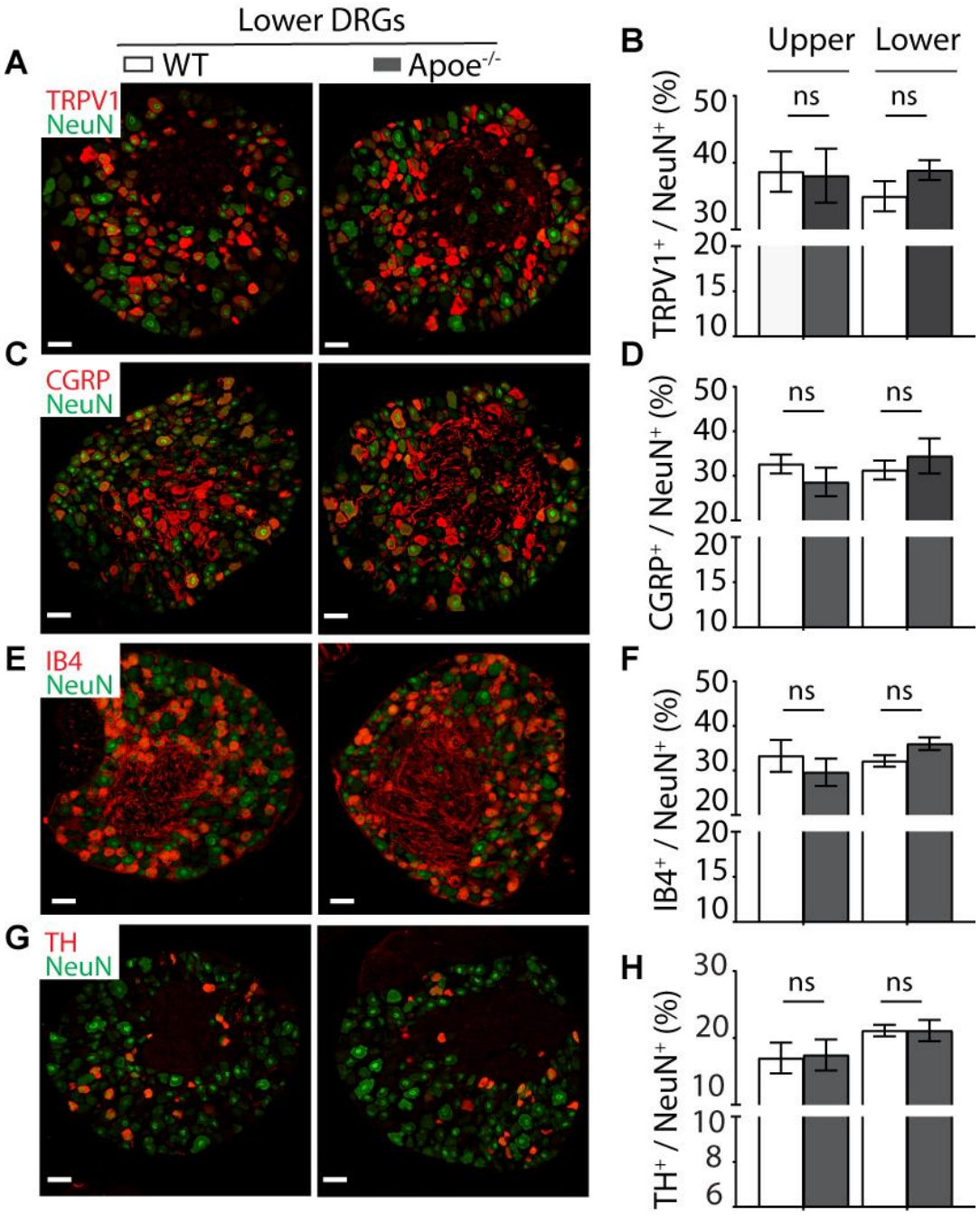

Figure 17. Subpopulations of Sensory Neurons in Thoracic DRGs of Adult WT and *Apoe*$^{-/-}$ Mice. Representative confocal images of the lower thoracic DRGs from adult WT and *Apoe*$^{-/-}$ mice. (A) TRPV1 designates the nociceptive sensory neuron marker (red); (C) CGRP designates the peptidergic sensory neuron marker (red); (E) IB4 designates the non-peptidergic sensory neuron marker (red); (G) TH designates the type C low-threshold mechanoreceptor marker (red); NeuN designates the pan-neuronal marker to stain all neurons (green). (B, D, F, H) Results were quantified as the percentage of the number of TRPV1^{+} neurons (WT = 6-8, *Apoe*$^{-/-}$ = 3-4), CGRP^{+} neurons (WT = 5-6, *Apoe*$^{-/-}$ = 5-6), IB4^{+} neurons (WT = 5, *Apoe*$^{-/-}$ = 5-7) or TH^{+} neurons (WT = 5, *Apoe*$^{-/-}$ = 5) among NeuN^{+} neurons. A minimum of 6 sections for the upper DRGs and 10 sections for the lower DRGs per mouse were used. Two-tailed unpaired Student´s t-test; data represent means per mouse ± SEM; ns, not significant. Scale bar: 50 µm.

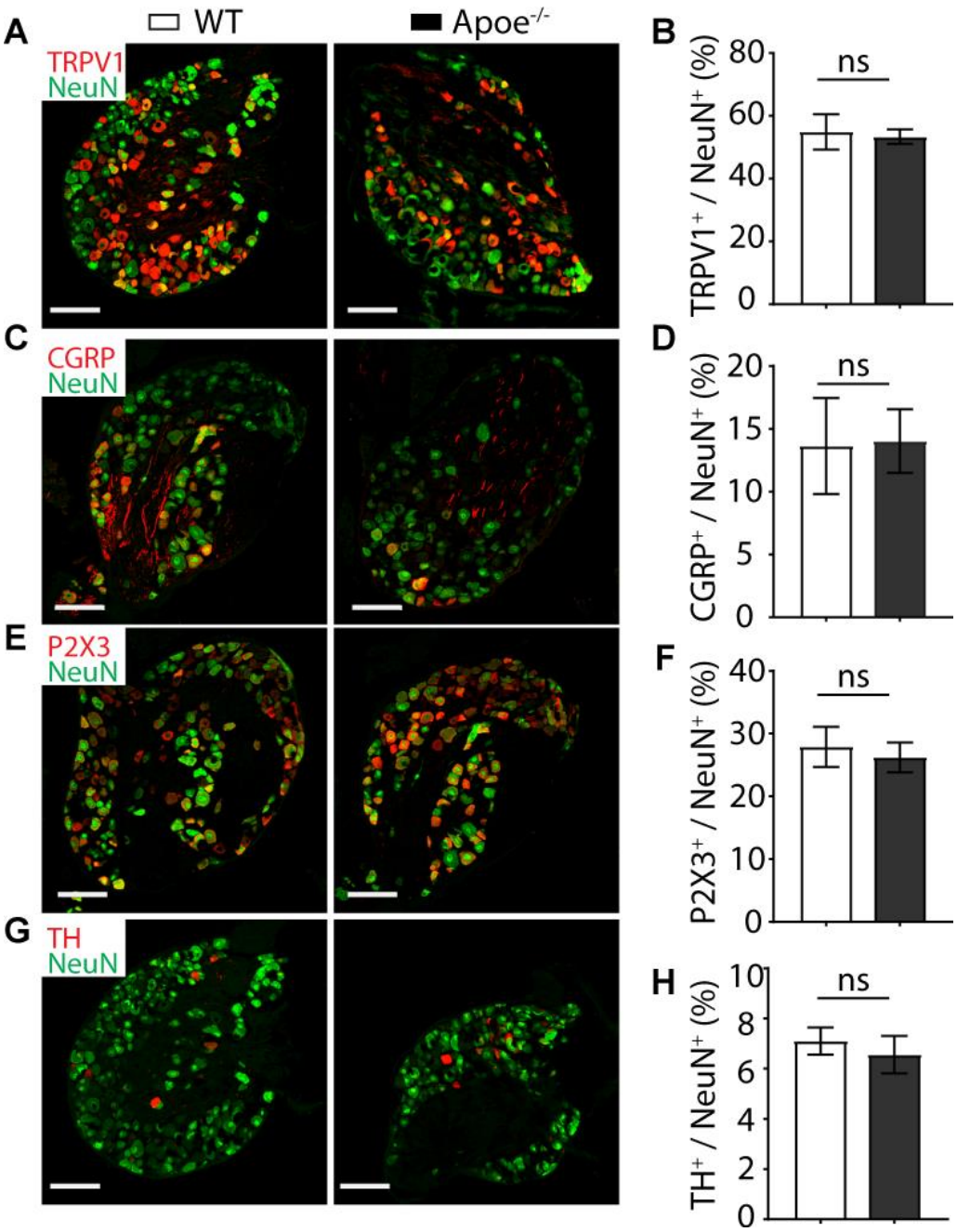

Figure 18. Subpopulations of Neurons in NGs of Adult WT and *Apoe*$^{-/-}$ Mice. Representative confocal images of the NGs from adult WT and *Apoe*$^{-/-}$ mice. (A) TRPV1 designates the nociceptive sensory neuron marker (red); (C) CGRP designates the peptidergic sensory neuron marker (red); (E) P2X3 designates the non-peptidergic sensory neuron marker (red); (G) TH designates the type C low-threshold mechanoreceptor marker (red); NeuN designates the pan-neuronal marker to stain neurons (green). (B, D, F, H) Results were quantified as the percentage of the number of TRPV1^{+} neurons, CGRP^{+} neurons, P2X3^{+} neurons or TH^{+} neurons among NeuN^{+} neurons. 3 mice from both WT and *Apoe*$^{-/-}$ mice, a minimum of 6 sections per mouse were used for the analyses. Scale bar: 50µm. Two-tailed unpaired Student´s t-test; data represent means per mouse ± SEM; ns, not significant.

3.1.3 Association of Atherosclerosis with Immune Cell Infiltration in the Peripheral Sensory Ganglia

The SPNS harbors two main types of ganglia: DRGs and NGs[49,52,168]. SPNS ganglia not only contain neurons but also non-neuronal cells including tissue macrophages, mast cells and T cells. We observed increased TRPV1$^+$ and CGRP$^+$ sensory axon networks in the adventitia of the aortic root and the abdominal aorta during atherosclerosis, as well as atherosclerosis-dependent TLO neogenesis in paraaortic ganglia and enhanced expression of immune-modulating genes in paraaortic ganglia in advanced atherosclerosis[38]. This data raised the question whether atherosclerosis is also associated with enhanced immune cells in peripheral sensory ganglia. To answer this question, innate immune cells, including CD68$^+$ macrophages / monocytes and Giemsa$^+$ mast cells; and adaptive immune cells, including CD3e$^+$ T cells were initially examined in the thoracic DRGs and NGs of adult WT and *Apoe*$^{-/-}$ mice. We found that macrophages were evenly distributed in DRGs, only sporadic T cells and mast cells were found in adult WT and *Apoe*$^{-/-}$ mice.

In the DRGs of adult WT mice (Fig. 19), the immune cell density showed a significant difference between the upper and lower segments. In particular, macrophages / monocytes showed a preference in the upper segment being >2-fold higher (0.42 ± 0.01) compared to the lower segment (0.17 ± 0.03) (Fig. 19 A and B). In contrast, both T cells and mast cells showed a preference in the lower segment: T cells were approximately 2-fold higher (4.22 ± 0.78) in the lower segment compared to the upper segment (1.91 ± 0.30) (Fig. 19 C and D), and mast cells were > 3-fold higher (5.00 ± 1.33) in the lower segment compared to the upper segment (1.41 ± 0.76) (Fig. 19 E and F). These data suggested that: I) the immune cell composition in thoracic DRGs differs between segments in adult WT mice; II) macrophages / monocytes are evenly distributed in thoracic DRGs and are more numerous in the upper segments in adult WT mice; III) both T cells and mast cells are rare in thoracic DRGs of adult WT mice, but preferentially present in the lower segments.

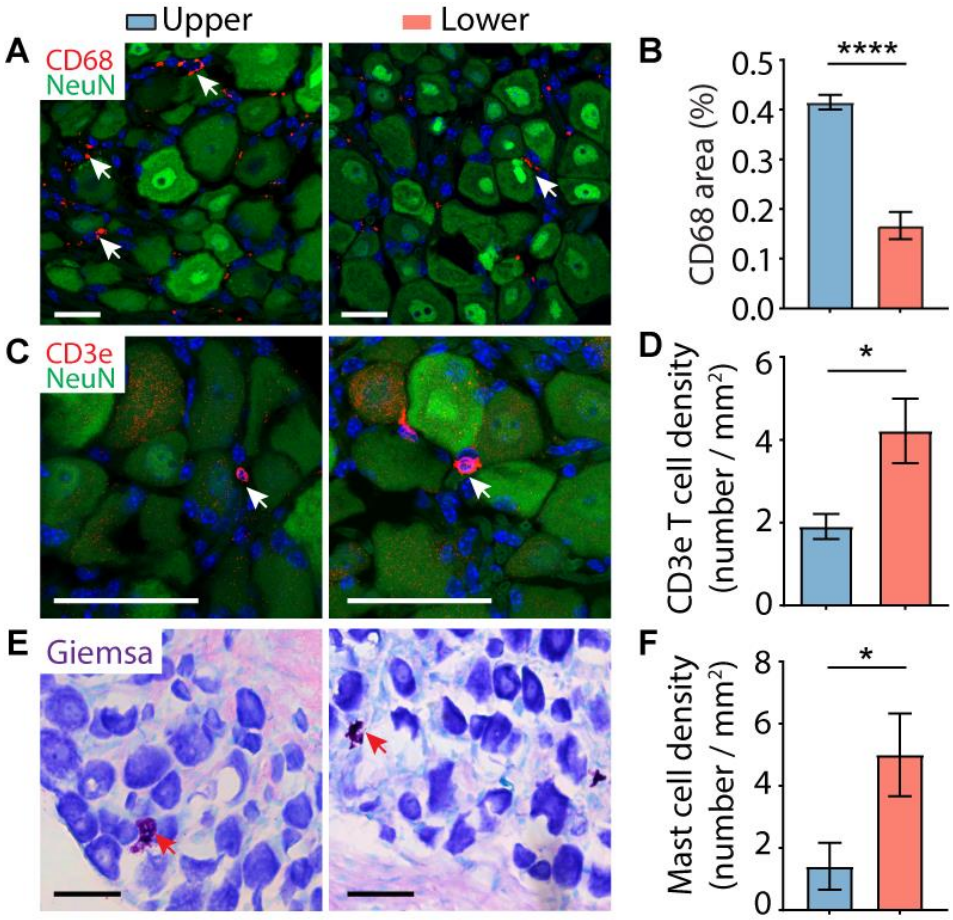

Figure 19. Immune Cells in Thoracic DRGs of Adult WT Mice. Representative confocal images show immune cells in the upper and lower thoracic DRGs of adult WT mice. (A) CD68 designates macrophage / monocytes (red, arrow). (C) CD3e designates T cells (red, arrow). NeuN designates neurons (green). (E) Giemsa staining designates mast cells, red arrows indicate mast cells. (B, D, F) Quantification: Macrophages / monocytes were quantified as the percentage of $CD68^+$ area per DRG area (B); T cells and mast cells were quantified as the density of $CD3e^+$ or $Giemsa^+$ cells per DRG area (mm^2) (D, F). 5-8 adult WT mice, a minimum of 6 sections for the upper DRGs and 10 sections for the lower DRGs per mouse were used for the analyses. Two-tailed unpaired Student´s t-test; data represent means per mouse ± SEM; *P < 0.05, ****P < 0.0001. Scale bar: 50 µm. upper: T1-5 DRGs; lower: T6-13 DRGs.

In the DRGs of adult *Apoe*$^{-/-}$ mice (Fig. 20), as in WT mice, the macrophages were evenly distributed. Both T cells and mast cells were rarely observed and randomly distributed across the soma. Mast cell content was 2-fold higher in the lower segment (14.00 ± 1.70) compared to the upper segment (7.00 ± 2.36) (Fig. 20 F). The difference in the distributoion of T cells and macrophages / monocytes between two segments did not reach significance (Fig. 20 B and D). To further examine the association of atherosclerosis and immune cells in thoracic DRGs, we analyzed the density of macrophages/monocytes, T cells and mast cells in adult WT versus *Apoe*$^{-/-}$ mice. When considering the mean values, the density of

macrophages / monocytes cells was 1.5-fold higher, T cells 2-fold higher, mast cells 5-fold higher in the upper segments of adult *Apoe*$^{-/-}$ mice compared to adult WT mice, but these numbers did not reach significance due to the large variation (Fig. 21 A). In the lower segment in *Apoe*$^{-/-}$ mice, the density of macrophages / monocytes cells was significantly 2-fold higher and of mast cells was significantly 3-fold higher compared to WT mice (Fig. 21 B).

In NGs, the density of CD68^{+} macrophages / monocytes in *Apoe*$^{-/-}$ mice was increased versus WT mice, but only a few were observed in both genotypes (Fig. 22). There were no T cells or mast cells in NGs of either WT or *Apoe*$^{-/-}$ mice (not shown). All these data indicated that: I) the immune cell composition in *Apoe*$^{-/-}$ mice are segmentally different in thoracic DRGs; II) atherosclerosis is associated with increased immune cell density in thoracic DRGs; III) atherosclerosis is mainly associated with changes in the number of immune cells in DRGs but not NGs.

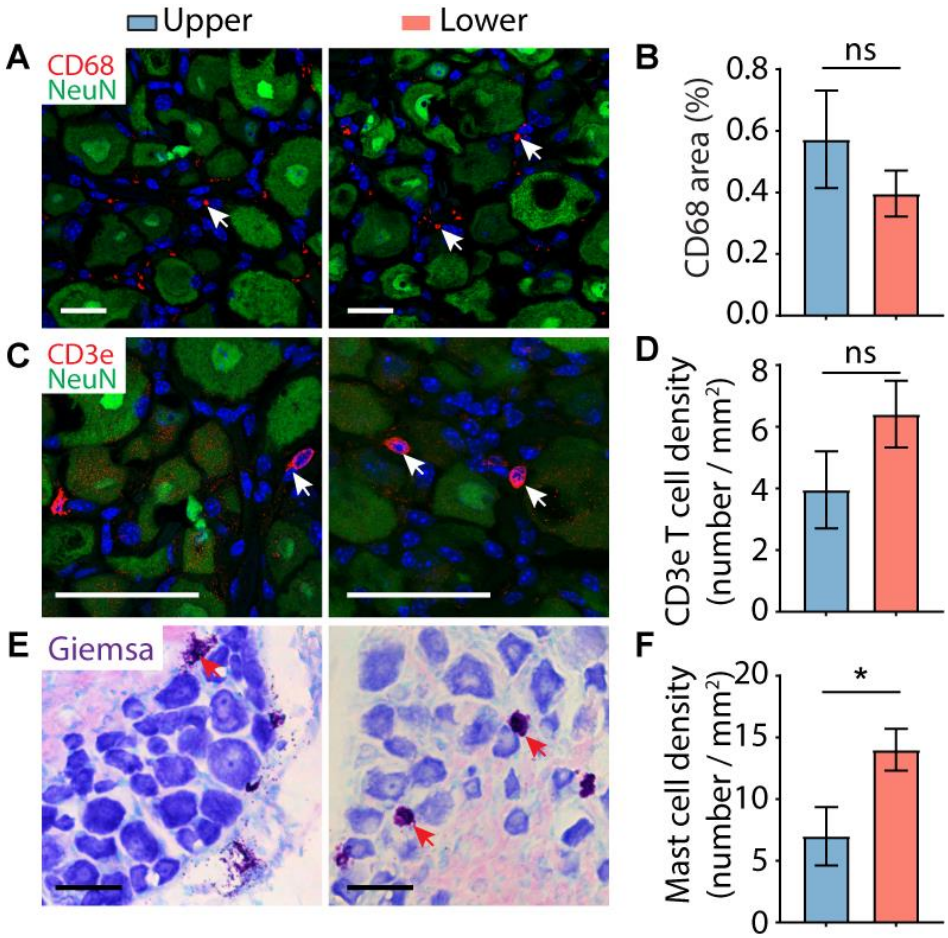

Figure 20. Immune Cells in Thoracic DRGs of Adult *Apoe*$^{-/-}$ Mice. Representative confocal images show immune cells in the upper and lower thoracic DRGs from adult *Apoe*$^{-/-}$ mice. (A) CD68 designates

macrophages / monocytes (red, arrow). (C) CD3e designates T cells (red, arrow). NeuN designates neurons (green). (E) Red arrows indicate the Giemsa$^+$ mast cells. (B, D, F) Quantification: (B) Macrophages / monocytes were quantified as the percentage of CD68$^+$ per DRG area. (D, F) T cells and mast cells were quantified as the density of CD3e$^+$ or Giemsa$^+$ cells per DRG area (mm^2). 4-7 adult *Apoe*$^{-/-}$ mice, a minimum of 6 sections for the upper DRGs and 10 sections for the lower DRGs per mouse were used for the analyses. Two-tailed unpaired Student´s t-test; data represent means per mouse ± SEM; *P < 0.05; ns, not significant. Scale bar: 50 µm. Upper: T1-5 DRGs; lower: T6-13 DRGs.

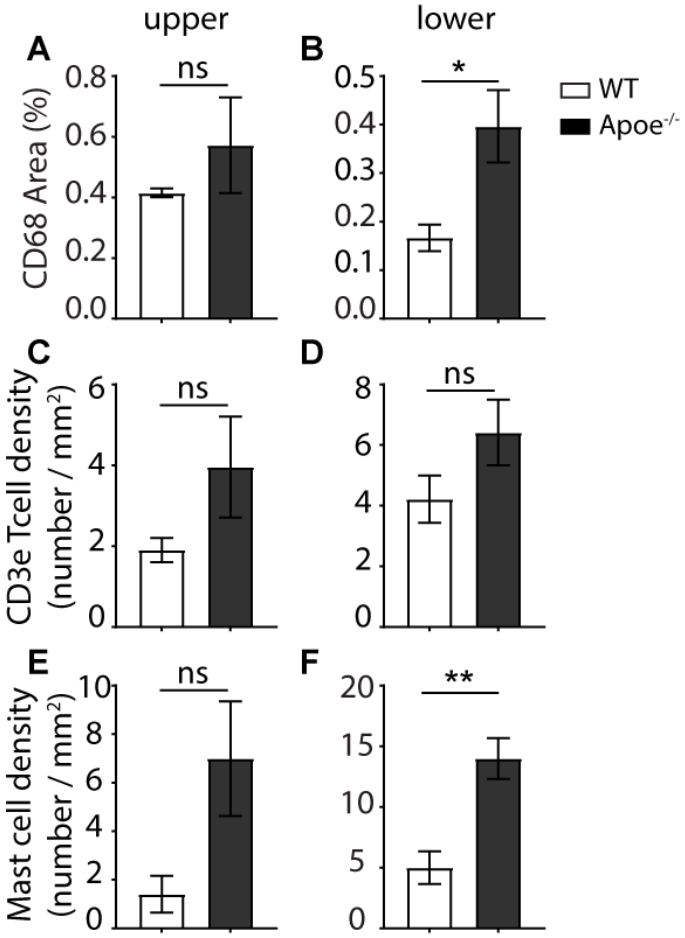

Figure 21. Atherosclerosis is Associated with Changes in the Immune Cell Composition in Lower Thoracic DRGs of Adult Mice. Quantification of CD68$^+$ macrophages / monocytes (A, B), CD3e$^+$ T cells (C, D) and Giemsa$^+$ mast cells (E, F) in thoracic DRGs from both adult WT (n = 5-8) and *Apoe*$^{-/-}$ (n = 4-7) mice. A minimum of 6 sections for the upper DRGs and 10 sections for the lower DRGs per mouse were used for the analyses. Two-tailed unpaired Student´s t-test; data represent means per mouse ± SEM; *P < 0.05, **P < 0.01, ns, not significant. upper: T1-5 DRGs; lower: T6-13 DRGs.

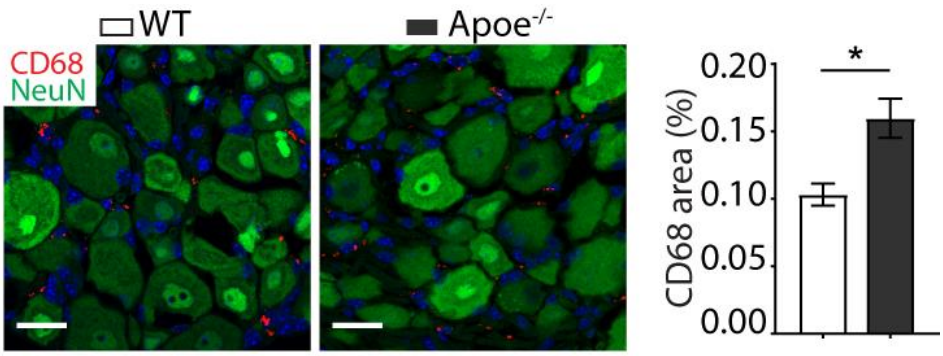

Figure 22. Immune Cells in NG of Adult WT and *Apoe*$^{-/-}$ Mice. Representative confocal images show macrophages / monocytes in NG from aged WT (n = 3) and *Apoe*$^{-/-}$ (n = 3) mice. Macrophages / monocytes were quantified as the percentage of CD68^{+} per NG area (mm^2). A minimum 6 sections per mouse were used for the analyses. Two-tailed unpaired Student´s t-test; data represent means per mouse ± SEM; *P < 0.05. Scale bar: 50 µm.

3.2 Association of Atherosclerosis with the SPNS in Aged Mice

3.2.1 Association of Atherosclerosis with Sensory Innervation in Aorta

To determine the sensory innervation patterns in aged mice, abdominal aortas were collected from WT and *Apoe*$^{-/-}$ mice around 76 wks. Aortas were prepared and sectioned as described in Methods. Axon density was quantified in sections from WT mice (Fig. 23 A), *Apoe*$^{-/-}$ mice without or with plaque but without ATLOs or ATLOs.

Compared to aged WT mice, TRPV1^{+} axon density in *Apoe*$^{-/-}$ mice was not increased at segments without plaque. However, a significant increase was observed in segments with plaque (Fig. 23 B) and a further increase in segments adjacent to ATLOs (Fig. 23 C). This was similar to the axon density determined using the CGRP marker. Compared to aged WT mice, we observed an increase in CGRP^{+} axons density in abdominal aorta adventitia with plaque (Fig. 24 B), which was further increased at ATLO-burdened segments (Fig. 24 C). All these data indicated that atherosclerosis is associated with the increased sensory axon density in abdominal aorta adventitia.

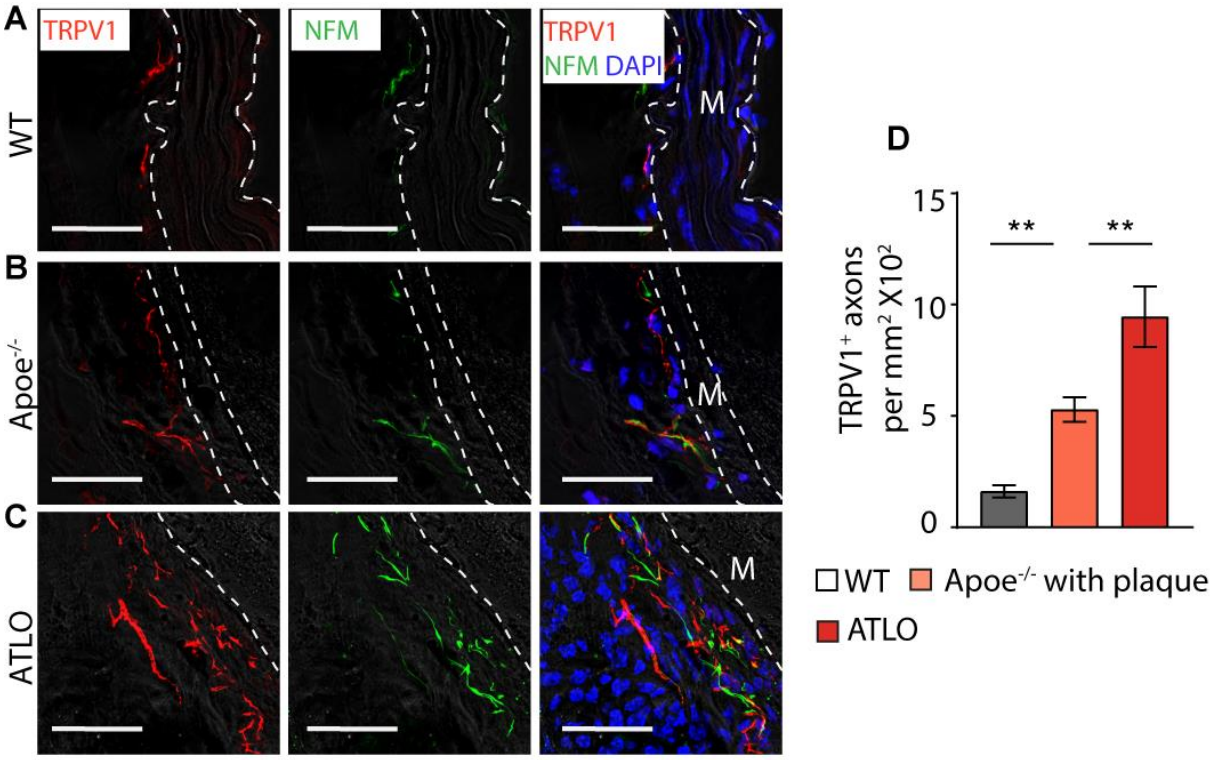

Figure 23. TRPV1 Sensory Axons in the Adventitia of Abdominal Aorta in Aged WT and *Apoe*$^{-/-}$ Mice. Overview of the TRPV1 axons distribution in the adventitia of from (A) WT mice; (B) *Apoe*$^{-/-}$ segments with plaque but without ALTO, (C) ATLO. The media (M) is marked by dashed lines. (D) Axon density was quantified as the number of TRPV1 axons of the adventitia area (per mm^2). WT = 6, *Apoe*$^{-/-}$ segments with plaque but without ATLO = 6, ATLO = 3. A minimum of 5 sections per mouse were used. . Ordinary one-way ANOVA; data represent means per mouse ± SEM; **P < 0.01. Scale bar: 50 μm.

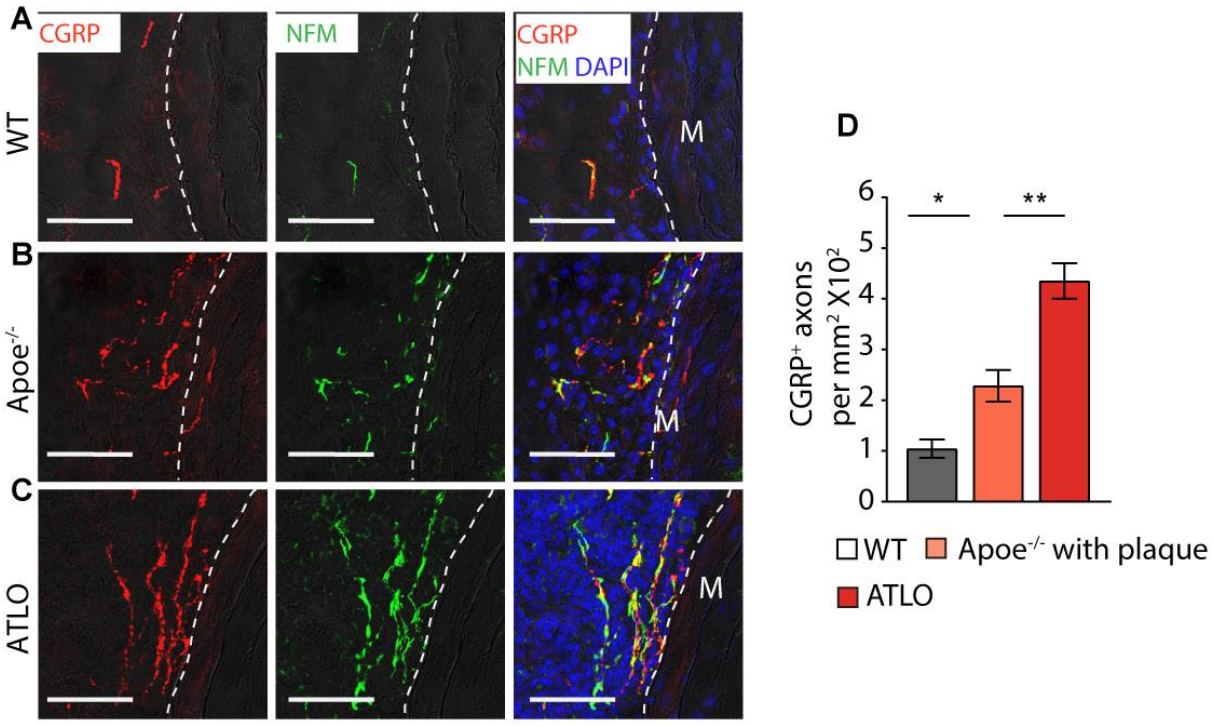

Figure 24. CGRP Sensory Axons in the Adventitia of Abdominal Aorta in Aged WT and *Apoe*$^{-/-}$ Mice. Overview of the distribution of CGRP axons in the adventitia of the aorta from (A) WT mice; (B) *Apoe*$^{-/-}$ segments with plaque but without ALTO, (C) ATLO. The media (M) is marked by dashed lines. (D) Axon density was quantified as the number of CGRP axons of the adventitia area (per mm^2). WT = 4, *Apoe*$^{-/-}$ segments with plaque but without ATLO = 4, ATLO = 5. A minimum of 5 sections per mouse were used for the analyses. Ordinary one-way ANOVA; data represent means per mouse ± SEM; **P < 0.01. Scale bar: 50 µm.

3.2.2 Association of Atherosclerosis with Neuronal Subpopulations of the Peripheral Sensory Ganglia

To determine the association of advanced atherosclerosis with neuronal subpopulations in peripheral sensory ganglia, thoracic DRGs and NGs from both WT and *Apoe*$^{-/-}$ mice around 76 wks were collected, prepared, sectioned and stained as described in Methods. We found no difference in the neuronal distribution in upper and lower thoracic DRGs between aged WT and *Apoe*$^{-/-}$ mice (Fig. 25), nor in NGs (Fig. 26). These data indicated that atherosclerosis was not associated with alterations of neuron subpopulations in either thoracic DRGs or NGs.

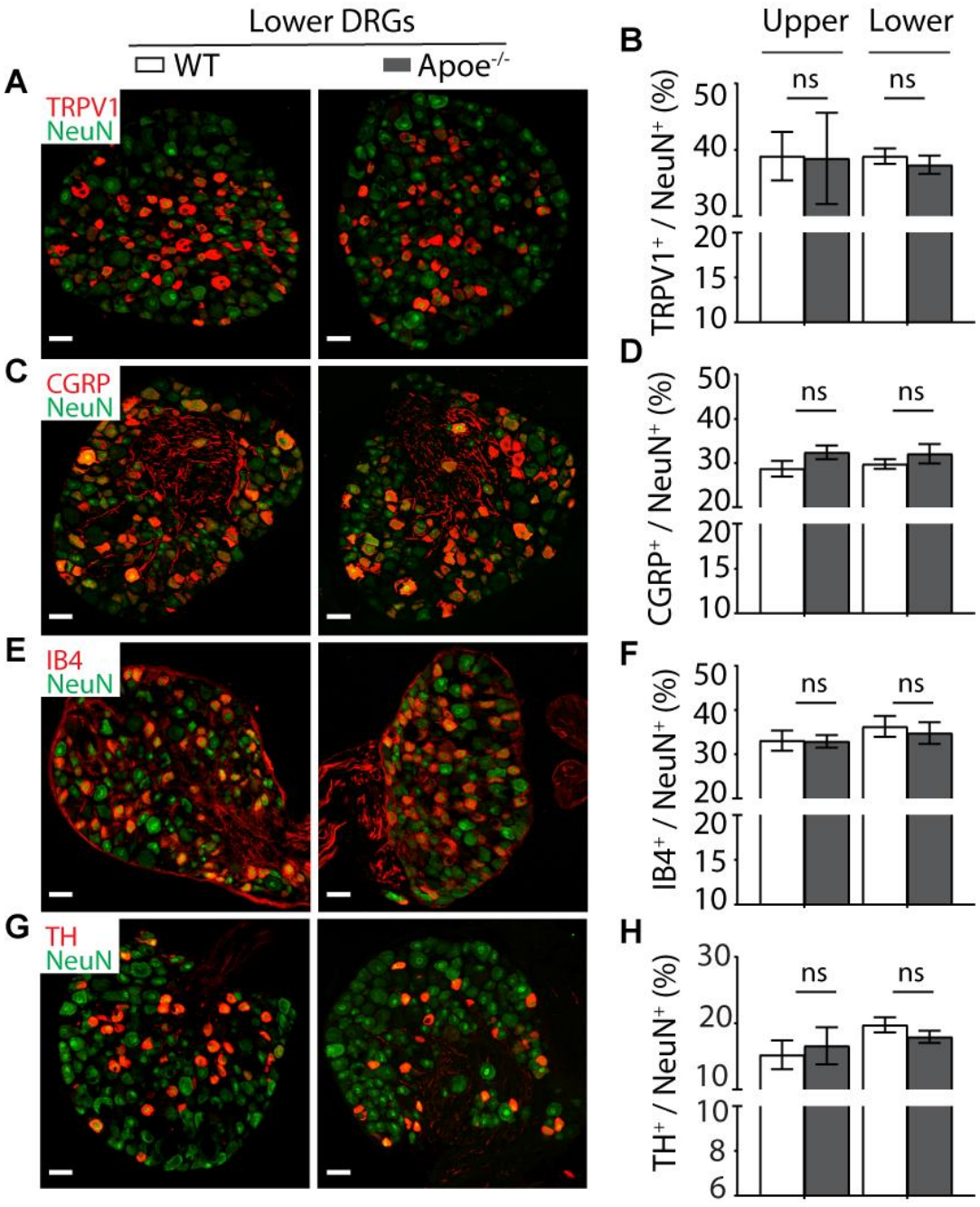

Figure 25. Subpopulations of Sensory Neurons in Thoracic DRGs of Aged WT and *Apoe*$^{-/-}$ Mice. Representative confocal images of the lower thoracic DRGs from aged WT and *Apoe*$^{-/-}$ mice. (A) TRPV1 designates the nociceptive sensory neuron marker (red); (C) CGRP designates the peptidergic sensory neuron marker (red); (E) IB4 designates the non-peptidergic sensory neuron marker (red); (G) TH designates the type C low-threshold mechanoreceptor marker (red); NeuN designates the pan-neuronal marker to stain all neurons (green). (B,D,F,H) Results were quantified as the percentage of the number of TRPV1$^+$ neurons (WT = 4-5, *Apoe*$^{-/-}$ = 5-8), CGRP$^+$ neurons (WT = 5, *Apoe*$^{-/-}$ = 5-8), IB4$^+$ neurons (WT = 5, *Apoe*$^{-/-}$ = 6-7) or TH$^+$ neurons (WT = 5, *Apoe*$^{-/-}$ = 5) among NeuN$^+$ neurons. A minimum of 6 sections for the upper DRGs and 10 sections for the lower DRGs per mouse were used. Two-tailed unpaired Student´s t-test; data represent means per mouse ± SEM; ns, not significant. Scale bar: 50 µm.

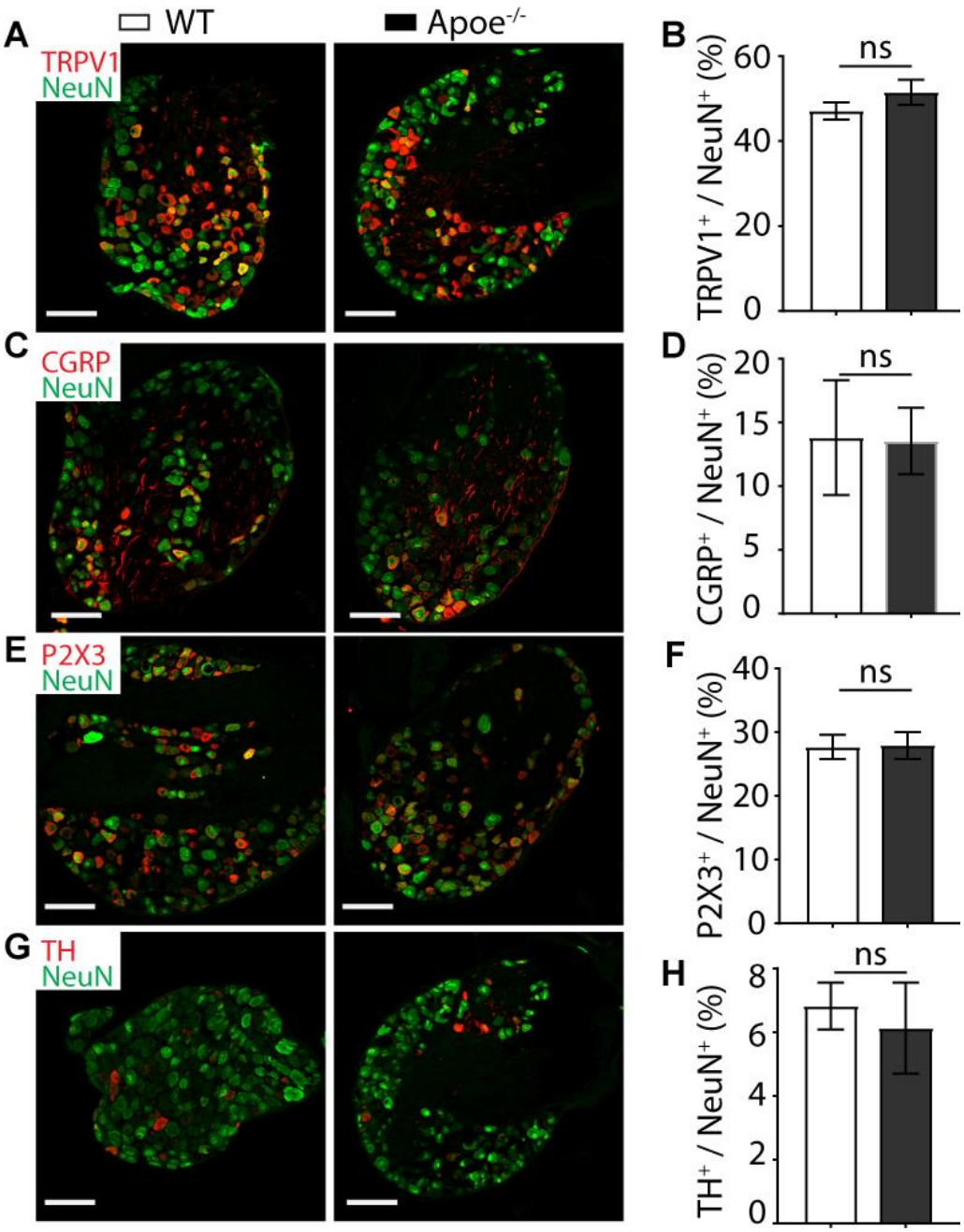

Figure 26. Subpopulations of Neurons in NGs of Aged WT and *Apoe*$^{-/-}$ Mice. Representative confocal images of the NGs from adult WT and *Apoe*$^{-/-}$ mice. (A) TRPV1 designates the nociceptive sensory neuron marker (red); (C) CGRP designates the peptidergic sensory neuron marker (red); (E) P2X3 designates the non-peptidergic sensory neuron marker (red); (G) TH designates the type C low-threshold mechanoreceptor marker (red); NeuN designates the pan-neuronal marker to stain neurons (green). (B, D, F, H) Results were quantified as the percentage of the number of TRPV1^{+} neurons, CGRP^{+} neurons, P2X3^{+} neurons and TH^{+} neurons among NeuN^{+} neurons. 3 mice from both WT and *Apoe*$^{-/-}$ mice, a minimum of 6 sections per mouse were used for the analyses. Two-tailed unpaired Student´s t-test; data represent means per mouse ± SEM; ns, not significant. Scale bar: 50µm.

3.2.3 Association of Atherosclerosis with Immune Cell Composition in the Peripheral Sensory Ganglia

We also investigated the relationship between atherosclerosis and immune cells in the peripheral sensory ganglia of aged mice. For this purpose, the thoracic DRGs and NGs from both WT and *Apoe*$^{-/-}$ mice at around 76 wks were stained as described in Methods.

In aged WT mice, we found no differences in the density of T cells and mast cells between segments (Fig. 19 D and F), whereas macrophages / monocytes infiltration was 5-fold higher in upper thoracic DRGs (0.91 ± 0.13) than in lower thoracic DRGs (0.18 ± 0.03), (Fig. 27 A). However, the macrophages / monocytes accumulation was only 2-fold higher in adult WT mice (Fig. 19 C). In aged *Apoe*$^{-/-}$ mice, there was no difference in the density of macrophages / monocytes between the two segments (Fig. 28 B). But both T cells and mast cells showed a significant preference in the lower segment as 4.45 ± 0.67 vs. 10.68 ± 1.25 for T cells (Fig. 28 D) and 5.79 ± 2.12 vs. 15.73 ± 2.68 for mast cells (Fig. 28 E). To further examine the effect of atherosclerosis on immune cell infiltration in DRGs, we compared the immune cell density in aged mice. In *Apoe*$^{-/-}$ mice, the density of macrophages/monocyte was significantly increased in lower thoracic DRGs compared to WT mice, but no difference in upper segments (Fig. 29 A and B); T cell denstity was significantly increased in both upper and lower segments in *Apoe*$^{-/-}$ mice versus WT mice (Fig. 29 C and D); mast cell density was also increased in *Apoe*$^{-/-}$ mice versus WT mice but did not reach a significance in the upper thoracic DRGs (Fig. 29 E and F).

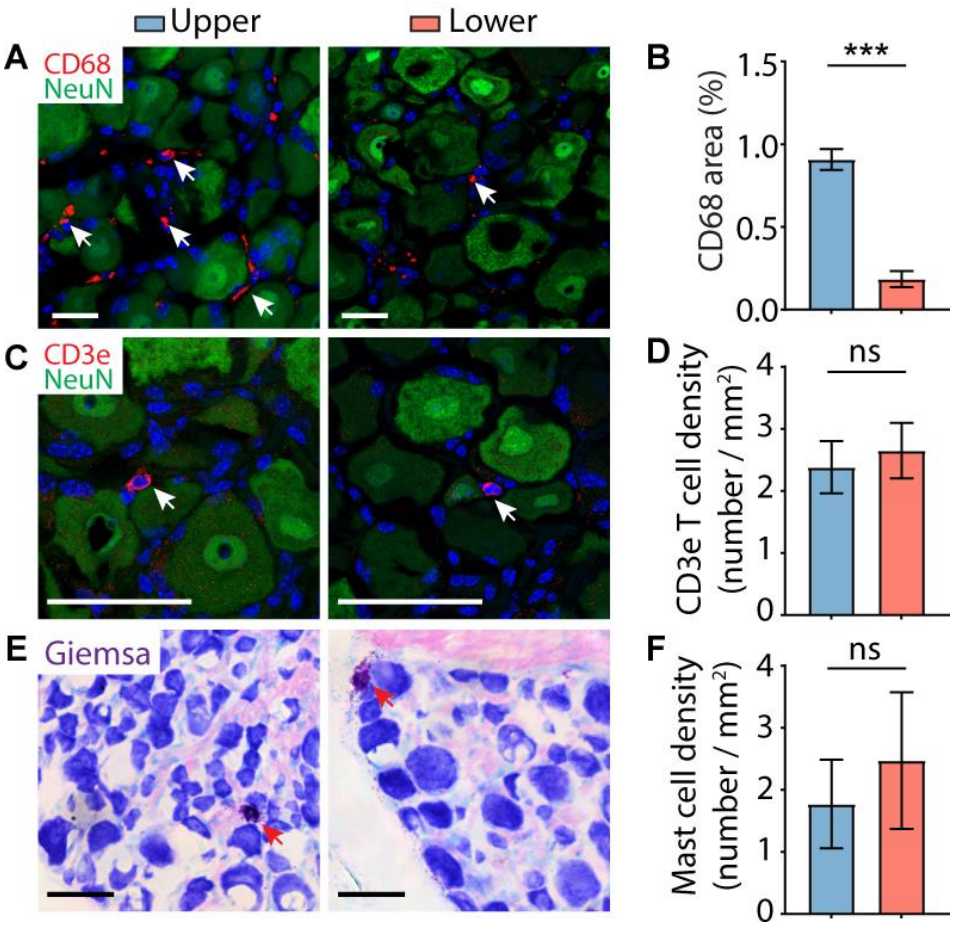

Figure 27. Immune Cells in Thoracic DRGs of Aged WT Mice. Representative confocal images show immune cells in the upper and lower thoracic DRGs of aged WT mice. (A) CD68 designates macrophage/monocytes (red, arrow). (C) CD3e designates T cells (red, arrow). NeuN designates all neurons (green). (E) red arrows indicate Giemsa$^+$ mast cells. (B, D, F) Quantification: (B) Macrophages / monocytes were quantified as the percentage of CD68$^+$ area per DRG area; (D, F) T cells and mast cells were quantified as the density of CD3e$^+$ or Giemsa$^+$ cells per DRG area (mm^2). 4-8 aged WT, a minimum of 6 sections for the upper DRGs and 10 sections for the lower DRGs per mouse were used for the analyses. Two-tailed unpaired Student´s t-test; data represent means per mouse ± SEM;*P < 0.05, ****P < 0.0001. upper: T1-5 DRGs; lower: T6-13 DRGs. Scale bar: 50 µm.

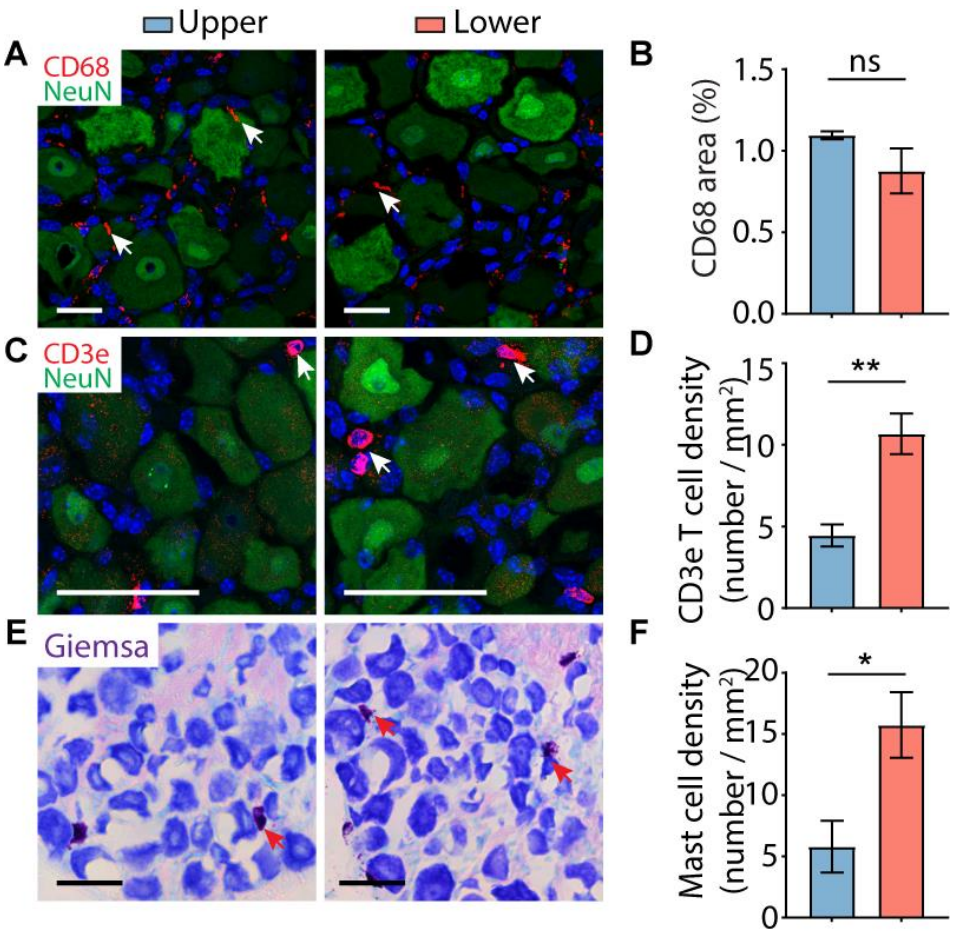

Figure 28. Immune Cells in Thoracic DRGs of Aged *Apoe*$^{-/-}$ Mice. Representative confocal images show immune cells in upper and lower thoracic DRGs of aged *Apoe*$^{-/-}$ mice. (A) CD68 designates macrophage/monocytes (red, arrow). (C) CD3e designates T cells (red, arrow). NeuN designates all neurons (green); (E) red arrows indicate Giemsa^{+} mast cells. (B, D, F) Quantification: (B) Macrophages / monocytes were quantified as the percentage of CD68^{+} area per DRG area; (D, F) T cells and mast cells were quantified as the density of CD3e^{+} or Giemsa^{+} cells per DRG area (mm^{2}). 4-8 aged WT, a minimum of 6 sections for the upper DRGs and 10 sections for the lower DRGs per mouse were used for the analyses. Two-tailed unpaired Student´s t-test; data represent means per mouse ± SEM; *P < 0.05, ****P < 0.0001. upper: T1-5 DRGs; lower: T6-13 DRGs. Scale bar: 50 µm.

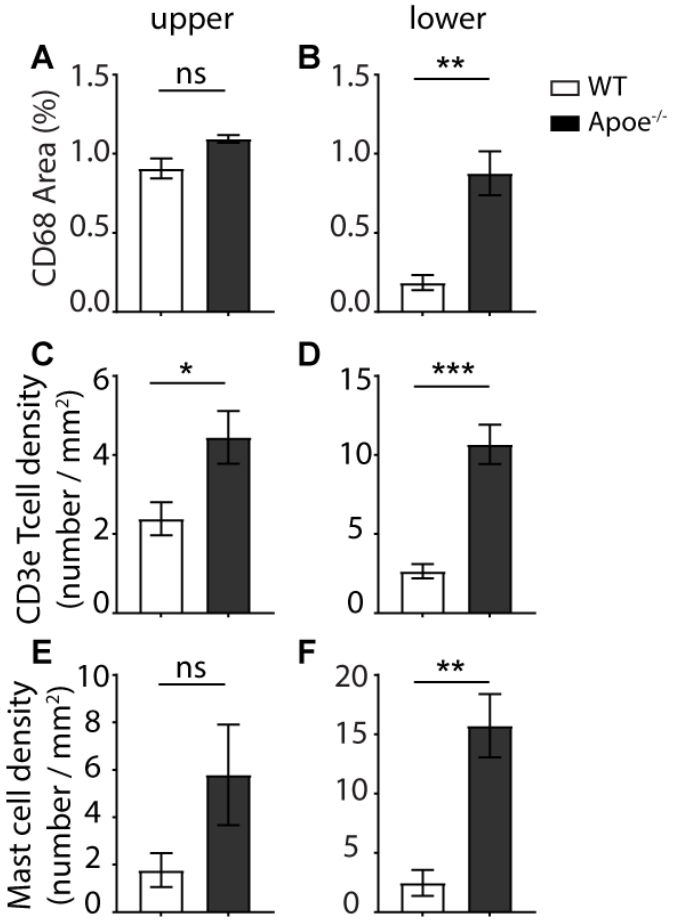

Figure 29. Association of Atherosclerosis with Immune Cell Infiltration in Lower Thoracic DRGs of Aged Mice. Quantification of CD68$^+$ macrophages / monocytes (A, B), CD3e$^+$ T cells (C, D) and Giemsa$^+$ mast cells (E, F) in thoracic DRGs from both aged WT (n = 4-8) and *Apoe*$^{-/-}$ (n = 4-8) mice. A minimum of 6 sections for the upper DRGs and 10 sections for the lower DRGs per mouse were used for the analyses. Two-tailed unpaired Student´s t-test; data represent means per mouse ± SEM; *P < 0.05, **P < 0.01, ***P < 0.001, ns, not significant. upper: T1-5 DRGs; lower: T6-13 DRGs.

Since we have observed immune cell clusters outside sympathetic perivascular ganglia capsules and the nerves sheaths in aged *Apoe*$^{-/-}$ mice, which are-termed as TLCs[38], we next wished to clarify whether TLCs were detectable around DRGs. The whole spine from aged WT and *Apoe*$^{-/-}$ mice was isolated and sectioned as described in Methods. We found DRG-TLCs in 3 of 5 aged *Apoe*$^{-/-}$ mice (Fig. 30), which were connected to the capsule but separated from the meninges and the SC. DRG-TLCs contained large numbers of CD68$^+$ macrophage/monocytes and B220$^+$ B cells but few T cells. These results, together with the immune cell in DRGs, suggested that: I) macrophage/monocytes in thoracic DRGs are increased in aged WT mice compared to adult WT mice; II) T cells and mast cells show a preference in lower thoracic DRGs in aged *Apoe*$^{-/-}$ mice; III) atherosclerosis is associated

with increased immune cells in lower thoracic DRGs; IV) atherosclerosis associates with TLCs adjacent to DRGs in aged *Apoe*$^{-/-}$ mice.

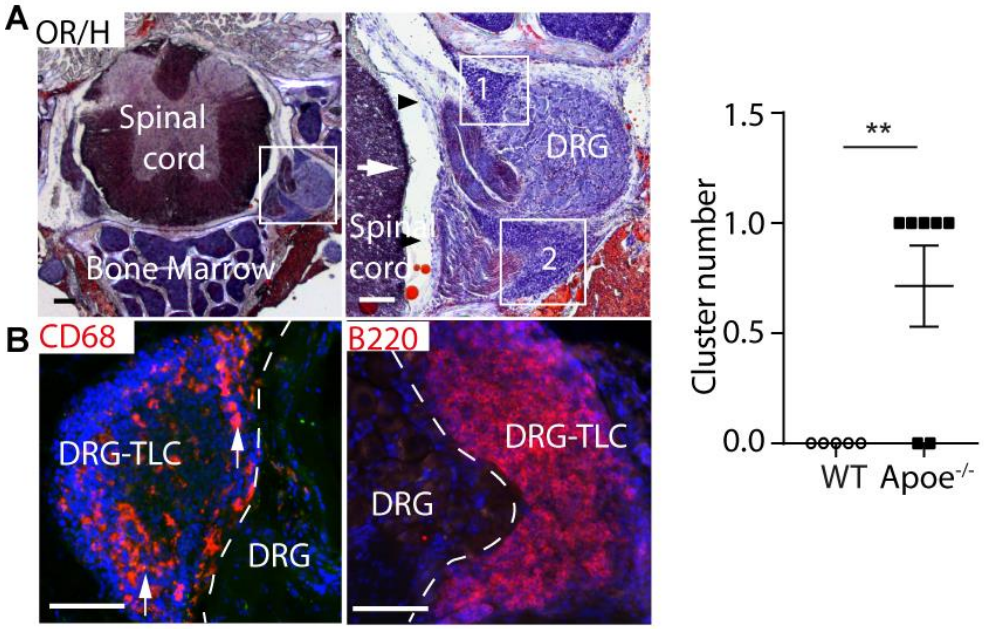

Figure 30. Structures and Cellularity of Epineural TLCs in Aged *Apoe*$^{-/-}$ Mice. (A) Representative ORO/H staining image shows the location of DRG-TLCs (left), the enlarged image shows the distance of DRG-TLCs from meninges (filled triangle) and the SC (right), 1 and 2 indicate the DRG-TLC structures; (B) representative immunofluorescence images indicated the cellularity of DRG-TLCs as CD68^{+} macrophages (arrow, left) and B220^{+} B cells (right). Two-tailed unpaired Student´s t-test; data represent means per mouse ± SEM; **P < 0.01. Scale bar: 50 µm.

In NGs, we only observed few CD68^{+} macrophage/monocytes but no T cells or mast cells (not shown) in either aged WT or *Apoe*$^{-/-}$ mice. The macrophage/monocytes was >5-fold higher in *Apoe*$^{-/-}$ mice compared to WT mice (Fig. 31), indicating a potential connection between atherosclerosis and sensory peripheral ganglia in DRGs but not NGs.

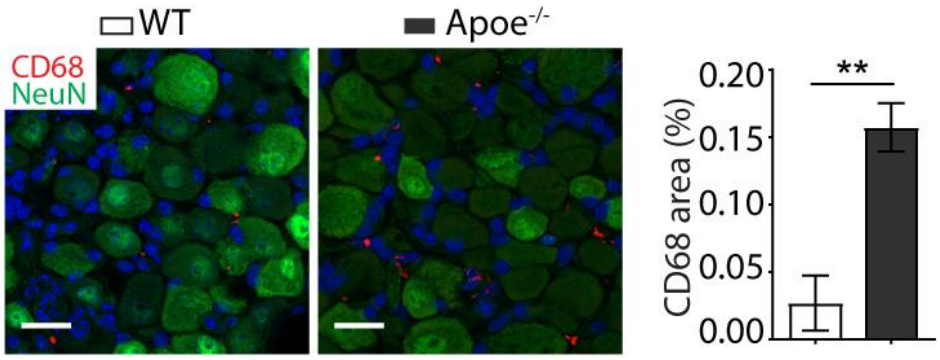

Figure 31. Immune Cells in NG of Aged WT and *Apoe*$^{-/-}$ Mice. Representative confocal images show macrophage/monocytes in NGs. Macrophages / monocytes were quantified as the percentage of CD68^{+} per NG area (mm^2). 3 Aged WT and *Apoe*$^{-/-}$ mice were used and a minimum 6 sections per mouse were used for the analyses. Two-tailed unpaired Student´s t-test; data represent means per mouse ± SEM; **P < 0.01. Scale bar: 50 µm.

3.3 Association of Atherosclerosis with CGRP Tissue Levels in the Aorta

Neurons actively communicate with the immune system through the release of neuropeptides stored in peripheral nerve-terminals. CGRP has been reported to be an important neuropeptide in different diseases including bacteria-induced infection[92,96,111] and pain[138]. Since we found increased TRPV1^{+} and CGRP^{+} sensory axons in *Apoe*$^{-/-}$ mice, we hypothesized that increased axons in atherosclerosis communicate with innervated tissues through the release of CGRP. To investigate this possibility, ascending arteries between the aortic root and the innominate artery of 5-8 adult WT and *Apoe*$^{-/-}$ mice aged at 32 wks were collected. The abodominal aorta between renal arteries of 5-8 aged WT and *Apoe*$^{-/-}$ mice aged around 78 wks were collected.

In adult mice, we found 10-fold higher CGRP tissue levels of the aorta in *Apoe*$^{-/-}$ mice compared to WT mice (291.00 ± 80.06 vs. 29.06 ± 7.02). In aged mice, CGRP levels were also nearly 10-fold higher in *Apoe*$^{-/-}$ mice compared to WT mice (740.80 ± 125.50 vs. 79.72 ± 8.03). Also, we found 3-fold higher CGRP levels in aged WT mice compared to adult mice and equally higher CGRP levels in aged *Apoe*$^{-/-}$ mice compared to adult mice. Importantly, there seems to be an ageing phenomenon involved in WT mice, and also possibly a different innervation patterns in different segments of aorta, as our previous data showed a higher innervation in abdominal aorta compared to thoracic aorta segments. These results revealed that increased CGRP levels in *Apoe*$^{-/-}$ mice may be associated with ageing and atherosclerosis.

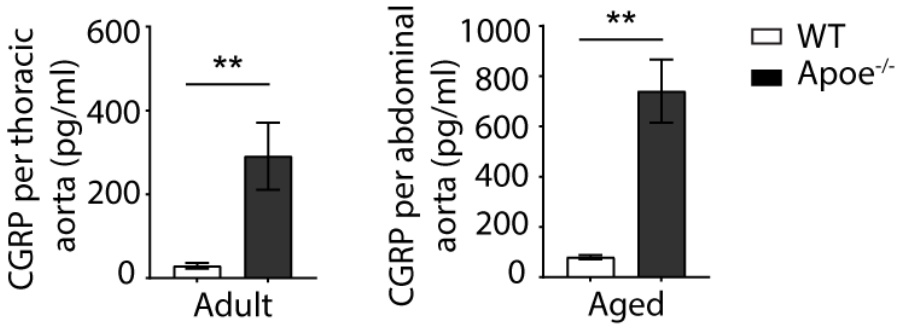

Figure 32. Atherosclerosis is Associated with Increased CGRP Levels in Aorta. The CGRP levels were determined by CGRP EIA. The ascending thoracic aorta from adult mice and perirenal abdominal aorta from aged mice were used. 5-8 adult and aged mice, from both WT and *Apoe*$^{-/-}$ mice, were used for the statistical analysis. CGRP levels was recorded as pg/ml. Two-tailed unpaired Student´s t-test; data represent means per mouse ± SEM; *P < 0.05, **P < 0.01.

3.4 Differential SPNS Gene Expression in Atherosclerotic Adventitia

We observed I) that sensory axons innervate the aorta adventitia, but not the adjacent media or intima; II) that adventitia innervations markedly increased in segments afflicted with atherosclerosis and that this phenomenon further increased in ATLOs; and III) that tissue CGRP levels were augmented in those aorta segments afflicted with atherosclerosis. Importantly, data from our lab showed that ATLO-innervating axons directly connect to immune cells and SMCs indicating interaction of axons with arterial wall constituents via putative neuro-adventitia junctions[38]. Immune cells and non-immune cells in secondary lymphoid organs (SLOs) have been shown to produce neuropeptides and express neuropeptide-receptors[112]. Since ATLOs harbor a mixture of innate and adaptive immune cells and non-immune cells, it is plausible that these cells can produce neuropeptides and express neuropeptide-receptors. Further more, our previous data supported this hypothesis and found candidate genes in ATLOs that were associated to axon maintance, axon neogenesis, axon guidance, and synaptic transmission, including growth associated protein 43, Semaphorin 3A and 3F, and Plexin D1 (Semaphorin 3E receptor)[29,37,38]. Among them, Semaphorin 3A and 3E have been reported to contain a functional role in atherosclerotic plaques via regulating the infiltration and retention of macrophages[169,170]. Moreover, we have found increased tissue CGRP levels in the plaque-burden aorta, and its receptor is also expressed by VSMCs and ECs[44,112]. All the data and studies related to neuroimmune interactions reminded us futher questions: I) what is the potential role of atherosclerosis in increased sensory innervations in aortic adventitia; and II) does ATLO strengthen SPNS neogenesis, maintance, and guidance and/or vice versa?

To give a systemic answer, we used our whole WT and *Apoe*$^{-/-}$ mice genome, mRNA expression array data bank[37,38], to detect different neuronal genes in separated abdominal aorta adventitia by LCM-based method and in whole aorta RNA products at different ages. For adventitia gene expression analyses, LCM-derived samples of WT adventitia, *Apoe*$^{-/-}$ plaque-free adventitia, and ATLOs were analyzed.

DE genes of interest were examined using gene ontology (GO)-terms based on the National Center for Biotechnology Information (http://www.ncbi.nlm.nih.gov/) and the GO data banks (http://www.geneontology.org/), which was also used to seek genes related to sensory aoxn neogenesis and guidance, sensory perception and ion channel molecules. Genes of interest including neuron projection (GO: 0043005, 116 genes), axon guidance (GO: 0007411, 10 genes), sensory perception (GO: 0007600, 32 genes), ion channel activity (GO: 0005216, 17 genes), ligand-gated ion channel activity (GO: 0015276, 3 genes) from a total of 1610 differentially regulated genes in aged WT and *Apoe*$^{-/-}$ mice (Fig. 33).

Numerous up-regulated genes were demonstrated in ATLO specifically, but no changes in the adventitia without adjacent plaque when compared with WT adventitia (Fig. 33). Highly up-regulated genes in ATLOS included: C-X-C motif ligand 4, C-X-C motif ligand 12, receptor of C-X-C motif ligand 12, Plexin B2, nerve growth factor (Ngf), synaptogyrin 2, myosin 5A, cell adhesion molecule 1, calcium/calmodulin-dependent protein kinase 1D, potassium intermediate/small conductance calcium-activated channel N4, and calcium channel alpha 1D, whereas down-regulated genes in ATLOS included: neuregulin 4, wingless-related MMTV integration site 5A, Syngr1, reticulon 4, Neurofibromin 1, growth arrest specific 1, aquaporin 1 and purinergic receptor P2X ligand-gated ion channel 5 (Fig. 33). Ngf regulates the growth and development of divergent neuronal pathways and their plasticity[171-173]. Semaphorins together with their Plexin and Neuropilin receptors were reported to maintain synaptic transmission in the developing and mature NS[174-176]. Moreover, Semaphorin 3A expression can be modulated by tissue calcium concentrations[177] and activation of TRPV1-mediated calcium influx has been implicated in atherosclerosis[171]. Conversly, reticulon 4 has been shown to inhit axon growth[178], and Nf1 deficiency resulted in survival of embryonic sensory neurons in a neurotrophin-independent manner[179]. Furthermore, ion channel genes were shown to play a role in sensing cellular calcium level, regulating synaptic plasticity and nerve conductance of peripheral sensory nerves[180,181].

Notably, axon growth and guidance genes including Ngf, PlxnB2 and ion channel genes Camk1d, Kcnn4 were up-regulated in ATLOs compared to aged WT and *Apoe*$^{-/-}$ plaque-free adventitia, whereas Semaphorin 3A was down regulated (Fig 34 B and C). These data indicated that numerous axonogenesis-related genes were up-regulated in plaque-burden adventitia segments whereas axon repellant genes were lower.

In addition to the LCM-based approach, we used total aorta microarray analyses to identify differential neuronal gene expression profiles of the aorta during ageing with respect to atherosclerosis and ATLOS development. Our own group previously established a large scale mouse whole genome mRNA data bank of the microanatomy of the normal and diseased aorta [29,37,38]. Because plaque and ATLOS gene expression were detected at 32 wks and 78 wks respectively, we used the data bank on total aorta from Wt and *Apoe*$^{-/-}$ mice aged at 6, 32, and 78 wks by interrogating the NS-related genes specifically. To analyze the effect of ageing on SPNS development, we detected multiple DE neuronal genes of interest such as neuron projection (GO: 0043005, 267 genes), axon guidance (GO: 0007411, 28 genes), sensory perception (GO: 0007600, 89 genes), ion channel activity (GO: 0005216, 58 genes), ligand-gated ion channel activity (GO: 0015276, 19 genes) in WT and *Apoe*$^{-/-}$ aortas (Fig. 34 A).

The mining of DE gene profiles in the diseased aorta throughout the lifespan discovered important candidates of neuroimmune interactions: Numerous SPNS genes were markedly upregulated as early as 32 wks when atherosclerosis had reached significant levels in the thoracic aorta, and were even higher at 78 wks. SPNS genes related to axon neogenesis and guidance as well as ion channel activity were up-regulated in adult *Apoe*$^{-/-}$ mice and further increased in aged *Apoe*$^{-/-}$ mice (Fig. 34). Heatmaps showed many up-regulated genes including Ngf, C-X-C motif ligand 12, C-X-C chemokine receptor type 4, Plexin B2, neuropilin 2 in aged *Apoe*$^{-/-}$ aortas, while Semaphorin 3A, neurotrophin 3, Ephrin type-B receptor 3 and Slit homolog 3 protein precursor were down-regulated in WT vs. *Apoe*$^{-/-}$ aorta during ageing. No significant differences were found in neuronal gene expression between WT and *Apoe*$^{-/-}$ aortas aged at 6 wks, but much higher differences in *Apoe*$^{-/-}$ aorta aged 32 wks and 78 wks compared to age-matched WT controls (Fig. 34 A). Semaphorins have previously been shown to be important in the development and maintenance of the immune and cardiovascular systems as well as in the SPNS development and guidance, while neuropilin 2, a Semaphorin 3 A receptor, guides axon growth during the NS

development[182,183]. Neuronal growth and development gene Ngf was highly up-regulated in WT vs. *Apoe*$^{-/-}$ mice. Specifically, expression of genes regulating axonogenesis and ion channel activities was higher in adventitia segments adjacent to atherosclerotic plaques (*nerve growth factor, calcium channel alpha 1D*), whereas gene expression of sensory axon repellants was lower in the same area (*Semaphorin 3A)* in aged *Apoe*$^{-/-}$ aorta vs. WT aorta. Notably, Semaphorin 3A showed a down-regulation tendency in aged *Apoe*$^{-/-}$ aorta vs. young and adult mice (Fig. 33). All the data suggested that age-dependent alteration in all SPNS-related GO-terms in *Apoe*$^{-/-}$ mice most likely represent genes expressed by the newly formed axons during atherosclerosis as well as recruited immune cells in local inflammatory pool in ATLOs.

In summary, the microarray data support the findings of enhanced adventitial sensory innervations in abdominal aorta and in *Apoe*$^{-/-}$ adventitia with plaques and with ATLOs. The data indicate that neuronal responses in atherosclerosis are segmentally organized by ATLOs and that ATLOs may promote axon sprouting in the plaque-laden area of the abdominal aorta. The microarray results combined with our IF and EIA data provide strong evidence for atherosclerosis-SPNS crosstalk in aged hyperlipidemic mouse aorta.

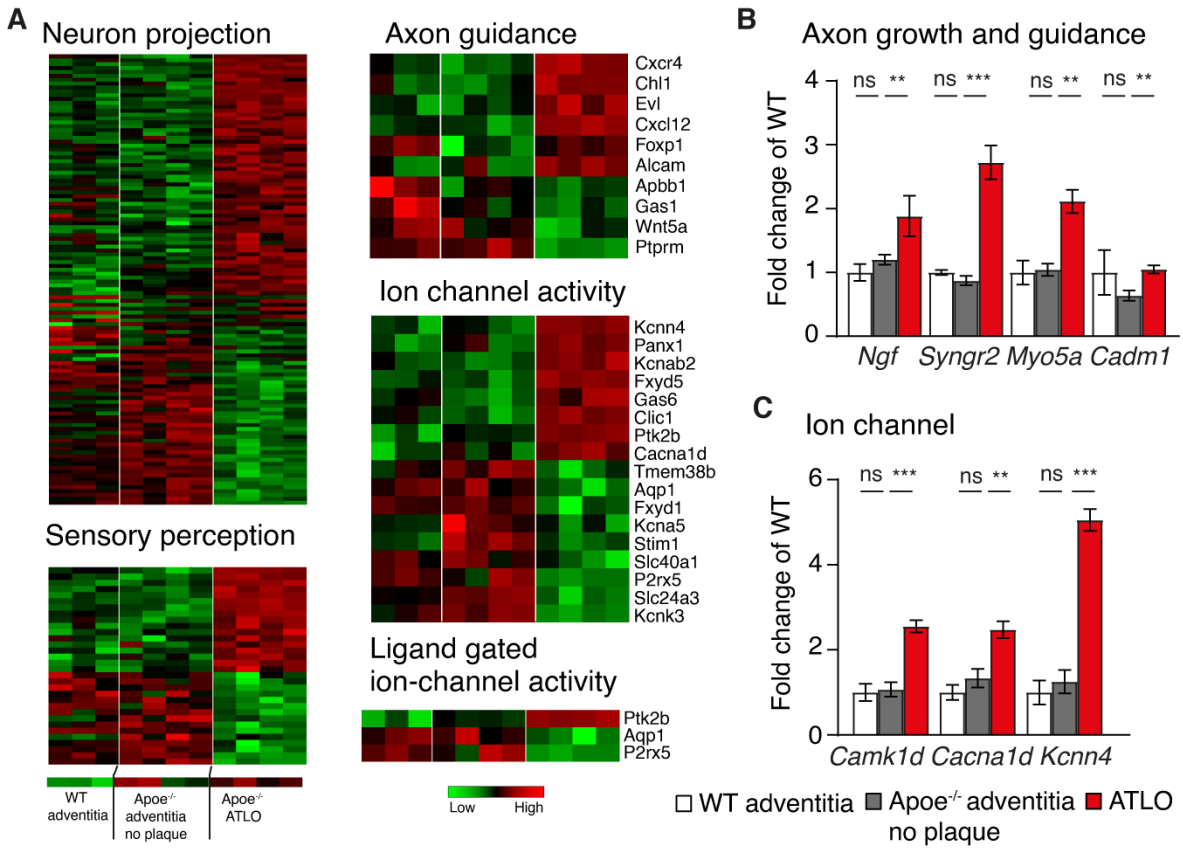

Figure 33. Neuronal Gene Expression in LCM-derived Abdominal Aorta Adventitia of Aged WT and *Apoe*$^{-/-}$ Mice. (A) DE genes heatmaps in abdominal adventitia RNA extracts from aged WT adventitia, *Apoe*$^{-/-}$ plaque-free abdominal aorta and ATLO. The GO-terms include: neuron projection (GO: 0043005), axon guidance (GO: 0007411), sensory perception (GO: 0007600), ion channel activity (GO: 0005216), ligand-gated ion channel activity (GO: 0015276). (B) Quantitation of axon growth and guidance related mRNA expression (log2 value) for NGF, Syngr2, Myo5a and Cadm1 in microarrays of LCM-derived WT adventitia, *Apoe*$^{-/-}$ plaque-free adventitia, and ATLOS. (C) Quantitation of ion channel related mRNA expression (log2 value) for Camk1d, Cacna1d and Kcnn4 in LCM-derived WT adventitia, *Apoe*$^{-/-}$ plaque-free adventitia, and ATLOS. Heatmaps showing significantly up- or down-regulated genes (ANOVA; RME ≤ 0.66) in the separated aorta laminae for the indicated NS-related GO-terms. 3 WT adventitia, 4 *Apoe*$^{-/-}$ plaque-free abdominal aorta and 4 ATLO. Data represent means per mouse ± SEM, based on the raw CEL-file microarrays data. Samples were compared using one-way ANOVA with Bonferroni's post-hoc test. **P < 0.01, ***P < 0.001. *Ngf*: nerve growth factor. *Syngr2*: synaptogyrin 2. *Myo5a*: myosin 5A. *Cadm1*: cell adhesion molecule 1. *Cacna1d*: calcium channel alpha 1D. *Kcnn4*: Potassium Calcium-Activated Channel Subfamily N Member 4.

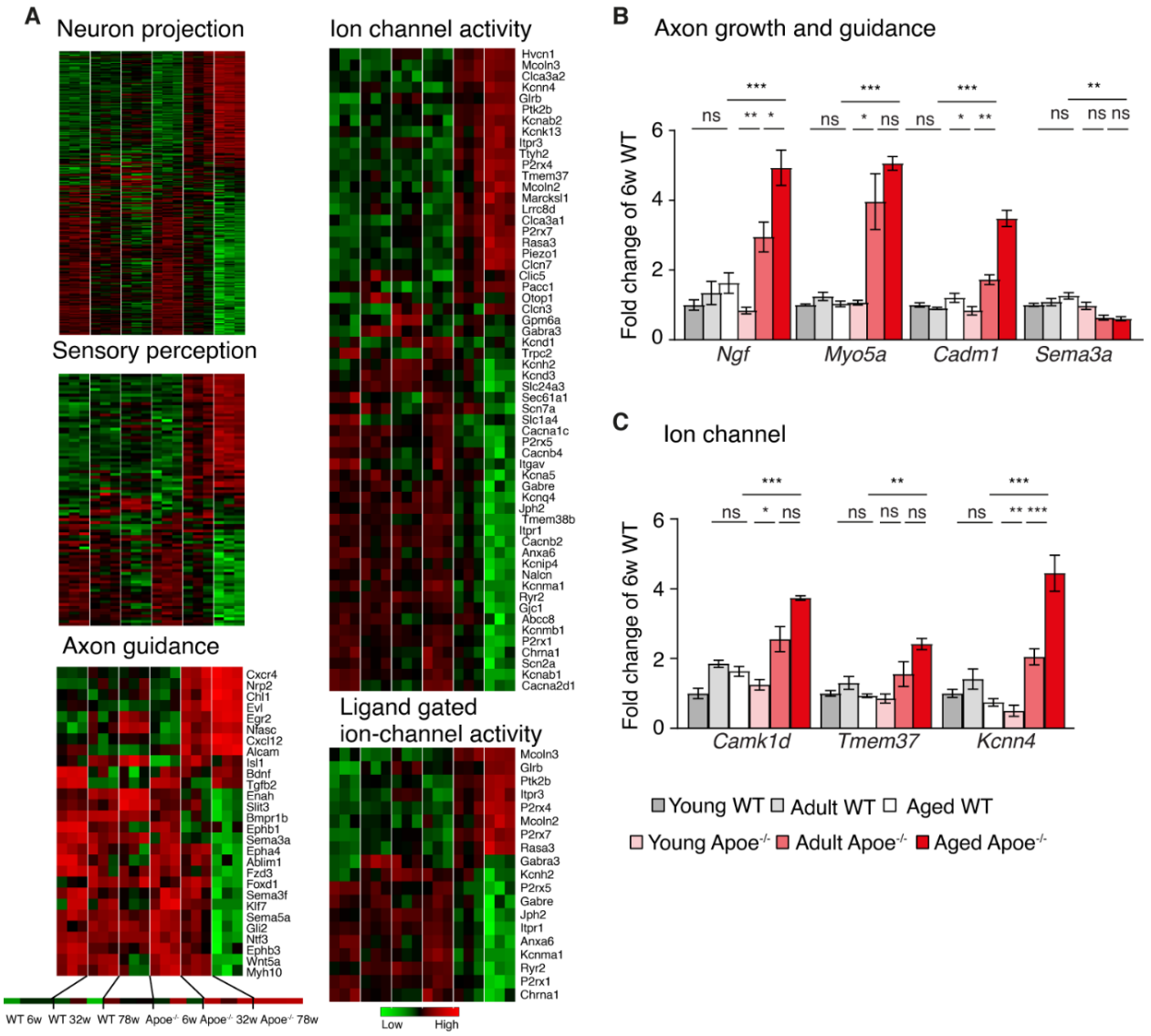

Figure 34. Differential Neuronal Gene Expression in WT and *Apoe*$^{-/-}$ Aortas. A) Heatmaps of DE genes in total aorta RNA extracts from WT and *Apoe*$^{-/-}$ mice aged 6, 32, and 78 wks. The GO-terms include: neuron projection (GO: 0043005), sensory perception (GO: 0007600), axon guidance (GO: 0007411), ion channel activity (GO: 0005216), ligand-gated ion channel activity (GO: 0015276). (B) Quantitation of axon growth and guidance related mRNA expression (log2 value) for Ngf, Myo5a, Cadm1 and Sema3a in WT and *Apoe*$^{-/-}$ mice during ageing. (C) Quantitation of ion channel related mRNA expression (log2 value) for Camk1d, Tmem37 and Kcnn4 in WT and *Apoe*$^{-/-}$ mice during ageing. Heatmaps showing significantly up- or down-regulated genes (ANOVA; RME ≤ 0.66). n = 3 per group. Data represent means per mouse ± SEM, based on the raw CEL-file microarrays data. Samples were analyzed by one-way ANOVA with Bonferroni's post-hoc test. **P < 0.01, ***P < 0.001. *Ngf*: nerve growth factor. *Syngr2*: synaptogyrin 2. *Myo5a*: myosin 5A. *Cadm1*: cell adhesion molecule 1. *Sema3a*: semaphorin 3A. *Camk1d*: calcium/calmodulin-dependent protein kinase 1D. *Kcnn4*: Potassium Calcium-Activated Channel Subfamily N Member 4.

3.5 Immune Cells in Peripheral Sensory Ganglia during Ageing

Since ageing was reported to have effects on both the immune and the NS, we also analyzed the effect of ageing on immune cell infiltration in the peripheral sensory ganglia of both WT and *Apoe*$^{-/-}$ mice. In WT mice, we found that ageing was associated with increased density of macrophages / monocytes in the upper segment but not the lower segment (Fig. 35 A and B), which explained the enhanced difference of the macrophages / monocytes infiltration between segments in aged WT mice (Fig. 26 A); and we observed reduced numbers of T cells (Fig. 35 C and D) and mast cells (Fig. 35 E and F) in the lower segment but not the upper segment. In *Apoe*$^{-/-}$ mice, ageing was associated with increased macrophages / monocytes infiltration in both the upper and the lower thoracic DRGs (Fig. 36 A and B), the increased T cell infiltration in the lower segment but not the upper one (Fig. 36 C and D), yet mast cell infiltration was not affected by ageing in *Apoe*$^{-/-}$ mice (Fig. 36 E and F). In NGs, we found decreased numbers of macrophage/monocytes during ageing in WT mice, but these numbers were unchanged versus *Apoe*$^{-/-}$ mice (Fig. 37). All these data indicated an important ageing phenotype in WT and *Apoe*$^{-/-}$ mice: I) ageing upregulates the macrophage / monocyte content in the upper segment but has no effect on the lower thoracic DRGs resulting in enhanced differences between the segments in WT mice; II) ageing downregulates the T cell and mast cell infiltration in the lower segment without affecting the upper segment; III) ageing is associated with increased numbers of macrophages / monocytes in both the upper and the lower segments of DRG in *Apoe*$^{-/-}$ mice; IV) ageing upregulates the number of T cells in the lower segment but has no effect on the upper thoracic DRGs; V) ageing has no effect on mast cells in *Apoe*$^{-/-}$ mice.

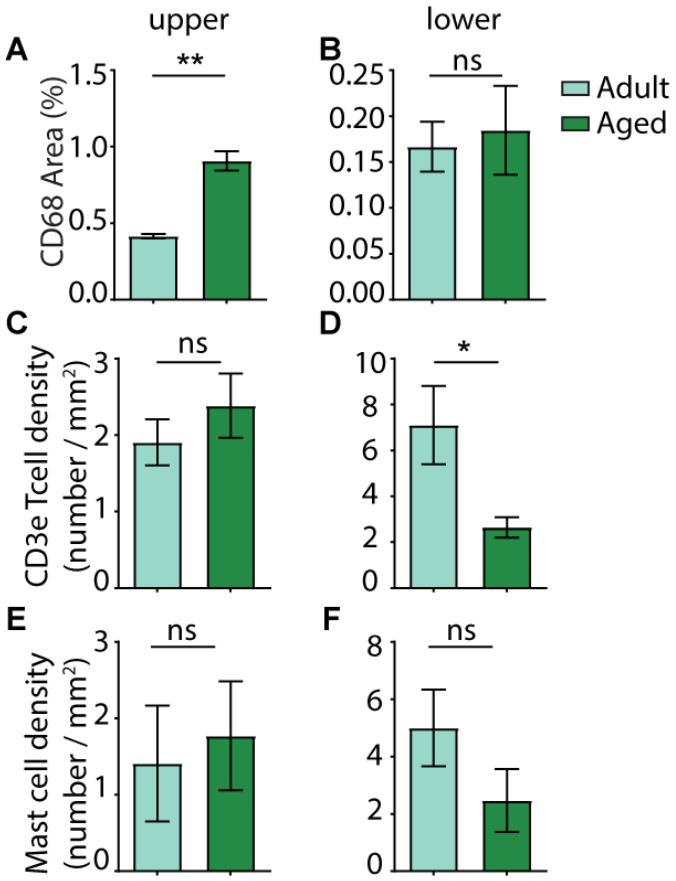

Figure 35. Quantification of Immune Cells in Thoracic DRGs of WT Mice during Ageing. Quantification of CD68⁺ macrophages / monocytes (A, B), CD3e⁺ T cells (C, D) and Giemsa⁺ mast cells (E, F) in WT mice during ageing in the upper and lower thoracic DRGs, respectively. 5-8 adult and 3-5 aged WT mice, a minimum of 6 sections per mouse were used for the analyses. Two-tailed unpaired Student´s t-test; data represent means per mouse ± SEM; *P < 0.05, **P < 0.01, ns, not significant. upper: T1-5 DRGs; lower: T6-13 DRGs.

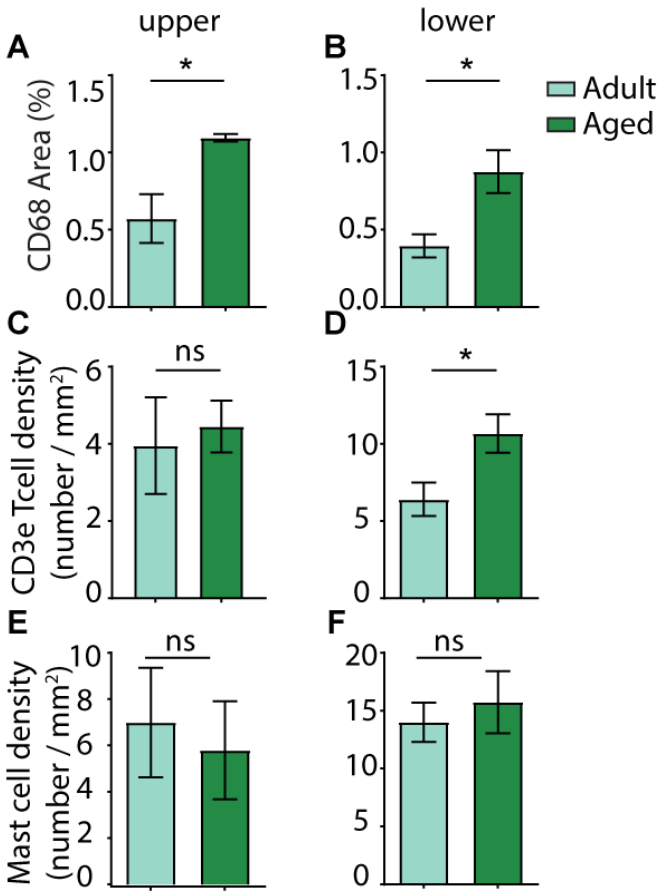

Figure 36. Quantification of Immune Cells in Thoracic DRGs of *Apoe*$^{-/-}$ Mice during Ageing. Quantification of CD68^{+} macrophages / monocytes (A, B), CD3e^{+} T cells (C, D) and Giemsa^{+} mast cells (E, F) in *Apoe*$^{-/-}$ mice during ageing in the upper and lower thoracic DRGs, respectively. 4-7 adult and 4-6 aged *Apoe*$^{-/-}$ mice, a minimum of 6 sections per mouse were used for the analyses. Two-tailed unpaired Student´s t-test; data represent means per mouse ± SEM; *P < 0.05, **P < 0.01, ns, not significant. upper: T1-5 DRGs; lower: T6-13 DRGs.

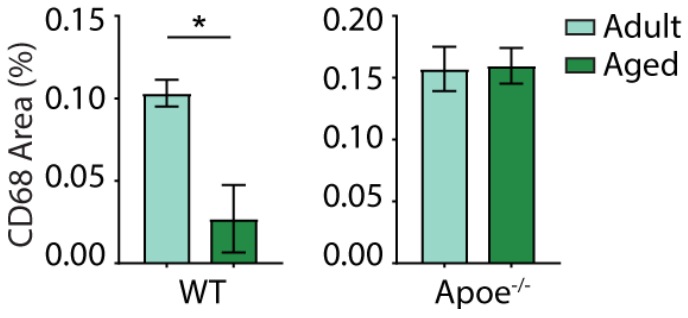

Figure 37. Quantification of Immune Cells in NGs during Ageing. Quantification of CD68^{+} macrophages / monocytes in both WT and *Apoe*$^{-/-}$ mice during ageing, 4 adult WT and *Apoe*$^{-/-}$ mice, 3 aged WT and *Apoe*$^{-/-}$ mice, a minimum of 6 sections per mouse were used for the analyses. Data represent means per mouse ± SEM; two-tailed unpaired Student´s t-test. *P < 0.05.

3.6 Pharmacological Depletion of TRPV1 in Sensory Neurons

We observed increased density of $CGRP^+$ and $TRPV1^+$ sensory axons in the plaque-laden aortic adventitia of both adult and aged *Apoe*$^{-/-}$ mice. Also, CGRP neuropeptide levels were increased in atherosclerotic aorta segments compared to age-matched WT mice. We next examined the functional impact of peripheral sensory innervation in atherosclerosis. As described in the introduction section, there are two broadly used chemicals for the depletion of TRPV1 in sensory neurons: capsaicin and RTX. We employed 3 pharmacological approaches using TRPV1-agonists to deplete TRPV1 in sensory neurons in the PNS: short-term capsaicin, short-term RTX, and long-term RTX treatment (see below).

3.6.1 Short-term Capsaicin Treatment

Apoe$^{-/-}$ mice aged at 28 wks were s.c. injected with capsaicin for three days with escalating doses (Fig 38 A). In the pilot experiments, all mice were treated under anesthesia with isoflurane inhalation[144]. But this treatment was associated with a severe mortality rate of 60% within 12 hours after capsaicin injection (Fig 38 B, capsaicin A). Two possibilities were considered: 1) capsaicin caused an immediate and intense irritation in mice, including pain and pulmonary edema; 2) inhalation anesthesia was unstable and short-lasting which aggravated the side effects of capsaicin. Pulmonary edema has been reported to be the main cause of high mortality due to capsaicin injection[160]. To ensure the efficiency of anesthesia, we changed from inhalation anesthesia to intraperitoneal injection anesthesia with ketamine/xylene. The injection dose of ketamine/xylene was controlled to ensure the general anesthesia lasted 1-1.5 hours to avoid deep anaesthesia and acute pain reactions indicated by arching the body or stress jumping. To reduce capsaicin-induced pulmonary edema, the drinking water was removed 3 hours prior to injection and 90% oxygen in an airtight recovery chamer was supplied for 2 hours after injection. Capsaicin injection alone was known to cause a 2-3°C decrease in body temperature[79], but we found that this condition was exacerbated by the high flux of oxygen in the recovery chamber, resulting in another main possible reason of death. Therefore, during wakeup, mice were rested on warming plate at 37°C to maintain the body core temperature. With the new protocol, more mice survived (Fig 38 B, capsaicin B). But it was still intolerable with a mortality rate at 40% in the capsaicin group. Most deaths happened on day 1 and day 2 (50 mg/kg) injection (Fig 38 B, red arrow).

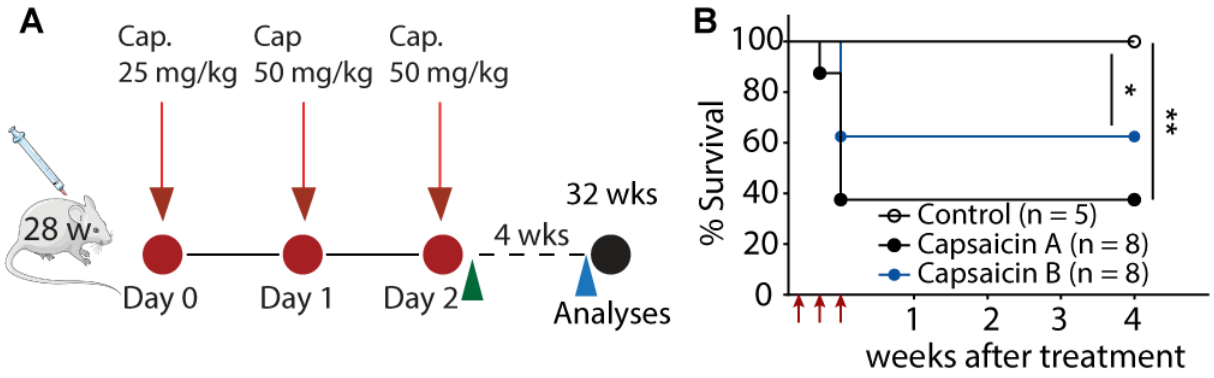

Figure 38. Short-term Capsaicin Treatment in Adult Mice. (A) Capsaicin treatment was established in *Apoe*$^{-/-}$ male mice aged at 28 wks. The treated group was injected s.c. daily with capsaicin (25, 50, and 50 mg/kg). The control group received the same dose of vehicle (10% ethanol and 10% Tween 80 in normal saline). Mice were fed with a normal diet and rested for 4 wks before sacrifice. Green arrow indicates the behavioral test 24 hours after the third injection. Blue arrow indicates blood sampling through the tail vein 2 days before sacrifice. (B) Survival curves of vehicle-treated mice (control, n = 5), capsaicin-treated mice in pilot experiment (capsaicin A, n = 8), capsaicin-treated mice with new protocol (capsaicin B, n = 8). Red arrows indicate capsaicin / vehicle injection time points. Log-rank (Mantel–Cox) test; *P < 0.05, **P < 0.01.

3.6.2 Short-term RTX Treatment

RTX is a functional analog of capsaicin but with a higher affinity than capsaicin[79]. Moreover, mice show a better tolerance to RTX compared to capsaicin: e.g. unlike capsaicin, RTX treatment does not induce severe and lethal pulmonary edema[80]. Recently, RTX-induced TRPV1^{+} sensory neuron treatment has been used in different diseases to investigate the potential role of sensory neuron innervation[92,95,96,130,139,184]. Given the high mortality rate caused by capsaicin, we established a short-term RTX treatment protocol in *Apoe*$^{-/-}$ male mice.

Apoe$^{-/-}$ mice aged at 28 wks were s.c. injected with RTX for three days with escalating doses of 30 (day 0), 70 (day 1), and 100 µg/kg (day 2) as shown in Fig. 39 A. Prior to injection, mice were removed from drinking water for 3 hours and anaesthetized with ketamine/xylene. To avoid incomplete absorption and local inflammation caused by repeated injection at one site, injections were conducted on the neck on day 0, on the right ventral side on day 1, and on the left ventral side on day 2. After injection, mice were given 90% oxygen in an airtight chamber for 2 hours. RTX, as capsaicin, has been reported to cause a drop in body temperature, which, however, is transient and returns back to normal levels after 3 hours[79]. Therefore, mice were regularly inspected twice a day to ensure that body temperature was at normal levels, one time immediately after RTX injection and another time 3 hours after

injection. With this RTX injection protocol, mortality was significantly reduced to 15% (Fig 39 B).

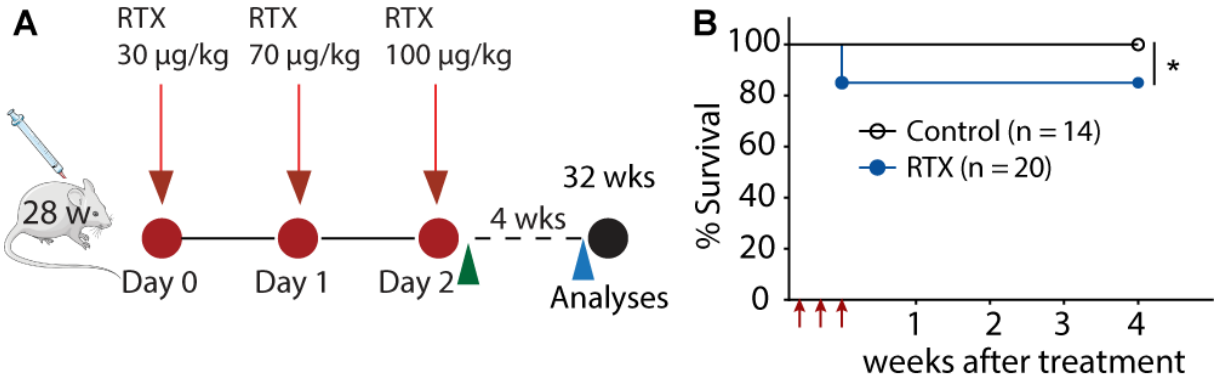

Figure 39. Short-term RTX Treatment in Adult Mice. (A) RTX treatment was established from 28 wks. The treated group was injected s.c. daily with three escalating doses of RTX (30, 70, and 100 µg/kg). The control group received the same amount of vehicle (2% DMSO with 0.15% Tween 80 in PBS). Mice were fed with a normal diet and rested for 4 wks before sacrifice. Green arrow indicates the behavioral test 24 hours after the third injection. Blue arrow indicates blood sampling through the tail vein 2 days before sacrifice. (B) Survival curves of vehicle-treated mice (control, n = 14), RTX-treated mice (n = 20). Red arrows indicate RTX / vehicle injection time points. Log-rank (Mantel–Cox) test; *P < 0.05.

To confirm successful establishment of RTX treatment, behavioral tests were performed 24 hours after the third injection, including an eye-wiping test and a hot-plate test (Fig. 40). We found that ablation of TRPV1 reduced the sensitivity of mice to a noxious chemical stimulus with a significantly reduced number of eyewipes from 18.8 ± 1.438 to 7.44 ± 1.203 (Fig. 40 A). TRPV1 ablation also reduced the sensitivity of mice to noxious heat (52°C) with a significantly prolonged latency to react to a thermal challenge from 15.71 ± 1.085 seconds to 56.30 ± 2.150 seconds (Fig. 40 B).

To confirm successful establishment of RTX treatment, the thoracic DRGs from the RTX and control groups were collected and sectioned to examine TRPV1 expression. Aortic roots were also collected and sectioned to observe changes of sensory innervation of the arterial wall. IF staining was done for TRPV1$^+$, CGRP$^+$, and NeuN$^+$ neuronal cell bodies in DRGs and for TRPV1$^+$ axons in aortic roots.

In DRGs, a CGRP antibody was used as a positive control since CGRP is expressed by but not limited to TRPV1$^+$ neurons[92]. In aortic root, TRPV1 was used for the TRPV1$^+$ sensory

axons in the adventitia. In DRGs, we found RTX treatment sharply reduced the percentage of TRPV1$^+$ neurons from 39.16 ± 2.428 to almost 0 (Fig. 41 C); reduced the percentage of CGRP$^+$ neurons, but not as sharply as TRPV1, from 33.89 ± 2.249 to 18.89 ± 1.368 (Fig. 41 D) as expected; the density of NeuN$^+$ neurons was reduced from 933.20 ± 57.93 to 556.30 ± 21.91 (Fig. 41 E), indicating that RTX treatment also involved deaths of the TRPV1-expressing neurons. In the aortic root, an almost complete depletion of TRPV1$^+$ axons in the adventitia of the aortic root was observed (Fig. 42). The data in DRGs together with the data on aortic roots showed that RTX treatment depletes both TRPV1-expressing sensory neurons and the TRPV1$^+$ axons, but precisely how many neurons died after RTX treatment remains to be determined. Using CGRP as a parameter indicated that a significant portion of TRPV1 neurons were eliminated. Yet, both the immunofluorescence and the behavioral results confirmed the successful establishment of RTX-mediated treatment in adult *Apoe*$^{-/-}$ mice.

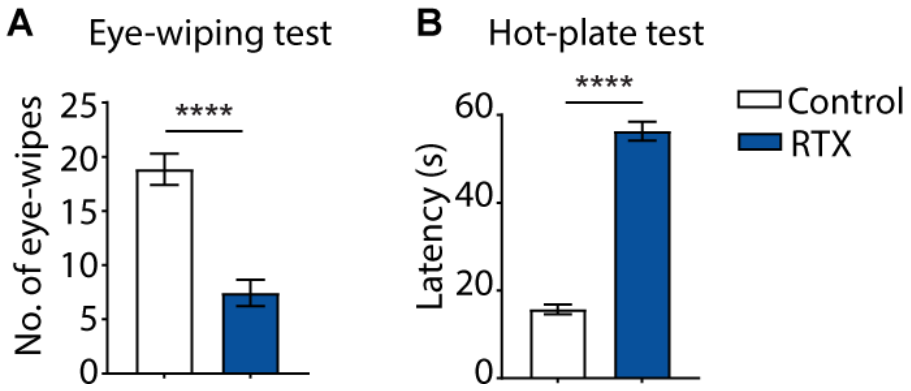

Figure 40. Pharmacological TRPV1 Ablation Led to Reduced Sensitivity to Noxious Stimuli. Vehicle treated (n = 7) or RTX-treated mice (n = 9) were assayed for the sensitivity to the noxious chemical stimuli (A) and noxious heat (B). (A) The sensitivity to chemical stimuli was recorded as the number of eye-wipes to 1% NH_4OH in 30 seconds. (B) The sensitivity to noxious heat was recorded as the latency of hindpaw lifting/licking/flinching following exposure to the hot plate set at 52°C was significantly delayed. Two-tailed unpaired Student´s t-test; data represent means per mouse ± SEM; ****P < 0.0001.

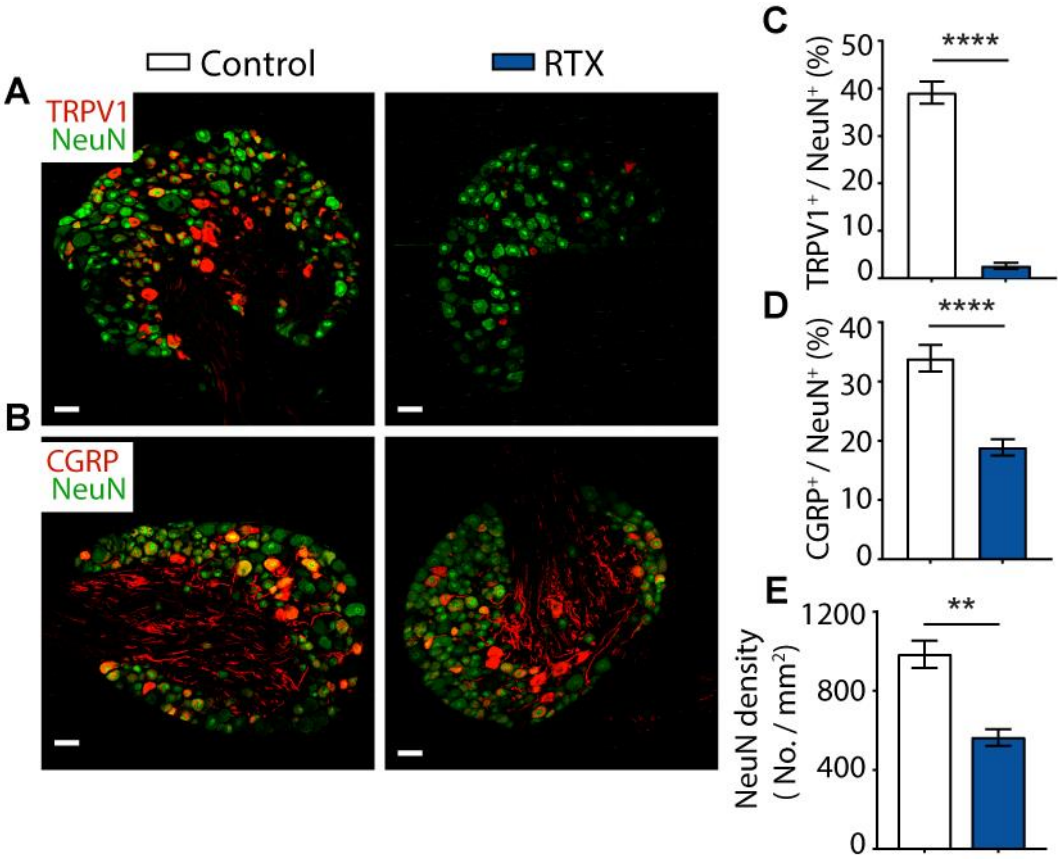

Figure 41. Ablation of TRPV1 after RTX Treatment. Immunofluorescence images and quantification shows the ablation of (A) TRPV1 and (B) CGRP in thoracic DRG (T1-T13). (C, D) TRPV1$^+$ and CGRP $^+$ neurons were quantified per NeuN$^+$ neurons. (E) NeuN$^+$ neurons were quantified as the number per DRG area. Data were analyzed in vehicle-treated (n = 7) or RTX-treated mice (n = 9) mice. A minimum of 10 sections for DRGs and 3 sections for aortic root were used per mouse for the quantification. Two-tailed unpaired Student´s t-test; data represent means per mouse ± SEM; ****P < 0.0001. Scale bar: 50 µm.

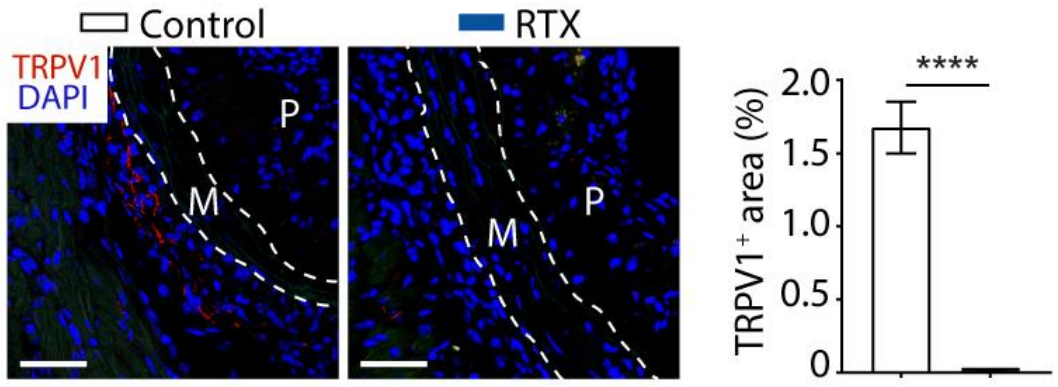

Figure 42. Ablation of TRPV1$^+$ Axons after RTX Treatment. Immunofluorescence images show TRPV1$^+$ axons in the control (n = 7) and RTX- (n = 9) treated mice determined in the aortic root. A minimum of 3 sections per mouse were used for the quantification. The area fraction was quantified as the TRPV1$^+$ area per

adventitia area. Data represents means per mouse ± SEM; two-tailed unpaired Student´s t-test. ****P < 0.0001. Scale bar: 50 µm. Dashed lines demarcate the media. M: media. P: plaque.

3.6.3 Long-term RTX Treatment

Given that atherosclerosis is a chronic progressive and slowly developing inflammatory disease, we established long-term RTX treatment to assess the impact of RTX on plaque growth. 8-weeks old male *Apoe*$^{-/-}$ mice were randomly divided into two groups to receive vehicle or RTX treatment, respectively. Mice were s.c. injected on three consecutive days with increasing doses 30 (day 0), 70 (day 1), and 100 µg/kg (day 2) or the same dose of vehicle as described in the short-term treatment protocol (Fig. 39 A and Fig. 43 A box1). Mice were then given repeated injections of 100 µg/kg RTX or vehicle every 4 wks (Fig. 43). To ensure survival, all mice were anaesthetized and maintained using the same protocol established for short-term RTX treatment. Death was observed during the repeated injection in both control and RTX groups but was limited to a relatively low mortality rate at the end of treatment, i.e. 20% in the control group and 30% in the RTX group (Fig. 43 B). This data is consistent with the interpretation that the majority of deaths occurred due to the anaesthesia and recovery periods within 24 hours but that RTX was also involved.

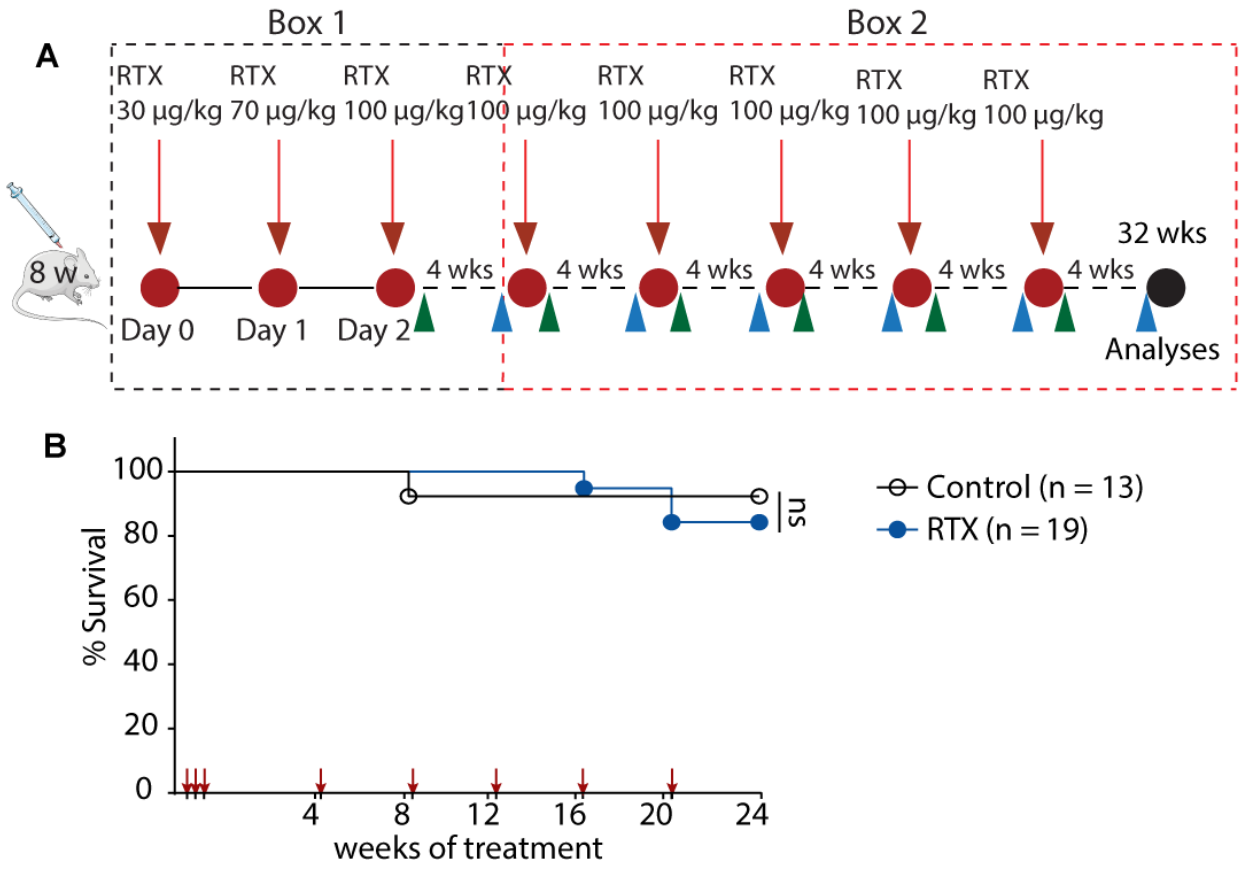

Figure 43. Long-term RTX Treatment Protocol in Adult Mice. Long-term RTX treatment was established

in young *Apoe*$^{-/-}$ mice at 8 wks. (Box 1) The treated group was injected s.c. daily with three escalating doses of RTX (30, 70, and 100 μg/kg). (Box 2) Mice were given repeated injection with a dose of 100 μg/kg every 4 wks after the three injections in Box1. Mice were rested for 4 wks after the last injection and sacrificed at 32 wks. The control group received the same dose of vehicle (2% DMSO with 0.15% Tween 80 in PBS). Green arrow indicates behavioral tests 24 hours after the injection. Blue arrow indicated blood sampling through tail vein 2 days before the injection or sacrifice. (B) Survival curves of vehicle-treated mice (control, n = 13), RTX-treated mice (n = 19). Red arrows indicate capsaicin / vehicle injection time points. Log-rank (Mantel–Cox) test; ns, not significant.

To confirm the successful establishment of long-term RTX treatment, behavioral tests were done 24 hours after the three consecutive injections every 24 hours after each repeated injection (Fig. 43 green arrow). The number of eyewipes to noxious chemical stimuli was significantly and consistently reduced after RTX treatment (Fig. 44 A), and the sensitivity to noxious heat was decreased (Fig. 44 B). The thoracic DRGs were also collected on sacrifice and stained for neuronal subpopulations. We found a dramatic decrease in TRPV1^{+} expression and a significant reduction in CGRP^{+} expression (Fig. 44 C). We also analyzed the number of total neurons as the NeuN^{+} cell bodies and found a significant decrease in the number of total neurons in DRGs (Fig. 44 D). Aortic root was also collected and stained for the depletion of axons. Almost complete ablation of TRPV1^{+} axons in the adventitia of the aortic root was noted (Fig. 44 E). All these data confirmed the successful establishment of long-term RTX treatment in young *Apoe*$^{-/-}$ mice.

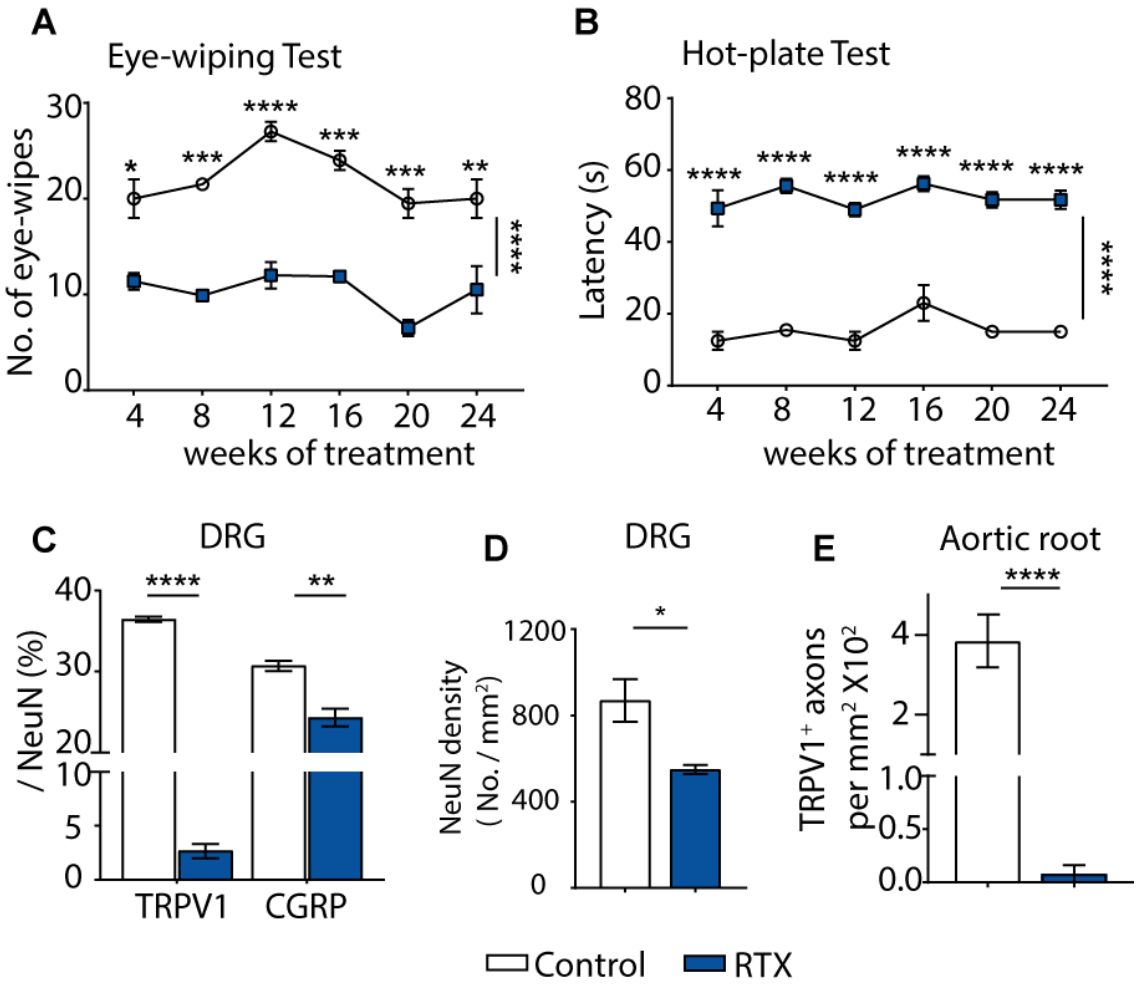

Figure 44. Long-term RTX Treatment in Adult *Apoe*$^{-/-}$ Mice. (A) Long-term RTX treatment led to reduced sensitivity to noxious chemical stimuli. The number of eye-wipes was counted within 30 seconds at 24 h after the injection. (B) Long-term RTX treatment led to reduced sensitivity to noxious heat. The latency to the heat response was counted within 60 seconds at 24 h after the injection. The X axes of (A) and (B) indicate the age of mice at the time of behavioral test. (C) The percentage of TRPV1$^+$ and CGRP$^+$ neurons from NeuN$^+$ total neurons in thoracic DRGs was reduced after the RTX treatment. (D) Total neurons in thoracic DRGs was recorded as the density of NeuN$^+$ neurons, control = 4, RTX = 4. (E) RTX treatment depleted the TRPV1$^+$ in axons in the adventitia. Control (n = 10) and RTX-treated mice (n = 14) were assayed for the specificity. Data represent means per mouse ± SEM; statistical analyses (A, B) by two-way ANOVA with Bonferroni's post hoc test for multiple comparisons, (C-E) two-tailed unpaired Student´s t-test. *P < 0.05, **P < 0.01, ***P < 0.001, ****P < 0.0001.

3.7 Short-term RTX Treatment in Adult *Apoe*$^{-/-}$ Mice

3.7.1 Effects of Short-term RTX Treatment on Physiological Parameters

Systematic deletion of TRPV1 by RTX treatment caused changes in various physiological parameters, including the body temperature[185], breathing features (like in lethal pulmonary edema)[79] and body weight[186]. To monitor the effect of RTX treatment on physiological

parameters in our experimental system, body weight was determined on the day of sacrifice. We found that RTX treatment did not change body weight (Fig. 45 A). Tissues/organs were also collected, including spleen, liver, lung, kidney (left), heart, gonadal adipose tissue (white adipose tissue) and brown adipose tissue from the back. The weight of tissue/organs was calculated as a ratio of the body weight of each mouse. Only the spleen weight/body weight was found to be significantly reduced after RTX treatment, but no other tissues or organs were affected (Fig. 45 B and C,). Blood was also collected to determine hematocrit parameters. Although there was a reduction in the absolute number of leukocytes and their subtypes, including lymphocytes, monocytes and granulocytes, the data did not reach statistical significance due to the large variability in the mouse cohort (Fig. 46 A). Plasma was collected to determine the effect of RTX treatment on lipid levels (Fig. 46 B). We found no effect of RTX treatment on blood lipid levels, including high density lipoprotein (HDL), LDL, very low-density lipoprotein (VLDL) and total cholesterol levels.

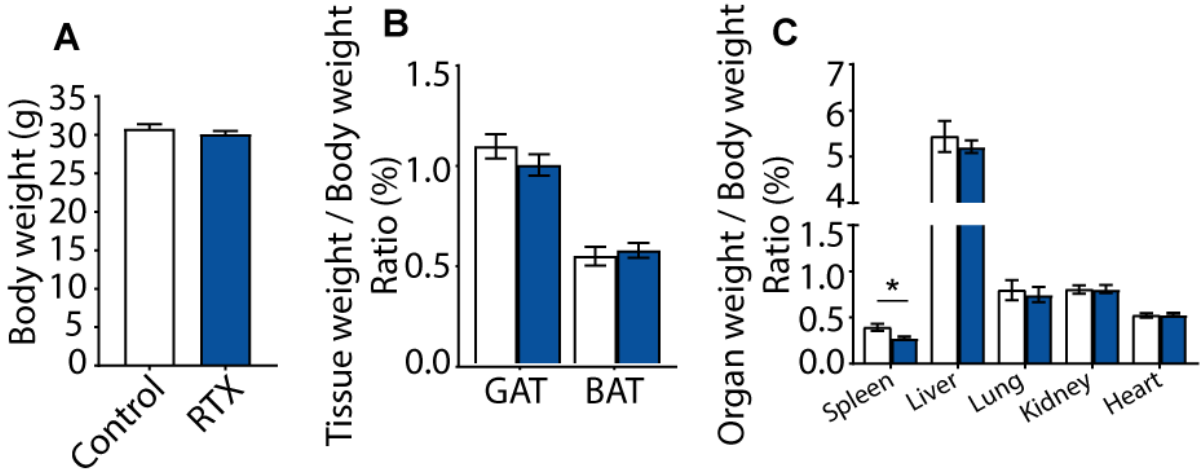

Figure 45. Body Weight and Relative Spleen Weight in RTX-treated Adult Mice. (A) The body weight was recorded on the day of sacrifice. (B, C) Tissue/organ weight was calculated as the ratio per total body weight. Statistical analyses by two-tailed unpaired Student´s t-test (*P < 0.05). Data was analyzed from vehicle-treated (n = 7) or RTX-treated mice (n = 9) mice. Two-tailed unpaired Student´s t-test; data represent means per mouse ± SEM; GAT: gonadal adipose tissue; BAT: brown adipose tissue.

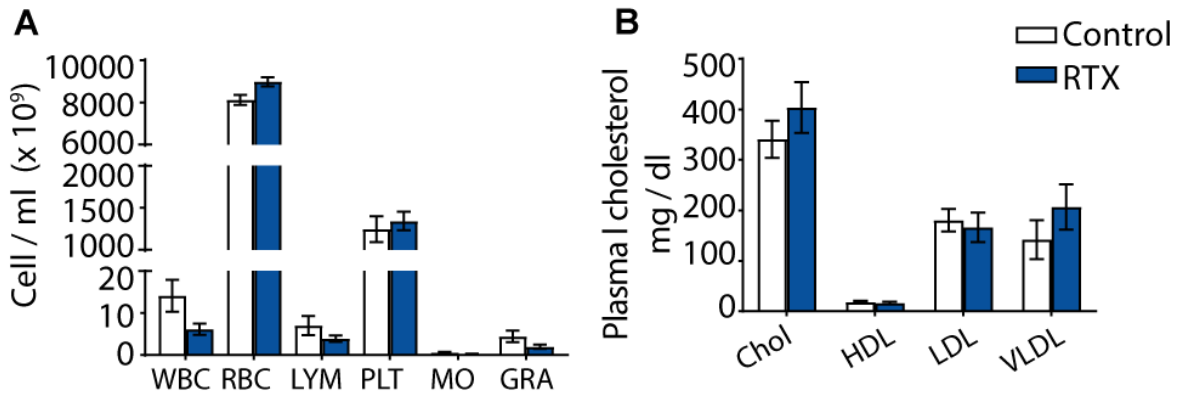

Figure 46. No changes in Haematological Parameters or Blood Lipids by RTX Treatment. (A) Blood samples were taken through heart puncture under anaesthesia for blood leukocyte counts.The total number of white blood cells (WBC), red blood cells (RBC), platelets (PLT), lymphocytes (LYM), monocytes (MO) and granulocytes (GRA) were determined. (B) Concentration of plasma lipids. Blood was taken one day before the sacrifice through tail vein. Data was analyzed from vehicle-treated (n = 7) or RTX-treated mice (n = 9) mice. Two-tailed unpaired Student´s t-test; data represent means per mouse ± SEM; HDL: high density lipoprotein; LDL: low density lipoprotein; VLDL: very low-density lipoprotein.

3.7.2 Effects of Short-term RTX Treatment on Leukocytes in SLOs

To determine the effect of RTX treatment on immune cells, the blood, spleen, inguinal LNs (iLNs), mesenteric LN (mLNs), paraaortic LNs including renal LNs (RLNs) and lumbar LNs (LLNs) were collected and examined by flow cytometry with the gating strategy for myeloid cells (Fig. 47 E) and lymphocytes (Fig. 47 B-D). The myeloid-cell population (Fig. 48 A, D, G), lymphoid-cell population (Fig. 48 B, E, H) and CD4-expressing lymphocytes (Fig. 48 C, F, I) were analyzed. All data are expressed as the percentage per total viable $CD45^+$ cells. We did not observe significant changes in the relative distribution of leukocyte subsets in blood (Fig. 48 A-C), spleen (Fig. 48 D-F) and other SLOs (not shown) between control and RTX treatment groups. In paraaortic LNs, RTX-treated mice had an increased frequency of $CD11b^+CD11c^+$ myeloid cells (Fig. 48 G), and $B220^+$ B cells, while the relative frequeny of $TCR\beta^+$ T cells decreased compared to the control group(Fig. 47 G). We also analysed the $CD8^+$ lymphocyte subtypes in blood and SLOs, including naïve T cells, effector memory T cells, central memory T cells, but found no difference between the control and RTX group (not shown).

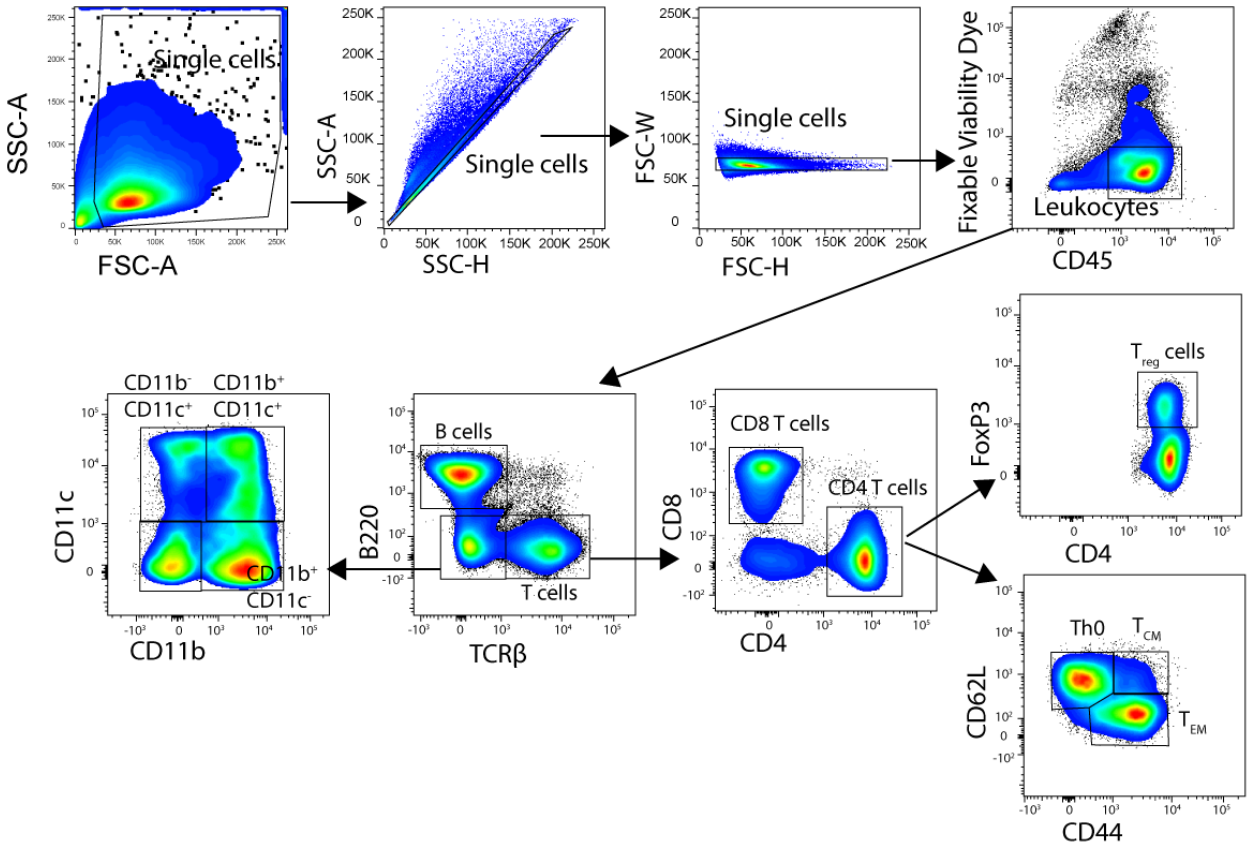

Figure 47. Flow Cytometry Gating Strategy for Immune Cells. The workflow shows the representative gating strategy of flow cytometry data from spleen after short-term RTX treatment in adult *Apoe*$^{-/-}$ mice at 32 wks. T_{reg}: regulatory T cell. Th0: naïve T cell. T_{CM}: central memory T cell. T_{EM}: effctor memory T cell.

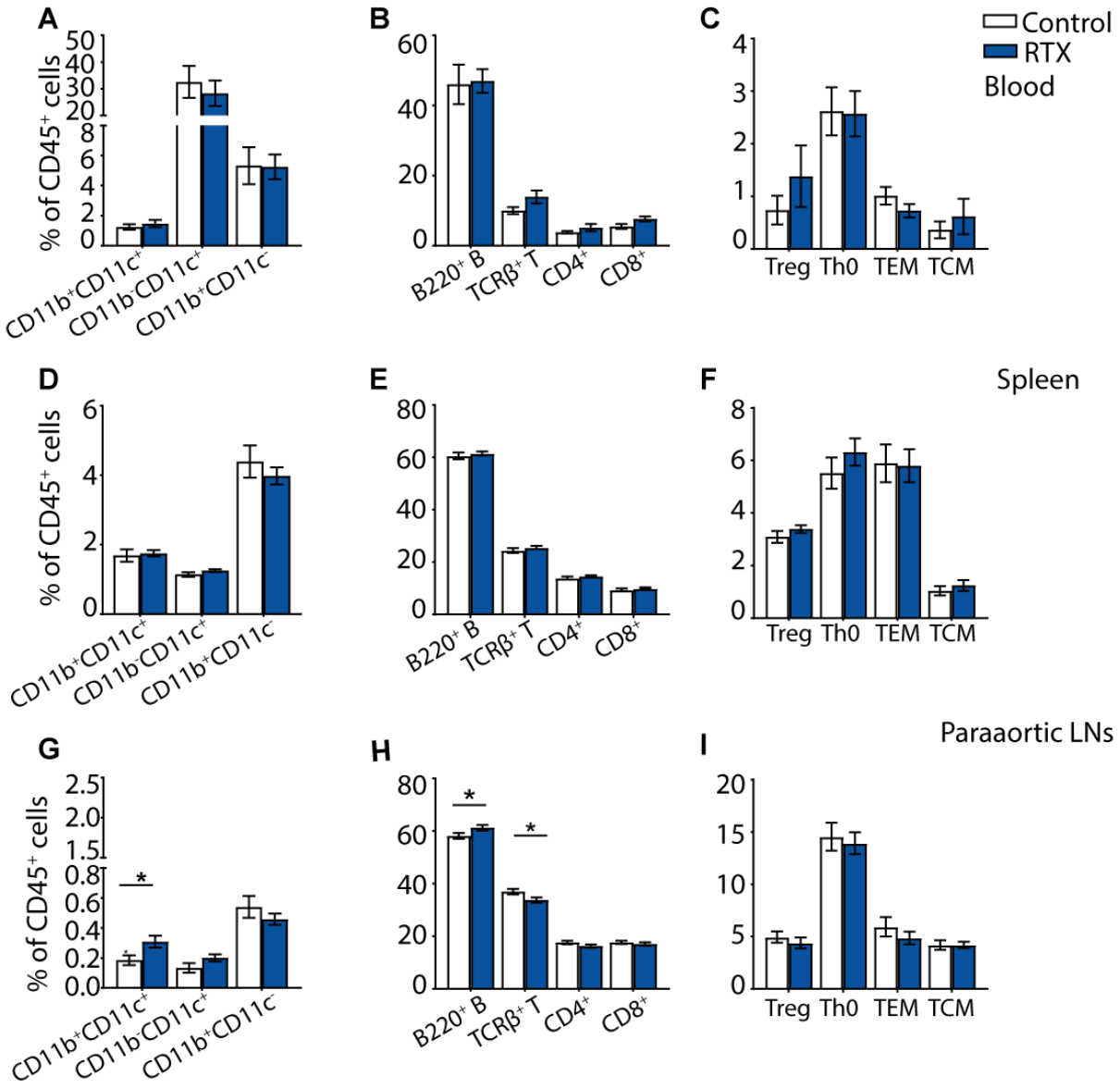

Figure 48. RTX Treatment Moderately Affected Immune Cell Subpopulations in Paraaortic LNs. Flow cytometric analysis of the B220^{-}TCRβ^{-} cell population (A, D, G), lymphocyte cell population (B, E, H) and CD4^{+} T cell population (C, F, I) from control (n = 12) and RTX-treated mice (n = 16) in blood (A-C), spleen (D-F), paraaortic LNs (G-I). Immune cells were calculated as the percentage of all CD45^{+} leukocytes. Two-tailed unpaired Student´s t-test; data represent means per mouse ± SEM; T_{reg}: regulatory T cell; Th0: naïve T cell; T_{EM}: effector memory T cell; T_{CM}: central memory T cell.

3.7.3 Effects of Short-term RTX Treatment on Atherosclerotic Progression.

To determine the potential effect of TRPV1 expression on atherosclerosis in adult *Apoe*$^{-/-}$ mice, the aortic root, the thoracic aorta including the aortic arch and descending aorta from control and RTX-treated mice were collected as described in Methods. The *en-face* staining data showed that RTX treatment had no effect on the lesion size in both aortic arch and

thoracic aorta (Fig. 49 A). Every 10th sections of aortic root and innominate artery were stained with ORO/H. ORO/H staining data showed that RTX treatment did not change the plaque size in aortic root (Fig. 50 B), but caused a significant 74.8% reduction of plaque size in innominate artery.

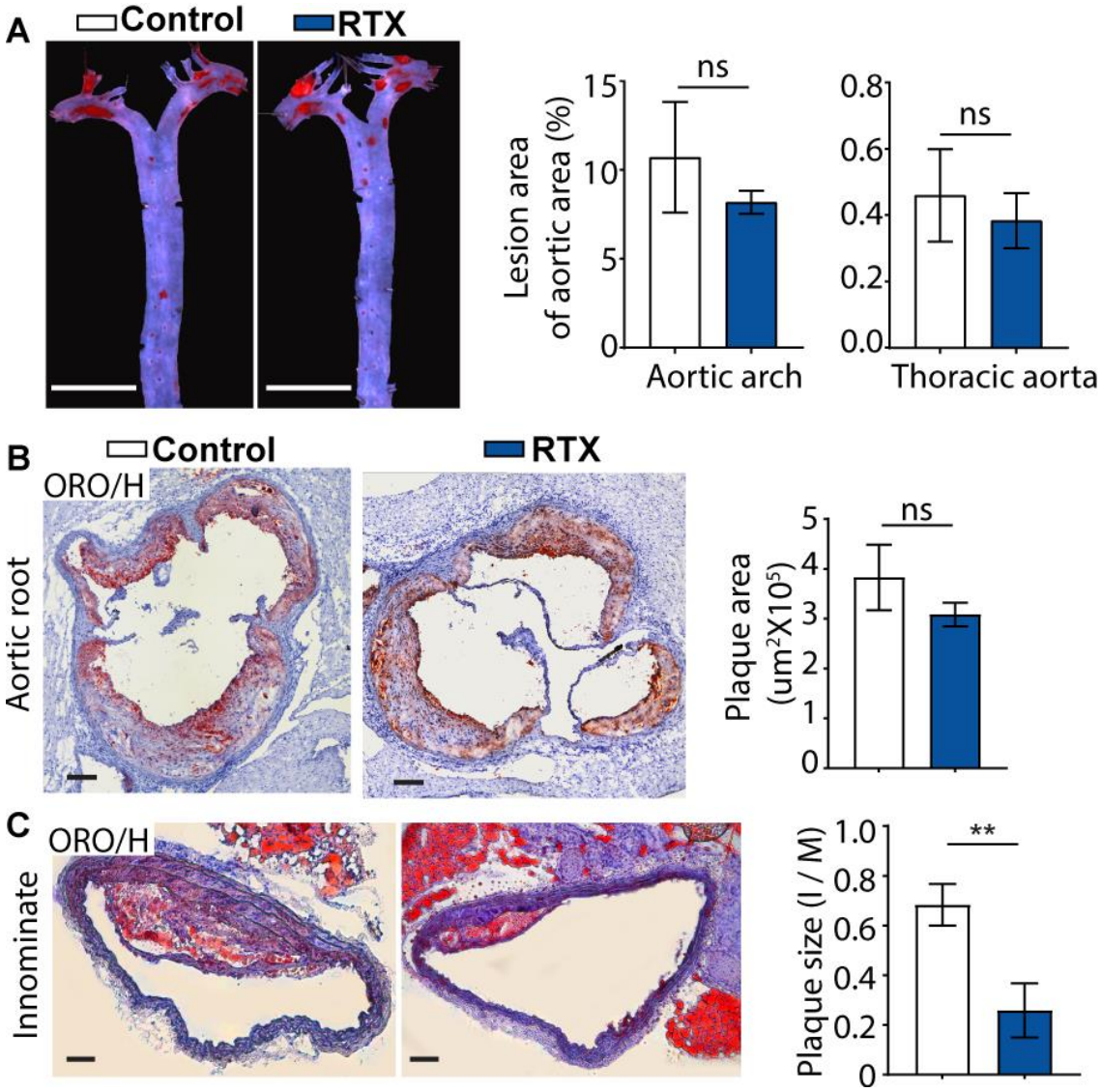

Figure 49. Short-term RTX Treatment Did not Affect Atherosclerotic Lesion Area. (A), Representative Sudan-IV *en-face* stained thoracic aorta (control = 6, RTX = 10) including the aortic arch, the branches and the descending aorta and quantification of absolute Sudan-IV-stained area as plaque areas. Statistical analyses by two-tailed unpaired Student´s t-test. Representative ORO/H-stained images in aortic roots (B, control = 10, RTX = 13) and innominate arteries (C, control = 6, RTX = 9). Plaque size in aortic roots was quantified as absolute ORO^+ area per mouse or along the distance from the aortic sinus. Plaque size in innominate artery was quantified as intima area/media area ratio (I/M). Two-tailed unpaired Student´s t-test; data represent means per mouse ± SEM; *P < 0.05, **P < 0.01, ***P < 0.001, ****P < 0.0001. Data represents means per mouse ± SEM. Scale bar (A) 0.5 cm, (B, C) 0.2 cm.

Next, the effect of short-term RTX treatment on lesion stages in aortic roots and innominate arteries was examined. In aortic root, most of the lesions were at an advanced stage in the control group, whereas RTX treatment did not cause differences in the distribution of lesion stages (Fig. 50 A and B). In innominate arteries, we found most of the lesions were at an early stage in control group. The ratio of lesion-free sections was significantly increased after RTX treatment (Fig. 50 C and D). Correspondingly, the ratio of sections at early lesion and fibroatheroma stage/advanced lesions tended to be decreased after RTX treatment, but did not reach significance. Therefore, we concluded that RTX treatment mostly affects the early, but not the advanced atherosclerotic plaque development at least during this short treatment time window of 4 weeks.

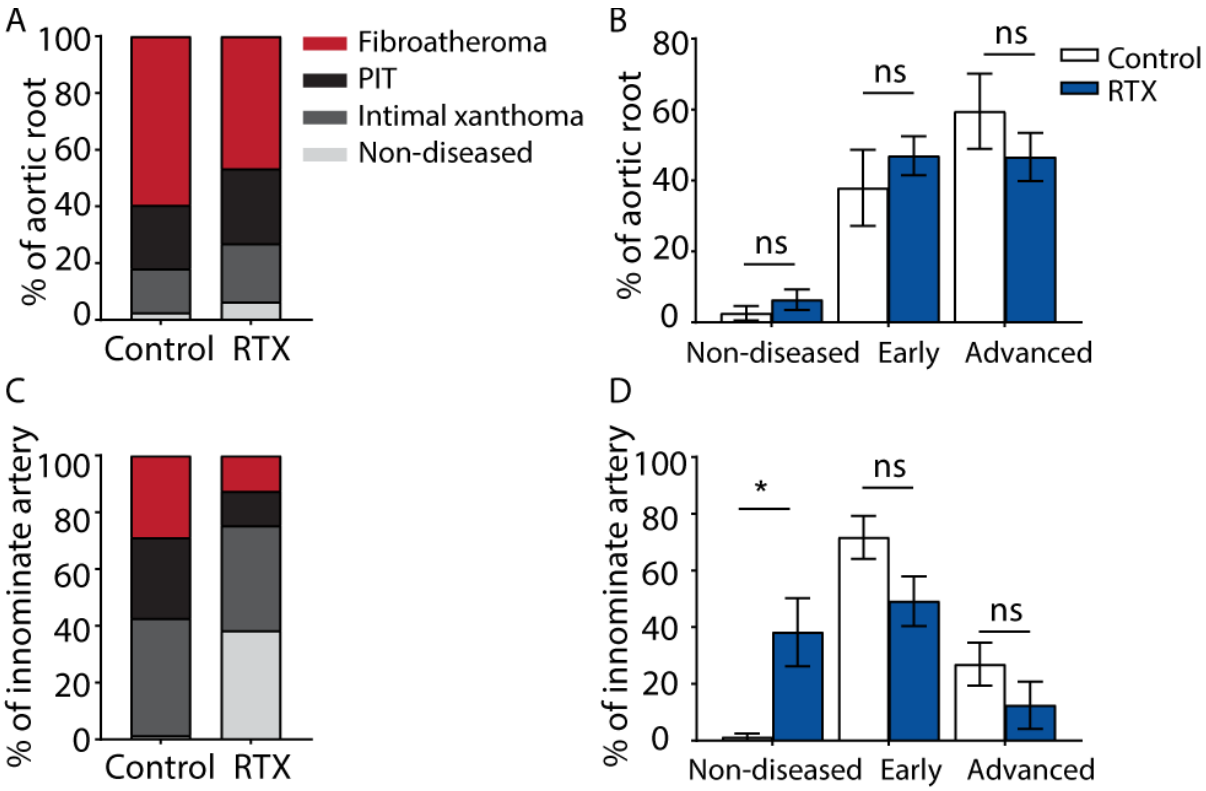

Figure 50. Effect of Short-term RTX Treatment on Atherosclerosis Progression. Lesion stages in aortic roots (A and B, control = 10, RTX = 13) and innominate arteries (C and D, control = 6, RTX = 9). Early lesion type contains intimal xanthoma and PIT. Advanced lesion type contains fibroatheroma. Statistical analyses in A and C by Chi-square test, B and D by two-way ANOVA with Bonferroni's post hoc test for multiple comparisons; data represent means per mouse ± SEM; ns, no significance. *P < 0.05. PIT: pathological intimal thickening.

We also examined the effect of short-term RTX treatment on the composition of aortic root

plaques, including macrophages, SMCs, and collagen content. No difference was found in CD68$^+$ monocytes/macrophages (Fig. 51 A) and Sirius red$^+$ collagen content (Fig. 51 C) between the control and RTX groups. However, RTX treatment caused a significant reduction in the percentage of SMA$^+$ plaque area (Fig. 51 B).

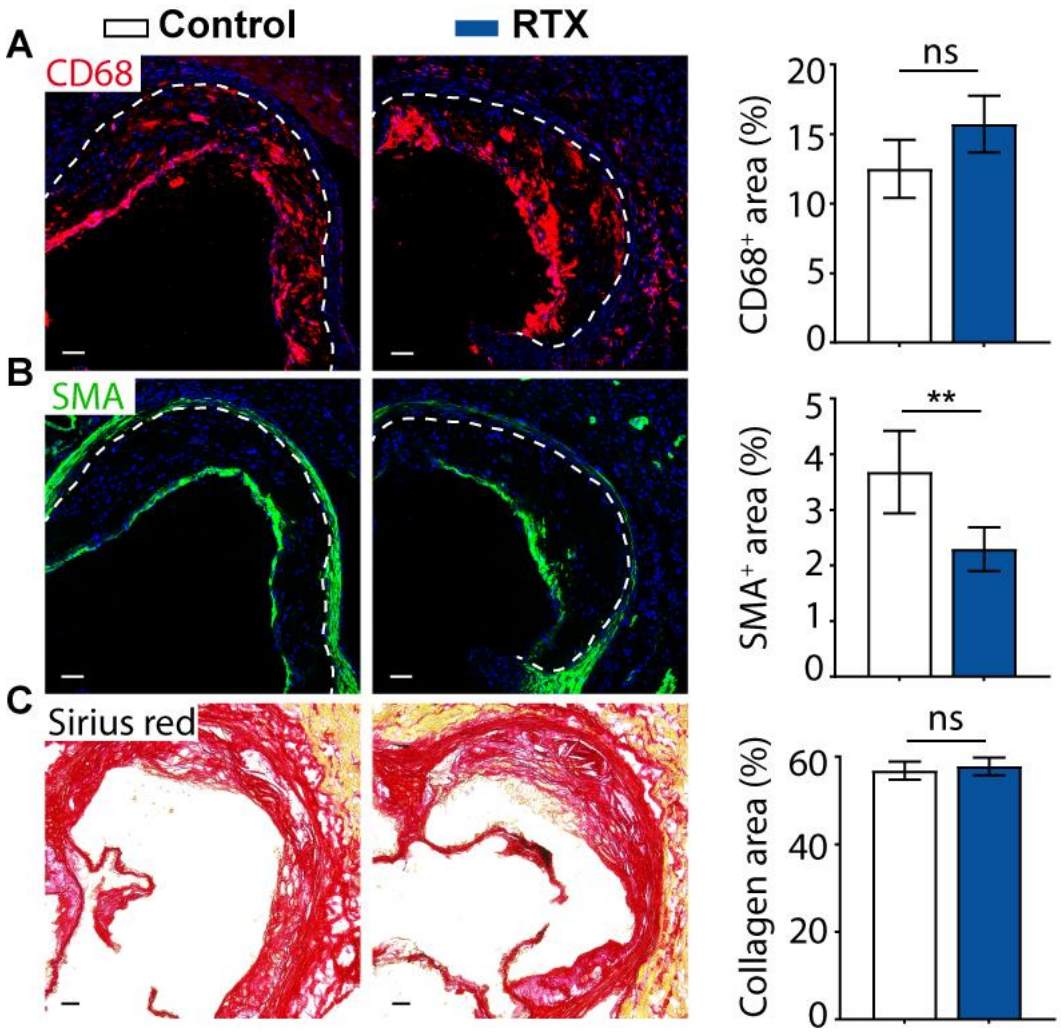

Figure 51. Short-term RTX Treatment Did not Affect Aortic Root Plaque Structure. Representative confocal images of aortic roots from control (n = 6) and RTX- (n = 9) treated mice. (A) CD68 staining for macrophages. (B) SMA staining for SMCs. (C) Sirius red staining for collagen. Dashed line indicates the inner border of the media. Data were quantified as the percentage of CD68$^+$, SMA$^+$ or Sirius red$^+$ area, respectively, per plaque area. Two-tailed unpaired Student´s t-test; data represent means per mouse ± SEM; **P < 0.01. Scale bar: 50 µm.

3.8 Long-term RTX Treatment in Adult *Apoe*$^{-/-}$ Mice

Given the chronicity and slow growth characteristics of atherosclerosis, advanced plaques in 32 wks adult *Apoe*$^{-/-}$ mice can be observed in aortic roots, while plaques developing in the

descending aorta and innominate artery are still at early stages. Short-term RTX treatment in adult mice starting at 28 wks mainly affected the plaque size in innominate artery and the thoracic aorta, but not in the aortic root. In addition, short-term RTX treatment was also tested in aged mice as a model of advanced plaque stage, but no effect on the aortic plaque size was observed (data not shown). It is conceivable that the 4 wks short-term RTX treatment may not be long enough to affect the advanced plaque development. To better clarify the question whether RTX affects atherosclerosis in a stage-dependent manner, a long-term RTX treatment experiment was performed in young *Apoe*$^{-/-}$ mice starting at the age of 8 wks.

3.8.1 Effects of Long-term RTX Treatment on Physiological Parameters

We again monitored the effect of RTX treatment in young mice on selected physiological parameters as described above for adult mice. Long-term RTX treatment showed no effect on body weight, tissue/organ weight and serum total cholesterol levels (Fig. 52 A-D).

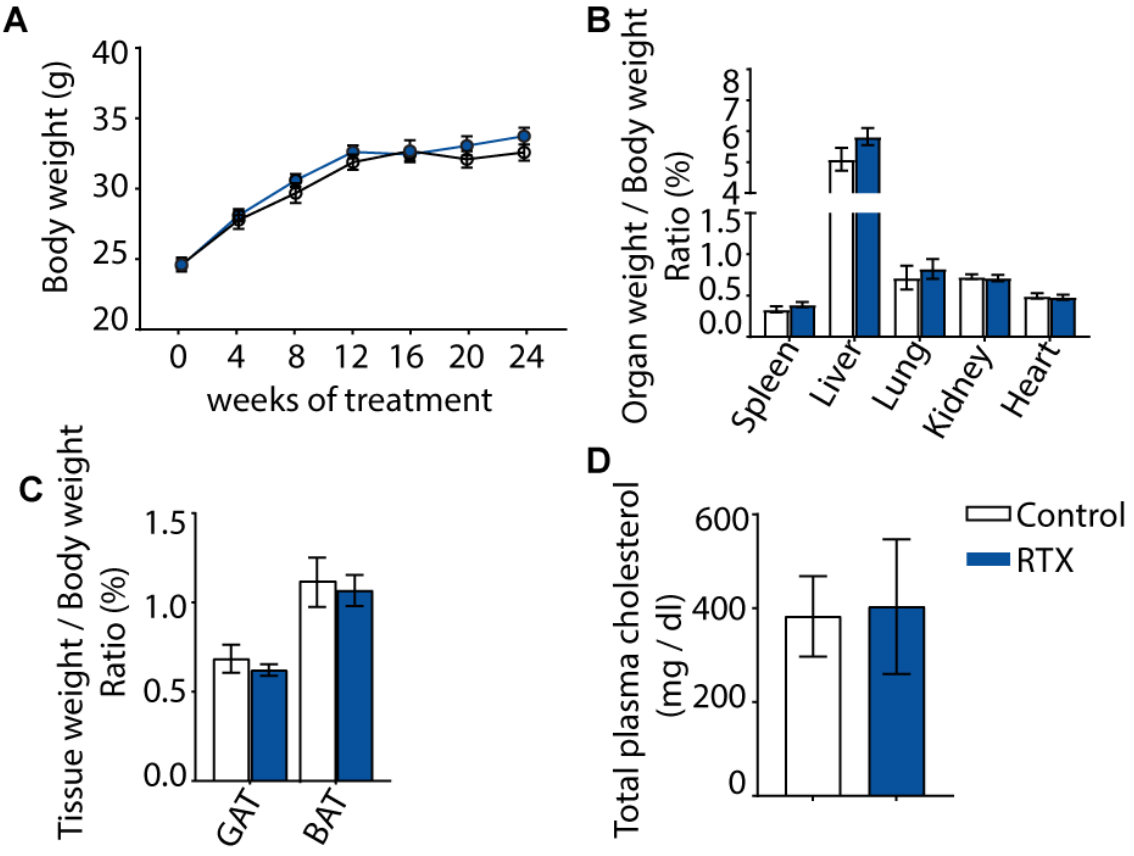

Figure 52. No Change in Body and Relative Tissue/Organ Weight or Plasma Cholesterol Levels by RTX. (A) Body weight, (B, C) organ weight normalized to body weight. (D) Total plasma cholesterol concentrations

were determined after sacrifice from control (n = 4) and RTX (n = 7) mice. Statistical analyses in A by two-way ANOVA with Bonferroni's post hoc test for multipule comparisons, in B - D by two-tailed unpaired Student´s t-test. Data represent means per mouse ± SEM. GAT: gonadal adipose tissue; BAT: brown adipose tissue.

3.8.2 Effects of Long-term RTX Treatment on Leukocytes in SLOs

To identify potential effects of long-term RTX treatment on leukocyte subsets during the progress of early atherosclerosis, blood, spleen, LNs adjacent to aortic arch, iLNs, mLNs, paraaortic LNs were collected and examined for immune cell compositions. The gating strategy for lymphoid cells is shown in Methods and Fig. 53 A. Since we found changes in myeloid cells after the short-term RTX treatment (Fig. 48 G), we established a new gating strategy to more detailed analysis of the subtypes of DCs and macrophages for the long-term treatment as shown in Methods and Fig. 54 A. We also established the gating strategy for progenitor cells in the bone marrow and spleen as shown in Methods and Fig. 55 A.

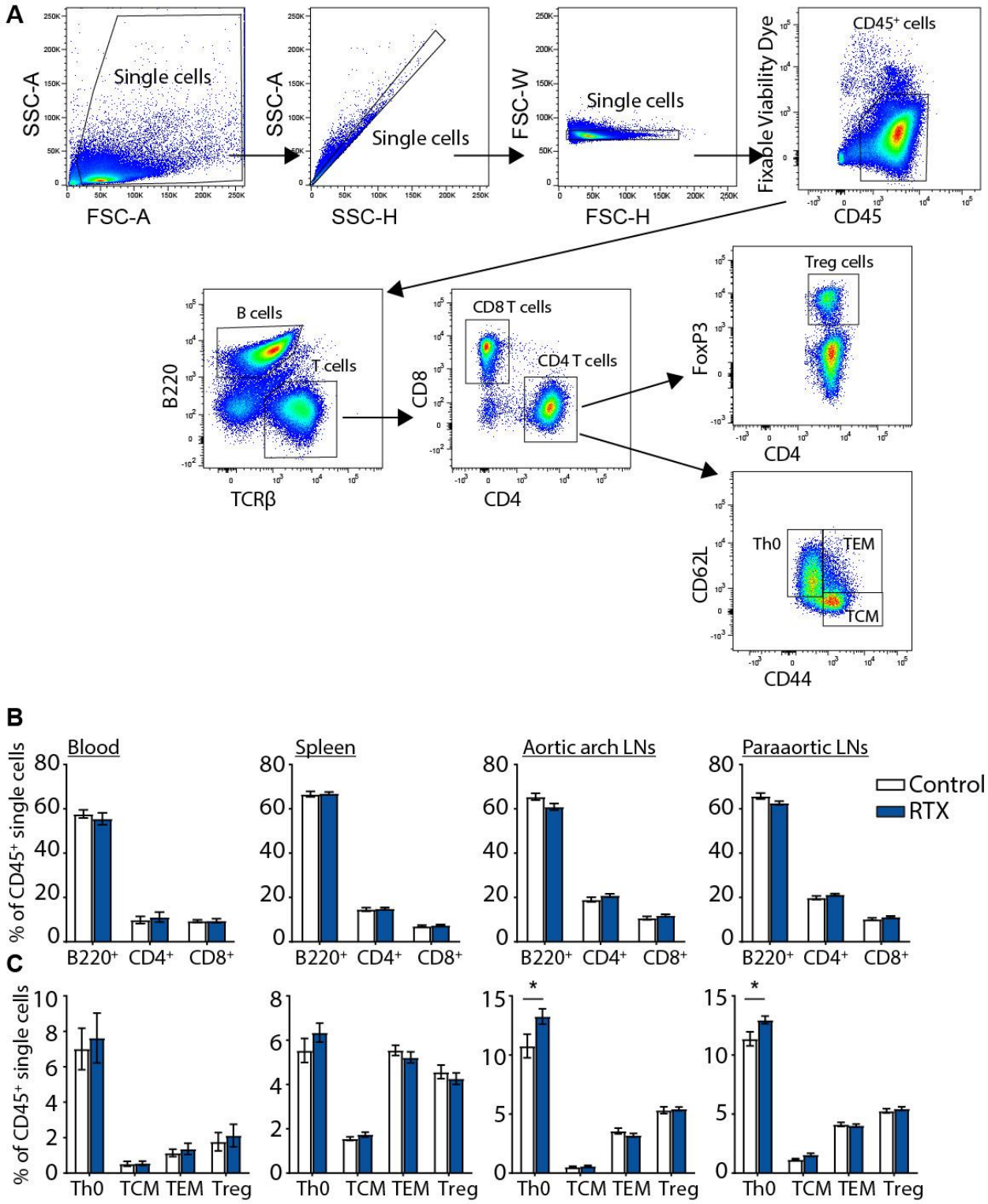

Figure 53. Long-term RTX Treatment Moderately Affected Lymphoyte Subpopulations in LNs. (A) The workflow shows the representative gating strategy of lymphocyte subpopulations in spleen for the long-term RTX treatment in adult *Apoe*$^{-/-}$ mice at 32 wks. (B) B cells, CD4$^+$ and CD8$^+$ T cells and (C) CD4$^+$ T subtypes in blood, spleen, aortic arch_LNs and the paraaortic LNs. Control n = 8, RTX n = 7. Data was quantified as the percentage of CD45$^+$ single cells. Two-tailed unpaired Student´s t-test; data represent means per mouse ± SEM; Th0: naïve T cell; T_{CM}: central memory T cell; T_{EM}: effector memory T cell; T_{reg}: regulatory T cell.

For lymphocyte subpopulations, B cells, $CD4^+$ and $CD8^+$ T cells and the $CD4^+$ T subtypes were analyzed. All data are expressed as the percentage from total $CD45^+$ cells. We found that the long-term RTX treatment mainly affects the lymphocyte subpopulations in aortic arch LNs and the paraaortic LNs (Fig. 53): the percentages of $B220^+$ B cells were significantly decreased while the $CD4^+$ T cells were increased in both the aortic arch LNs and the paraaortic LNs, but not the blood and spleen (Fig. 53 B). We further analyzed the $CD4^+$ T subtypes and found significantly increased Th0 cells in both the aortic arch LNs and the paraaortic LNs, significantly increased T_{CM} cells in paraaortic LNs, but no changes were observed in T_{EM} and T_{reg} cells (Fig. 53 C). We also quantified the $CD8^+$ T subset but found no differences between the control and RTX treatment groups. For myeloid cell subpopulations, DCs and macrophages were analyzed. All data are expressed as percentage of total $CD45^+$ single cells. RTX treatment only increased the mature DC frequencies in paraaortic LNs (Fig. 54 B). For progenitor cells, no differences were found in the subtypes after the RTX treatment in both bone marrow and spleen (Fig. 55 B). All these data suggested that the long-term RTX treatment mainly affects the lymphoid cell populations but not the myeloid cells or the progenitors but also the red cell count. In lymphoid cells, mainly $CD4^+$ T cells and its subtypes $CD4^+$ Th0 cells in the aortic arch_LNs and the paraaortic LNs are affected. These data indicated that important T cell subtypes and the red cells are affected by RTX.

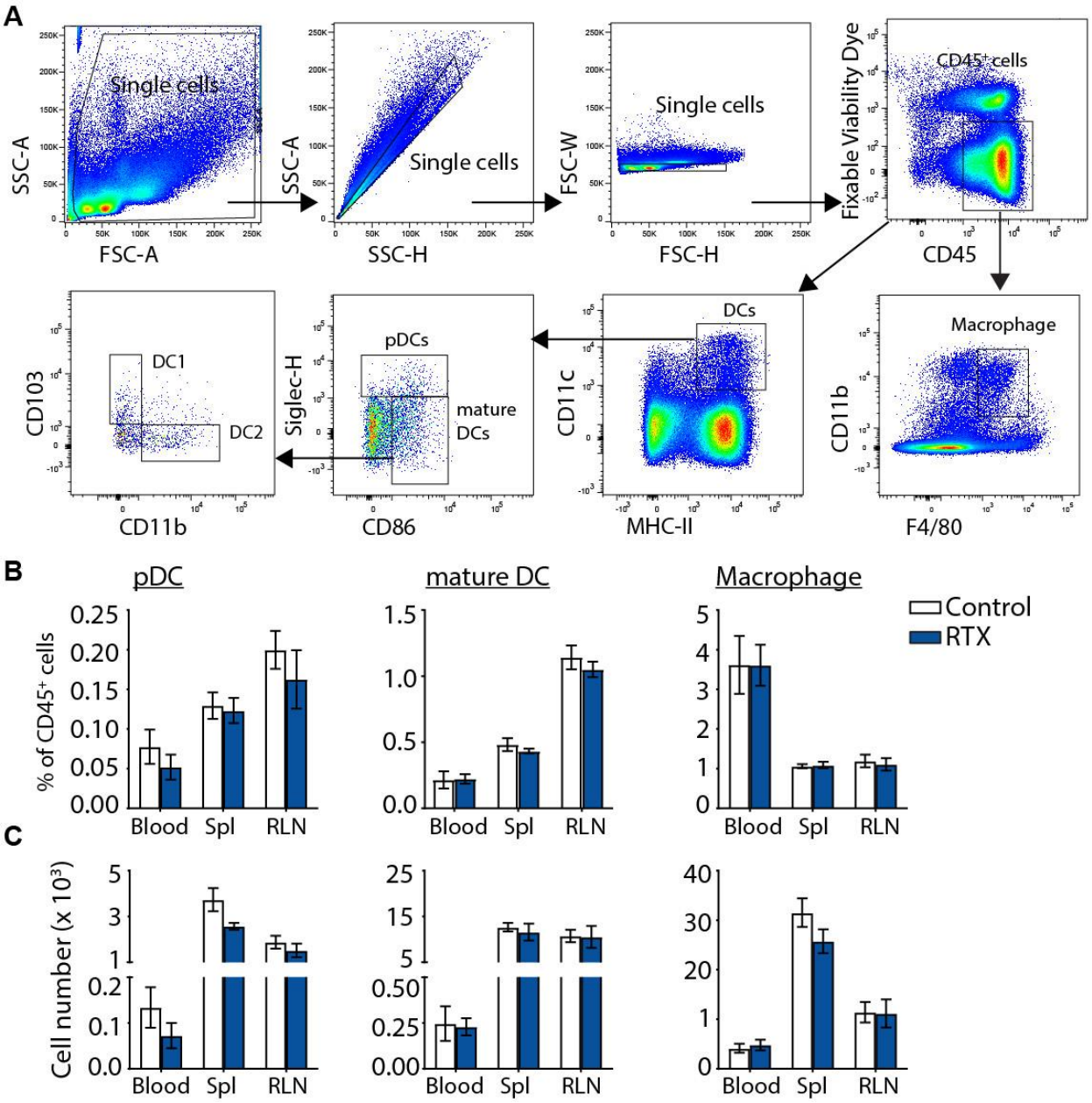

Figure 54. Long-term RTX Treatment Affected Myeloid Cell Subpopulations in Paraaortic LNs. (A) The workflow shows the gating strategy of myeloid cell subpopulations in spleen in treated mouse. (B) Shows the myeloid cells as the percentage of $CD45^+$ cells, including mature DC, pDCs and macrophages in blood, spleen, aortic arch LNs and the paraaortic LNs. (C) shows the absolute cell numbers of the populations. Control n = 8, RTX n = 7. Data was quantified as the percentage of $CD45^+$. Two-tailed unpaired Student´s t-test; data represent means per mouse ± SEM; pDC, plasmacytoid DC.

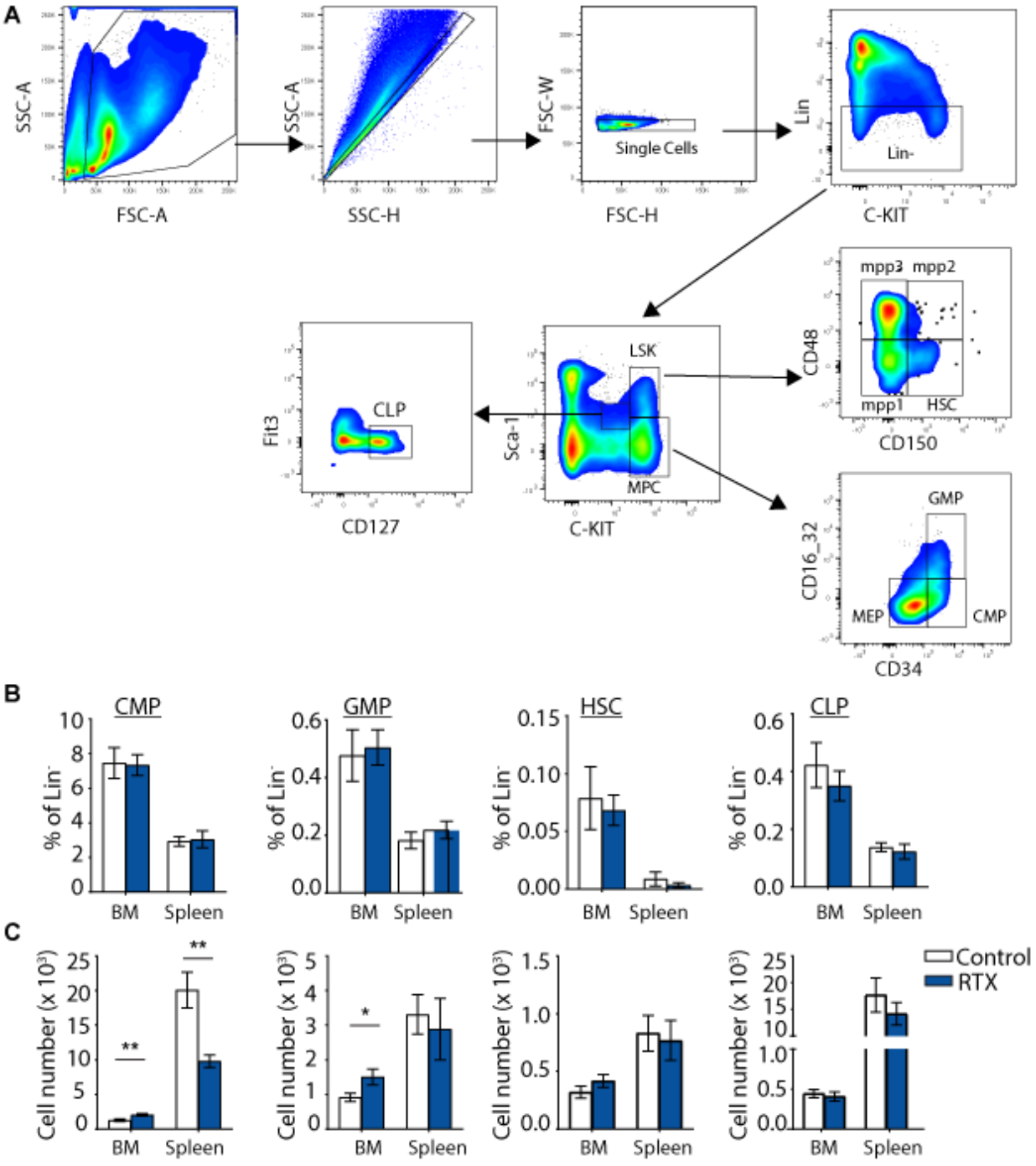

Figure 55. Long-term RTX Treatment Had no Effects on Progenitor Subpopulations. (A) The workflow shows the representative gating strategy of progenitor subpopulations in bone marrow in treated mouse. (B) Shows progenitor subpopulations as the percentage of Lin$^-$ cells, including CMP, GMP, HSC and CLP in bone marrow and spleen. (C) shows the absolute cell numbers of the subpopulations. Control n = 8, RTX n = 7. Statistical analyses by two-tailed unpaired Student´s t-test. Data represents means per mouse ± SEM. CMP, common myeloid progenitor; GMP, granulocyte-monocyte progenitor cell; HSC, haematopoietic stem cell; CLP, common lymphoid progenitors.

3.8.3 Effects of Long-term RTX Treatment on Atherosclerotic Plaque Progression

To determine effects of long-term RTX treatment on the progression of atherosclerosis, aortic roots, innominate arteries, thoracic aorta including the arch and branches from control and RTX-treated mice were collected. Long-term RTX treatment caused a significantly > 2-fold decrease in lesion area of aortic arch but no changes in the descending artery (Fig. 56 A-B). of the analysis of the innominate artery showed a 5-fold decrease in ORO/H stained plaque size after RTX treatment. It is important to note that 4 out of 7 innominate arteries from RTX group were not burdened with plaque at all, whereas all innominate arteries of vehicle-treated animals were burdened with plaques (Fig. 56 C).

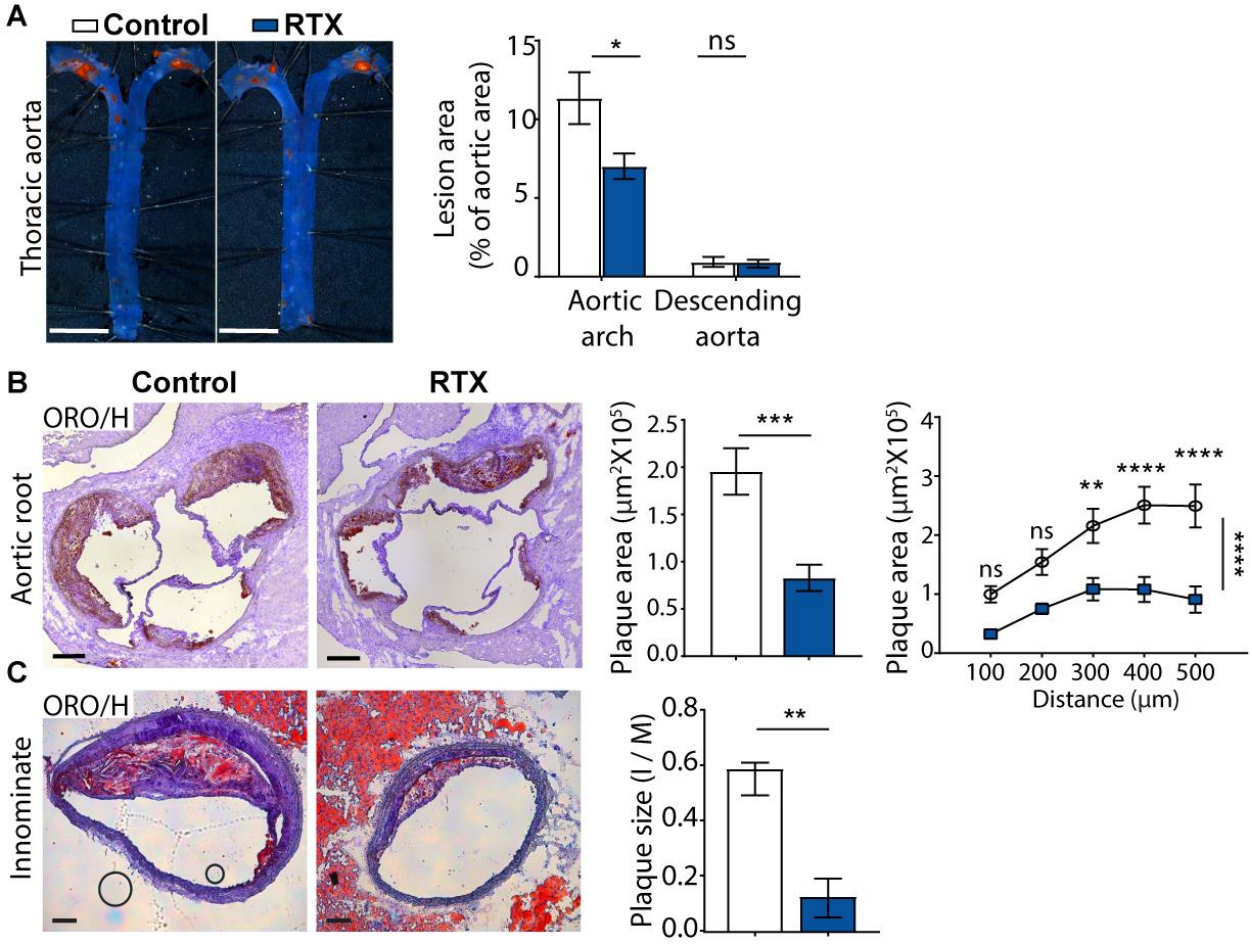

Figure 56. Long-term RTX Treatment Reduces Atherosclerotic Lesion Area. (A), Representative Sudan-IV *en-face* stained thorax aorta (contro = 12, RTX = 14) including the the aortic arch and the descending aorta Quantification of absolute Sudan-IV stained area as plaque areas. Statistical analyses by two-tailed unpaired Student´s t-test. Representative ORO/H stained images in aortic root (B, control = 12, RTX = 14) and innominate artery (C, control = 4, RTX = 7). Plaque size in serial sections of aortic root was quantified as absolute ORO⁺ area per mouse. Statistical analyses by two-tailed unpaired Student´s t-test and two-way ANOVA with Bonferroni's post hoc test for multiple comparisons. Plaque size in innominate artery was

quantified as intima area/media area ratio (I/M). *P < 0.05, **P < 0.01, ***P < 0.001, ****P < 0.0001. Data represents means per mouse ± SEM. Scale bar (A) 0.5 cm, (B, C) 0.2 cm.

In aortic roots (Fig 57. A and B), the ratio of sections without lesions was significantly increased after long-term RTX treatment, whereas the percentage of fibroatheroma stage/advanced lesions was significantly decreased. In innominate arteries (Fig 57. C and D), there was a dramatical increase of sections without any lesion after long-term RTX treatment with 54.3% compared to 1.9% in the control group. Instead, there was complete loss of sections with fibroatheroma stage/advanced lesions after long-term RTX treatment compared to 25% in the control group. All these data in aortic root and innominate artery indicated that long-term RTX treatment potently attenuated the progression of atherosclerosis.

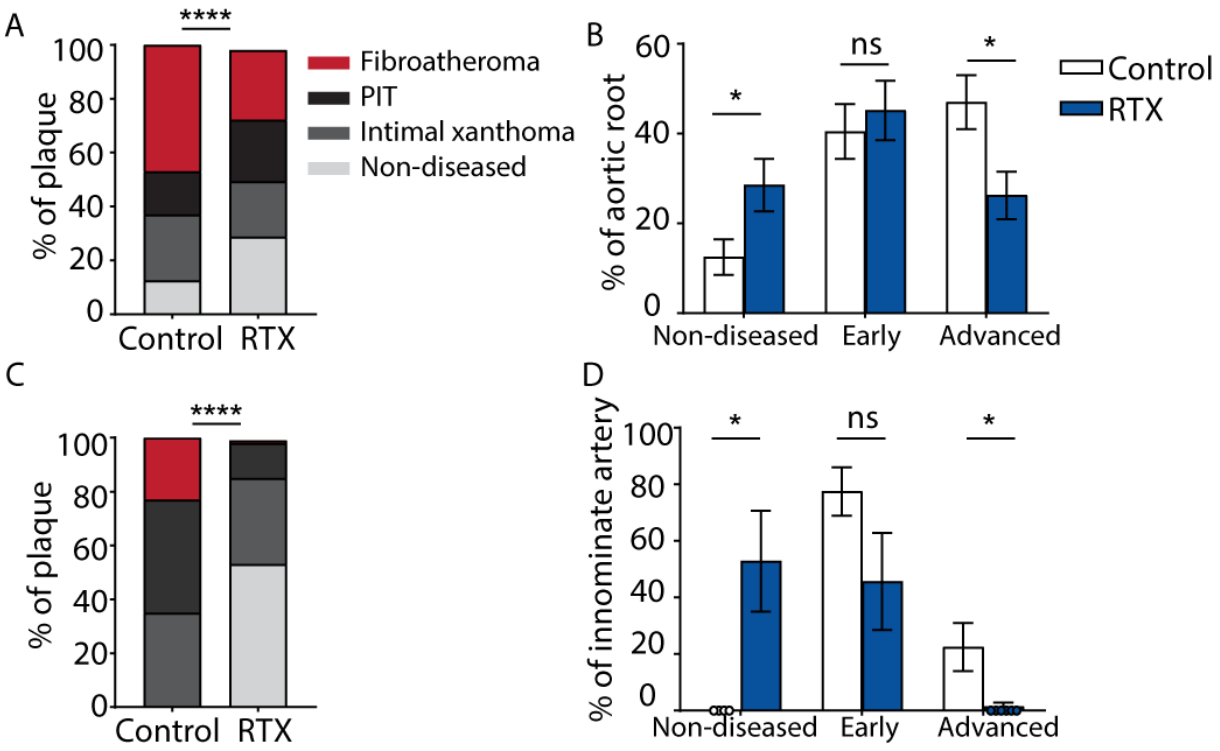

Figure 57. Long-term RTX Treatment Attenuated Atherosclerosis Progression. Lesion stages in aortic root (A and B, control = 10, RTX = 15) and innominate artery (C and D, control = 4, RTX = 7). Early lesions include intimal xanthoma and PIT. Advanced lesions include fibroatheroma. Statistical analyses in A and C by Chi-square test, B and D by two-way ANOVA with Bonferroni's post hoc test for multiple comparisons. Data represent means per mouse ± SEM, ns, no significance. *P < 0.05. PIT: pathological intimal thickening.

Every 10th section was chosen to determine plaque cellularity and other components in the aortic root. IF staining for macrophages and SMCs, Sirius red staining for collagen. We

observed that RTX treatment led to a marked decrease in plaque macrophages (Fig. 58 A), yet sharply reduced percentage of SMA (Fig. 58 B) and also significantly reduced the percentage of collagen (Fig. 58 C). These data revealed an anti- atherosclerosis effect of RTX by reducing plaque sizes and attenuating plaque progression.

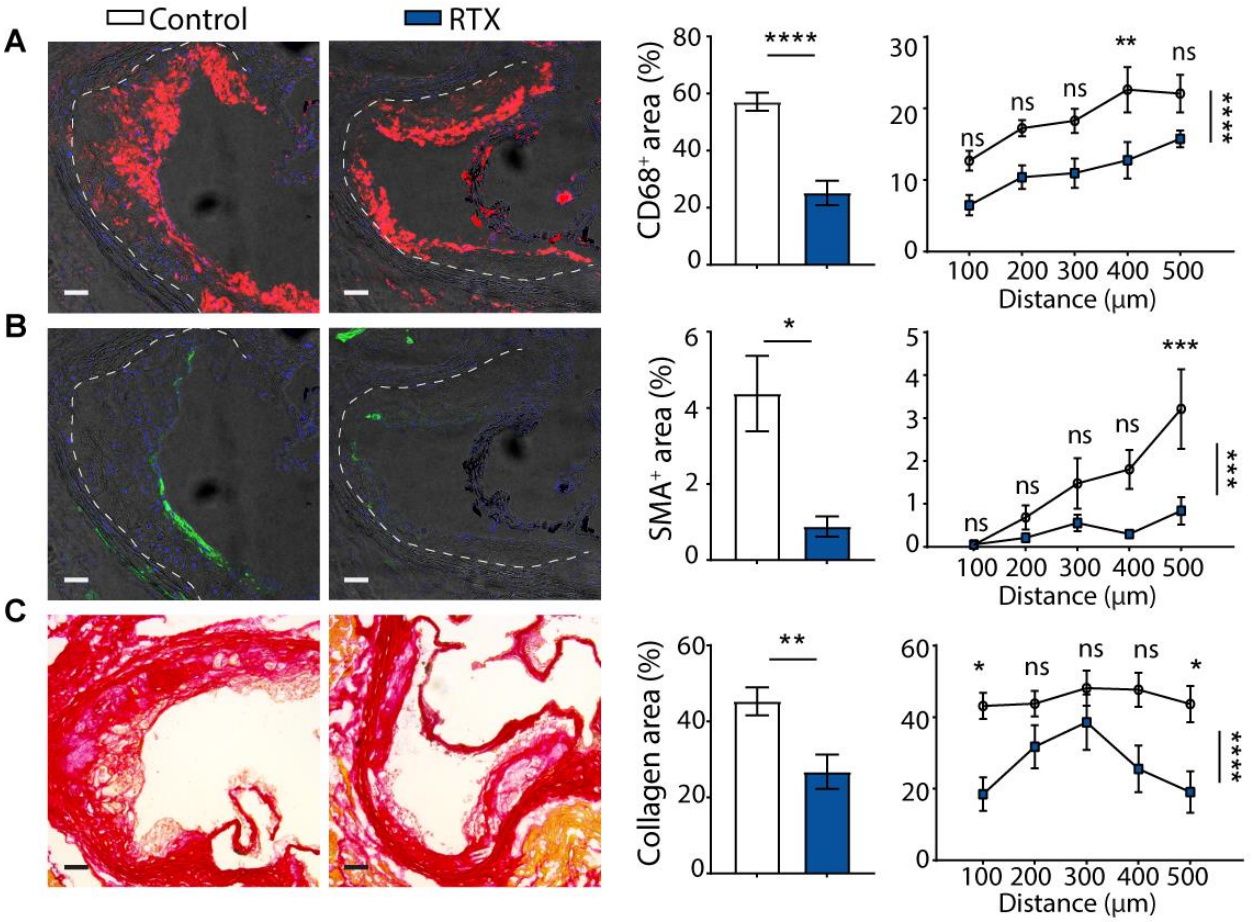

Figure 58. Long-term Depletion of TRPV1 Affect Plaque Structure of Aortic Root. Representative confocal images of aortic root from control (n = 7) and RTX- (n = 7) treated mice. (A) CD68 staining for macrophages, (B) SMA staining for SMCs, (C) Sirius red staining for collagen. Dashed line indicates the inner border of the media. Data was quantified as the percentage of $CD68^+$, SMA^+, Sirius red^+ area / plaque area per mouse or along the distance from the aortic sinus. Statistical analyses by two-tailed unpaired Student´s t-test and two-way ANOVA with Bonferroni's post hoc test for multiple comparisons. *P < 0.05, **P < 0.01, ***P < 0.001, ****P < 0.0001. Scale bar: 50 µm.

3.8.4 Effects of Long-term RTX Treatment on Apoptosis in the Aortic Root

It has been reported that apoptosis is implicated in the progression of atherosclerosis[31]. For this reason, we determined apoptosis in aortic root plaque through the TUNEL assay. Apoptosis was defined as the density of $TUNEL^+$ cells per lesion area of aortic root sections.

We found long-term RTX treatment significantly increased the density of TUNEL⁺ cells within aortic root plaque (Fig. 59), indicating increased apoptosis.

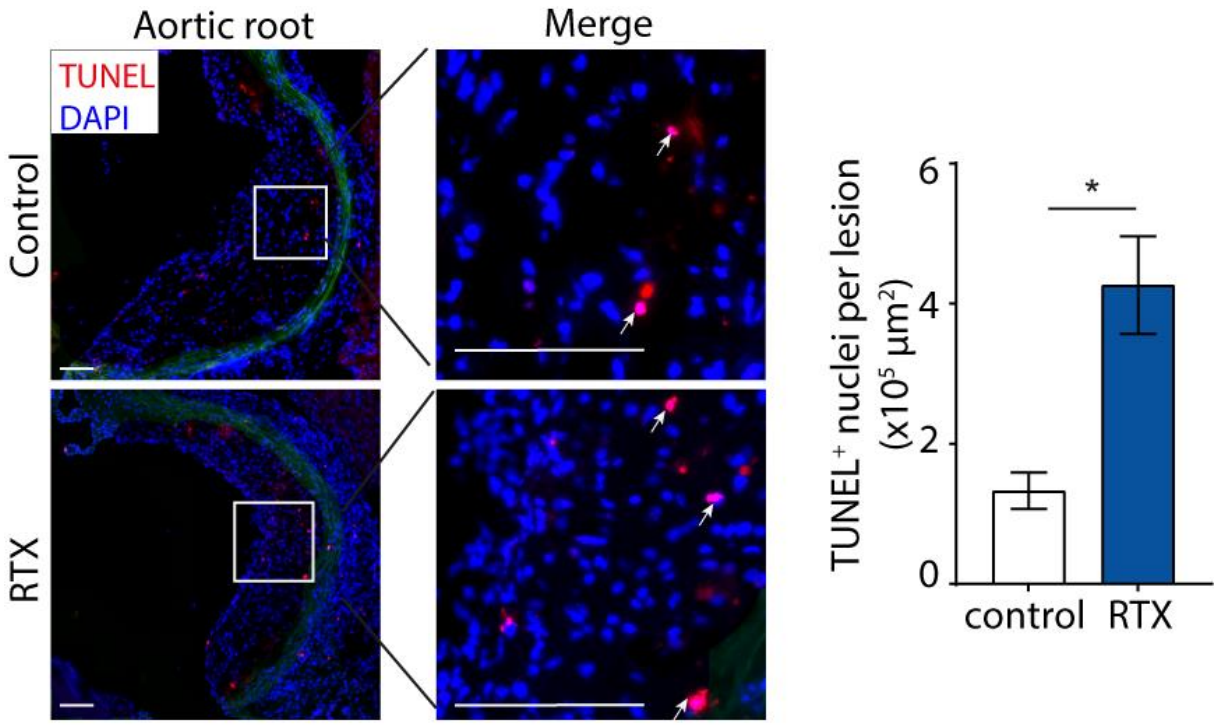

Figure 59. Long-term RTX Treatment Increased Apoptosis in Aortic Root Plaques. Representative thunder images of TUNEL stained aortic root from control (n = 3) and RTX (n = 3) group (left). The white square gives a view of the magnification of a region of lesion as indicated in the middle. Arrow indicates a TUNEL⁺ nucleus. Data was quantified as the density of TUNEL⁺ cells per lesion area of aortic root sections. Two-tailed unpaired Student´s t-test; data represent means per mouse ± SEM; *P < 0.05. Scale bar: 100 µm.

3.8.5 Effects of Long-term RTX Treatment on Aortic CGRP Content

The ascending aortas between the aortic root and innominate artery were collected from both control and RTX-treated groups and CGRP neuropeptide levels were measured using the CGRP-EIA assay as described in Methods. We found the the CGRP levels were reduced by long-term RTX treatment as expected.

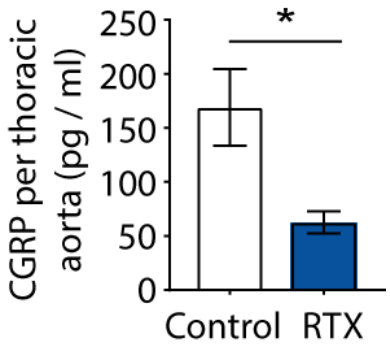

Figure 60. Long-term RTX Treatment Reduced CGRP Tissue Levels. CGRP levels were determined using the CGRP EIA kit. The ascending aorta from control (n = 5) and RTX (n = 6) groups were collected for the EIA assay. CGRP levels were recorded as pg/ml. Two-tailed unpaired Student´s t-test; data represent means per mouse ± SEM; *P < 0.05.

3.8.6 Effects of Long-term RTX treatment on Immune Cells in DRGs

Since we had found that atherosclerosis is related to an increase in immune cells in DRGs and that atherosclerosis was attenuated by RTX, we wondered whether the increased immune cells in DRG were likewise reduced by RTX. T6-13 DRG sections were stained for macrophages / monocytes and mast cells. We found that RTX treatment did not cause significant reductions in either macrophages / monocytes or mast cells; compared to the *Apoe*$^{-/-}$ mice without any treatment, the control group showed insignificant increase but the RTX group did not show alterations of the macrophages / monocytes and mast cells; thus, compared to the WT mice, the immune cells showed a significant increase, no matter with/without treatment or vehicle / RTX treatment (Fig. 61).

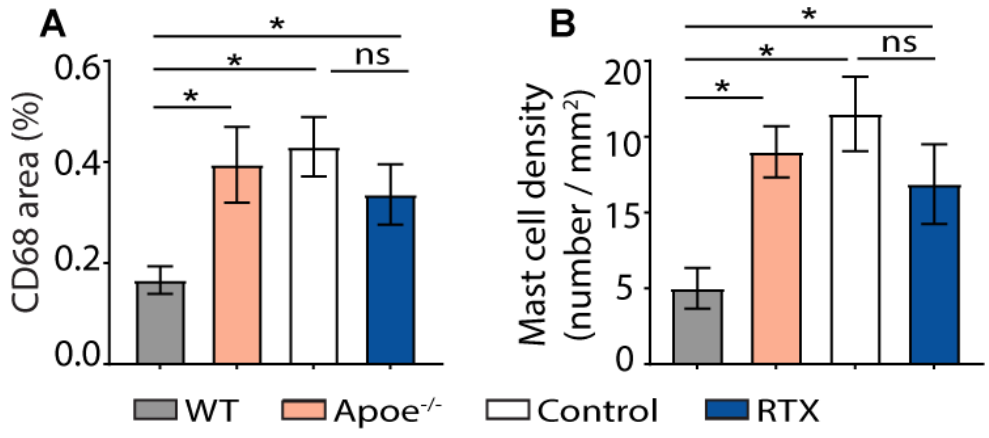

Figure 61. Immune Cells in DRGs after RTX Treatment. CD68^{+} macrophages / monocytes and Giemsa^{+} mast cells in WT mice (n = 8), *Apoe*$^{-/-}$ mice (n = 4-6), control *Apoe*$^{-/-}$ mice (n = 4), RTX *Apoe*$^{-/-}$ mice (n = 8). A minimum of 10 sections per mouse were used for the analyses. . Data represent means per mouse ± SEM; Ordinary one-way ANOVA. *P < 0.05. ns, not significant.

4 DISCUSSION

Data reported above can be summarized as follows: atherosclerosis is associated with a marked increase in the density of sensory axons in the adventitia of aorta segments that are burdened by plaques and further increase in ATLOs; the distribution of immune cells in thoracic DRGs is different between upper and lower segments in WT mice and during ageing; atherosclerosis is associated with additional alterations of distinct immune cell subsets in DRGs; pharmacological depletion of TRPV1 for extended periods of time reduces atherosclerosis progression. These data provide extensive mechanistic and functional evidence that the SPNS has profound effect on atherosclerosis. Further work is required to confirm this data using genetic models of TRPV1 deletion before clinical studies in humans can be considered.

4.1 Sensory Neuroimmune Interactions in the Arterial Wall during Atherosclerosis

To understand neuroimmune communications in atherosclerosis, we examined the innervation patterns of the SPNS in the arterial wall. Altered sensory neuronal function and innervation patterns, caused by interactions with immune dysregulation and inflammation, have been established before but nothing is known about atherosclerosis[111,187,188]. Anand *et al* reported increased TRPV1$^+$ fiber density in the inflamed human oesophagus[188] and in the human rectosigmoid with irritable bowel syndrome[188]. In contrast, Chiu *et al* demonstrated loss of innervating CGRP$^+$ sensory axons at the lesion centers after bacterial infection of the skin[187]. These data indicated that the dysregulation of the SPNS in diseases remains to be better understood. Here, we demonstrated that both the TRPV1$^+$ or CGRP$^+$ sensory axons are detectable at low density in the healthy aortic root and aorta of WT mice. At early stages of atherosclerosis, TRPV1$^+$ and CGRP$^+$ axon density in the adventitia of aortic roots in plaque-containing segments increase. At more advanced disease stages, the axon density within the adventitia of diseased aorta segments shows a strong correlation with plaque development, reaching even higher levels in ATLOs where the inflammatory component of adventitia restructuring is intense[38].

The increased axon density at target locations may be caused by signals that originate in the neuronal cell bodies or it may be caused at the level of axon endings via locally derived signals to act on the axons. To examine these possibilities, we sought to examine changes

that my occur in the related ganglia of the adventitia sensory axons as reported for acute knee inflammation[189]. However, we did not observe changes of neuronal subpopulations in both thoracic DRGs and NGs neither in early nor advanced atherosclerosis. Our analysis included both TRPV1$^+$ nociceptive neurons and CGRP$^+$ peptidergice neurons and IB4$^+$/P2X3$^+$ nonpeptidergic neurons. We therefore have reasons to believe that atherosclerosis induces neogenesis of sensory axons which occurs at the terminal axon endings as a locally regulated sprouting phenomenon (Fig 61). In addition, TRPV1 was reported to be expressed in cultured VSMCs or arteries[190-192], though we were not able to observe TRPV1 immunofluorescence positivity in aortic media SMCs in tissue sections (Fig 15 and 23) or TRPV1 protein level in acutely isolated aortic media by Western blots (not shown).

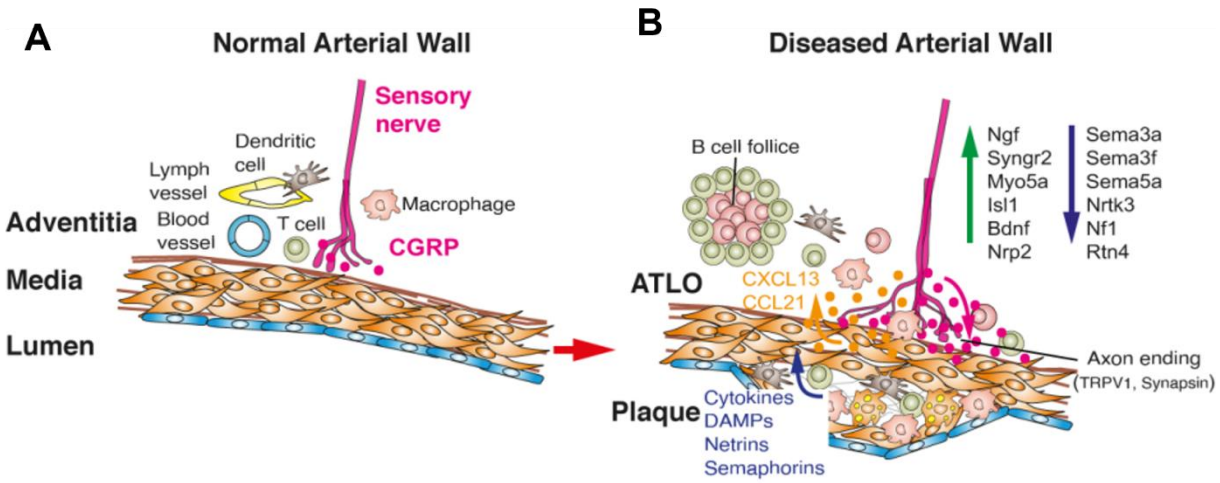

Figure 61. Interaction between the SPNS, the Immune System and the Cardiovascular System at Adventitia of Diseased Artery Segments. (A) SPNS innervation in the adventitia of the normal arteries; (B) Interaction of ATLOs, SPNS, and the arterial wall in the adventitia of advanced diseased arteries. Green arrow indicates upregulation of genes involved in axon neogenesis; blue arrow indicates downregulation of genes associated with inhibition and guidance of axons. Ngf: nerve growth factor; Syngr2: synaptogyrin 2; Nrp2: neuropilin 2; Myo5a: myosin 5A; Isl1: ISL LIM homeobox 1; Bdnf: brain derived neurotrophic factor; Sema3a: semaphorin 3A; Nrtk3: neurotrophic receptor tyrosine kinase 3; Nf1: Neurofibromin 1; Rtn4: reticulon 4; DAMPs: damage-associated molecular patterns.

4.2 Segmental Differences of Immune Cell Distribution in WT DRGs

Peripheral ganglia are known to contain a variety of immune cells. In this thesis, the existence of macrophages/monocytes, T cells, and mast cells in thoracic DRGs was confirmed. Importantly, a segmental difference in the distribution of immune cells in thoracic

DRG segments was documented. The sensory axons that innervate different organs/tissues are coming from different segments of DRGs, for example, the axons that innervate the aortic root mainly come from cervical and upper thoracic DRGs. Although the functional implications of these differences are not clear at this point, it is possible that the segmental difference of immune cell numbers in DRGs may be related to the distinct innervated organs/tissues and their interaction with the SPNS. Furthermore, the segment difference was more prominent in adult compared to aged mice. This indicates that ageing may affect immune cells in the ganglia of the PNS: the sole increase in macrophages / monocytes in the upper DRGs, but no changes in T cells or mast cells requires further work since each of these cells may affect ganglia biology in differential ways. Meanwhile, ageing was observed to reduce the T cells and mast cells in the lower DRGs, while no effect on macrophages / monocytes was noted. The findings of this thesis raise important questions: Does ageing affect the innervated organs/tissues? Are immune cells in DRGs guided via the innervating axon-neuronal cell body direction? These questions need to be answered in the future.

4.3 Atherosclerosis Affects the Immune Cell Infiltration Patterns in DRGs

Immune cell expansion and inflammatory responses in DRGs are reported when distant nerves are experimentally injured[193,194]. Is it conceivable that similar responses occur in DRGs even if there is no injury but neogenesis of distant nerves? In this thesis, through comparing the immune cell density between adult and aged *Apoe*$^{-/-}$ mice, we found increased macrophages / monocytes in both upper and lower DRGs in aged *Apoe*$^{-/-}$ mice, increased T cells in lower DRGs but unchanged mast cells. Is this caused by ageing? Since atherosclerosis is at an advanced stage in aged *Apoe*$^{-/-}$ mice and the sensory axons innervating the diseased aorta adventitia is associated with a higher CGRP tissue content, this raises the possibility that the increased immune cell density in DRGs is induced by advanced atherosclerosis in *Apoe*$^{-/-}$ mice. Comparing the immune cell density between WT and *Apoe*$^{-/-}$ mice, we observed that the content of immune cells in the lower thoracic DRGs is more pronounced in *Apoe*$^{-/-}$ mice and further increased in aged *Apoe*$^{-/-}$ mice[38]. Taken together, we conclude that two major factors are associated with increased DRG inflammation by immune cells, i.e. ageing and atherosclerosis.

4.4 Establishment of Long-term Pharmacological TRPV1 Depletion

RTX-mediated depletion of TRPV1 includes the killing of sensory neurons via apoptosis.

Previous reports have used short time windows of RTX treament (4 wks)[95,138,139]. We also established short-term RTX treatment in *Apoe*$^{-/-}$ mice but the effect of short-term RTX treatment on atherosclerotic lesion in aortic arch, descending aorta and aortic root was not statistically significant due to the slow growing of plaques in mice on a normal chow diet. Yet, these data yielded the interesting observation that RTX may affect early lesions in the innominate artery where there was a statistically significant attenuation of plaque size, rather than advanced complex lesions/plaques in aortic root. For this purpose, we established long-term RTX treatment for 6 month in young *Apoe*$^{-/-}$ mice aged at 8 wks to assess its impact on plaque growth, and regularly performed behavioral test over time to determine the efficacy of the pharmacological treatment. In addition to reduced TRPV1^{+} neuronal subpopulation in DRGs, and almost completely disappeared TRPV1 axons in aortic adventitia confirmed the efficacy of long-term pharmacological treatment. Moreover, similar body weight, relative tissues/organs weight, and serum cholesterol levels between treated and control mice indicate the normal physiological parameters post-long-term RTX treatment. In summary, we successfully established long-term RTX treatment of TRPV1 expressing sensory neurons in hyperlipidemic mice.

4.5 TRPV1 Depletion Affects the Progression of Atherosclerosis

In this thesis, we established both the short and long-term treatment. Short-term treatment started at age of 28 wks, while long-term treatment was initiated in 8 wk-old mice , with both end points when mice reached 32 wks of age. Both the short and long-term treatment caused plaque size reduction in the innominate artery. 4 out of 7 innominate arteries developed no plaque after the long-term treatment, while they contained plaque in all control mice (Fig. 56). To the best of our knowledge, this unprecedented striking anti-atherosclerotic effect has not been reported by any other pharmacological intervention so far. Considering the phases of atherosclerosis progression, the aortic root develops advanced plaques as one of the first sites at the age of around 30 wks in *Apoe*$^{-/-}$ mice fed with chow diet[17]. Then the disease spreads to the aortic arch, the innominate artery and principal branches of the aortic arch and finally to the descending and abdominal aorta over time. Therefore, short-term treatment starting at age of 28 wks was likely too late to affect the initiation of plaque in aortic root. Yet, 4 wks turned out to be long enough to affect the lesion progression in the innominate artery, but not enough to inhibit the advanced plaque progression in aortic roots. VSMCs are essential and critical for plaque growth at all stages, but differ in their roles and the effects of phenotype switching or proliferation or loss at different stages of

atherogenesis[23,25-27,32,195]. Intimal xanthomas are considered as early events of atherosclerosis which mainly contain VSMCs (Fig 14). In Intimal xanthomas, VSMCs undergo the phenotype switching by losing their contractile phenotype and acquiring a synthetic and proliferative phenotype, which allows intimal xanthomad to develop into PITs (Fig 14)[23]. However, phenotypic switching seems to be a reversible process, at least in the early stages[23,25,196], and thus making this stage most likely initiator of atherosclerotic plaque development and therapeutically modifiable[196]. Furthermore, long-term RTX treatment decreased total monocyte/macrophages area, VSMCs and collagen area. The reduced VSMCs and collagen contents are linked to the early plaque stage, which barely contains VSMCs and collagen but foam cells[23,25,32]. In summary, pharmacological depletion of TRPV1 by RTX treatment attenuates atherosclerosis progression by reducing myeloid cells and fibrous components in the lesion.

During long-term RTX treatment, the effect of the drug is two-fold i.e. neuronal death is involved in a significant number of DRG neurons in addition to elimination of TRPV1 on the surface of surviving neurons. This particular circumstance may be unique to pharmaceuticals targeting TRPV1. More work will be required to compare the current body of data with genetic models of TRPV1 deletion. Similar caveats relate to the effects of RTX on immune cells in the circulation and in the bone marrow and secondary lymphoid organs. All these considerations lead us to suggest the importance of genetically TRPV1 knockout mice to reevaluate the bona fide effect of the TRPV1-mediated pain pathway in atherosclerosis, which needs to be followed up in future studies. It will be of interest to examine the relationship between early and advanced lesion development in genetically inducible TRPV1 knockout mice on *Apoe* background at various disease stages and mouse ages[31,190,197,198].

5 REFERENCES

1 Glass, C. K. & Witztum, J. L. Atherosclerosis: The road ahead. *Cell* **104**, 503-516, doi:Doi 10.1016/S0092-8674(01)00238-0 (2001).

2 Breslow, J. L. Cardiovascular disease burden increases, NIH funding decreases. *Nat Med* **3**, 600-601, doi:Doi 10.1038/Nm0697-600 (1997).

3 Lusis, A. J. Atherosclerosis. *Nature* **407**, 233-241, doi:Doi 10.1038/35025203 (2000).

4 Braunwald, E. Shattuck lecture - Cardiovascular medicine at the turn of the millennium: Triumphs, concerns, and opportunities. *New Engl J Med* **337**, 1360-1369, doi:Doi 10.1056/Nejm199711063371906 (1997).

5 Foks, A. C. & Bot, I. Preface: Pathology and Pharmacology of Atherosclerosis. *European journal of pharmacology* **816**, 1-2, doi:10.1016/j.ejphar.2017.10.052 (2017).

6 Napoli, C. *et al.* Fatty streak formation occurs in human fetal aortas and is greatly enhanced by maternal hypercholesterolemia - Intimal accumulation of low density lipoprotein and its oxidation precede monocyte recruitment into early atherosclerotic lesions. *J Clin Invest* **100**, 2680-2690, doi:Doi 10.1172/Jci119813 (1997).

7 Galkina, E. & Ley, K. Immune and inflammatory mechanisms of atherosclerosis (*). *Annual review of immunology* **27**, 165-197, doi:10.1146/annurev.immunol.021908.132620 (2009).

8 Libby, P. Inflammation in atherosclerosis. *Nature* **420**, 868-874, doi:10.1038/nature01323 (2002).

9 Hansson, G. K. & Hermansson, A. The immune system in atherosclerosis. *Nature immunology* **12**, 204-212, doi:10.1038/ni.2001 (2011).

10 Nathan, C. & Ding, A. Nonresolving inflammation. *Cell* **140**, 871-882, doi:10.1016/j.cell.2010.02.029 (2010).

11 Nagenborg, J., Goossens, P., Biessen, E. A. L. & Donners, M. Heterogeneity of atherosclerotic plaque macrophage origin, phenotype and functions: Implications for treatment. *European journal of pharmacology* **816**, 14-24, doi:10.1016/j.ejphar.2017.10.005 (2017).

12 Gil-Pulido, J. & Zernecke, A. Antigen-presenting dendritic cells in atherosclerosis. *European journal of pharmacology* **816**, 25-31, doi:10.1016/j.ejphar.2017.08.016 (2017).

13 Kovanen, P. T. & Bot, I. Mast cells in atherosclerotic cardiovascular disease - Activators and actions. *European journal of pharmacology* **816**, 37-46, doi:10.1016/j.ejphar.2017.10.013 (2017).

14 Hansson, G. K. & Libby, P. The immune response in atherosclerosis: a double-edged sword. *Nat Rev Immunol* **6**, 508-519, doi:10.1038/nri1882 (2006).

15 Emini Veseli, B. *et al.* Animal models of atherosclerosis. *European journal of pharmacology* **816**, 3-13, doi:10.1016/j.ejphar.2017.05.010 (2017).

16 Lee, Y. T. *et al.* Animal models of atherosclerosis. *Biomedical reports* **6**, 259-266, doi:10.3892/br.2017.843 (2017).

17 Nakashima, Y., Plump, A. S., Raines, E. W., Breslow, J. L. & Ross, R. *Apoe*-Deficient Mice Develop Lesions of All Phases of Atherosclerosis Throughout the Arterial Tree. *Arterioscler Thromb* **14**, 133-140, doi:Doi 10.1161/01.Atv.14.1.133 (1994).

18 Spanbroek, R. *et al.* Expanding expression of the 5-lipoxygenase pathway within the arterial wall during human atherogenesis. *Proc Natl Acad Sci U S A* **100**, 1238-1243, doi:10.1073/pnas.242716099 (2003).

19 Plump, A. S. *et al.* Severe hypercholesterolemia and atherosclerosis in apolipoprotein E-deficient mice created by homologous recombination in ES cells. *Cell* **71**, 343-353 (1992).

20 Libby, P. *et al.* Atherosclerosis. *Nat Rev Dis Primers* **5**, 56, doi:10.1038/s41572-019-0106-z (2019).

21 Mehta, A. & Shapiro, M. D. Apolipoproteins in vascular biology and atherosclerotic disease. *Nat Rev Cardiol*, doi:10.1038/s41569-021-00613-5 (2021).

22 Libby, P. The changing landscape of atherosclerosis. *Nature* **592**, 524-533, doi:10.1038/s41586-021-03392-8 (2021).

23 Basatemur, G. L., Jorgensen, H. F., Clarke, M. C. H., Bennett, M. R. & Mallat, Z. Vascular smooth muscle cells in atherosclerosis. *Nat Rev Cardiol* **16**, 727-744, doi:10.1038/s41569-019-0227-9 (2019).

24 Roy, P., Orecchioni, M. & Ley, K. How the immune system shapes atherosclerosis: roles of innate and adaptive immunity. *Nat Rev Immunol*, doi:10.1038/s41577-021-00584-1 (2021).

25 Grootaert, M. O. J. & Bennett, M. R. Vascular smooth muscle cells in atherosclerosis: time for a re-

assessment. *Cardiovasc Res* **117**, 2326-2339, doi:10.1093/cvr/cvab046 (2021).

26 Hu, D., Yin, C., Luo, S., Habenicht, A. J. R. & Mohanta, S. K. Vascular Smooth Muscle Cells Contribute to Atherosclerosis Immunity. *Front Immunol* **10**, 1101, doi:10.3389/fimmu.2019.01101 (2019).

27 Yin, C., Mohanta, S. K., Srikakulapu, P., Weber, C. & Habenicht, A. J. Artery Tertiary Lymphoid Organs: Powerhouses of Atherosclerosis Immunity. *Front Immunol* **7**, 387, doi:10.3389/fimmu.2016.00387 (2016).

28 Haley, K. J. *et al.* Overexpression of eotaxin and the CCR3 receptor in human atherosclerosis: using genomic technology to identify a potential novel pathway of vascular inflammation. *Circulation* **102**, 2185-2189 (2000).

29 Hu, D. *et al.* Artery Tertiary Lymphoid Organs Control Aorta Immunity and Protect against Atherosclerosis via Vascular Smooth Muscle Cell Lymphotoxin beta Receptors. *Immunity* **42**, 1100-1115, doi:10.1016/j.immuni.2015.05.015 (2015).

30 Baardman, J. & Lutgens, E. Regulatory T Cell Metabolism in Atherosclerosis. *Metabolites* **10**, doi:10.3390/metabo10070279 (2020).

31 Virmani, R., Kolodgie, F. D., Burke, A. P., Farb, A. & Schwartz, S. M. Lessons from sudden coronary death: a comprehensive morphological classification scheme for atherosclerotic lesions. *Arterioscler Thromb Vasc Biol* **20**, 1262-1275, doi:10.1161/01.atv.20.5.1262 (2000).

32 Miano, J. M., Fisher, E. A. & Majesky, M. W. Fate and State of Vascular Smooth Muscle Cells in Atherosclerosis. *Circulation* **143**, 2110-2116, doi:10.1161/CIRCULATIONAHA.120.049922 (2021).

33 Mohanta, S. K. *et al.* Artery tertiary lymphoid organs contribute to innate and adaptive immune responses in advanced mouse atherosclerosis. *Circulation research* **114**, 1772-1787, doi:10.1161/CIRCRESAHA.114.301137 (2014).

34 Aloisi, F. & Pujol-Borrell, R. Lymphoid neogenesis in chronic inflammatory diseases. *Nat Rev Immunol* **6**, 205-217, doi:10.1038/nri1786 (2006).

35 Weih, F., Grabner, R., Hu, D. S., Beer, M. & Habenicht, A. J. R. Control of dichotomic innate and adaptive immune responses by artery tertiary lymphoid organs in atherosclerosis. *Front Physiol* **3**, doi:Artn 22610.3389/Fphys.2012.00226 (2012).

36 Moos, M. P. *et al.* The lamina adventitia is the major site of immune cell accumulation in standard chow-fed apolipoprotein E-deficient mice. *Arterioscler Thromb Vasc Biol* **25**, 2386-2391, doi:10.1161/01.ATV.0000187470.31662.fe (2005).

37 Grabner, R. *et al.* Lymphotoxin beta receptor signaling promotes tertiary lymphoid organogenesis in the aorta adventitia of aged *Apoe-/-* mice. *The Journal of experimental medicine* **206**, 233-248, doi:10.1084/jem.20080752 (2009).

38 Mohanta, S. K. *et al.* Neuroimmune cardiovascular interfaces control atherosclerosis. *Nature*, doi:10.1038/s41586-022-04673-6 (2022).

39 Kaiser, J. T., Reddy, V. & Lugo-Pico, J. G. in *StatPearls* (2021).

40 Goldstein, B. Anatomy of the peripheral nervous system. *Phys Med Rehabil Clin N Am* **12**, 207-236 (2001).

41 Waxenbaum, J. A., Reddy, V. & Varacallo, M. in *StatPearls* (2021).

42 Rao, M. & Gershon, M. D. The bowel and beyond: the enteric nervous system in neurological disorders. *Nat Rev Gastroenterol Hepatol* **13**, 517-528, doi:10.1038/nrgastro.2016.107 (2016).

43 Klose, C. S. N. & Veiga-Fernandes, H. Neuroimmune interactions in peripheral tissues. *Eur J Immunol* **51**, 1602-1614, doi:10.1002/eji.202048812 (2021).

44 Udit, S., Blake, K. & Chiu, I. M. Somatosensory and autonomic neuronal regulation of the immune response. *Nat Rev Neurosci*, doi:10.1038/s41583-021-00555-4 (2022).

45 Spencer, N. J. & Hu, H. Enteric nervous system: sensory transduction, neural circuits and gastrointestinal motility. *Nat Rev Gastroenterol Hepatol* **17**, 338-351, doi:10.1038/s41575-020-0271-2 (2020).

46 Kunze, W. A., Bornstein, J. C. & Furness, J. B. Identification of sensory nerve cells in a peripheral organ (the intestine) of a mammal. *Neuroscience* **66**, 1-4, doi:10.1016/0306-4522(95)00067-s (1995).

47 Mercado-Perez, A. & Beyder, A. Gut feelings: mechanosensing in the gastrointestinal tract. *Nat Rev Gastroenterol Hepatol* **19**, 283-296, doi:10.1038/s41575-021-00561-y (2022).

48 Uesaka, T., Young, H. M., Pachnis, V. & Enomoto, H. Development of the intrinsic and extrinsic innervation of the gut. *Dev Biol* **417**, 158-167, doi:10.1016/j.ydbio.2016.04.016 (2016).

49 Basbaum, A. I., Bautista, D. M., Scherrer, G. & Julius, D. Cellular and molecular mechanisms of pain. *Cell* **139**, 267-284, doi:10.1016/j.cell.2009.09.028 (2009).

50 <Neuroscience - D.Purves, et al.pdf>.

51 Lumpkin, E. A. & Caterina, M. J. Mechanisms of sensory transduction in the skin. *Nature* **445**, 858-865, doi:10.1038/nature05662 (2007).

52 Wood, J. N. Chapter 5 Molecular mechanisms of nociception and pain. *Handbook of clinical neurology* **81**, 49-59, doi:10.1016/S0072-9752(06)80009-6 (2006).

53 Patapoutian, A., Tate, S. & Woolf, C. J. Transient receptor potential channels: targeting pain at the source. *Nat Rev Drug Discov* **8**, 55-68, doi:10.1038/nrd2757 (2009).

54 Chu, C., Artis, D. & Chiu, I. M. Neuro-immune Interactions in the Tissues. *Immunity* **52**, 464-474, doi:10.1016/j.immuni.2020.02.017 (2020).

55 Dubin, A. E. & Patapoutian, A. Nociceptors: the sensors of the pain pathway. *J Clin Invest* **120**, 3760-3772, doi:10.1172/JCI42843 (2010).

56 Das, S. *et al.* Innervation: the missing link for biofabricated tissues and organs. *NPJ Regen Med* **5**, 11, doi:10.1038/s41536-020-0096-1 (2020).

57 Julius, D. & Basbaum, A. I. Molecular mechanisms of nociception. *Nature* **413**, 203-210, doi:10.1038/35093019 (2001).

58 Braz, J., Solorzano, C., Wang, X. & Basbaum, A. I. Transmitting pain and itch messages: a contemporary view of the spinal cord circuits that generate gate control. *Neuron* **82**, 522-536, doi:10.1016/j.neuron.2014.01.018 (2014).

59 Hunt, S. P. & Mantyh, P. W. The molecular dynamics of pain control. *Nat Rev Neurosci* **2**, 83-91, doi:10.1038/35053509 (2001).

60 Peier, A. M. *et al.* A TRP channel that senses cold stimuli and menthol. *Cell* **108**, 705-715, doi:10.1016/s0092-8674(02)00652-9 (2002).

61 Tominaga, M. *et al.* The cloned capsaicin receptor integrates multiple pain-producing stimuli. *Neuron* **21**, 531-543, doi:10.1016/s0896-6273(00)80564-4 (1998).

62 Elokely, K. *et al.* Understanding TRPV1 activation by ligands: Insights from the binding modes of capsaicin and resiniferatoxin. *P Natl Acad Sci USA* **113**, E137-E145, doi:10.1073/pnas.1517288113 (2016).

63 Wang, D. H. Transient receptor potential vanilloid channels in hypertension, inflammation, and end organ damage: an imminent target of therapy for cardiovascular disease? *Curr Opin Cardiol* **23**, 356-363, doi:Doi 10.1097/Hco.0b013e32830460ad (2008).

64 Clapham, D. E. TRP channels as cellular sensors. *Nature* **426**, 517-524, doi:10.1038/nature02196 (2003).

65 Ramsey, I. S., Delling, M. & Clapham, D. E. An introduction to TRP channels. *Annual review of physiology* **68**, 619-647, doi:10.1146/annurev.physiol.68.040204.100431 (2006).

66 Song, M. Y. & Yuan, J. X. Introduction to TRP channels: structure, function, and regulation. *Advances in experimental medicine and biology* **661**, 99-108, doi:10.1007/978-1-60761-500-2_6 (2010).

67 Kwan, K. Y. *et al.* TRPA1 contributes to cold, mechanical, and chemical nociception but is not essential for hair-cell transduction. *Neuron* **50**, 277-289, doi:10.1016/j.neuron.2006.03.042 (2006).

68 Proudfoot, C. J. *et al.* Analgesia mediated by the TRPM8 cold receptor in chronic neuropathic pain. *Curr Biol* **16**, 1591-1605, doi:10.1016/j.cub.2006.07.061 (2006).

69 Tracey, W. D. Nociception. *Current Biology* **27**, R129-R133, doi:DOI 10.1016/j.cub.2017.01.037 (2017).

70 Caterina, M. J. *et al.* The capsaicin receptor: a heat-activated ion channel in the pain pathway. *Nature* **389**, 816-824 (1997).

71 Nagy, I. & Rang, H. Noxious heat activates all capsaicin-sensitive and also a sub-population of capsaicin-insensitive dorsal root ganglion neurons. *Neuroscience* **88**, 995-997, doi:Doi 10.1016/S0306-4522(98)00535-1 (1999).

72 Rosenbaum, T. & Simon, S. A. in *TRP Ion Channel Function in Sensory Transduction and Cellular Signaling Cascades Frontiers in Neuroscience* (eds W. B. Liedtke & S. Heller) (2007).

73 Moriyama, T. *et al.* Possible involvement of P2Y2 metabotropic receptors in ATP-induced transient receptor potential vanilloid receptor 1-mediated thermal hypersensitivity. *The Journal of neuroscience : the official journal of the Society for Neuroscience* **23**, 6058-6062 (2003).

74 Pinho-Ribeiro, F. A., Verri, W. A. & Chiu, I. M. Nociceptor Sensory Neuron-Immune Interactions in Pain and Inflammation. *Trends Immunol* **38**, 5-19, doi:10.1016/j.it.2016.10.001 (2017).

75 Aneiros, E. *et al.* The biophysical and molecular basis of TRPV1 proton gating. *Embo J* **30**, 994-1002, doi:10.1038/emboj.2011.19 (2011).

76 Fischer, M. J. M., Ciotu, C. I. & Szallasi, A. The Mysteries of Capsaicin-Sensitive Afferents. *Front Physiol* **11**, 554195, doi:10.3389/fphys.2020.554195 (2020).

77 Szallasi, A. & Blumberg, P. M. Vanilloid (capsaicin) receptors and mechanisms. *Pharmacol Rev* **51**, 159-211 (1999).

78 Yang, F. & Zheng, J. Understand spiciness: mechanism of TRPV1 channel activation by capsaicin. *Protein Cell* **8**, 169-177, doi:10.1007/s13238-016-0353-7 (2017).

79 Szallasi, A. & Blumberg, P. M. Resiniferatoxin, a Phorbol-Related Diterpene, Acts as an Ultrapotent Analog of Capsaicin, the Irritant Constituent in Red Pepper. *Neuroscience* **30**, 515-520, doi:Doi 10.1016/0306-4522(89)90269-8 (1989).

80 Szolcsanyi, J., Szallasi, A., Szallasi, Z., Joo, F. & Blumberg, P. M. Resiniferatoxin - an Ultrapotent Selective Modulator of Capsaicin-Sensitive Primary Afferent Neurons. *J Pharmacol Exp Ther* **255**, 923-928 (1990).

81 Nagy, J. I. Capsaicins Action on the Nervous-System. *Trends Neurosci* **5**, 362-365, doi:Doi 10.1016/0166-2236(82)90205-3 (1982).

82 Szallasi, A. The Vanilloid (Capsaicin) Receptor - Receptor Types and Species-Differences. *Gen Pharmacol-Vasc S* **25**, 223-243, doi:Doi 10.1016/0306-3623(94)90049-3 (1994).

83 Bujak, J. K., Kosmala, D., Szopa, I. M., Majchrzak, K. & Bednarczyk, P. Inflammation, Cancer and Immunity-Implication of TRPV1 Channel. *Frontiers in oncology* **9**, 1087, doi:10.3389/fonc.2019.01087 (2019).

84 Chiu, I. M. Infection, Pain, and Itch. *Neurosci Bull* **34**, 109-119, doi:10.1007/s12264-017-0098-1 (2018).

85 Baral, P., Mills, K., Pinho-Ribeiro, F. A. & Chiu, I. M. Pain and Itch: Beneficial or Harmful to Antimicrobial Defense? *Cell Host Microbe* **19**, 755-759, doi:10.1016/j.chom.2016.05.010 (2016).

86 Hescham, S. A. *et al.* Magnetothermal nanoparticle technology alleviates parkinsonian-like symptoms in mice. *Nat Commun* **12**, 5569, doi:10.1038/s41467-021-25837-4 (2021).

87 Anand, P. & Bley, K. Topical capsaicin for pain management: therapeutic potential and mechanisms of action of the new high-concentration capsaicin 8% patch. *British journal of anaesthesia* **107**, 490-502, doi:10.1093/bja/aer260 (2011).

88 Kun, J. *et al.* Effect of Surgical and Chemical Sensory Denervation on Non-neural Expression of the Transient Receptor Potential Vanilloid 1 (TRPV1) Receptors in the Rat. *J Mol Neurosci* **48**, 795-803, doi:10.1007/s12031-012-9766-9 (2012).

89 Vyklicky, L. *et al.* Calcium-Dependent Desensitization of Vanilloid Receptor TRPV1: A Mechanism Possibly Involved in Analgesia Induced by Topical Application of Capsaicin. *Physiol Res* **57**, S59-S68 (2008).

90 Dogan, M. D. *et al.* Lipopolysaccharide fever is initiated via a capsaicin-sensitive mechanism independent of the subtype-1 vanilloid receptor. *Brit J Pharmacol* **143**, 1023-1032, doi:10.1038/sj.bjp.0705977 (2004).

91 Kissin, I. & Szallasi, A. Therapeutic Targeting of TRPV1 by Resiniferatoxin, from Preclinical Studies to Clinical Trials. *Curr Top Med Chem* **11**, 2159-2170, doi:Doi 10.2174/156802611796904924 (2011).

92 Baral, P. *et al.* Nociceptor sensory neurons suppress neutrophil and gammadelta T cell responses in bacterial lung infections and lethal pneumonia. *Nat Med* **24**, 417-426, doi:10.1038/nm.4501 (2018).

93 Czaja, K., Burns, G. A. & Ritter, R. C. Capsaicin-induced neuronal death and proliferation of the primary sensory neurons located in the nodose ganglia of adult rats. *Neuroscience* **154**, 621-630, doi:10.1016/j.neuroscience.2008.03.055 (2008).

94 Farazifard, R., Safarpour, F., Sheibani, V. & Javan, M. Eye-wiping test: a sensitive animal model for acute trigeminal pain studies. *Brain Res Brain Res Protoc* **16**, 44-49, doi:10.1016/j.brainresprot.2005.10.003 (2005).

95 Riol-Blanco, L. *et al.* Nociceptive sensory neurons drive interleukin-23-mediated psoriasiform skin inflammation. *Nature* **510**, 157-161, doi:10.1038/nature13199 (2014).

96 Lai, N. Y. *et al.* Gut-Innervating Nociceptor Neurons Regulate Peyer's Patch Microfold Cells and SFB Levels to Mediate Salmonella Host Defense. *Cell* **180**, 33-+, doi:10.1016/j.cell.2019.11.014 (2020).

97 Hsieh, Y. L. *et al.* Role of peptidergic nerve terminals in the skin: reversal of thermal sensation by calcitonin gene-related peptide in TRPV1-depleted neuropathy. *PLoS One* **7**, e50805, doi:10.1371/journal.pone.0050805 (2012).

98 Caterina, M. J. *et al.* Impaired nociception and pain sensation in mice lacking the capsaicin receptor. *Science* **288**, 306-313, doi:DOI 10.1126/science.288.5464.306 (2000).

99 Muratori, L. *et al.* Generation of New Neurons in Dorsal Root Ganglia in Adult Rats after Peripheral Nerve Crush Injury. *Neural Plast* **2015**, doi:Artn 86054610.1155/2015/860546 (2015).

100 Garami, A. *et al.* Thermoregulatory phenotype of the Trpv1 knockout mouse: thermoeffector dysbalance with hyperkinesis. *The Journal of neuroscience : the official journal of the Society for Neuroscience* **31**, 1721-1733, doi:10.1523/JNEUROSCI.4671-10.2011 (2011).

101 Lee, E. *et al.* Transient receptor potential vanilloid type-1 channel regulates diet-induced obesity, insulin resistance, and leptin resistance. *FASEB J* **29**, 3182-3192, doi:10.1096/fj.14-268300 (2015).

102 Riera, C. E. *et al.* TRPV1 pain receptors regulate longevity and metabolism by neuropeptide signaling. *Cell* **157**, 1023-1036, doi:10.1016/j.cell.2014.03.051 (2014).

103 Steinman, L. Elaborate interactions between the immune and nervous systems. *Nature immunology* **5**, 575-581, doi:10.1038/ni1078 (2004).

104 Pavlov, V. A. & Tracey, K. J. Neural circuitry and immunity. *Immunologic research* **63**, 38-57, doi:10.1007/s12026-015-8718-1 (2015).

105 Foster, S. L., Seehus, C. R., Woolf, C. J. & Talbot, S. Sense and Immunity: Context-Dependent Neuro-Immune Interplay. *Front Immunol* **8**, 1463, doi:10.3389/fimmu.2017.01463 (2017).

106 Ansel, J. C., Brown, J. R., Payan, D. G. & Brown, M. A. Substance P selectively activates TNF-alpha gene expression in murine mast cells. *Journal of immunology* **150**, 4478-4485 (1993).

107 Kawashima, K., Fujii, T., Moriwaki, Y. & Misawa, H. Critical roles of acetylcholine and the muscarinic and nicotinic acetylcholine receptors in the regulation of immune function. *Life Sci* **91**, 1027-1032, doi:10.1016/j.lfs.2012.05.006 (2012).

108 Kawashima, K., Fujii, T., Moriwaki, Y., Misawa, H. & Horiguchi, K. Non-neuronal cholinergic system in regulation of immune function with a focus on alpha7 nAChRs. *Int Immunopharmacol* **29**, 127-134, doi:10.1016/j.intimp.2015.04.015 (2015).

109 Talbot, S., Foster, S. L. & Woolf, C. J. Neuroimmunity: Physiology and Pathology. *Annual review of immunology* **34**, 421-447, doi:10.1146/annurev-immunol-041015-055340 (2016).

110 Delgado, M. VIP: a very important peptide in T helper differentiation. *Trends Immunol* **24**, 221-224, doi:10.1016/s1471-4906(03)00069-3 (2003).

111 Pinho-Ribeiro, F. A. *et al.* Blocking Neuronal Signaling to Immune Cells Treats Streptococcal Invasive Infection. *Cell* **173**, 1083-1097 e1022, doi:10.1016/j.cell.2018.04.006 (2018).

112 Huang, S. *et al.* Lymph nodes are innervated by a unique population of sensory neurons with immunomodulatory potential. *Cell*, doi:10.1016/j.cell.2020.11.028 (2020).

113 Schaible, H. G. Nociceptive neurons detect cytokines in arthritis. *Arthritis Res Ther* **16**, 470, doi:10.1186/s13075-014-0470-8 (2014).

114 Binshtok, A. M. *et al.* Nociceptors are interleukin-1beta sensors. *The Journal of neuroscience : the official journal of the Society for Neuroscience* **28**, 14062-14073, doi:10.1523/JNEUROSCI.3795-08.2008 (2008).

115 Chiu, I. M., von Hehn, C. A. & Woolf, C. J. Neurogenic inflammation and the peripheral nervous system in host defense and immunopathology. *Nature neuroscience* **15**, 1063-1067, doi:10.1038/nn.3144 (2012).

116 Ghasemlou, N., Chiu, I. M., Julien, J. P. & Woolf, C. J. CD11b+Ly6G- myeloid cells mediate mechanical inflammatory pain hypersensitivity. *Proc Natl Acad Sci U S A* **112**, E6808-6817, doi:10.1073/pnas.1501372112 (2015).

117 Aich, A., Afrin, L. B. & Gupta, K. Mast Cell-Mediated Mechanisms of Nociception. *Int J Mol Sci* **16**, 29069-29092, doi:10.3390/ijms161226151 (2015).

118 Chatterjea, D. & Martinov, T. Mast cells: versatile gatekeepers of pain. *Mol Immunol* **63**, 38-44, doi:10.1016/j.molimm.2014.03.001 (2015).

119 Foreman, J. C. Peptides and neurogenic inflammation. *British medical bulletin* **43**, 386-400 (1987).

120 Weidner, C. *et al.* Acute effects of substance P and calcitonin gene-related peptide in human skin--a microdialysis study. *The Journal of investigative dermatology* **115**, 1015-1020, doi:10.1046/j.1523-1747.2000.00142.x (2000).

121 Veres, T. Z. *et al.* Spatial interactions between dendritic cells and sensory nerves in allergic airway inflammation. *Am J Resp Cell Mol* **37**, 553-561, doi:10.1165/rcmb.2007-00870C (2007).

122 Hosoi, J. *et al.* Regulation of Langerhans cell function by nerves containing calcitonin gene-related peptide. *Nature* **363**, 159-163, doi:10.1038/363159a0 (1993).

123 Franco, R., Pacheco, R., Lluis, C., Ahern, G. P. & O'Connell, P. J. The emergence of neurotransmitters as immune modulators. *Trends Immunol* **28**, 400-407, doi:10.1016/j.it.2007.07.005 (2007).

124 Rochlitzer, S. *et al.* The neuropeptide calcitonin gene-related peptide affects allergic airway inflammation

by modulating dendritic cell function. *Clinical and experimental allergy : journal of the British Society for Allergy and Clinical Immunology* **41**, 1609-1621, doi:10.1111/j.1365-2222.2011.03822.x (2011).

125 Jimeno, R. *et al.* Effect of VIP on the balance between cytokines and master regulators of activated helper T cells. *Immunol Cell Biol* **90**, 178-186, doi:10.1038/icb.2011.23 (2012).

126 Talbot, S. *et al.* Silencing Nociceptor Neurons Reduces Allergic Airway Inflammation. *Neuron* **87**, 341-354, doi:10.1016/j.neuron.2015.06.007 (2015).

127 Goetzl, E. J. *et al.* Enhanced delayed-type hypersensitivity and diminished immediate-type hypersensitivity in mice lacking the inducible VPAC(2) receptor for vasoactive intestinal peptide. *Proc Natl Acad Sci U S A* **98**, 13854-13859, doi:10.1073/pnas.241503798 (2001).

128 Delgado, M. VIP: a very important peptide in T helper differentiation. *Trends in immunology* **24**, 221-224, doi:10.1016/S1471-4906(03)00069-3 (2003).

129 Cunin, P. *et al.* The tachykinins substance P and hemokinin-1 favor the generation of human memory Th17 cells by inducing IL-1beta, IL-23, and TNF-like 1A expression by monocytes. *Journal of immunology* **186**, 4175-4182, doi:10.4049/jimmunol.1002535 (2011).

130 Cohen, J. A. *et al.* Cutaneous TRPV1(+) Neurons Trigger Protective Innate Type 17 Anticipatory Immunity. *Cell* **178**, 919-+, doi:10.1016/j.cell.2019.06.022 (2019).

131 Cabral, L. D. & Giusti-Paiva, A. The Transient Receptor Potential Vanilloid 1 Antagonist Capsazepine Improves the Impaired Lung Mechanics during Endotoxemia. *Basic & clinical pharmacology & toxicology* **119**, 421-427, doi:10.1111/bcpt.12605 (2016).

132 Erin, N., Boyer, P. J., Bonneau, R. H., Clawson, G. A. & Welch, D. R. Capsaicin-mediated denervation of sensory neurons promotes mammary tumor metastasis to lung and heart. *Anticancer Res* **24**, 1003-1009 (2004).

133 Erin, N. Role of sensory neurons, neuroimmune pathways, and transient receptor potential vanilloid 1 (TRPV1) channels in a murine model of breast cancer metastasis. *Cancer Immunol Immun* **69**, 307-314, doi:10.1007/s00262-019-02463-0 (2020).

134 Vinuesa, A. G. *et al.* Vanilloid Receptor-1 Regulates Neurogenic Inflammation in Colon and Protects Mice from Colon Cancer. *Cancer Res* **72**, 1705-1716, doi:10.1158/0008-5472.CAN-11-3693 (2012).

135 Pavlov, V. A., Chavan, S. S. & Tracey, K. J. Molecular and Functional Neuroscience in Immunity. *Annual Review of Immunology, Vol 36* **36**, 783-812, doi:10.1146/annurev-immunol-042617-053158 (2018).

136 Chavan, S. S., Pavlov, V. A. & Tracey, K. J. Mechanisms and Therapeutic Relevance of Neuro-immune Communication. *Immunity* **46**, 927-942, doi:10.1016/j.immuni.2017.06.008 (2017).

137 Filtjens, J. *et al.* Nociceptive sensory neurons promote CD8 T cell responses to HSV-1 infection. *Nat Commun* **12**, 2936, doi:10.1038/s41467-021-22841-6 (2021).

138 Chiu, I. M. *et al.* Bacteria activate sensory neurons that modulate pain and inflammation. *Nature* **501**, 52-57, doi:10.1038/nature12479 (2013).

139 Kashem, S. W. *et al.* Nociceptive Sensory Fibers Drive Interleukin-23 Production from CD301b+ Dermal Dendritic Cells and Drive Protective Cutaneous Immunity. *Immunity* **43**, 515-526, doi:10.1016/j.immuni.2015.08.016 (2015).

140 Costigan, M., Scholz, J. & Woolf, C. J. Neuropathic pain: a maladaptive response of the nervous system to damage. *Annual review of neuroscience* **32**, 1-32, doi:10.1146/annurev.neuro.051508.135531 (2009).

141 Chavan, S. S., Ma, P. C. & Chiu, I. M. Neuro-immune interactions in inflammation and host defense: Implications for transplantation. *Am J Transplant* **18**, 556-563, doi:10.1111/ajt.14515 (2018).

142 Yam, M. F. *et al.* General Pathways of Pain Sensation and the Major Neurotransmitters Involved in Pain Regulation. *Int J Mol Sci* **19**, doi:10.3390/ijms19082164 (2018).

143 Ali, A., Pisipati, S. & Tewari, A. Words of wisdom: Re: Autonomic nerve development contributes to prostate cancer progression. *European urology* **65**, 665-666, doi:10.1016/j.eururo.2013.11.021 (2014).

144 Kadekawa, K. *et al.* The role of capsaicin-sensitive C-fiber afferent pathways in the control of micturition in spinal-intact and spinal cord-injured mice. *Am J Physiol Renal Physiol* **313**, F796-F804, doi:10.1152/ajprenal.00097.2017 (2017).

145 Borbely, E. *et al.* Capsaicin-sensitive sensory nerves exert complex regulatory functions in the serum-transfer mouse model of autoimmune arthritis. *Brain, behavior, and immunity* **45**, 50-59, doi:10.1016/j.bbi.2014.12.012 (2015).

146 Perl, E. R. Timeline - Ideas about pain, a historical view. *Nature Reviews Neuroscience* **8**, 71-80,

doi:10.1938/nrn2042 (2007).
147 Scholz, J. & Woolf, C. J. The neuropathic pain triad: neurons, immune cells and glia. *Nature neuroscience* **10**, 1361-1368, doi:10.1038/nn1992 (2007).
148 Mirakaj, V., Dalli, J., Granja, T., Rosenberger, P. & Serhan, C. N. Vagus nerve controls resolution and pro-resolving mediators of inflammation. *The Journal of experimental medicine* **211**, 1037-1048, doi:10.1084/jem.20132103 (2014).
149 Wang, L. H., Luo, M., Wang, Y. P. & Wang, D. H. Impaired vasodilation in response to perivascular nerve stimulation in mesenteric arteries of TRPV1-null mutant mice. *J Hypertens* **24**, 2399-2408, doi:DOI 10.1097/01.hjh.0000251900.78051.56 (2006).
150 Feng, N. H., Lee, H. H., Shiang, J. C. & Ma, M. C. Transient receptor potential vanilloid type 1 channels act as mechanoreceptors and cause substance P release and sensory activation in rat kidneys. *Am J Physiol-Renal* **294**, F316-F325, doi:10.1152/ajprenal.00308.2007 (2008).
151 Li, J. P. & Wang, D. H. Increased GFR and renal excretory function by activation of TRPV1 in the isolated perfused kidney. *Pharmacol Res* **57**, 239-246, doi:10.1016/j.phrs.2008.01.011 (2008).
152 Birder, L. A. *et al.* Altered urinary bladder function in mice lacking the vanilloid receptor TRPV1. *Nature neuroscience* **5**, 856-860, doi:10.1038/nn902 (2002).
153 Shanks, J., de Morais, S. D. B., Gao, L., Zucker, I. H. & Wang, H. J. TRPV1 (Transient Receptor Potential Vanilloid 1) Cardiac Spinal Afferents Contribute to Hypertension in Spontaneous Hypertensive Rat. *Hypertension* **74**, 910-920, doi:10.1161/Hypertensionaha.119.13285 (2019).
154 Marrone, M. C. *et al.* TRPV1 channels are critical brain inflammation detectors and neuropathic pain biomarkers in mice. *Nature Communications* **8**, doi:Artn 1529210.1038/Ncomms15292 (2017).
155 Hurtado-Zayala, J. I. *et al.* TRPV1 regulates excitatory innervation of OLM neurons in the hippocampus. *Nature Communications* **8**, doi:Artn 1587810.1038/Ncomms15878 (2017).
156 Cavanaugh, D. J. *et al.* Trpv1 reporter mice reveal highly restricted brain distribution and functional expression in arteriolar smooth muscle cells. *The Journal of neuroscience : the official journal of the Society for Neuroscience* **31**, 5067-5077, doi:10.1523/JNEUROSCI.6451-10.2011 (2011).
157 Yoshida, A. *et al.* TRPV1 is crucial for proinflammatory STAT3 signaling and thermoregulation-associated pathways in the brain during inflammation. *Sci Rep* **6**, 26088, doi:10.1038/srep26088 (2016).
158 Zhang, Y. *et al.* TRPV1 channel mediates NLRP3 inflammasome-dependent neuroinflammation in microglia. *Cell Death Dis* **12**, 1159, doi:10.1038/s41419-021-04450-9 (2021).
159 Saria, A., Skofitsch, G. & Lembeck, F. Distribution of capsaicin in rat tissues after systemic administration. *J Pharm Pharmacol* **34**, 273-275, doi:10.1111/j.2042-7158.1982.tb04245.x (1982).
160 Offley, S. C. *et al.* Capsaicin-sensitive sensory neurons contribute to the maintenance of trabecular bone integrity. *J Bone Miner Res* **20**, 257-267, doi:10.1359/Jbmr.041108 (2005).
161 De Jonge, F. *et al.* Effect of intestinal inflammation on capsaicin-sensitive afferents in the ileum of Schistosoma mansoni-infected mice. *Histochemistry and cell biology* **119**, 477-484, doi:10.1007/s00418-003-0532-5 (2003).
162 Rinne, P. *et al.* Melanocortin 1 Receptor Deficiency Promotes Atherosclerosis in Apolipoprotein E(-/-) Mice. *Arterioscler Thromb Vasc Biol* **38**, 313-323, doi:10.1161/ATVBAHA.117.310418 (2018).
163 Mohanta, S., Yin, C., Weber, C., Hu, D. & Habenicht, A. J. Aorta Atherosclerosis Lesion Analysis in Hyperlipidemic Mice. *Bio-protocol* **6**, doi:10.21769/bioprotoc.1833 (2016).
164 Maier, B. *et al.* A conserved dendritic-cell regulatory program limits antitumour immunity. *Nature* **580**, 257-262, doi:10.1038/s41586-020-2134-y (2020).
165 Bonacina, F. *et al.* Myeloid apolipoprotein E controls dendritic cell antigen presentation and T cell activation. *Nat Commun* **9**, 3083, doi:10.1038/s41467-018-05322-1 (2018).
166 Subramanian, M. & Tabas, I. Dendritic cells in atherosclerosis. *Semin Immunopathol* **36**, 93-102, doi:10.1007/s00281-013-0400-x (2014).
167 Beer, M. *et al.* Laser-capture microdissection of hyperlipidemic/*Apoe*(-)/(-) mouse aorta atherosclerosis. *Methods Mol Biol* **755**, 417-428, doi:10.1007/978-1-61779-163-5_35 (2011).
168 Berthoud, H. R. & Neuhuber, W. L. Functional and chemical anatomy of the afferent vagal system. *Auton Neurosci* **85**, 1-17, doi:10.1016/S1566-0702(00)00215-0 (2000).
169 Wanschel, A. *et al.* Neuroimmune guidance cue Semaphorin 3E is expressed in atherosclerotic plaques and regulates macrophage retention. *Arterioscler Thromb Vasc Biol* **33**, 886-893,

doi:10.1161/ATVBAHA.112.300941 (2013).

170 Randolph, G. J. & Gautier, E. L. Emerging roles of neural guidance molecules in atherosclerosis: sorting out the complexity. *Arterioscler Thromb Vasc Biol* **33**, 882-883, doi:10.1161/ATVBAHA.113.301346 (2013).

171 Woolf, C. J. Central sensitization: uncovering the relation between pain and plasticity. *Anesthesiology* **106**, 864-867, doi:10.1097/01.anes.0000264769.87038.55 (2007).

172 Vermeiren, S., Bellefroid, E. J. & Desiderio, S. Vertebrate Sensory Ganglia: Common and Divergent Features of the Transcriptional Programs Generating Their Functional Specialization. *Front Cell Dev Biol* **8**, 587699, doi:10.3389/fcell.2020.587699 (2020).

173 Guo, J. U. *et al.* Neuronal activity modifies the DNA methylation landscape in the adult brain. *Nature neuroscience* **14**, 1345-1351, doi:10.1038/nn.2900 (2011).

174 Zhu, B. *et al.* ER-associated degradation regulates Alzheimer's amyloid pathology and memory function by modulating gamma-secretase activity. *Nat Commun* **8**, 1472, doi:10.1038/s41467-017-01799-4 (2017).

175 Orr, B. O., Fetter, R. D. & Davis, G. W. Retrograde semaphorin-plexin signalling drives homeostatic synaptic plasticity. *Nature* **550**, 109-113, doi:10.1038/nature24017 (2017).

176 Keller, M., Mirakaj, V., Koeppen, M. & Rosenberger, P. Neuronal guidance proteins in cardiovascular inflammation. *Basic Res Cardiol* **116**, 6, doi:10.1007/s00395-021-00847-x (2021).

177 Fukamachi, S. *et al.* Modulation of semaphorin 3A expression by calcium concentration and histamine in human keratinocytes and fibroblasts. *J Dermatol Sci* **61**, 118-123, doi:10.1016/j.jdermsci.2010.11.012 (2011).

178 GrandPre, T., Nakamura, F., Vartanian, T. & Strittmatter, S. M. Identification of the Nogo inhibitor of axon regeneration as a Reticulon protein. *Nature* **403**, 439-444, doi:10.1038/35000226 (2000).

179 Vogel, K. S., Brannan, C. I., Jenkins, N. A., Copeland, N. G. & Parada, L. F. Loss of neurofibromin results in neurotrophin-independent survival of embryonic sensory and sympathetic neurons. *Cell* **82**, 733-742, doi:10.1016/0092-8674(95)90470-0 (1995).

180 Takemoto-Kimura, S. *et al.* Calmodulin kinases: essential regulators in health and disease. *J Neurochem* **141**, 808-818, doi:10.1111/jnc.14020 (2017).

181 Mongan, L. C. *et al.* The distribution of small and intermediate conductance calcium-activated potassium channels in the rat sensory nervous system. *Neuroscience* **131**, 161-175, doi:10.1016/j.neuroscience.2004.09.062 (2005).

182 Yazdani, U. & Terman, J. R. The semaphorins. *Genome Biol* **7**, 211, doi:10.1186/gb-2006-7-3-211 (2006).

183 Takahashi, T., Nakamura, F., Jin, Z., Kalb, R. G. & Strittmatter, S. M. Semaphorins A and E act as antagonists of neuropilin-1 and agonists of neuropilin-2 receptors. *Nature neuroscience* **1**, 487-493, doi:10.1038/2203 (1998).

184 Zhang, X. *et al.* Nociceptive Sensory Fibers Drive Interleukin-23 Production in a Murine Model of Psoriasis via Calcitonin Gene-Related Peptide. *Front Immunol* **12**, 743675, doi:10.3389/fimmu.2021.743675 (2021).

185 Baskaran, P. *et al.* TRPV1 activation counters diet-induced obesity through sirtuin-1 activation and PRDM-16 deacetylation in brown adipose tissue. *Int J Obesity* **41**, 739-749, doi:10.1038/ijo.2017.16 (2017).

186 Christie, S., Wittert, G. A., Li, H. & Page, A. J. Involvement of TRPV1 Channels in Energy Homeostasis. *Front Endocrinol* **9**, doi:Artn 42010.3389/Fendo.2018.00420 (2018).

187 Akbar, A. *et al.* Increased capsaicin receptor TRPV1-expressing sensory fibres in irritable bowel syndrome and their correlation with abdominal pain. *Gut* **57**, 923-929, doi:10.1136/gut.2007.138982 (2008).

188 Matthews, P. J. *et al.* Increased capsaicin receptor TRPV1 nerve fibres in the inflamed human oesophagus. *Eur J Gastroenterol Hepatol* **16**, 897-902, doi:10.1097/00042737-200409000-00014 (2004).

189 Chakrabarti, S. *et al.* Acute inflammation sensitizes knee-innervating sensory neurons and decreases mouse digging behavior in a TRPV1-dependent manner. *Neuropharmacology* **143**, 49-62, doi:10.1016/j.neuropharm.2018.09.014 (2018).

190 Gao, W. *et al.* Copper sulfide nanoparticles as a photothermal switch for TRPV1 signaling to attenuate atherosclerosis. *Nature Communications* **9**, doi:ARTN 23110.1038/s41467-017-02657-z (2018).

191 Li, B. H. *et al.* TRPV1 activation impedes foam cell formation by inducing autophagy in oxLDL-treated vascular smooth muscle cells. *Cell Death & Disease* **5**, doi:Artn E118210.1038/Cddis.2014.146 (2014).

192 Ma, L. *et al.* Activation of TRPV1 reduces vascular lipid accumulation and attenuates atherosclerosis.

Cardiovasc Res **92**, 504-513, doi:10.1093/cvr/cvr245 (2011).

193 Hu, P., Bembrick, A. L., Keay, K. A. & McLachlan, E. M. Immune cell involvement in dorsal root ganglia and spinal cord after chronic constriction or transection of the rat sciatic nerve. *Brain, behavior, and immunity* **21**, 599-616, doi:10.1016/j.bbi.2006.10.013 (2007).

194 Yu, X. *et al.* Dorsal root ganglion macrophages contribute to both the initiation and persistence of neuropathic pain. *Nat Commun* **11**, 264, doi:10.1038/s41467-019-13839-2 (2020).

195 Checkouri, E., Blanchard, V. & Meilhac, O. Macrophages in Atherosclerosis, First or Second Row Players? *Biomedicines* **9**, doi:10.3390/biomedicines9091214 (2021).

196 Pan, H. *et al.* Single-Cell Genomics Reveals a Novel Cell State During Smooth Muscle Cell Phenotypic Switching and Potential Therapeutic Targets for Atherosclerosis in Mouse and Human. *Circulation* **142**, 2060-2075, doi:10.1161/CIRCULATIONAHA.120.048378 (2020).

197 Meir, K. S. & Leitersdorf, E. Atherosclerosis in the apolipoprotein-E-deficient mouse: a decade of progress. *Arterioscler Thromb Vasc Biol* **24**, 1006-1014, doi:10.1161/01.ATV.0000128849.12617.f4 (2004).

198 Stary, H. C. *et al.* A Definition of Initial, Fatty Streak, and Intermediate Lesions of Atherosclerosis - a Report from the Committee on Vascular-Lesions of the Council on Arteriosclerosis, American-Heart-Association. *Circulation* **89**, 2462-2478 (1994).

6 ACKNOWLEDGEMENTS

First, I would like to give my sincere appreciation to my supervisors Univ.-Prof. Dr. rer. nat. Sabine Steffens and Prof. Dr. med. Andreas J R Habenicht for the opportunity to pursue my Ph.D. work in IPEK. I appreciate their patience and constructive suggestions during my work, as well as their academic and scientific assistance to my thesis. Without their supervision, I would not have been able to arrive where I am now.

I especially thank my direct supervisor, Dr. Sarajo Mohanta. He is not only an experienced researcher himself, but also an excellent Instructor. For the past 6 years, he spent time and patience in guiding my project and training my logical thinking as a rigorous scientist. He did not require me being right every time but encouraged me to seek the possibilities as much as I can and, therefore, explore the science from multiple aspects. I would like to acknowledge Yuanfang for his help in my experiments as an excellent senior colleague. I further thank Shu for his FACS help. I would like to thank Zhihua, Yutao and Chuankai for their kind help without any hesitation when I needed them. Further, I thank Zhe, Xi, Mingyang and Rui for their help in my experiments. With all the help from all of you, I get where I am now. I appreciate to be one of the big family of the Habenicht group. Finally, I would like to thank the ZVH for their support in my animal experiments and the colleagues in the Garden Pavillon for their contribution to our lab.

I especially give my uppermost gratitude to my family. It is their selfless and endless love, education, understanding, and support that shaped who am I and give me the faith and choices to reach different possibilities that I have desired in my whole life.

7 AFFIDAVIT

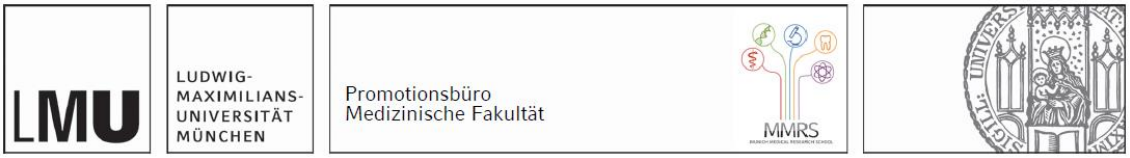

Affidavit

Sun Ting

_____

Surname, first name

Goethestr. 72

_____

Street

80336 München Deutschland

_____

Zip code, town, country

I hereby declare, that the submitted thesis entitled:

Crosstalk Between the Sensory Peripheral Nervous System and Atherosclerosis in Hyperlipidemic Mice is my own work. I have only used the sources indicated and have not made unauthorized use of services of a third party. Where the work of others has been quoted or reproduced, the source is always given.

I further declare that the submitted thesis or parts thereof have not been presented as part of an examination degree to any other university.

Munich, 22.05.2023 Ting Sun

_____ _____

Place, date Signature doctoral candidate

8 Publication List

1. **Sun T**, Li Y, Förstera B, Stanic K, Lu S, Steffens S, Yin C, Ertürk A, Megens RTA, Weber C, Habenicht A, Mohanta SK. Tissue Clearing Approaches in Atherosclerosis. Methods Mol Biol. 2022.
2. Mohanta, S.K., Peng, L., Li, Y. Lu S, **Sun T**…et al. Neuroimmune cardiovascular interfaces control atherosclerosis. Nature (2022).
3. Varasteh Z, Mohanta S, Robu S, Braeuer M, Li Y, Omidvari N, Topping G, **Sun T**, Nekolla SG, Richter A, Weber C, Habenicht A, Haberkorn UA, Weber WA. Molecular Imaging of Fibroblast Activity After Myocardial Infarction Using a 68Ga-Labeled Fibroblast Activation Protein Inhibitor, FAPI-04. J Nucl Med. 2019 Dec.

9 SUPPLEMENT

Table S1. Probe sets of up and down-regulated transcripts in aged WT and *Apoe*$^{-/-}$ abdominal aorta adventitia.

Differential expression of probe sets were determined as described in Methods for different peripheral sensory nervous system related Gene Ontology (GO) terms in LCM-derived abdominal aorta adventitia from 3 WT adventitia, 4 *Apoe*$^{-/-}$ without plaque and 4 ATLO at age of 78 wks. The following GO-terms were analyzed from total genes: A) neuron projection (GO: 0043005), B) axon guidance (GO: 0007411), C) sensory perception (GO: 0007600), D) ion channel activity (GO: 0005216), E) ligand-gated ion channel activity (GO: 0015276). Further data are displayed as heat maps in Fig. 33. Probe sets are ordered according to fold change between aorta adentitia without plaque from 78 wks old *Apoe*$^{-/-}$ mice versus ATLO. Gene symbols and gene names are indicated for ease of reading. Columns of the mean value for each gene show signal intensity without normalization.

A. Neuron projection (GO: 0043005)

Affymetrix Probe set ID	Gene Symbol	Gene Name	Entrez Gene ID	Mean WT aorta adventitia 78 wks	Mean *Apoe*$^{-/-}$ aorta adventitia no plaque 78wks	Mean *Apoe*$^{-/-}$ aorta adventitia with ATLO 78wks	Fold change *Apoe*$^{-/-}$ aorta no plaque *vs.* ATLO	p ANOVA
1415857_at	Emb	embigin	13723	246	33	698	21.2	0.0020
1418945_at	Mmp3	matrix metallopeptidase 3	17392	2278	1206	9869	8.18	0.0030
1416246_a_at	Coro1a	coronin, actin binding protein 1A	12721	586	614	4470	7.28	0.0010
1455269_a_at	Coro1a	coronin, actin binding protein 1A	12721	729	1006	6703	6.66	0.0005
1448710_at	Cxcr4	chemokine (C-X-C motif) receptor 4	12767	173	108	679	6.28	0.0006
1455332_x_at	Fcgr2b	Fc receptor, IgG, low affinity IIb	14130	467	380	2273	5.98	0.0002
1417795_at	Chl1	cell adhesion molecule L1-like	12661	91	70	410	5.89	0.0030
1417976_at	Ada	adenosine deaminase	11486	86	67	347	5.21	0.0200
1451941_a_at	Fcgr2b	Fc receptor, IgG, low affinity IIb	14130	616	347	1789	5.16	0.0009
1422105_at	Cd3e	CD3 antigen, epsilon polypeptide	12501	52	65	325	5.03	0.0200
1435477_s_at	Fcgr2b	Fc receptor, IgG, low affinity IIb	14130	1291	1062	5157	4.86	0.0003
1424542_at	S100a4	S100 calcium binding protein A4	20198	1068	763	3688	4.83	0.0010
1451987_at	Arrb2	arrestin, beta 2	216869	190	164	731	4.45	0.0002
1435945_a_at	Kcnn4	potassium intermediate/small conductance calcium-activated channel, subfamily N, member 4	16534	145	186	822	4.41	0.0020
1416956_at	Kcnab2	potassium voltage-gated channel, shaker-related subfamily, beta member 2	16498	103	80	327	4.09	0.0007
1435476_a_at	Fcgr2b	Fc receptor, IgG, low affinity IIb	14130	1584	960	3643	3.79	0.0003
1449473_s_at	Cd40	CD40 antigen	21939	82	106	366	3.47	0.0020
1416882_at	Rgs10	regulator of G-protein signalling 10	67865	666	498	1262	2.53	0.0050
1423478_at	Prkcb	protein kinase C, beta	18751	128	169	405	2.39	0.0070
1417379_at	Iqgap1	IQ motif containing GTPase activating protein 1	29875	1088	837	2001	2.39	0.0050
1419296_at	Arhgap4	Rho GTPase activating protein 4	171207	114	114	387	3.38	0.0020

Affymetrix Probe set ID	Gene Symbol	Gene Name	Entrez Gene ID	Mean WT aorta adventitia 78 wks	Mean *Apoe*$^{-/-}$ aorta adventitia no plaque 78wks	Mean *Apoe*$^{-/-}$ aorta adventitia with ATLO 78wks	Fold change *Apoe*$^{-/-}$ aorta no plaque *vs.* ATLO	p ANOVA
1454268_a_at	Cyba	cytochrome b-245, alpha polypeptide	13057	927	877	2963	3.38	0.0020
1459546_s_at	Enpp1	ectonucleotide pyrophosphatase/phosphodiesterase 1	18605	176	127	426	3.35	0.0010
1460419_a_at	Prkcb	protein kinase C, beta	18751	558	515	1600	3.11	0.0010
1448950_at	Il1r1	interleukin 1 receptor, type I	16177	304	400	1241	3.1	0.0010
1438115_a_at	Slc9a3r1	solute carrier family 9 (sodium/hydrogen exchanger), member 3 regulator 1	26941	572	319	973	3.05	0.0020
1424208_at	Ptger4	prostaglandin E receptor 4 (subtype EP4)	19219	497	455	1375	3.02	0.0004
1420380_at	Ccl2	chemokine (C-C motif) ligand 2	20296	97	93	277	2.99	0.0200
1450020_at	Cx3cr1	chemokine (C-X3-C motif) receptor 1	13051	111	120	358	2.98	0.0100
1456380_x_at	Cnn3	calponin 3, acidic	71994	421	795	2324	2.92	0.0100
1415856_at	Emb	embigin	13723	357	250	730	2.92	0.0040
1455796_x_at	Olfm1	olfactomedin 1	56177	236	232	674	2.9	0.0300
1419221_a_at	Rgs14	regulator of G-protein signaling 14	51791	378	220	592	2.7	0.0030
1424181_at	6-Sep	septin 6	56526	246	152	410	2.69	0.0060
1449591_at	Casp4	caspase 4, apoptosis-related cysteine peptidase	12363	321	251	668	2.66	0.0030
1426239_s_at	Arrb2	arrestin, beta 2	216869	467	606	1606	2.65	0.0005
1438116_x_at	Slc9a3r1	solute carrier family 9 (sodium/hydrogen exchanger), member 3 regulator 1	26941	643	446	1181	2.65	0.0010
1460555_at	Ripor2	RHO family interacting cell polarization regulator 2	193385	240	276	720	2.61	0.0060
1420979_at	Pak1	p21 (RAC1) activated kinase 1	18479	92	85	220	2.59	0.0070
1421525_a_at	Naip5	NLR family, apoptosis inhibitory protein 5	17951	113	97	224	2.31	0.0300
1451310_a_at	Ctsl	cathepsin L	13039	4744	2422	5478	2.26	0.0007
1423135_at	Thy1	thymus cell antigen 1, theta	21838	1210	1017	2298	2.26	0.0060
1421917_at	Pdgfra	platelet derived growth factor receptor, alpha polypeptide	18595	2511	1052	2377	2.26	0.0060

Affymetrix Probe set ID	Gene Symbol	Gene Name	Entrez Gene ID	Mean WT aorta adventitia 78 wks	Mean *Apoe*$^{-/-}$ aorta adventitia no plaque 78wks	Mean *Apoe*$^{-/-}$ aorta adventitia with ATLO 78wks	Fold change *Apoe*$^{-/-}$ aorta no plaue *vs.* ATLO	p ANOVA
1416759_at	Mical1	microtubule associated monooxygenase, calponin and LIM domain containing 1	171580	195	209	469	2.25	0.0060
1426744_at	Srebf2	sterol regulatory element binding factor 2	20788	206	98	217	2.23	0.0040
1415903_at	Slc38a1	solute carrier family 38, member 1	105727	355	247	540	2.19	0.0090
1436958_x_at	Tpm3	tropomyosin 3, gamma	59069	2270	2037	4370	2.15	0.0010
1415849_s_at	Stmn1	stathmin 1	16765	1019	545	1160	2.13	0.0500
1449315_at	Tenm3	teneurin transmembrane protein 3	23965	163	95	202	2.12	0.0100
1417676_a_at	Ptpro	protein tyrosine phosphatase, receptor type, O	19277	290	203	424	2.09	0.0300
1439440_x_at	Twf2	twinfilin actin binding protein 2	23999	465	836	1743	2.08	0.0002
1434653_at	Ptk2b	PTK2 protein tyrosine kinase 2 beta	19229	211	345	718	2.08	0.0005
1449018_at	Pfn1	profilin 1	18643	1301	964	1989	2.06	0.0200
1431394_a_at	Lrrk2	leucine-rich repeat kinase 2	66725	342	219	451	2.06	0.0070
1450033_a_at	Stat1	signal transducer and activator of transcription 1	20846	577	396	806	2.04	0.0300
1419754_at	Myo5a	myosin VA	17918	241	258	525	2.03	0.0060
1423326_at	Entpd1	ectonucleoside triphosphate diphosphohydrolase 1	12495	314	224	456	2.03	0.0200
1450027_at	Sdc3	syndecan 3	20970	499	538	1074	2	0.0010
1428103_at	Adam10	a disintegrin and metallopeptidase domain 10	11487	1643	1784	3559	1.99	0.0020
1426301_at	Alcam	activated leukocyte cell adhesion molecule	11658	141	209	395	1.89	0.0300
1451992_at	Grk2	G protein-coupled receptor kinase 2	110355	286	337	634	1.88	0.0004
1426300_at	Alcam	activated leukocyte cell adhesion molecule	11658	152	175	327	1.87	0.0200
1420622_a_at	Hspa8	heat shock protein 8	15481	2008	4254	7834	1.84	0.0020
1416514_a_at	Fscn1	fascin actin-bundling protein 1	14086	696	1277	2268	1.78	0.0030

Affymetrix Probe set ID	Gene Symbol	Gene Name	Entrez Gene ID	Mean WT aorta adventitia 78 wks	Mean *Apoe*$^{-/-}$ aorta adventitia no plaque 78wks	Mean *Apoe*$^{-/-}$ aorta adventitia with ATLO 78wks	Fold change *Apoe*$^{-/-}$ aorta no plaue *vs.* ATLO	p ANOVA
1427260_a_at	Tpm3	tropomyosin 3, gamma	59069	2558	2975	5173	1.74	0.0080
1448279_at	Arpc3	actin related protein 2/3 complex, subunit 3	56378	2398	2856	4949	1.73	0.0020
1431292_a_at	Twf2	twinfilin actin binding protein 2	23999	161	216	341	1.58	0.0090
1438992_x_at	Atf4	activating transcription factor 4	11911	903	1366	2100	1.54	0.0020
1417869_s_at	Ctsz	cathepsin Z	64138	1441	2202	3160	1.43	0.0005
1433829_a_at	Hnrnpa2b1	heterogeneous nuclear ribonucleoprotein A2/B1	53379	2431	3886	5245	1.35	0.0020
1434272_at	Cpeb2	cytoplasmic polyadenylation element binding protein 2	231207	219	521	694	1.33	0.0200
1432466_a_at	*Apoe*	apolipoprotein E	11816	14332	96	127	1.31	0.0002
1417627_a_at	Limk1	LIM-domain containing, protein kinase	16885	147	244	303	1.24	0.0200
1438176_x_at	Snap47	synaptosomal-associated protein, 47	67826	2977	1478	1822	1.23	0.0200
1435884_at	Itsn1	intersectin 1 (SH3 domain protein 1A)	16443	305	514	630	1.23	0.0200
1425492_at	Bmpr1a	bone morphogenetic protein receptor, type 1A	12166	1146	564	677	1.2	0.0010
1438506_s_at	Abi1	abl-interactor 1	11308	174	389	462	1.19	0.0020
1426645_at	Hsp90aa1	heat shock protein 90, alpha (cytosolic), class A member 1	15519	2856	1044	1175	1.13	0.0200
1460251_at	Fas	Fas (TNF receptor superfamily member 6)	14102	194	493	416	1.19	0.0080
1423893_x_at	Apbb1	amyloid beta (A4) precursor protein-binding, family B, member 1	11785	559	315	263	1.2	0.0100
1421955_a_at	Nedd4	neural precursor cell expressed, developmentally down-regulated 4	17999	520	262	197	1.33	0.0200
1438067_at	Nf1	neurofibromin 1	18015	255	169	126	1.35	0.0020
1416936_at	Aatk	apoptosis-associated tyrosine kinase	11302	375	248	176	1.41	0.0300
1415840_at	Elovl5	ELOVL family member 5, elongation of long chain fatty acids (yeast)	68801	5398	3751	2627	1.43	0.0070

Affymetrix Probe set ID	Gene Symbol	Gene Name	Entrez Gene ID	Mean WT aorta adventitia 78 wks	Mean *Apoe*$^{-/-}$ aorta adventitia no plaque 78wks	Mean *Apoe*$^{-/-}$ aorta adventitia with ATLO 78wks	Fold change *Apoe*$^{-/-}$ aorta no plaue *vs.* ATLO	p ANOVA
1436342_a_at	Ubxn1	UBX domain protein 1	225896	499	1479	882	1.68	0.0008
1451200_at	Kif1b	kinesin family member 1B	16561	1062	797	472	1.69	0.0060
1450650_at	Myo10	myosin X	17909	74	202	115	1.76	0.0040
1416418_at	Gabarapl1	gamma-aminobutyric acid (GABA) A receptor-associated protein-like 1	57436	961	779	438	1.78	0.0200
1436930_x_at	Hmbs	hydroxymethylbilane synthase	15288	346	791	443	1.78	0.0050
1423363_at	Sort1	sortilin 1	20661	252	511	284	1.8	0.0200
1416419_s_at	Gabarapl1	gamma-aminobutyric acid (GABA) A receptor-associated protein-like 1	57436	2258	1665	917	1.81	0.0100
1419301_at	Fzd4	frizzled class receptor 4	14366	1285	1168	619	1.89	0.0100
1421116_a_at	Rtn4	reticulon 4	68585	1981	1673	886	1.89	0.0030
1450468_at	Myoc	myocilin	17926	493	184	96	1.92	0.0030
1449183_at	Comt	catechol-O-methyltransferase	12846	3957	3057	1530	2	0.0050
1416203_at	Aqp1	aquaporin 1	11826	2374	2250	1117	2.01	0.0060
1426463_at	Gphn	gephyrin	268566	234	235	116	2.03	0.0030
1428835_at	Myh14	myosin, heavy polypeptide 14	71960	335	400	196	2.04	0.0070
1456036_x_at	Gsto1	glutathione S-transferase omega 1	14873	1871	3391	1659	2.04	0.0007
1426521_at	D230025D16Rik	RIKEN cDNA D230025D16 gene	234678	282	349	168	2.08	0.0100
1436945_x_at	Stim1	stromal interaction molecule 1	20866	326	678	311	2.18	0.0006
1424078_s_at	Pex6	peroxisomal biogenesis factor 6	224824	467	718	326	2.2	0.0010
1451226_at	Pex6	peroxisomal biogenesis factor 6	224824	671	892	404	2.21	0.0020
1419247_at	Rgs2	regulator of G-protein signaling 2	19735	1393	2367	1040	2.28	0.0200
1452031_at	Slc1a3	solute carrier family 1 (glial high affinity glutamate transporter), member 3	20512	631	790	339	2.33	0.0090
1450955_s_at	Sort1	sortilin 1	20661	303	393	168	2.34	0.0010
1417702_a_at	Hnmt	histamine N-methyltransferase	140483	332	505	216	2.34	0.0200
1452782_a_at	Txn2	thioredoxin 2	56551	628	893	379	2.36	0.0090

Affymetrix Probe set ID	Gene Symbol	Gene Name	Entrez Gene ID	Mean WT aorta adventitia 78 wks	Mean *Apoe*$^{-/-}$ aorta adventitia no plaque 78wks	Mean *Apoe*$^{-/-}$ aorta adventitia with ATLO 78wks	Fold change *Apoe*$^{-/-}$ aorta no plaue *vs.* ATLO	p ANOVA
1453206_at	Acad9	acyl-Coenzyme A dehydrogenase family, member 9	229211	315	430	182	2.36	0.0005
1423362_at	Sort1	sortilin 1	20661	1445	1859	784	2.37	0.0006
1449214_a_at	Opa1	OPA1, mitochondrial dynamin like GTPase	74143	191	411	171	2.41	0.0090
1450519_a_at	Prkaca	protein kinase, cAMP dependent, catalytic, alpha	18747	829	1070	438	2.44	0.0020
1449097_at	Txnrd2	thioredoxin reductase 2	26462	225	462	188	2.45	0.0020
1421557_x_at	Txn2	thioredoxin 2	56551	692	1219	496	2.45	0.0080
1455136_at	Atp1a2	ATPase, Na+/K+ transporting, alpha 2 polypeptide	98660	371	412	165	2.5	0.0080
1451312_at	Ndufs7	NADH:ubiquinone oxidoreductase core subunit S7	75406	3216	3765	1488	2.53	0.0030
1450659_at	Rgs7	regulator of G protein signaling 7	24012	612	612	230	2.67	0.0200
1426340_at	Slc1a3	solute carrier family 1 (glial high affinity glutamate transporter), member 3	20512	668	895	332	2.7	0.0030
1417251_at	Palmd	palmdelphin	114301	688	898	332	2.71	0.0006
1419107_at	Ophn1	oligophrenin 1	94190	223	416	147	2.83	0.0050
1417421_at	S100a1	S100 calcium binding protein A1	20193	1208	1340	473	2.83	0.0002
1449379_at	Kdr	kinase insert domain protein receptor	16542	922	1344	460	2.92	0.0003
1424313_a_at	Ndufs7	NADH:ubiquinone oxidoreductase core subunit S7	75406	4278	7203	2447	2.94	0.0020
1426785_s_at	Mgll	monoglyceride lipase	23945	4158	6890	2338	2.95	0.0040
1450391_a_at	Mgll	monoglyceride lipase	23945	2951	4634	1549	2.99	0.0040
1422470_at	Bnip3	BCL2/adenovirus E1B interacting protein 3	12176	4837	5747	1919	2.99	0.0004
1426235_a_at	Glul	glutamate-ammonia ligase (glutamine synthetase)	14645	1762	2441	813	3	0.0010
1453836_a_at	Mgll	monoglyceride lipase	23945	1691	2149	690	3.12	0.0020

Affymetrix Probe set ID	Gene Symbol	Gene Name	Entrez Gene ID	Mean WT aorta adventitia 78 wks	Mean *Apoe*$^{-/-}$ aorta adventitia no plaque 78wks	Mean *Apoe*$^{-/-}$ aorta adventitia with ATLO 78wks	Fold change *Apoe*$^{-/-}$ aorta no plaue *vs.* ATLO	p ANOVA
1425534_at	Stau2	staufen double-stranded RNA binding protein 2	29819	235	319	99	3.23	0.0010
1419814_s_at	S100a1	S100 calcium binding protein A1	20193	3867	5634	1700	3.31	0.0020
1455961_at	Mme	membrane metallo endopeptidase	17380	904	1246	350	3.56	0.0007
1450344_a_at	Ptger3	prostaglandin E receptor 3 (subtype EP3)	19218	1672	1654	447	3.7	0.0060
1434893_at	Atp1a2	ATPase, Na+/K+ transporting, alpha 2 polypeptide	98660	1736	2841	755	3.76	0.0010
1427465_at	Atp1a2	ATPase, Na+/K+ transporting, alpha 2 polypeptide	98660	1229	2588	681	3.8	0.0020
1415984_at	Acadm	acyl-Coenzyme A dehydrogenase, medium chain	11364	12039	12144	3085	3.94	0.0008
1452308_a_at	Atp1a2	ATPase, Na+/K+ transporting, alpha 2 polypeptide	98660	1408	1811	454	3.99	0.0030
1434100_x_at	Ppargc1a	peroxisome proliferative activated receptor, gamma, coactivator 1 alpha	19017	126	249	42	5.93	0.0040
1437751_at	Ppargc1a	peroxisome proliferative activated receptor, gamma, coactivator 1 alpha	19017	158	251	41	6.08	0.0090
1422852_at	Cib2	calcium and integrin binding family member 2	56506	1273	1672	266	6.3	0.0008
1456395_at	Ppargc1a	peroxisome proliferative activated receptor, gamma, coactivator 1 alpha	19017	288	355	50	7.05	0.0060
1415984_at	Acadm	acyl-Coenzyme A dehydrogenase, medium chain	11364	12039	12144	3085	3.94	0.0008
1452308_a_at	Atp1a2	ATPase, Na+/K+ transporting, alpha 2 polypeptide	98660	1408	1811	454	3.99	0.0030
1434100_x_at	Ppargc1a	peroxisome proliferative activated receptor, gamma, coactivator 1 alpha	19017	126	249	42	5.93	0.0040
1437751_at	Ppargc1a	peroxisome proliferative activated receptor, gamma, coactivator 1 alpha	19017	158	251	41	6.08	0.0090
1422852_at	Cib2	calcium and integrin binding family member 2	56506	1273	1672	266	6.3	0.0008

Affymetrix Probe set ID	Gene Symbol	Gene Name	Entrez Gene ID	Mean WT aorta adventitia 78 wks	Mean *Apoe*$^{-/-}$ aorta adventitia no plaque 78wks	Mean *Apoe*$^{-/-}$ aorta adventitia with ATLO 78wks	Fold change *Apoe*$^{-/-}$ aorta no plaue *vs.* ATLO	p ANOVA
1456395_at	Ppargc1a	peroxisome proliferative activated receptor, gamma, coactivator 1 alpha	19017	288	355	50	7.05	0.0060
1449265_at	Casp1	caspase 1	12362	399	301	772	2.56	0.0010
1418099_at	Tnfrsf1b	tumor necrosis factor receptor superfamily, member 1b	21938	249	293	744	2.54	0.0005

B. Axon guidance (GO: 0007411)

Affymetrix Probe set ID	Gene Symbol	Gene Name	Entrez Gene ID	Mean WT aorta adventitia 78 wks	Mean *Apoe*$^{-/-}$ aorta adventitia no plaque 78wks	Mean *Apoe*$^{-/-}$ aorta adventitia with ATLO 78wks	Fold change *Apoe*$^{-/-}$ aorta no plaue *vs.* ATLO	p ANOVA
1448710_at	Cxcr4	chemokine (C-X-C motif) receptor 4	12767	173	108	679	6.28	0.0006
1417795_at	Chl1	cell adhesion molecule with homology	12661	91	70	410	5.89	0.003
1434920_a_at	Evl	Ena-vasodilator stimulated phosphoprotein	14026	241	258	922	3.57	0.006
1448823_at	Cxcl12	chemokine (C-X-C motif) ligand 12	20315	5201	4107	14034	3.42	0.0006
1421141_a_at	Foxp1	forkhead box P1	108655	149	87	194	2.24	0.03
1450106_a_at	Evl	Ena-vasodilator stimulated phosphoprotein	14026	98	123	267	2.17	0.01
1421142_s_at	Foxp1	forkhead box P1	108655	369	167	324	1.94	0.007
1426301_at	Alcam	activated leukocyte cell adhesion molecule	11658	141	209	395	1.89	0.03
1426300_at	Alcam	activated leukocyte cell adhesion molecule	11658	152	175	327	1.87	0.02
1417574_at	Cxcl12	chemokine (C-X-C motif) ligand 12	20315	929	1295	2254	1.74	0.001
1423893_x_at	Apbb1	amyloid beta (A4) precursor protein-binding, family B, member 1	11785	559	315	263	-1.2	0.01
1416855_at	Gas1	growth arrest specific 1	14451	4395	2200	1609	-1.37	0.003
1436791_at	Wnt5a	wingless-related MMTV integration site 5A	22418	274	220	130	-1.68	0.02
1422541_at	Ptprm	protein tyrosine phosphatase, receptor type, M	19274	821	889	371	-2.4	0.0006

C. Sensory perception (GO: 0007600)

Affymetrix Probe set ID	Gene Symbol	Gene Name	Entrez Gene ID	Mean WT aorta adventitia 78 wks	Mean *Apoe*$^{-/-}$ aorta adventitia no plaque 78wks	Mean *Apoe*$^{-/-}$ aorta adventitia with ATLO 78wks	Fold change *Apoe*$^{-/-}$ aorta no plaue *vs.* ATLO	p ANOVA
1423607_at	Lum	lumican	17022	2694	1189	8359	7.03	0.0005
1448710_at	Cxcr4	chemokine (C-X-C motif) receptor 4	12767	176	111	677	6.12	0.0006
1421186_at	Ccr2	chemokine (C-C motif) receptor 2	12772	203	280	1641	5.85	0.0004
1425225_at	Fcgr4	Fc receptor, IgG, low affinity IV	246256	192	178	1033	5.79	0.0010
1448591_at	Ctss	cathepsin S	13040	2586	2558	13285	5.19	0.0002
1451987_at	Arrb2	arrestin, beta 2	216869	194	168	729	4.34	0.0002
1423669_at	Col1a1	collagen, type I, alpha 1	12842	907	971	3737	3.85	0.0200
1448823_at	Cxcl12	chemokine (C-X-C motif) ligand 12	20315	5242	4093	15383	3.76	0.0005
1438115_a_at	Slc9a3r1	solute carrier family 9 (sodium/hydrogen exchanger), member 3 regulator 1	26941	573	324	966	2.98	0.0020
1437874_s_at	Hexb	hexosaminidase B	15212	2115	1431	4099	2.86	0.0002
1460180_at	Hexb	hexosaminidase B	15212	801	620	1726	2.79	0.0030
1426239_s_at	Arrb2	arrestin, beta 2	216869	470	606	1585	2.62	0.0005
1438116_x_at	Slc9a3r1	solute carrier family 9 (sodium/hydrogen exchanger), member 3 regulator 1	26941	642	449	1169	2.6	0.0010
1460555_at	Ripor2	RHO family interacting cell polarization regulator 2	193385	244	281	718	2.56	0.0060
1421188_at	Ccr2	chemokine (C-C motif) receptor 2	12772	145	229	579	2.53	0.0010
1424067_at	Icam1	intercellular adhesion molecule 1	15894	494	540	1320	2.44	0.0040
1424683_at	Retreg1	reticulophagy regulator 1	66270	731	545	1276	2.34	0.0200
1455494_at	Col1a1	collagen, type I, alpha 1	12842	947	1434	3320	2.32	0.0100
1419754_at	Myo5a	myosin VA	17918	245	263	527	2.01	0.0060
1427974_s_at	Cacna1d	calcium channel, voltage-dependent, L type, alpha 1D subunit	12289	90	120	228	1.9	0.0090
1451992_at	Grk2	G protein-coupled receptor kinase 2	110355	290	341	633	1.85	0.0004

Affymetrix Probe set ID	Gene Symbol	Gene Name	Entrez Gene ID	Mean WT aorta adventitia 78 wks	Mean *Apoe*$^{-/-}$ aorta adventitia no plaque 78wks	Mean *Apoe*$^{-/-}$ aorta adventitia with ATLO 78wks	Fold change *Apoe*$^{-/-}$ aorta no plaue *vs.* ATLO	p ANOVA
1416892_s_at	Fam107b	family with sequence similarity 107, member B	66540	742	854	1547	1.81	0.0100
1417574_at	Cxcl12	chemokine (C-X-C motif) ligand 12	20315	923	1280	2221	1.73	0.0010
1455792_x_at	Ndn	necdin	17984	1872	1521	898	1.69	0.0300
1419301_at	Fzd4	frizzled class receptor 4	14366	1271	1156	619	1.87	0.0100
1421116_a_at	Rtn4	reticulon 4	68585	1952	1652	880	1.88	0.0030
1421960_at	Adcy3	adenylate cyclase 3	104111	1124	889	467	1.9	0.0300
1416203_at	Aqp1	aquaporin 1	11826	2341	2218	1107	2	0.0060
1449183_at	Comt	catechol-O-methyltransferase	12846	3924	3027	1511	2	0.0050
1428835_at	Myh14	myosin, heavy polypeptide 14	71960	340	404	200	2.02	0.0070
1449893_a_at	Lrig1	leucine-rich repeats and immunoglobulin-like domains 1	16206	234	302	144	2.1	0.0100
1452031_at	Slc1a3	solute carrier family 1 (glial high affinity glutamate transporter), member 3	20512	631	787	344	2.29	0.0090
1449214_a_at	Opa1	OPA1, mitochondrial dynamin like GTPase	74143	195	414	174	2.38	0.0090
1450883_a_at	Cd36	CD36 molecule	12491	8694	9607	3928	2.45	0.0030
1426340_at	Slc1a3	solute carrier family 1 (glial high affinity glutamate transporter), member 3	20512	667	889	336	2.64	0.0030
1423166_at	Cd36	CD36 molecule	12491	10771	8170	3062	2.67	0.0004
1423420_at	Adrb1	adrenergic receptor, beta 1	11554	88	293	102	2.88	0.0100
1450391_a_at	Mgll	monoglyceride lipase	23945	2911	4631	1530	3.03	0.0040
1426785_s_at	Mgll	monoglyceride lipase	23945	4136	7080	2307	3.07	0.0030
1448499_a_at	Ephx2	epoxide hydrolase 2, cytoplasmic	13850	3282	4825	1570	3.07	0.0030
1453836_a_at	Mgll	monoglyceride lipase	23945	1669	2118	688	3.08	0.0020
1434210_s_at	Lrig1	leucine-rich repeats and immunoglobulin-like domains 1	16206	244	282	88	3.22	0.0004
1455961_at	Mme	membrane metallo endopeptidase	17380	898	1233	354	3.48	0.0007
1450884_at	Cd36	CD36 molecule	12491	1537	2245	541	4.15	0.0006

D. Ion channel activity (GO: 0005216)

Affymetrix Probe set ID	Gene Symbol	Gene Name	Entrez Gene ID	Mean WT aorta adventitia 78 wks	Mean *Apoe*$^{-/-}$ aorta adventitia no plaque 78wks	Mean *Apoe*$^{-/-}$ aorta adventitia with ATLO 78wks	Fold change *Apoe*$^{-/-}$ aorta no plaue *vs.* ATLO	p ANOVA
1435945_a_at	Kcnn4	potassium intermediate/small conductance calcium-activated channel, subfamily N, member 4	16534	148	190	817	4.31	0.0020
1416379_at	Panx1	pannexin 1	55991	34	64	263	4.08	0.0060
1416956_at	Kcnab2	potassium voltage-gated channel, shaker-related subfamily, beta member 2	16498	105	82	331	4.05	0.0007
1418296_at	Fxyd5	FXYD domain-containing ion transport regulator 5	18301	1134	975	3197	3.28	0.0004
1417399_at	Gas6	growth arrest specific 6	14456	3628	2164	6703	3.1	0.0020
1416656_at	Clic1	chloride intracellular channel 1	114584	1376	933	2609	2.8	0.0007
1434653_at	Ptk2b	PTK2 protein tyrosine kinase 2 beta	19229	215	350	716	2.04	0.0005
1427974_s_at	Cacna1d	calcium channel, voltage-dependent, L type, alpha 1D subunit	12289	90	120	228	1.9	0.0090
1424700_at	Tmem38b	transmembrane protein 38B	52076	721	1000	499	2	0.0060
1416203_at	Aqp1	aquaporin 1	11826	2341	2218	1107	2	0.0060
1421374_a_at	Fxyd1	FXYD domain-containing ion transport regulator 1	56188	2833	2997	1485	2.02	0.0030
1417680_at	Kcna5	potassium voltage-gated channel, shaker-related subfamily, member 5	16493	151	265	127	2.1	0.0200
1436945_x_at	Stim1	stromal interaction molecule 1	20866	330	676	315	2.14	0.0006
1417061_at	Slc40a1	solute carrier family 40 (iron-regulated transporter), member 1	53945	419	441	202	2.18	0.0200
1449433_at	P2rx5	purinergic receptor P2X, ligand-gated ion channel, 5	94045	332	295	94	3.13	0.0080
1424308_at	Slc24a3	solute carrier family 24 (sodium/potassium/calcium exchanger), member 3	94249	957	1690	448	3.77	0.0005
1425341_at	Kcnk3	potassium channel, subfamily K, member 3	16527	593	1258	147	8.53	0.0004

E. Ligand-gated ion channel activity (GO: 0015276)

Affymetrix Probe set ID	Gene Symbol	Gene Name	Entrez Gene ID	Mean WT aorta adventitia 78 wks	Mean *Apoe*$^{-/-}$ aorta adventitia no plaque 78wks	Mean *Apoe*$^{-/-}$ aorta adventitia with ATLO 78wks	Fold change *Apoe*$^{-/-}$ aorta no plaue *vs.* ATLO	p ANOVA
1434653_at	Ptk2b	PTK2 protein tyrosine kinase 2 beta	19229	215	350	716	2.04	0.0005
1416203_at	Aqp1	aquaporin 1	11826	2341	2218	1107	2	0.0060
1449433_at	P2rx5	purinergic receptor P2X, ligand-gated ion channel, 5	94045	332	295	94	3.13	0.0080

Table S2. Probe sets of total aorta up and down-regulated transcripts of WT and *Apoe*$^{-/-}$ mice during aging.

Differential expression of probe sets were determined as described in Methods for different peripheral sensory nervous system related Gene Ontology (GO) terms in LCM-derived abdominal aorta adventitia from 3 WT and 3 *Apoe*$^{-/-}$ mice each at 6, 32, and 78 weeks. The following GO-terms were analyzed from total genes: A) neuron projection (GO: 0043005), B) axon guidance (GO: 0007411), C) sensory perception (GO: 0007600), D) ion channel activity (GO: 0005216), E) ligand-gated ion channel activity (GO: 0015276). Further data are displayed as heat maps in Fig. 34. Probe sets are ordered according to fold change between aorta from 78 wks old *Apoe*$^{-/-}$ mice versus 6 wks old WT mice. Gene symbols and gene names are indicated for ease of reading. Columns of the mean value for each gene show signal intensity without normalization.

A. Neuron projection (GO: 0043005)

Affymetrix Probe set ID	Gene Symbol	Gene Name	Entrez Gene ID	Mean WT aorta 6 wks	Mean WT aorta 32 wks	Mean WT aorta 78 wks	Mean *Apoe*$^{-/-}$ aorta 6 wks	Mean *Apoe*$^{-/-}$ aorta 32 wks	Mean *Apoe*$^{-/-}$ aorta 78 wks	Fold change *Apoe*$^{-/-}$ 78 wks *vs.* *WT* 6 wks	p. ANOVA
1450476_at	Cnr2	cannabinoid receptor 2 (macrophage)	12802	10	10	11	8	53	209	26.84	0.0004
1423478_at	Prkcb	protein kinase C, beta	18751	16	30	23	23	185	358	15.24	0.0001
1448710_at	Cxcr4	chemokine (C-X-C motif) receptor 4	12767	80	112	107	77	529	1120	14.5	0.0000
1455269_a_at	Coro1a	coronin, actin binding protein 1A	12721	169	336	625	275	1527	3332	12.12	0.0000
1416246_a_at	Coro1a	coronin, actin binding protein 1A	12721	334	325	498	336	1586	3943	11.75	0.0000
1419127_at	Npy	neuropeptide Y	109648	108	319	439	119	643	1319	11.11	0.0050
1436778_at	Cybb	cytochrome b-245, beta polypeptide	13058	329	376	637	312	1584	3259	10.45	0.0000
1432466_a_at	*Apoe*	apolipoprotein E	11816	7518	5330	5505	19	179	189	9.91	0.0000
1420380_at	Ccl2	chemokine (C-C motif) ligand 2	20296	99	49	126	95	414	915	9.65	0.0001
1435945_a_at	Kcnn4	potassium intermediate/small conductance calcium-activated channel, subfamily N, member 4	16534	337	460	250	158	692	1501	9.51	0.0001
1424471_at	Rapgef3	Rap guanine nucleotide exchange factor (GEF) 3	223864	48	79	109	30	179	247	8.2	0.0070
1460419_a_at	Prkcb	protein kinase C, beta	18751	250	359	588	265	1076	2126	8.01	0.0000
1417788_at	Sncg	synuclein, gamma	20618	439	893	1492	340	1742	2668	7.85	0.0000
1427005_at	Plk2	polo like kinase 2	20620	211	135	344	171	520	1291	7.54	0.0000
1459850_x_at	Glrb	glycine receptor, beta subunit	14658	10	52	233	82	120	582	7.13	0.0001
1451987_at	Arrb2	arrestin, beta 2	216869	170	188	174	147	568	986	6.71	0.0000
1429055_at	Shtn1	shootin 1	71653	151	242	229	146	492	829	5.67	0.0000
1435349_at	Nrp2	neuropilin 2	18187	144	221	258	172	631	1151	6.7	0.0000
1436779_at	Cybb	cytochrome b-245, beta polypeptide	13058	262	334	357	246	864	1603	6.52	0.0000
1435190_at	Chl1	cell adhesion molecule L1-like	12661	94	82	109	75	200	449	5.99	0.0005
1419675_at	Ngf	nerve growth factor	18049	96	124	154	81	284	480	5.92	0.0002
1422125_at	Htr2b	5-hydroxytryptamine (serotonin) receptor 2B	15559	74	115	147	105	386	615	5.84	0.0001
1450731_s_at	Tnfrsf21	tumor necrosis factor receptor superfamily, member 21	94185	139	239	322	135	462	774	5.75	0.0001
1435477_s_at	Fcgr2b	Fc receptor, IgG, low affinity IIb	14130	736	720	1048	705	2176	3922	5.56	0.0000

Affymetrix Probe set ID	Gene Symbol	Gene Name	Entrez Gene ID	Mean WT aorta 6 wks	Mean WT aorta 32 wks	Mean WT aorta 78 wks	Mean *Apoe*$^{-/-}$ aorta 6 wks	Mean *Apoe*$^{-/-}$ aorta 32 wks	Mean *Apoe*$^{-/-}$ aorta 78 wks	Fold change *Apoe*$^{-/-}$ 78 wks *vs. WT* 6 wks	p. ANOVA
1424942_a_at	Myc	myelocytomatosis oncogene	17869	145	158	147	90	250	500	5.53	0.0004
1418945_at	Mmp3	matrix metallopeptidase 3	17392	1354	2996	3346	1377	5598	7489	5.44	0.0000
1449591_at	Casp4	caspase 4, apoptosis-related cysteine peptidase	12363	239	302	476	205	875	1102	5.37	0.0000
1428347_at	Cyfip2	cytoplasmic FMR1 interacting protein 2	76884	129	283	365	168	489	903	5.36	0.0000
1421525_a_at	Naip5	NLR family, apoptosis inhibitory protein 5	17951	99	123	146	113	349	594	5.26	0.0000
1415803_at	Cx3cl1	chemokine (C-X3-C motif) ligand 1	20312	262	349	622	278	772	1458	5.24	0.0000
1451941_a_at	Fcgr2b	Fc receptor, IgG, low affinity IIb	14130	549	458	690	506	1472	2594	5.13	0.0000
1434653_at	Ptk2b	PTK2 protein tyrosine kinase 2 beta	19229	261	463	424	263	748	1346	5.12	0.0000
1418099_at	Tnfrsf1b	tumor necrosis factor receptor superfamily, member 1b	21938	300	400	416	308	986	1555	5.05	0.0000
1455332_x_at	Fcgr2b	Fc receptor, IgG, low affinity IIb	14130	254	277	421	334	907	1444	4.32	0.0000
1451767_at	Ncf1	neutrophil cytosolic factor 1	17969	110	121	84	95	284	470	4.93	0.0003
1424902_at	Plxdc1	plexin domain containing 1	72324	107	148	151	104	277	509	4.91	0.0000
1419754_at	Myo5a	myosin VA	17918	220	271	225	234	836	1112	4.76	0.0000
1416956_at	Kcnab2	potassium voltage-gated channel, shaker-related subfamily, beta member 2	16498	55	104	109	89	245	420	4.74	0.0100
1427038_at	Penk	preproenkephalin	18619	426	738	1575	396	1376	1826	4.61	0.0000
1456778_at	Nrp2	neuropilin 2	18187	177	400	352	199	748	912	4.59	0.0000
1457724_at	Ctsl	cathepsin L	13039	178	162	117	167	534	753	4.52	0.0000
1422823_at	Eps8	epidermal growth factor receptor pathway substrate 8	13860	247	296	317	207	683	922	4.45	0.0001
1431320_a_at	Myo5a	myosin VA	17918	242	253	283	248	618	1092	4.4	0.0001
1450027_at	Sdc3	syndecan 3	20970	682	646	963	681	1884	3001	4.4	0.0000
1422978_at	Cybb	cytochrome b-245, beta polypeptide	13058	193	211	199	204	619	883	4.33	0.0000
1417262_at	Ptgs2	prostaglandin-endoperoxide synthase 2	19225	431	303	473	332	902	1423	4.29	0.0003
1456772_at	Ncf1	neutrophil cytosolic factor 1	17969	319	324	310	341	805	1460	4.28	0.0001
1417378_at	Cadm1	cell adhesion molecule 1	54725	353	320	421	290	608	1230	4.24	0.0000
1434069_at	Prex1	phosphatidylinositol-3,4,5-trisphosphate-dependent Rac exchange factor 1	277360	329	307	310	286	624	1159	4.06	0.0000

Affymetrix Probe set ID	Gene Symbol	Gene Name	Entrez Gene ID	Mean WT aorta 6 wks	Mean WT aorta 32 wks	Mean WT aorta 78 wks	Mean *Apoe*$^{-/-}$ aorta 6 wks	Mean *Apoe*$^{-/-}$ aorta 32 wks	Mean *Apoe*$^{-/-}$ aorta 78 wks	Fold change *Apoe*$^{-/-}$ 78 wks *vs. WT* 6 wks	p. ANOVA
1434447_at	Met	met proto-oncogene	17295	104	240	130	88	282	347	3.97	0.0070
1449265_at	Casp1	caspase 1	12362	205	299	339	216	539	845	3.91	0.0000
1450414_at	Pdgfb	platelet derived growth factor, B polypeptide	18591	315	569	533	320	676	1084	3.38	0.0000
1420980_at	Pak1	p21 (RAC1) activated kinase 1	18479	206	351	527	184	452	714	3.88	0.0002
1426239_s_at	Arrb2	arrestin, beta 2	216869	426	477	568	505	857	1941	3.84	0.0000
1440802_at	Clasp2	CLIP associating protein 2	76499	80	60	195	60	65	228	3.8	0.0001
1417297_at	Itpr3	inositol 1,4,5-triphosphate receptor 3	16440	224	280	499	214	476	812	3.79	0.0000
1420653_at	Tgfb1	transforming growth factor, beta 1	21803	516	538	551	440	1292	1670	3.79	0.0000
1417669_at	Abhd12	abhydrolase domain containing 12	76192	836	923	961	750	1736	2842	3.79	0.0007
1436205_at	Nfasc	neurofascin	269116	115	213	425	121	331	448	3.71	0.0001
1438115_a_at	Slc9a3r1	solute carrier family 9 (sodium/hydrogen exchanger), member 3 regulator 1	26941	477	584	767	476	1007	1751	3.68	0.0001
1417676_a_at	Ptpro	protein tyrosine phosphatase, receptor type, O	19277	240	281	311	226	530	822	3.64	0.0000
1422824_s_at	Eps8	epidermal growth factor receptor pathway substrate 8	13860	281	335	416	234	637	846	3.61	0.0000
1450070_s_at	Pak1	p21 (RAC1) activated kinase 1	18479	121	221	345	128	285	461	3.59	0.0000
1439662_at	Homer1	homer scaffolding protein 1	26556	101	190	47	61	194	216	3.54	0.0200
1454268_a_at	Cyba	cytochrome b-245, alpha polypeptide	13057	2532	2330	3388	2574	5556	9049	3.52	0.0000
1449473_s_at	Cd40	CD40 antigen	21939	84	45	100	68	145	230	3.39	0.0300
1428340_s_at	Atp13a2	ATPase type 13A2	74772	321	410	405	338	632	1139	3.37	0.0000
1417376_a_at	Cadm1	cell adhesion molecule 1	54725	233	253	273	241	443	802	3.33	0.0000
1417870_x_at	Ctsz	cathepsin Z	64138	2419	2069	2395	2250	4491	7458	3.31	0.0000
1416882_at	Rgs10	regulator of G-protein signalling 10	67865	904	825	1195	831	1420	2749	3.31	0.0000
1415804_at	Cx3cl1	chemokine (C-X3-C motif) ligand 1	20312	67	134	123	78	315	258	3.3	0.0030

Affymetrix Probe set ID	Gene Symbol	Gene Name	Entrez Gene ID	Mean WT aorta 6 wks	Mean WT aorta 32 wks	Mean WT aorta 78 wks	Mean *Apoe*$^{-/-}$ aorta 6 wks	Mean *Apoe*$^{-/-}$ aorta 32 wks	Mean *Apoe*$^{-/-}$ aorta 78 wks	Fold change *Apoe*$^{-/-}$ 78 wks *vs. WT* 6 wks	p. ANOVA
1425525_a_at	P2rx4	purinergic receptor P2X, ligand-gated ion channel 4	18438	981	1075	1000	992	2007	3273	3.3	0.0000
1452202_at	Pde2a	phosphodiesterase 2A, cGMP-stimulated	207728	132	257	146	97	229	315	3.24	0.0020
1417869_s_at	Ctsz	cathepsin Z	64138	1722	2299	1558	1723	4678	5493	3.19	0.0000
1450970_at	Got1	glutamic-oxaloacetic transaminase 1, soluble	14718	316	334	392	278	478	879	3.16	0.0000
1417377_at	Cadm1	cell adhesion molecule 1	54725	70	106	76	97	176	303	3.13	0.0300
1423135_at	Thy1	thymus cell antigen 1, theta	21838	627	1056	1441	602	1257	1828	3.04	0.0001
1426528_at	Nrp2	neuropilin 2	18187	374	498	438	366	711	1099	3.01	0.0001
1419296_at	Arhgap4	Rho GTPase activating protein 4	171207	98	128	194	112	189	335	2.98	0.0020
1451596_a_at	Sphk1	sphingosine kinase 1	20698	244	221	377	250	360	741	2.96	0.0000
1438116_x_at	Slc9a3r1	solute carrier family 9 (sodium/hydrogen exchanger), member 3 regulator 1	26941	604	787	1064	645	1379	1902	2.95	0.0010
1451461_a_at	Aldoc	aldolase C, fructose-bisphosphate	11676	126	87	166	81	126	236	2.91	0.0030
1460337_at	Sh3kbp1	SH3-domain kinase binding protein 1	58194	628	699	666	509	952	1468	2.88	0.0010
1436051_at	Myo5a	myosin VA	17918	576	563	492	535	998	1526	2.85	0.0000
1436482_a_at	Sdc3	syndecan 3	20970	142	143	248	206	465	583	2.83	0.0000
1419248_at	Rgs2	regulator of G-protein signaling 2	19735	540	1177	1138	676	1606	1890	2.8	0.0000
1417551_at	Cln3	ceroid lipofuscinosis, neuronal 3, juvenile (Batten, Spielmeyer-Vogt disease)	12752	315	423	385	292	578	824	2.83	0.0000
1421385_a_at	Myo7a	myosin VIIA	17921	228	269	272	241	408	673	2.79	0.0000
1447830_s_at	Rgs2	regulator of G-protein signaling 2	19735	325	819	863	463	974	1266	2.74	0.0003
1440481_at	Stat1	signal transducer and activator of transcription 1	20846	104	104	103	117	165	316	2.71	0.0020
1424208_at	Ptger4	prostaglandin E receptor 4 (subtype EP4)	19219	470	631	955	533	1065	1426	2.68	0.0002
1452527_a_at	P2rx4	purinergic receptor P2X, ligand-gated ion channel 4	18438	795	656	705	788	1380	2060	2.62	0.0000

Affymetrix Probe set ID	Gene Symbol	Gene Name	Entrez Gene ID	Mean WT aorta 6 wks	Mean WT aorta 32 wks	Mean WT aorta 78 wks	Mean *Apoe*$^{-/-}$ aorta 6 wks	Mean *Apoe*$^{-/-}$ aorta 32 wks	Mean *Apoe*$^{-/-}$ aorta 78 wks	Fold change *Apoe*$^{-/-}$ 78 wks *vs. WT* 6 wks	p. ANOVA
1460365_a_at	Dnm1	dynamin 1	13429	360	488	540	351	619	915	2.6	0.0003
1452746_at	Atp13a2	ATPase type 13A2	74772	800	794	851	851	1406	2205	2.59	0.0000
1424507_at	Rin1	Ras and Rab interactor 1	225870	105	121	132	79	196	198	2.52	0.0010
1425863_a_at	Ptpro	protein tyrosine phosphatase, receptor type, O	19277	102	107	114	87	203	218	2.52	0.0009
1417094_at	Acot7	acyl-CoA thioesterase 7	70025	404	518	624	385	624	957	2.49	0.0002
1420915_at	Stat1	signal transducer and activator of transcription 1	20846	300	422	402	313	628	778	2.49	0.0000
1434222_at	Sipa1l1	signal-induced proliferation-associated 1 like 1	217692	323	423	492	281	437	682	2.43	0.0070
1423055_at	Nsg1	neuron specific gene family member 1	18196	534	536	906	481	817	1167	2.43	0.0005
1436958_x_at	Tpm3	tropomyosin 3, gamma	59069	1979	1809	2504	1784	2952	4300	2.41	0.0000
1419247_at	Rgs2	regulator of G-protein signaling 2	19735	748	1143	1209	815	1459	1820	2.23	0.0001
1420979_at	Pak1	p21 (RAC1) activated kinase 1	18479	117	153	183	151	188	365	2.41	0.0002
1443086_at	Alcam	activated leukocyte cell adhesion molecule	11658	132	94	114	110	183	263	2.38	0.0030
1421073_a_at	Ptger4	prostaglandin E receptor 4 (subtype EP4)	19219	112	115	133	96	219	228	2.37	0.0007
1425656_a_at	Baiap2	brain-specific angiogenesis inhibitor 1-associated protein 2	108100	191	142	181	165	240	382	2.32	0.0006
1437302_at	Adrb2	adrenergic receptor, beta 2	11555	177	216	102	100	244	233	2.32	0.0200
1447707_s_at	Pde2a	phosphodiesterase 2A, cGMP-stimulated	207728	449	827	783	473	891	1092	2.31	0.0001
1434272_at	Cpeb2	cytoplasmic polyadenylation element binding protein 2	231207	622	600	726	538	711	1214	2.26	0.0004
1416371_at	Apod	apolipoprotein D	11815	474	1606	1672	607	1712	1358	2.24	0.0000
1431619_a_at	Dtnbp1	dystrobrevin binding protein 1	94245	606	702	737	566	907	1258	2.22	0.0002
1451435_at	Cux1	cut-like homeobox 1	13047	555	875	1049	728	1068	1618	2.22	0.0000
1425536_at	Stx3	syntaxin 3	20908	726	546	694	525	780	1156	2.2	0.0000
1454731_at	Myo10	myosin X	17909	403	404	522	450	547	989	2.2	0.0001
1433532_a_at	Mbp	myelin basic protein	17196	199	406	286	170	516	373	2.2	0.0005

Affymetrix Probe set ID	Gene Symbol	Gene Name	Entrez Gene ID	Mean WT aorta 6 wks	Mean WT aorta 32 wks	Mean WT aorta 78 wks	Mean *Apoe*$^{-/-}$ aorta 6 wks	Mean *Apoe*$^{-/-}$ aorta 32 wks	Mean *Apoe*$^{-/-}$ aorta 78 wks	Fold change *Apoe*$^{-/-}$ 78 wks *vs.* *WT* 6 wks	p. ANOVA
1416514_a_at	Fscn1	fascin actin-bundling protein 1	14086	639	483	355	708	1135	1424	2.01	0.0003
1437467_at	Alcam	activated leukocyte cell adhesion molecule	11658	1218	853	801	1161	1573	2332	2.01	0.0000
1459866_x_at	Cyfip1	cytoplasmic FMR1 interacting protein 1	20430	2214	1931	4813	2570	2430	5622	2.19	0.0030
1424542_at	S100a4	S100 calcium binding protein A4	20198	5382	5627	6301	4561	9582	9924	2.18	0.0000
1418701_at	Comt	catechol-O-methyltransferase	12846	365	543	655	378	654	819	2.17	0.0010
1416531_at	Gsto1	glutathione S-transferase omega 1	14873	1050	1347	1262	1054	1423	2257	2.14	0.0007
1450033_a_at	Stat1	signal transducer and activator of transcription 1	20846	462	539	381	447	740	951	2.12	0.0008
1425733_a_at	Eps8	epidermal growth factor receptor pathway substrate 8	13860	241	257	253	231	392	488	2.12	0.0000
1448564_at	Cib1	calcium and integrin binding 1 (calmyrin)	23991	634	676	740	622	957	1300	2.09	0.0020
1450982_at	Slc9a3r1	solute carrier family 9 (sodium/hydrogen exchanger), member 3 regulator 1	26941	536	653	742	514	866	1072	2.09	0.0007
1417627_a_at	Limk1	LIM-domain containing, protein kinase	16885	172	228	202	165	299	343	2.08	0.0050
1444089_at	Sptbn1	spectrin beta, non-erythrocytic 1	20742	369	360	441	417	549	868	2.08	0.0000
1418829_a_at	Eno2	enolase 2, gamma neuronal	13807	196	295	276	201	357	415	2.07	0.0002
1450020_at	Cx3cr1	chemokine (C-X3-C motif) receptor 1	13051	104	116	64	146	283	302	2.06	0.0003
1426475_at	Hmbs	hydroxymethylbilane synthase	15288	292	401	439	312	504	637	2.04	0.0020
1417868_a_at	Ctsz	cathepsin Z	64138	5736	5108	5096	4892	8001	10740	2.2	0.0000
1424470_a_at	Rapgef3	Rap guanine nucleotide exchange factor (GEF) 3	223864	331	405	457	280	487	612	2.19	0.0020
1436930_x_at	Hmbs	hydroxymethylbilane synthase	15288	265	265	397	278	386	564	2.03	0.0050
1453367_a_at	Abhd12	abhydrolase domain containing 12	76192	660	580	481	603	1117	1206	2	0.0000
1450468_at	Myoc	myocilin	17926	219	361	481	191	426	374	1.96	0.0020
1456873_at	Clic5	chloride intracellular channel 5	224796	253	465	378	199	416	388	1.95	0.0020

Affymetrix Probe set ID	Gene Symbol	Gene Name	Entrez Gene ID	Mean WT aorta 6 wks	Mean WT aorta 32 wks	Mean WT aorta 78 wks	Mean *Apoe*$^{-/-}$ aorta 6 wks	Mean *Apoe*$^{-/-}$ aorta 32 wks	Mean *Apoe*$^{-/-}$ aorta 78 wks	Fold change *Apoe*$^{-/-}$ 78 wks *vs.* *WT* 6 wks	p. ANOVA
1460415_a_at	Cd40	CD40 antigen	21939	95	54	83	119	130	222	1.88	0.0100
1428937_at	Atp2b1	ATPase, Ca++ transporting, plasma membrane 1	67972	988	727	740	912	1089	1668	1.83	0.0003
1422852_at	Cib2	calcium and integrin binding family member 2	56506	230	850	551	281	546	504	1.79	0.0002
1428104_at	Tpx2	TPX2, microtubule-associated	72119	192	118	95	112	209	198	1.77	0.0050
1435495_at	Adora1	adenosine A1 receptor	11539	149	258	96	89	185	158	1.77	0.0040
1436037_at	Itga4	integrin alpha 4	16401	583	457	457	585	753	1018	1.74	0.0020
1439505_at	Clic5	chloride intracellular channel 5	224796	161	350	237	141	320	232	1.65	0.0030
1430640_a_at	Prkar2b	protein kinase, cAMP dependent regulatory, type II beta	19088	273	1257	331	312	979	500	1.6	0.0010
1450766_at	Pde6h	phosphodiesterase 6H, cGMP-specific, cone, gamma	78600	93	148	197	78	106	120	1.53	0.0060
1431592_a_at	Sh3kbp1	SH3-domain kinase binding protein 1	58194	404	428	249	388	639	583	1.5	0.0080
1441248_at	Clcn3	chloride channel, voltage-sensitive 3	12725	133	79	240	167	115	249	1.49	0.0050
1456475_s_at	Prkar2b	protein kinase, cAMP dependent regulatory, type II beta	19088	311	2027	528	462	1538	687	1.49	0.0002
1416041_at	Sgk1	serum/glucocorticoid regulated kinase 1	20393	4259	2102	2122	2774	3162	4106	1.48	0.0030
1448280_at	Syp	synaptophysin	20977	132	270	250	150	227	203	1.35	0.0100
1448260_at	Uchl1	ubiquitin carboxy-terminal hydrolase L1	22223	921	1386	2253	1093	1256	1577	1.44	0.0010
1431292_a_at	Twf2	twinfilin actin binding protein 2	23999	311	331	170	266	334	381	1.43	0.0080
1437466_at	Alcam	activated leukocyte cell adhesion molecule	11658	1174	896	721	1080	1307	1484	1.37	0.0005
1450344_a_at	Ptger3	prostaglandin E receptor 3 (subtype EP3)	19218	189	660	478	329	427	445	1.36	0.0001
1432269_a_at	Sh3kbp1	SH3-domain kinase binding protein 1	58194	291	194	129	248	350	336	1.36	0.0030
1427567_a_at	Tpm3	tropomyosin 3, gamma	59069	1164	720	702	1098	1349	1470	1.34	0.0000
1422474_at	Pde4b	phosphodiesterase 4B, cAMP specific	18578	496	1257	1183	659	1373	860	1.3	0.0004
1426300_at	Alcam	activated leukocyte cell adhesion molecule	11658	837	704	452	853	812	1083	1.27	0.0003
1435293_at	Adam22	a disintegrin and metallopeptidase domain 22	11496	188	320	465	205	304	258	1.26	0.0009
1450693_at	Rgs17	regulator of G-protein signaling 17	56533	216	245	525	224	301	274	1.22	0.0050

Affymetrix Probe set ID	Gene Symbol	Gene Name	Entrez Gene ID	Mean WT aorta 6 wks	Mean WT aorta 32 wks	Mean WT aorta 78 wks	Mean *Apoe*$^{-/-}$ aorta 6 wks	Mean *Apoe*$^{-/-}$ aorta 32 wks	Mean *Apoe*$^{-/-}$ aorta 78 wks	Fold change *Apoe*$^{-/-}$ 78 wks *vs.* *WT* 6 wks	p. ANOVA
1434202_a_at	Fam107a	family with sequence similarity 107, member A	268709	1684	1340	1384	806	854	699	-1.15	0.0060
1433888_at	Atp2b2	ATPase, Ca++ transporting, plasma membrane 2	11941	184	246	187	166	238	119	-1.4	0.0300
1420375_at	Kif3a	kinesin family member 3A	16568	880	427	407	698	599	474	-1.47	0.0010
1449281_at	Nrtn	neurturin	18188	798	1222	1747	897	950	1097	1.22	0.0020
1438664_at	Prkar2b	protein kinase, cAMP dependent regulatory, type II beta	19088	256	2072	512	455	1650	549	1.21	0.0000
1436334_at	Synj1	synaptojanin 1	104015	306	248	175	344	389	411	1.2	0.0040
1422168_a_at	Bdnf	brain derived neurotrophic factor	12064	379	154	134	211	196	244	1.16	0.0100
1426301_at	Alcam	activated leukocyte cell adhesion molecule	11658	1020	869	430	1033	1316	1191	1.15	0.0001
1439779_at	Rgs17	regulator of G-protein signaling 17	56533	211	296	499	185	242	213	1.15	0.0002
1456741_s_at	Gpm6a	glycoprotein m6a	234267	321	375	691	339	405	372	1.1	0.0050
1416936_at	Aatk	apoptosis-associated tyrosine kinase	11302	183	256	405	222	288	238	1.07	0.0010
1418815_at	Cdh2	cadherin 2	12558	290	241	136	332	384	337	1.01	0.0001
1456392_at	Negr1	neuronal growth regulator 1	320840	135	179	244	102	133	103	1.01	0.0010
1426464_at	Nr1d1	nuclear receptor subfamily 1, group D, member 1	217166	503	1455	1219	638	1230	634	-1.01	0.0040
1434943_at	Morn4	MORN repeat containing 4	226123	180	227	391	256	195	254	-1.01	0.0050
1434203_at	Fam107a	family with sequence similarity 107, member A	268709	745	546	497	307	259	304	-1.01	0.0100
1436957_at	Gabra3	gamma-aminobutyric acid (GABA) A receptor, subunit alpha 3	14396	1378	2766	2277	1588	2137	1495	-1.06	0.0003
1437064_at	Ar	androgen receptor	11835	496	815	1038	657	700	592	-1.11	0.0010
1425558_at	Klc3	kinesin light chain 3	232943	386	420	414	179	259	156	-1.15	0.0100
1460191_at	Ykt6	YKT6 v-SNARE homolog (S. cerevisiae)	56418	639	360	282	493	511	428	-1.15	0.0020
1428174_x_at	Khsrp	KH-type splicing regulatory protein	16549	779	614	1240	817	555	701	-1.17	0.0100
1417319_at	Nectin3	nectin cell adhesion molecule 3	58998	242	192	118	204	171	170	-1.2	0.0060
1450923_at	Tgfb2	transforming growth factor, beta 2	21808	1865	763	913	1661	846	1372	-1.21	0.0000
1421152_a_at	Gnao1	guanine nucleotide binding protein, alpha O	14681	391	682	797	526	501	423	-1.24	0.0060
1438702_at	Flrt2	fibronectin leucine rich transmembrane protein 2	399558	744	444	356	678	594	542	-1.25	0.0040

Affymetrix Probe set ID	Gene Symbol	Gene Name	Entrez Gene ID	Mean WT aorta 6 wks	Mean WT aorta 32 wks	Mean WT aorta 78 wks	Mean *Apoe*$^{-/-}$ aorta 6 wks	Mean *Apoe*$^{-/-}$ aorta 32 wks	Mean *Apoe*$^{-/-}$ aorta 78 wks	Fold change *Apoe*$^{-/-}$ 78 wks *vs.* *WT* 6 wks	p. ANOVA
1423250_a_at	Tgfb2	transforming growth factor, beta 2	21808	1242	785	543	952	797	724	-1.31	0.0020
1423414_at	Ptgs1	prostaglandin-endoperoxide synthase 1	19224	804	672	555	715	1095	537	-1.33	0.0090
1451285_at	Fus	fused in sarcoma	233908	3015	1440	2559	3248	2524	2366	-1.37	0.0200
1460214_at	Pcp4	Purkinje cell protein 4	18546	178	200	303	147	184	96	-1.53	0.0010
1423941_at	Camk2g	calcium/calmodulin-dependent protein kinase II gamma	12325	2202	3139	3420	2603	2708	1672	-1.56	0.0003
1425270_at	Kif1b	kinesin family member 1B	16561	446	260	160	355	267	226	-1.57	0.0003
1422553_at	Pten	phosphatase and tensin homolog	19211	1496	1011	617	1534	1229	973	-1.58	0.0060
1458492_x_at	Ntm	neurotrimin	235106	274	111	166	270	84	171	-1.58	0.0070
1444240_at	Shank1	SH3 and multiple ankyrin repeat domains 1	243961	377	214	162	282	209	177	-1.59	0.0004
1436819_at	6-Sep	septin 6	56526	411	539	598	456	460	286	-1.6	0.0003
1457528_at	Slc4a7	solute carrier family 4, sodium bicarbonate cotransporter, member 7	218756	533	329	262	488	353	304	-1.61	0.0100
1420416_at	Sema3a	sema domain, immunoglobulin domain (Ig), short basic domain, secreted, (semaphorin) 3A	20346	592	635	742	571	371	353	-1.62	0.0007
1421102_a_at	Vamp3	vesicle-associated membrane protein 3	22319	854	629	418	881	615	540	-1.63	0.0001
1449522_at	Unc5c	unc-5 netrin receptor C	22253	1347	1626	1830	1126	1257	695	-1.62	0.0000
1427004_at	Fbxo2	F-box protein 2	230904	200	409	410	252	289	155	-1.63	0.0040
1433600_at	Adra2a	adrenergic receptor, alpha 2a	11551	514	662	743	565	691	344	-1.64	0.0050
1430485_at	Trpc2	transient receptor potential cation channel, subfamily C, member 2	22064	269	195	129	257	191	156	-1.65	0.0060
1423363_at	Sort1	sortilin 1	20661	352	496	192	369	390	219	-1.68	0.0005
1449423_at	Mast1	microtubule associated serine/threonine kinase 1	56527	306	376	167	313	290	186	-1.68	0.0200
1432419_a_at	Mob2	MOB kinase activator 2	101513	1324	1399	1661	1368	872	777	-1.76	0.0000
1420472_at	Mtpn	myotrophin	14489	1844	1008	761	1637	1166	915	-1.79	0.0000
1435730_at	Cacna1c	calcium channel, voltage-dependent, L type, alpha 1C subunit	12288	438	514	485	417	308	233	-1.79	0.0020
1455779_at	Map1a	microtubule-associated protein 1 A	17754	667	856	1039	817	703	455	-1.8	0.0010

Affymetrix Probe set ID	Gene Symbol	Gene Name	Entrez Gene ID	Mean WT aorta 6 wks	Mean WT aorta 32 wks	Mean WT aorta 78 wks	Mean *Apoe*$^{-/-}$ aorta 6 wks	Mean *Apoe*$^{-/-}$ aorta 32 wks	Mean *Apoe*$^{-/-}$ aorta 78 wks	Fold change *Apoe*$^{-/-}$ 78 wks *vs.* *WT* 6 wks	p. ANOVA
1435720_at	Kcnd3	potassium voltage-gated channel, Shal-related family, member 3	56543	1020	1487	1601	1042	1028	561	-1.86	0.0001
1418690_at	Ptprz1	protein tyrosine phosphatase, receptor type Z, polypeptide 1	19283	342	326	409	325	286	174	-1.87	0.0100
1450040_at	Timp2	tissue inhibitor of metalloproteinase 2	21858	4561	3836	2257	4847	4523	2578	-1.88	0.0000
1455188_at	Ephb1	Eph receptor B1	270190	416	222	152	277	142	147	-1.89	0.0009
1436043_at	Scn7a	sodium channel, voltage-gated, type VII, alpha	20272	824	1112	671	989	1056	524	-1.89	0.0001
1422178_a_at	Rab17	RAB17, member RAS oncogene family	19329	213	333	377	302	202	157	-1.92	0.0040
1451840_at	Kcnip4	Kv channel interacting protein 4	80334	341	250	323	305	243	158	-1.93	0.0010
1443618_at	Pdzd2	PDZ domain containing 2	68070	187	169	199	217	111	108	-2	0.0200
1449262_s_at	Lin7c	lin-7 homolog C (C. elegans)	22343	1110	489	615	915	519	466	-1.96	0.0008
1455831_at	Fus	fused in sarcoma	233908	319	143	154	313	286	159	-1.97	0.0020
1423331_a_at	Nectin3	nectin cell adhesion molecule 3	58998	798	487	362	703	494	355	-1.98	0.0000
1437497_a_at	Hsp90aa1	heat shock protein 90, alpha (cytosolic), class A member 1	15519	5723	2848	2686	4499	2669	2264	-1.99	0.0005
1427489_at	Itga8	integrin alpha 8	241226	13018	11974	11136	12649	10626	6308	-2.01	0.0000
1436876_at	Rgs7bp	regulator of G-protein signalling 7 binding protein	52882	1395	1561	1446	1411	1562	697	-2.02	0.0001
1451109_a_at	Nedd4	neural precursor cell expressed, developmentally down-regulated 4	17999	8225	6612	5788	8615	6658	4257	-2.02	0.0000
1423550_at	Slc1a4	solute carrier family 1 (glutamate/neutral amino acid transporter), member 4	55963	586	212	291	513	186	253	-2.03	0.0000
1459457_at	Camk2d	calcium/calmodulin-dependent protein kinase II, delta	108058	781	570	418	816	545	401	-2.04	0.0010
1426864_a_at	Ncam1	neural cell adhesion molecule 1	17967	5818	5284	6280	5493	4292	2691	-2.04	0.0009
1447941_x_at	Braf	Braf transforming gene	109880	308	267	194	382	218	186	-2.05	0.0030
1449865_at	Sema3a	sema domain, immunoglobulin domain (Ig), short basic domain, secreted, (semaphorin) 3A	20346	309	247	260	222	152	108	-2.05	0.0003

Affymetrix Probe set ID	Gene Symbol	Gene Name	Entrez Gene ID	Mean WT aorta 6 wks	Mean WT aorta 32 wks	Mean WT aorta 78 wks	Mean *Apoe*$^{-/-}$ aorta 6 wks	Mean *Apoe*$^{-/-}$ aorta 32 wks	Mean *Apoe*$^{-/-}$ aorta 78 wks	Fold change *Apoe*$^{-/-}$ 78 wks *vs.* *WT* 6 wks	p. ANOVA
1432004_a_at	Dnm2	dynamin 2	13430	392	371	174	429	440	208	-2.07	0.0001
1420833_at	Vamp2	vesicle-associated membrane protein 2	22318	498	681	392	508	505	243	-2.09	0.0007
1421860_at	Clstn1	calsyntenin 1	65945	710	713	756	814	590	394	-2.07	0.0040
1417755_at	Topors	topoisomerase I binding, arginine/serine-rich	106021	278	173	138	277	188	134	-2.07	0.0050
1421297_a_at	Cacna1c	calcium channel, voltage-dependent, L type, alpha 1C subunit	12288	629	646	550	657	396	317	-2.08	0.0000
1450038_s_at	Usp9x	ubiquitin specific peptidase 9, X chromosome	22284	602	551	524	735	457	354	-2.08	0.0060
1433147_at	Cald1	caldesmon 1	109624	1079	780	591	1043	719	502	-2.08	0.0005
1419256_at	Sptbn1	spectrin beta, non-erythrocytic 1	20742	1848	1034	1192	1997	1043	960	-2.08	0.0000
1434112_at	Adgrl2	adhesion G protein-coupled receptor L2	99633	3516	3026	2819	3646	2598	1753	-2.08	0.0000
1418898_at	Lin7c	lin-7 homolog C (C. elegans)	22343	810	374	328	666	386	319	-2.09	0.0002
1424893_at	Ndel1	nudE neurodevelopment protein 1 like 1	83431	589	345	258	562	383	269	-2.09	0.0006
1452379_at	Auts2	autism susceptibility candidate 2	319974	398	364	179	331	255	158	-2.09	0.0060
1429021_at	Epha4	Eph receptor A4	13838	285	252	191	281	263	134	-2.1	0.0020
1457139_at	Auts2	autism susceptibility candidate 2	319974	3168	2656	2496	3522	2293	1676	-2.1	0.0040
1426565_at	Igf1r	insulin-like growth factor I receptor	16001	855	656	557	894	689	425	-2.11	0.0000
1416756_at	Dnajb1	DnaJ heat shock protein family (Hsp40) member B1	81489	2462	1085	967	2023	835	959	-2.11	0.0200
1425511_at	Mark1	MAP/microtubule affinity regulating kinase 1	226778	1032	681	697	1004	585	473	-2.12	0.0020
1434788_at	Fzd3	frizzled class receptor 3	14365	340	236	236	278	208	131	-2.12	0.0006
1460546_at	Lgi3	leucine-rich repeat LGI family, member 3	213469	213	255	104	201	230	94	-2.13	0.0010
1421629_at	Gabre	gamma-aminobutyric acid (GABA) A receptor, subunit epsilon	14404	337	347	271	360	259	169	-2.13	0.0090
1427293_a_at	Auts2	autism susceptibility candidate 2	319974	535	351	201	468	318	210	-2.22	0.0090
1449504_at	Kpna1	karyopherin (importin) alpha 1	16646	295	179	139	275	182	129	-2.13	0.0040
1426086_a_at	Fmr1	fragile X mental retardation 1	14265	310	177	173	262	139	123	-2.14	0.0080
1427495_at	Scn7a	sodium channel, voltage-gated, type VII, alpha	20272	317	406	219	385	317	179	-2.15	0.0005
1439860_at	Eef2k	eukaryotic elongation factor-2 kinase	13631	424	585	342	604	529	281	-2.15	0.0010
1460286_at	6-Sep	septin 6	56526	208	240	236	260	178	121	-2.15	0.0040

Affymetrix Probe set ID	Gene Symbol	Gene Name	Entrez Gene ID	Mean WT aorta 6 wks	Mean WT aorta 32 wks	Mean WT aorta 78 wks	Mean *Apoe*$^{-/-}$ aorta 6 wks	Mean *Apoe*$^{-/-}$ aorta 32 wks	Mean *Apoe*$^{-/-}$ aorta 78 wks	Fold change *Apoe*$^{-/-}$ 78 wks *vs.* *WT* 6 wks	p. ANOVA
1415784_at	Vps35	VPS35 retromer complex component	65114	968	762	522	962	802	443	-2.17	0.0002
1435721_at	Kcnq4	potassium voltage-gated channel, subfamily Q, member 4	60613	819	826	890	904	626	416	-2.17	0.0001
1415877_at	Dpysl3	dihydropyrimidinase-like 3	22240	1396	989	1066	1613	1105	742	-2.17	0.0100
1423872_a_at	Dag1	dystroglycan 1	13138	1787	1488	1041	2019	1467	926	-2.18	0.0005
1434766_at	Prkaa2	protein kinase, AMP-activated, alpha 2 catalytic subunit	108079	979	1180	867	982	830	448	-2.19	0.0000
1435933_at	Scn2a	sodium channel, voltage-gated, type II, alpha	110876	447	462	580	585	392	266	-2.2	0.0030
1425491_at	Bmpr1a	bone morphogenetic protein receptor, type 1A	12166	1823	1470	1341	1657	1225	752	-2.2	0.0000
1418497_at	Fgf13	fibroblast growth factor 13	14168	1336	1516	1982	1500	1170	678	-2.21	0.0001
1417279_at	Itpr1	inositol 1,4,5-trisphosphate receptor 1	16438	4139	4007	4177	4481	3246	2015	-2.22	0.0000
1425292_at	Dtna	dystrobrevin alpha	13527	745	384	270	468	297	208	-2.25	0.0001
1424768_at	Cald1	caldesmon 1	109624	10281	10865	8718	11685	10483	5170	-2.26	0.0000
1433825_at	Ntrk3	neurotrophic tyrosine kinase, receptor, type 3	18213	2815	3219	2805	3246	2590	1433	-2.26	0.0000
1438680_at	Auts2	autism susceptibility candidate 2	319974	3299	2291	2458	3970	1826	1654	-2.4	0.0000
1443823_s_at	Atp1a2	ATPase, Na+/K+ transporting, alpha 2 polypeptide	98660	4204	4898	4399	4678	3867	2059	-2.27	0.0020
1438354_x_at	Cnn3	calponin 3, acidic	71994	1722	1768	1095	1089	920	478	-2.28	0.0050
1437390_x_at	Stx1a	syntaxin 1A (brain)	20907	2144	2174	1812	2304	1827	1008	-2.28	0.0000
1437631_at	Kcnip4	Kv channel interacting protein 4	80334	388	394	367	309	316	135	-2.3	0.0001
1416168_at	Serpinf1	serine (or cysteine) peptidase inhibitor, clade F, member 1	20317	9990	7808	6654	9590	7008	4163	-2.3	0.0000
1434893_at	Atp1a2	ATPase, Na+/K+ transporting, alpha 2 polypeptide	98660	1696	2456	2107	2034	2020	882	-2.31	0.0002
1434917_at	Cobl	cordon-bleu WH2 repeat	12808	698	431	535	635	387	274	-2.32	0.0005
1449416_at	Fzd4	frizzled class receptor 4	14366	155	197	60	170	133	73	-2.33	0.0001
1417307_at	Dmd	dystrophin, muscular dystrophy	13405	3103	3461	3449	3440	2644	1467	-2.35	0.0001
1423630_at	Cygb	cytoglobin	114886	2890	3281	1850	2751	3544	1172	-2.35	0.0040
1428967_at	Igf1r	insulin-like growth factor I receptor	16001	571	494	387	594	476	253	-2.35	0.0010
1433504_at	Pygb	brain glycogen phosphorylase	110078	2663	2588	3256	2997	2770	1273	-2.35	0.0001

Affymetrix Probe set ID	Gene Symbol	Gene Name	Entrez Gene ID	Mean WT aorta 6 wks	Mean WT aorta 32 wks	Mean WT aorta 78 wks	Mean *Apoe*$^{-/-}$ aorta 6 wks	Mean *Apoe*$^{-/-}$ aorta 32 wks	Mean *Apoe*$^{-/-}$ aorta 78 wks	Fold change *Apoe*$^{-/-}$ 78 wks *vs.* *WT* 6 wks	p. ANOVA
1458534_at	Rgs7bp	regulator of G-protein signalling 7 binding protein	52882	491	461	651	493	349	208	-2.37	0.0000
1427646_a_at	Arhgef2	rho/rac guanine nucleotide exchange factor (GEF) 2	16800	707	443	469	802	425	336	-2.39	0.0100
1426057_a_at	Epha3	Eph receptor A3	13837	354	175	106	275	185	114	-2.41	0.0000
1448676_at	Camk2b	calcium/calmodulin-dependent protein kinase II, beta	12323	525	405	276	404	329	167	-2.41	0.0002
1423221_at	Tubb4a	tubulin, beta 4A class IVA	22153	1339	1400	884	1627	1253	670	-2.43	0.0004
1441507_at	Sptbn1	spectrin beta, non-erythrocytic 1	20742	639	537	336	783	564	320	-2.45	0.0001
1427385_s_at	Actn1	actinin, alpha 1	109711	1942	1837	2378	2301	1743	939	-2.45	0.0006
1449315_at	Tenm3	teneurin transmembrane protein 3	23965	1017	756	612	937	628	382	-2.46	0.0002
1448541_at	Klc1	kinesin light chain 1	16593	682	412	303	673	442	274	-2.46	0.0002
1448468_a_at	Kcnab1	potassium voltage-gated channel, shaker-related subfamily, beta member 1	16497	5653	5003	5882	5456	3743	2217	-2.46	0.0000
1439527_at	Pgr	progesterone receptor	18667	1070	1270	1283	1023	564	415	-2.46	0.0002
1456131_x_at	Dag1	dystroglycan 1	13138	1930	1503	1015	2194	1497	889	-2.47	0.0004
1454015_a_at	Cdh13	cadherin 13	12554	1231	695	718	1498	818	606	-2.47	0.0020
1437967_at	Ccdc141	coiled-coil domain containing 141	545428	787	564	576	530	462	215	-2.47	0.0003
1456072_at	Ppp1r9a	protein phosphatase 1, regulatory subunit 9A	243725	572	559	542	620	434	251	-2.47	0.0040
1425987_a_at	Kcnma1	potassium large conductance calcium-activated channel, subfamily M, alpha member 1	16531	869	718	649	1004	538	406	-2.48	0.0002
1428948_at	Kcnma1	potassium large conductance calcium-activated channel, subfamily M, alpha member 1	16531	1313	1673	1494	1674	1297	711	-2.36	0.0004
1450384_at	Bace1	beta-site APP cleaving enzyme 1	23821	646	484	315	716	484	304	-2.36	0.0005
1424398_at	Dhx36	DEAH (Asp-Glu-Ala-His) box polypeptide 36	72162	1099	832	305	975	944	413	-2.36	0.0001
1450123_at	Ryr2	ryanodine receptor 2, cardiac	20191	572	746	831	798	452	315	-2.54	0.0000
1429463_at	Prkaa2	protein kinase, AMP-activated, alpha 2 catalytic subunit	108079	1407	1460	827	1475	1117	580	-2.54	0.0005
1457562_at	Rps6kb1	ribosomal protein S6 kinase, polypeptide 1	72508	173	89	64	179	107	76	-2.37	0.0200

Affymetrix Probe set ID	Gene Symbol	Gene Name	Entrez Gene ID	Mean WT aorta 6 wks	Mean WT aorta 32 wks	Mean WT aorta 78 wks	Mean *Apoe*$^{-/-}$ aorta 6 wks	Mean *Apoe*$^{-/-}$ aorta 32 wks	Mean *Apoe*$^{-/-}$ aorta 78 wks	Fold change *Apoe*$^{-/-}$ 78 wks *vs.* *WT* 6 wks	p. ANOVA
1435553_at	Pdzd2	PDZ domain containing 2	68070	1339	1509	1274	1664	1206	656	-2.54	0.0000
1448665_at	Dmd	dystrophin, muscular dystrophy	13405	3866	4810	3735	4342	3542	1754	-2.48	0.0005
1455876_at	Slc4a7	solute carrier family 4, sodium bicarbonate cotransporter, member 7	218756	406	208	215	352	227	142	-2.48	0.0020
1421042_at	Arhgef2	rho/rac guanine nucleotide exchange factor (GEF) 2	16800	1304	849	791	1487	796	594	-2.5	0.0007
1427569_a_at	Utrn	utrophin	22288	1009	880	682	985	673	392	-2.51	0.0002
1425575_at	Epha3	Eph receptor A3	13837	1622	1172	800	1599	964	625	-2.56	0.0001
1427465_at	Atp1a2	ATPase, Na+/K+ transporting, alpha 2 polypeptide	98660	1924	1820	1671	2017	1459	784	-2.57	0.0006
1423671_at	Dner	delta/notch-like EGF repeat containing	227325	323	165	139	247	143	96	-2.57	0.0001
1456069_at	Dtna	dystrobrevin alpha	13527	792	393	280	510	261	198	-2.58	0.0000
1431973_at	6-Sep	septin 6	56526	216	231	334	234	115	90	-2.6	0.0090
1456505_at	Braf	Braf transforming gene	109880	505	296	155	502	323	191	-2.62	0.0003
1425071_s_at	Ntrk3	neurotrophic tyrosine kinase, receptor, type 3	18213	1353	1313	1101	1485	1088	562	-2.64	0.0000
1421866_at	Nr3c1	nuclear receptor subfamily 3, group C, member 1	14815	726	301	383	682	476	257	-2.65	0.0002
1437559_at	Rgs7bp	regulator of G-protein signalling 7 binding protein	52882	841	957	658	931	892	351	-2.65	0.0000
1424770_at	Cald1	caldesmon 1	109624	6315	3969	3287	6151	4239	2306	-2.67	0.0090
1454729_at	Tmem108	transmembrane protein 108	81907	246	193	158	345	172	129	-2.67	0.0010
1450439_at	Hcfc1	host cell factor C1	15161	378	249	201	398	254	149	-2.67	0.0100
1450939_at	Entpd1	ectonucleoside triphosphate diphosphohydrolase 1	12495	1011	867	639	1015	660	351	-2.89	0.0003
1460028_at	Grip2	glutamate receptor interacting protein 2	243547	2007	2011	2386	2297	1629	856	-2.68	0.0010
1422863_s_at	Pdlim5	PDZ and LIM domain 5	56376	3167	1691	1849	3366	1639	1254	-2.69	0.0000
1422329_a_at	Ntrk3	neurotrophic tyrosine kinase, receptor, type 3	18213	444	460	378	557	350	207	-2.69	0.0010
1422862_at	Pdlim5	PDZ and LIM domain 5	56376	1326	526	692	1270	512	472	-2.69	0.0010
1429178_at	Tenm3	teneurin transmembrane protein 3	23965	883	599	517	884	508	326	-2.71	0.0000
1421276_a_at	Dst	dystonin	13518	2715	2134	2214	2977	1577	1095	-2.72	0.0000
1426066_a_at	Dtna	dystrobrevin alpha	13527	435	343	359	463	323	164	-2.82	0.0000

Affymetrix Probe set ID	Gene Symbol	Gene Name	Entrez Gene ID	Mean WT aorta 6 wks	Mean WT aorta 32 wks	Mean WT aorta 78 wks	Mean *Apoe*$^{-/-}$ aorta 6 wks	Mean *Apoe*$^{-/-}$ aorta 32 wks	Mean *Apoe*$^{-/-}$ aorta 78 wks	Fold change *Apoe*$^{-/-}$ 78 wks *vs.* *WT* 6 wks	p. ANOVA
1425574_at	Epha3	Eph receptor A3	13837	550	193	247	534	236	189	-2.82	0.0000
1448366_at	Stx1a	syntaxin 1A (brain)	20907	603	579	500	677	411	239	-2.83	0.0001
1441531_at	Plcb4	phospholipase C, beta 4	18798	489	342	224	437	344	154	-2.83	0.0020
1449551_at	Myo1c	myosin IC	17913	3167	2442	1694	3434	2163	1205	-2.85	0.0000
1416180_a_at	Rdx	radixin	19684	1075	434	416	923	531	324	-2.85	0.0000
1429768_at	Dtna	dystrobrevin alpha	13527	1176	1275	984	1264	864	437	-2.89	0.0002
1419592_at	Unc5c	unc-5 netrin receptor C	22253	899	521	732	739	391	256	-2.89	0.0000
1420518_a_at	Igsf9	immunoglobulin superfamily, member 9	93842	648	634	643	921	509	317	-2.9	0.0020
1439556_at	Ncam1	neural cell adhesion molecule 1	17967	840	957	1281	1242	644	374	-3.32	0.0040
1429794_a_at	P2rx1	purinergic receptor P2X, ligand-gated ion channel, 1	18436	562	467	669	525	501	180	-2.92	0.0006
1460719_a_at	P2rx1	purinergic receptor P2X, ligand-gated ion channel, 1	18436	1108	837	919	1096	787	374	-2.93	0.0000
1427019_at	Ptprz1	protein tyrosine phosphatase, receptor type Z, polypeptide 1	19283	3136	3922	3540	3893	3168	1327	-2.93	0.0000
1418852_at	Chrna1	cholinergic receptor, nicotinic, alpha polypeptide 1 (muscle)	11435	340	234	184	328	187	110	-3	0.0050
1421471_at	Npy1r	neuropeptide Y receptor Y1	18166	1628	1362	1385	1301	828	434	-3	0.0001
1450462_at	Crhr2	corticotropin releasing hormone receptor 2	12922	221	256	193	293	209	97	-3.02	0.0006
1422861_s_at	Pdlim5	PDZ and LIM domain 5	56376	1520	574	587	1358	499	448	-3.03	0.0000
1422803_at	Fstl3	follistatin-like 3	83554	2205	1588	1502	2567	1449	840	-3.06	0.0000
1455886_at	Cbl	Casitas B-lineage lymphoma	12402	268	191	60	223	236	72	-3.09	0.0070
1450037_at	Usp9x	ubiquitin specific peptidase 9, X chromosome	22284	470	480	247	568	439	182	-3.12	0.0010
1452284_at	Ptprz1	protein tyrosine phosphatase, receptor type Z, polypeptide 1	19283	5834	6396	6604	6978	4095	2212	-3.15	0.0002
1427280_at	Scn2a	sodium channel, voltage-gated, type II, alpha	110876	405	391	294	526	320	165	-3.19	0.0010
1434802_s_at	Ntf3	neurotrophin 3	18205	1438	1549	1601	1608	1120	505	-3.19	0.0001
1420924_at	Timp2	tissue inhibitor of metalloproteinase 2	21858	4447	2888	1116	4616	3785	1443	-3.2	0.0000

Affymetrix Probe set ID	Gene Symbol	Gene Name	Entrez Gene ID	Mean WT aorta 6 wks	Mean WT aorta 32 wks	Mean WT aorta 78 wks	Mean *Apoe*$^{-/-}$ aorta 6 wks	Mean *Apoe*$^{-/-}$ aorta 32 wks	Mean *Apoe*$^{-/-}$ aorta 78 wks	Fold change *Apoe*$^{-/-}$ 78 wks *vs.* *WT* 6 wks	p. ANOVA
1451550_at	Ephb3	Eph receptor B3	13845	655	344	323	633	328	130	-4.86	0.0060
1421413_a_at	Pdlim5	PDZ and LIM domain 5	56376	1083	385	357	952	358	297	-3.21	0.0000
1450786_x_at	Pdlim5	PDZ and LIM domain 5	56376	3095	1273	1382	2923	1191	895	-3.27	0.0000
1416504_at	Ulk1	unc-51 like kinase 1	22241	331	259	149	310	231	94	-3.29	0.0200
1429946_at	Ccdc141	coiled-coil domain containing 141	545428	384	95	125	330	127	100	-3.29	0.0001
1421955_a_at	Nedd4	neural precursor cell expressed, developmentally down-regulated 4	17999	4175	2268	1932	4365	2670	1326	-3.29	0.0000
1447547_at	Ltbp1	latent transforming growth factor beta binding protein 1	268977	889	729	643	927	611	281	-3.3	0.0005
1421239_at	Il6st	interleukin 6 signal transducer	16195	1217	641	455	1220	907	366	-3.33	0.0000
1426285_at	Lama2	laminin, alpha 2	16773	2405	1443	1377	2413	1245	720	-3.35	0.0000
1450659_at	Rgs7	regulator of G protein signaling 7	24012	1300	1179	1027	1206	720	359	-3.36	0.0000
1424605_at	Pcsk5	proprotein convertase subtilisin/kexin type 5	18552	339	216	176	392	164	115	-3.41	0.0040
1419223_a_at	Dtna	dystrobrevin alpha	13527	778	568	466	766	439	205	-3.74	0.0000
1425070_at	Ntrk3	neurotrophic tyrosine kinase, receptor, type 3	18213	432	387	283	506	358	133	-3.79	0.0020
1426865_a_at	Ncam1	neural cell adhesion molecule 1	17967	4525	3020	2488	4655	2914	1221	-3.81	0.0000
1450803_at	Ntf3	neurotrophin 3	18205	1538	1352	1448	1623	1055	421	-3.86	0.0001
1456329_at	Prtg	protogenin	235472	173	161	99	230	116	59	-3.88	0.0050
1418430_at	Kif5b	kinesin family member 5B	16573	2416	1642	741	2530	1690	636	-3.98	0.0001
1425338_at	Plcb4	phospholipase C, beta 4	18798	1538	1246	1279	1626	869	406	-4	0.0003
1453724_a_at	Serpinf1	serine (or cysteine) peptidase inhibitor, clade F, member 1	20317	5890	3518	3372	5656	2741	1400	-4.04	0.0000
1460305_at	Itga3	integrin alpha 3	16400	702	715	415	747	569	184	-4.05	0.0020
1427688_a_at	Ptprs	protein tyrosine phosphatase, receptor type, S	19280	213	90	64	211	124	51	-4.11	0.0300
1421850_at	Map1b	microtubule-associated protein 1B	17755	321	179	106	278	160	67	-4.14	0.0050
1454043_a_at	Kcnab1	potassium voltage-gated channel, shaker-related subfamily, beta member 1	16497	2379	1571	1474	2214	1077	512	-4.33	0.0000

Affymetrix Probe set ID	Gene Symbol	Gene Name	Entrez Gene ID	Mean WT aorta 6 wks	Mean WT aorta 32 wks	Mean WT aorta 78 wks	Mean *Apoe*$^{-/-}$ aorta 6 wks	Mean *Apoe*$^{-/-}$ aorta 32 wks	Mean *Apoe*$^{-/-}$ aorta 78 wks	Fold change *Apoe*$^{-/-}$ 78 wks *vs.* *WT* 6 wks	p. ANOVA
1450437_a_at	Ncam1	neural cell adhesion molecule 1	17967	633	313	183	560	291	127	-4.4	0.0003
1439713_at	Itga1	integrin alpha 1	109700	410	304	118	425	278	92	-4.61	0.0002
1440970_at	Kalrn	kalirin, RhoGEF kinase	545156	393	365	487	325	275	70	-4.65	0.0020
1437339_s_at	Pcsk5	proprotein convertase subtilisin/kexin type 5	18552	2529	1852	1567	2521	1556	524	-4.81	0.0000
1427771_x_at	Itgb1	integrin beta 1 (fibronectin receptor beta)	16412	1680	2297	732	2442	1692	505	-4.83	0.0010
1451406_a_at	Pcsk5	proprotein convertase subtilisin/kexin type 5	18552	1148	753	930	1212	645	249	-4.86	0.0001
1441057_at	Myh10	myosin, heavy polypeptide 10, non-muscle	77579	233	220	105	293	218	57	-5.16	0.0020
1418431_at	Kif5b	kinesin family member 5B	16573	565	266	138	528	333	102	-5.2	0.0003
1443315_at	Dmd	dystrophin, muscular dystrophy	13405	623	553	418	811	338	146	-5.55	0.0001
1421851_at	Map1b	microtubule-associated protein 1B	17755	2988	1811	1372	2899	1315	505	-5.74	0.0000
1450397_at	Map1b	microtubule-associated protein 1B	17755	439	236	98	416	256	67	-6.2	0.0100
1424848_at	Kcnma1	potassium large conductance calcium-activated channel, subfamily M, alpha member 1	16531	198	143	95	211	133	29	-7.2	0.0050
1456379_x_at	Dner	delta/notch-like EGF repeat containing	227325	429	105	86	281	116	33	-8.55	0.0000
1453860_s_at	Nr3c1	nuclear receptor subfamily 3, group C, member 1	14815	227	81	46	174	103	20	-8.62	0.0050
1425339_at	Plcb4	phospholipase C, beta 4	18798	1620	749	623	1624	622	118	-13.82	0.0030

B. Axon guidance (GO: 0007411)

Affymetrix Probe set ID	Gene Symbol	Gene Name	Entrez Gene ID	Mean WT aorta 6 wks	Mean WT aorta 32 wks	Mean WT aorta 78 wks	Mean *Apoe*$^{-/-}$ aorta 6 wks	Mean *Apoe*$^{-/-}$ aorta 32 wks	Mean *Apoe*$^{-/-}$ aorta 78 wks	Fold change *Apoe*$^{-/-}$ 78 wks *vs.* *WT* 6 wks	p. ANOVA
1427682_a_at	Egr2	early growth response 2	13654	23	75	125	39	203	395	10.2	0.000800
1448710_at	Cxcr4	chemokine (C-X-C motif) receptor 4	12767	80	112	107	77	529	1120	14.5	0.000010
1435349_at	Nrp2	neuropilin 2	18187	144	221	258	172	631	1151	6.7	0.000004
1435190_at	Chl1	cell adhesion molecule with homology to L1CAM	12661	94	82	109	75	200	449	5.99	0.000500
1417574_at	Cxcl12	chemokine (C-X-C motif) ligand 12	20315	577	562	615	474	1216	2174	4.58	0.000010
1434920_a_at	Evl	Ena-vasodilator stimulated phosphoprotein	14026	401	319	244	361	1291	1927	5.34	0.000003
1427683_at	Egr2	early growth response 2	13654	116	167	305	129	304	582	4.52	0.000040
1450106_a_at	Evl	Ena-vasodilator stimulated phosphoprotein	14026	204	102	102	167	472	644	3.85	0.000010
1436205_at	Nfasc	neurofascin	269116	115	213	425	121	331	448	3.71	0.000100
1426528_at	Nrp2	neuropilin 2	18187	374	498	438	366	711	1099	3.01	0.000100
1443086_at	Alcam	activated leukocyte cell adhesion molecule	11658	132	94	114	110	183	263	2.38	0.003000
1448823_at	Cxcl12	chemokine (C-X-C motif) ligand 12	20315	5885	5864	6394	5182	8384	10772	2.08	0.000007
1440885_at	Evl	Ena-vasodilator stimulated phosphoprotein	14026	280	281	310	280	349	578	2.06	0.000200
1437467_at	Alcam	activated leukocyte cell adhesion molecule	11658	1218	853	801	1161	1573	2332	2.01	0.000010
1450723_at	Isl1	ISL1 transcription factor, LIM/homeodomain	16392	263	345	497	169	404	302	1.79	0.000200
1437466_at	Alcam	activated leukocyte cell adhesion molecule	11658	1174	896	721	1080	1307	1484	1.37	0.000500
1426300_at	Alcam	activated leukocyte cell adhesion molecule	11658	837	704	452	853	812	1083	1.27	0.000300
1422168_a_at	Bdnf	brain derived neurotrophic factor	12064	379	154	134	211	196	244	1.16	0.010000
1426301_at	Alcam	activated leukocyte cell adhesion molecule	11658	1020	869	430	1033	1316	1191	1.15	0.000050
1450923_at	Tgfb2	transforming growth factor, beta 2	21808	1865	763	913	1661	846	1372	-1.21	0.000020
1423250_a_at	Tgfb2	transforming growth factor, beta 2	21808	1242	785	543	952	797	724	-1.31	0.002000
1424801_at	Enah	enabled homolog (Drosophila)	13800	4220	5157	6251	4372	3675	2948	-1.48	0.000007

Affymetrix Probe set ID	Gene Symbol	Gene Name	Entrez Gene ID	Mean WT aorta 6 wks	Mean WT aorta 32 wks	Mean WT aorta 78 wks	Mean *Apoe*$^{-/-}$ aorta 6 wks	Mean *Apoe*$^{-/-}$ aorta 32 wks	Mean *Apoe*$^{-/-}$ aorta 78 wks	Fold change *Apoe*$^{-/-}$ 78 wks *vs. WT* 6 wks	p. ANOVA
1420416_at	Sema3a	sema domain, immunoglobulin domain (Ig), short basic domain, secreted, (semaphorin) 3A	20346	592	635	742	571	371	353	-1.62	0.000700
1427086_at	Slit3	slit homolog 3 (Drosophila)	20564	3299	3281	4585	3368	3146	2243	-1.5	0.000200
1420508_at	Sema3f	sema domain, immunoglobulin domain (Ig), short basic domain, secreted, (semaphorin) 3F	20350	612	478	695	562	440	339	-1.66	0.009000
1421624_a_at	Enah	enabled homolog (Drosophila)	13800	655	503	706	521	380	293	-1.78	0.000020
1437312_at	Bmpr1b	bone morphogenetic protein receptor, type 1B	12167	793	878	772	646	485	356	-1.82	0.000080
1455188_at	Ephb1	Eph receptor B1	270190	416	222	152	277	142	147	-1.89	0.000900
1449865_at	Sema3a	sema domain, immunoglobulin domain (Ig), short basic domain, secreted, (semaphorin) 3A	20346	309	247	260	222	152	108	-2.05	0.000300
1429021_at	Epha4	Eph receptor A4	13838	285	252	191	281	263	134	-2.1	0.002000
1453103_at	Ablim1	actin-binding LIM protein 1	226251	792	461	382	680	551	323	-2.11	0.001000
1434788_at	Fzd3	frizzled homolog 3 (Drosophila)	14365	340	236	236	278	208	131	-2.12	0.000600
1418876_at	Foxd1	forkhead box D1	15229	128	211	207	170	219	79	-2.16	0.000300
1425840_a_at	Sema3f	sema domain, immunoglobulin domain (Ig), short basic domain, secreted, (semaphorin) 3F	20350	1159	829	701	1090	946	494	-2.21	0.005000
1419356_at	Klf7	Kruppel-like factor 7 (ubiquitous)	93691	791	730	543	1009	720	437	-2.31	0.020000
1437673_at	Wnt5a	wingless-related MMTV integration site 5A	22418	246	284	183	201	226	85	-2.37	0.003000
1422872_at	Bmpr1b	bone morphogenetic protein receptor, type 1B	12167	284	214	97	201	174	84	-2.41	0.002000
1442223_at	Enah	enabled homolog (Drosophila)	13800	2649	1163	1426	2010	803	803	-2.5	0.000300
1437422_at	Sema5a	sema domain, seven thrombospondin repeats (type 1 and type 1-like), transmembrane domain (TM) and short cytoplasmic domain, (semaphorin) 5A	20356	1698	981	693	1562	940	534	-2.93	0.001000
1434776_at	Sema5a	sema domain, seven thrombospondin repeats (type 1 and type 1-like), transmembrane domain (TM) and short cytoplasmic domain, (semaphorin) 5A	20356	1173	1042	923	1225	893	465	-2.64	0.000050
1434802_s_at	Ntf3	neurotrophin 3	18205	1438	1549	1601	1608	1120	505	-3.19	0.000100
1459211_at	Gli2	GLI-Kruppel family member GLI2	14633	626	825	781	942	651	293	-3.22	0.000600
1436791_at	Wnt5a	wingless-related MMTV integration site 5A	22418	706	850	713	786	717	241	-3.26	0.000020
1450803_at	Ntf3	neurotrophin 3	18205	1538	1352	1448	1623	1055	421	-3.86	0.000100

Affymetrix Probe set ID	Gene Symbol	Gene Name	Entrez Gene ID	Mean WT aorta 6 wks	Mean WT aorta 32 wks	Mean WT aorta 78 wks	Mean *Apoe*$^{-/-}$ aorta 6 wks	Mean *Apoe*$^{-/-}$ aorta 32 wks	Mean *Apoe*$^{-/-}$ aorta 78 wks	Fold change *Apoe*$^{-/-}$ 78 wks *vs.* *WT* 6 wks	p. ANOVA
1451550_at	Ephb3	Eph receptor B3	13845	655	344	323	633	328	130	-4.86	0.006000
1448818_at	Wnt5a	wingless-related MMTV integration site 5A	22418	653	606	253	721	519	140	-5.14	0.000008
1441057_at	Myh10	myosin, heavy polypeptide 10, non-muscle	77579	233	220	105	293	218	57	-5.16	0.002000
1431162_a_at	Enah	enabled homolog (Drosophila)	13800	321	104	108	260	80	14	-19.06	0.000100

C. Sensory perception (GO: 0007600)

Affymetrix Probe set ID	Gene Symbol	Gene Name	Entrez Gene ID	Mean WT aorta 6 wks	Mean WT aorta 32 wks	Mean WT aorta 78 wks	Mean *Apoe*$^{-/-}$ aorta 6 wks	Mean *Apoe*$^{-/-}$ aorta 32 wks	Mean *Apoe*$^{-/-}$ aorta 78 wks	Fold change *Apoe*$^{-/-}$ 78 wks *vs.* *WT* 6 wks	p. ANOVA
1429987_at	Cemip	cell migration inducing protein, hyaluronan binding	80982	12	29	79	16	451	1050	63.93	0.000003
1450476_at	Cnr2	cannabinoid receptor 2 (macrophage)	12802	10	10	11	8	53	209	26.84	0.000400
1416022_at	Fabp5	fatty acid binding protein 5, epidermal	16592	641	989	563	495	8105	10154	20.5	0.000001
1437540_at	Mcoln3	mucolipin 3	171166	26	9	18	26	287	468	18.26	0.000200
1423017_a_at	Il1rn	interleukin 1 receptor antagonist	16181	28	37	44	48	291	700	14.5	0.000020
1448710_at	Cxcr4	chemokine (C-X-C motif) receptor 4	12767	80	112	107	77	529	1120	14.5	0.000010
1416021_a_at	Fabp5	fatty acid binding protein 5, epidermal	16592	1408	1807	1261	1121	10967	12391	11.05	0.000001
1420380_at	Ccl2	chemokine (C-C motif) ligand 2	20296	99	49	126	95	414	915	9.65	0.000100
1451798_at	Il1rn	interleukin 1 receptor antagonist	16181	98	150	116	116	554	1063	9.17	0.000003
1450567_a_at	Col2a1	collagen, type II, alpha 1	12824	245	84	34	189	1152	1603	8.49	0.000010
1448591_at	Ctss	cathepsin S	13040	1679	1944	2492	1825	12208	13868	7.6	0.000000
1421186_at	Ccr2	chemokine (C-C motif) receptor 2	12772	154	154	132	130	619	939	7.21	0.000030
1459850_x_at	Glrb	glycine receptor, beta subunit	14658	10	52	233	82	120	582	7.13	0.000080
1424683_at	Retreg1	reticulophagy regulator 1	66270	264	569	755	338	885	2321	6.87	0.000000

Affymetrix Probe set ID	Gene Symbol	Gene Name	Entrez Gene ID	Mean WT aorta 6 wks	Mean WT aorta 32 wks	Mean WT aorta 78 wks	Mean *Apoe*$^{-/-}$ aorta 6 wks	Mean *Apoe*$^{-/-}$ aorta 32 wks	Mean *Apoe*$^{-/-}$ aorta 78 wks	Fold change *Apoe*$^{-/-}$ 78 wks *vs. WT* 6 wks	p. ANOVA
1423166_at	Cd36	CD36 molecule	12491	794	3237	1578	835	4019	4649	5.57	0.000008
1424942_a_at	Myc	myelocytomatosis oncogene	17869	145	158	147	90	250	500	5.53	0.000400
1447643_x_at	Snai2	snail family zinc finger 2	20583	733	428	1253	398	856	2082	5.24	0.040000
1419754_at	Myo5a	myosin VA	17918	220	271	225	234	836	1112	4.76	0.000002
1427038_at	Penk	preproenkephalin	18619	426	738	1575	396	1376	1826	4.61	0.000007
1417574_at	Cxcl12	chemokine (C-X-C motif) ligand 12	20315	577	562	615	474	1216	2174	4.58	0.000010
1431320_a_at	Myo5a	myosin VA	17918	242	253	283	248	618	1092	4.4	0.000060
1455745_at	Cln8	ceroid-lipofuscinosis, neuronal 8	26889	98	39	150	92	119	397	4.33	0.010000
1417262_at	Ptgs2	prostaglandin-endoperoxide synthase 2	19225	431	303	473	332	902	1423	4.29	0.000300
1421187_at	Ccr2	chemokine (C-C motif) receptor 2	12772	59	71	18	57	218	244	4.27	0.000100
1425663_at	Il1rn	interleukin 1 receptor antagonist	16181	121	123	181	149	304	623	4.18	0.000100
1450883_a_at	Cd36	CD36 molecule	12491	1224	4327	1699	1492	5328	5773	3.87	0.000010
1426239_s_at	Arrb2	arrestin, beta 2	216869	426	477	568	505	857	1941	3.84	0.000010
1417297_at	Itpr3	inositol 1,4,5-triphosphate receptor 3	16440	224	280	499	214	476	812	3.79	0.000020
1438115_a_at	Slc9a3r1	solute carrier family 9 (sodium/hydrogen exchanger), member 3 regulator 1	26941	477	584	767	476	1007	1751	3.68	0.000090
1425525_a_at	P2rx4	purinergic receptor P2X, ligand-gated ion channel 4	18438	981	1075	1000	992	2007	3273	3.3	0.000005
1424067_at	Icam1	intercellular adhesion molecule 1	15894	715	772	949	690	1677	2170	3.14	0.000001
1451987_at	Arrb2	arrestin, beta 2	216869	170	188	174	147	568	986	6.71	0.000020
1425225_at	Fcgr4	Fc receptor, IgG, low affinity IV	246256	145	232	360	298	877	1955	6.56	0.000002
1419675_at	Ngf	nerve growth factor	18049	96	124	154	81	284	480	5.92	0.000200
1416892_s_at	Fam107b	family with sequence similarity 107, member B	66540	515	646	686	571	1000	1685	2.95	0.000006
1436051_at	Myo5a	myosin VA	17918	576	563	492	535	998	1526	2.85	0.000007
1450505_a_at	Retreg1	reticulophagy regulator 1	66270	130	125	139	123	192	339	2.77	0.003000
1439787_at	P2rx7	purinergic receptor P2X, ligand-gated ion channel, 7	18439	335	463	522	352	719	922	2.62	0.000002
1452527_a_at	P2rx4	purinergic receptor P2X, ligand-gated ion channel 4	18438	795	656	705	788	1380	2060	2.62	0.000020
1449024_a_at	Hexa	hexosaminidase A	15211	3981	4203	4253	3815	6526	9294	2.44	0.000001

Affymetrix Probe set ID	Gene Symbol	Gene Name	Entrez Gene ID	Mean WT aorta 6 wks	Mean WT aorta 32 wks	Mean WT aorta 78 wks	Mean *Apoe*$^{-/-}$ aorta 6 wks	Mean *Apoe*$^{-/-}$ aorta 32 wks	Mean *Apoe*$^{-/-}$ aorta 78 wks	Fold change *Apoe*$^{-/-}$ 78 wks *vs. WT* 6 wks	p. ANOVA
1438116_x_at	Slc9a3r1	solute carrier family 9 (sodium/hydrogen exchanger), member 3 regulator 1	26941	604	787	1064	645	1379	1902	2.95	0.001000
1421188_at	Ccr2	chemokine (C-C motif) receptor 2	12772	167	187	236	166	349	465	2.81	0.000200
1421385_a_at	Myo7a	myosin VIIA	17921	228	269	272	241	408	673	2.79	0.000030
1418580_at	Rtp4	receptor transporter protein 4	67775	519	477	640	466	962	1217	2.61	0.000040
1460365_a_at	Dnm1	dynamin 1	13429	360	488	540	351	619	915	2.6	0.000300
1450884_at	Cd36	CD36 molecule	12491	147	624	269	200	508	484	2.42	0.000040
1442542_at	Eya4	EYA transcriptional coactivator and phosphatase 4	14051	106	135	124	100	196	240	2.4	0.000200
1460180_at	Hexb	hexosaminidase B	15212	2074	1861	1956	2155	3581	5176	2.4	0.000005
1419853_a_at	P2rx7	purinergic receptor P2X, ligand-gated ion channel, 7	18439	138	186	113	129	250	300	2.33	0.002000
1437302_at	Adrb2	adrenergic receptor, beta 2	11555	177	216	102	100	244	233	2.32	0.020000
1452014_a_at	Igf1	insulin-like growth factor 1	16000	1344	786	740	1302	1591	2903	2.23	0.000070
1417932_at	Il18	interleukin 18	16173	266	241	362	270	475	594	2.2	0.004000
1433532_a_at	Mbp	myelin basic protein	17196	199	406	286	170	516	373	2.2	0.000500
1418701_at	Comt	catechol-O-methyltransferase	12846	365	543	655	378	654	819	2.17	0.001000
1426886_at	Cln5	ceroid-lipofuscinosis, neuronal 5	211286	708	716	771	700	1008	1483	2.12	0.000100
1450982_at	Slc9a3r1	solute carrier family 9 (sodium/hydrogen exchanger), member 3 regulator 1	26941	536	653	742	514	866	1072	2.09	0.000700
1416893_at	Fam107b	family with sequence similarity 107, member B	66540	81	89	166	154	255	320	2.08	0.003000
1448823_at	Cxcl12	chemokine (C-X-C motif) ligand 12	20315	5885	5864	6394	5182	8384	10772	2.08	0.000007
1450148_at	Mcoln3	mucolipin 3	171166	126	148	159	118	236	245	2.07	0.006000
1448509_at	Fam107b	family with sequence similarity 107, member B	66540	265	271	320	302	355	610	2.02	0.010000
1456873_at	Clic5	chloride intracellular channel 5	224796	253	465	378	199	416	388	1.95	0.002000
1423607_at	Lum	lumican	17022	7942	5208	7261	6566	11380	12368	1.88	0.000002
1435495_at	Adora1	adenosine A1 receptor	11539	149	258	96	89	185	158	1.77	0.004000
1437347_at	Ednrb	endothelin receptor type B	13618	604	655	708	488	1040	812	1.66	0.040000
1439505_at	Clic5	chloride intracellular channel 5	224796	161	350	237	141	320	232	1.65	0.003000
1450766_at	Pde6h	phosphodiesterase 6H, cGMP-specific, cone, gamma	78600	93	148	197	78	106	120	1.53	0.006000

Affymetrix Probe set ID	Gene Symbol	Gene Name	Entrez Gene ID	Mean WT aorta 6 wks	Mean WT aorta 32 wks	Mean WT aorta 78 wks	Mean *Apoe*$^{-/-}$ aorta 6 wks	Mean *Apoe*$^{-/-}$ aorta 32 wks	Mean *Apoe*$^{-/-}$ aorta 78 wks	Fold change *Apoe*$^{-/-}$ 78 wks *vs. WT* 6 wks	p. ANOVA
1438166_x_at	Ndufs4	NADH:ubiquinone oxidoreductase core subunit S4	17993	240	491	382	281	370	311	1.11	0.000300
1424003_at	Pomk	protein-O-mannose kinase	74653	150	310	173	185	347	177	-1.04	0.020000
1423414_at	Ptgs1	prostaglandin-endoperoxide synthase 1	19224	804	672	555	715	1095	537	-1.33	0.009000
1420852_a_at	B3gnt2	UDP-GlcNAc:betaGal beta-1,3-N-acetylglucosaminyltransferase 2	53625	713	332	345	527	362	395	-1.34	0.000300
1437401_at	Igf1	insulin-like growth factor 1	16000	3422	1365	1164	3131	1932	2309	-1.36	0.000010
1433888_at	Atp2b2	ATPase, Ca++ transporting, plasma membrane 2	11941	184	246	187	166	238	119	-1.4	0.030000
1434413_at	Igf1	insulin-like growth factor 1	16000	5137	2144	1819	4645	2785	3305	-1.41	0.000002
1423669_at	Col1a1	collagen, type I, alpha 1	12842	13743	5856	4505	14133	8852	9505	-1.49	0.000001
1421114_a_at	Epyc	epiphycan	13516	430	409	316	409	632	264	-1.55	0.006000
1444240_at	Shank1	SH3 and multiple ankyrin repeat domains 1	243961	377	214	162	282	209	177	-1.59	0.000400
1457528_at	Slc4a7	solute carrier family 4, sodium bicarbonate cotransporter, member 7	218756	533	329	262	488	353	304	-1.61	0.010000
1433600_at	Adra2a	adrenergic receptor, alpha 2a	11551	514	662	743	565	691	344	-1.64	0.005000
1418534_at	Fzd2	frizzled class receptor 2	57265	1454	1890	2149	1830	1602	1021	-1.79	0.002000
1455779_at	Map1a	microtubule-associated protein 1 A	17754	667	856	1039	817	703	455	-1.8	0.001000
1455188_at	Ephb1	Eph receptor B1	270190	416	222	152	277	142	147	-1.89	0.000900
1449533_at	Tmem100	transmembrane protein 100	67888	512	525	354	432	507	228	-1.89	0.009000
1420387_at	Mpv17	MpV17 mitochondrial inner membrane protein	17527	1011	1760	1472	1602	1784	820	-1.95	0.020000
1440374_at	Pde1c	phosphodiesterase 1C	18575	82	110	211	51	90	78	1.53	0.010000
1419519_at	Igf1	insulin-like growth factor 1	16000	1239	830	842	1231	1164	1823	1.48	0.002000
1448260_at	Uchl1	ubiquitin carboxy-terminal hydrolase L1	22223	921	1386	2253	1093	1256	1577	1.44	0.001000
1423285_at	Coch	cochlin	12810	313	356	613	213	274	272	1.28	0.004000
1435721_at	Kcnq4	potassium voltage-gated channel, subfamily Q, member 4	60613	819	826	890	904	626	416	-2.17	0.000050
1452385_at	Usp53	ubiquitin specific peptidase 53	99526	746	717	478	744	579	342	-2.17	0.000200
1437591_a_at	Wdr1	WD repeat domain 1	22388	4182	3195	2647	4569	2911	2069	-2.21	0.000600
1456401_at	Cacnb2	calcium channel, voltage-dependent, beta 2 subunit	12296	897	857	993	941	619	422	-2.23	0.000300

Affymetrix Probe set ID	Gene Symbol	Gene Name	Entrez Gene ID	Mean WT aorta 6 wks	Mean WT aorta 32 wks	Mean WT aorta 78 wks	Mean *Apoe*$^{-/-}$ aorta 6 wks	Mean *Apoe*$^{-/-}$ aorta 32 wks	Mean *Apoe*$^{-/-}$ aorta 78 wks	Fold change *Apoe*$^{-/-}$ 78 wks *vs. WT* 6 wks	p. ANOVA
1460647_a_at	Nr2f6	nuclear receptor subfamily 2, group F, member 6	13864	548	268	250	589	280	292	-2.01	0.000600
1418533_s_at	Fzd2	frizzled class receptor 2	57265	1179	1358	1420	1520	1179	745	-2.04	0.001000
1426864_a_at	Ncam1	neural cell adhesion molecule 1	17967	5818	5284	6280	5493	4292	2691	-2.04	0.000900
1416513_at	Lamb2	laminin, beta 2	16779	2960	2931	2397	3051	2454	1472	-2.07	0.000900
1436912_at	Cacnb4	calcium channel, voltage-dependent, beta 4 subunit	12298	188	190	136	206	178	98	-2.1	0.000900
1418532_at	Fzd2	frizzled class receptor 2	57265	987	1111	1082	1452	843	673	-2.16	0.003000
1434644_at	Tbl1x	transducin (beta)-like 1 X-linked	21372	717	691	484	803	632	353	-2.27	0.000030
1425911_a_at	Fgfr1	fibroblast growth factor receptor 1	14182	2689	2462	1520	2733	2404	1179	-2.32	0.000080
1449416_at	Fzd4	frizzled class receptor 4	14366	155	197	60	170	133	73	-2.33	0.000100
1428948_at	Kcnma1	potassium large conductance calcium-activated channel, subfamily M, alpha member 1	16531	1313	1673	1494	1674	1297	711	-2.36	0.000400
1450384_at	Bace1	beta-site APP cleaving enzyme 1	23821	646	484	315	716	484	304	-2.36	0.000500
1451758_at	Lamc3	laminin gamma 3	23928	660	609	738	782	547	322	-2.43	0.000300
1425987_a_at	Kcnma1	potassium large conductance calcium-activated channel, subfamily M, alpha member 1	16531	869	718	649	1004	538	406	-2.48	0.000200
1455876_at	Slc4a7	solute carrier family 4, sodium bicarbonate cotransporter, member 7	218756	406	208	215	352	227	142	-2.48	0.002000
1435383_x_at	Ndn	necdin	17984	2452	2158	1894	2563	2106	993	-2.58	0.000010
1434776_at	Sema5a	sema domain, seven thrombospondin repeats (type 1 and type 1-like), transmembrane domain (TM) and short cytoplasmic domain, (semaphorin) 5A	20356	1173	1042	923	1225	893	465	-2.64	0.000050
1449094_at	Gjc1	gap junction protein, gamma 1	14615	1922	1945	1714	1813	1474	687	-2.64	0.000040
1455792_x_at	Ndn	necdin	17984	1755	1284	1276	1795	1136	672	-2.67	0.000001
1425594_at	Lamc3	laminin gamma 3	23928	813	623	783	829	528	302	-2.75	0.000100
1420523_at	Ccdc50	coiled-coil domain containing 50	67501	709	419	231	594	364	214	-2.77	0.000020
1434643_at	Tbl1x	transducin (beta)-like 1 X-linked	21372	635	479	272	660	525	232	-2.84	0.004000
1444706_at	Nav2	neuron navigator 2	78286	498	427	270	526	428	185	-2.84	0.003000

Affymetrix Probe set ID	Gene Symbol	Gene Name	Entrez Gene ID	Mean WT aorta 6 wks	Mean WT aorta 32 wks	Mean WT aorta 78 wks	Mean *Apoe*$^{-/-}$ aorta 6 wks	Mean *Apoe*$^{-/-}$ aorta 32 wks	Mean *Apoe*$^{-/-}$ aorta 78 wks	Fold change *Apoe*$^{-/-}$ 78 wks *vs.* *WT* 6 wks	p. ANOVA
1415923_at	Ndn	necdin	17984	2186	1652	1489	2317	1765	764	-3.03	0.000003
1439556_at	Ncam1	neural cell adhesion molecule 1	17967	840	957	1281	1242	644	374	-3.32	0.004000
1420925_at	Tub	tubby bipartite transcription factor	22141	1457	1557	1616	1506	1087	433	-3.48	0.000200
1415900_a_at	Kit	KIT proto-oncogene receptor tyrosine kinase	16590	224	229	153	266	226	74	-3.58	0.030000
1435382_at	Ndn	necdin	17984	2585	2248	2023	2687	2385	1192	-2.25	0.000003
1442827_at	Tlr4	toll-like receptor 4	21898	413	183	137	320	208	142	-2.26	0.000900
1437422_at	Sema5a	sema domain, seven thrombospondin repeats (type 1 and type 1-like), transmembrane domain (TM) and short cytoplasmic domain, (semaphorin) 5A	20356	1698	981	693	1562	940	534	-2.93	0.001000
1421471_at	Npy1r	neuropeptide Y receptor Y1	18166	1628	1362	1385	1301	828	434	-3	0.000090
1450462_at	Crhr2	corticotropin releasing hormone receptor 2	12922	221	256	193	293	209	97	-3.02	0.000600
1430309_at	Nipbl	NIPBL cohesin loading factor	71175	555	342	115	493	442	131	-3.78	0.006000
1426865_a_at	Ncam1	neural cell adhesion molecule 1	17967	4525	3020	2488	4655	2914	1221	-3.81	0.000010
1450437_a_at	Ncam1	neural cell adhesion molecule 1	17967	633	313	183	560	291	127	-4.4	0.000300
1442467_at	Nav2	neuron navigator 2	78286	256	224	391	668	223	146	-4.57	0.004000
1447787_x_at	Gjc1	gap junction protein, gamma 1	14615	569	290	297	541	293	79	-6.83	0.010000
1424848_at	Kcnma1	potassium large conductance calcium-activated channel, subfamily M, alpha member 1	16531	198	143	95	211	133	29	-7.2	0.005000
1452476_at	Cacnb2	calcium channel, voltage-dependent, beta 2 subunit	12296	315	253	396	482	262	39	-12.48	0.000800

D. Ion channel activity (GO: 0005216)

Affymetrix Probe set ID	Gene Symbol	Gene Name	Entrez Gene ID	Mean WT aorta 6 wks	Mean WT aorta 32 wks	Mean WT aorta 78 wks	Mean *Apoe*$^{-/-}$ aorta 6 wks	Mean *Apoe*$^{-/-}$ aorta 32 wks	Mean *Apoe*$^{-/-}$ aorta 78 wks	Fold change *Apoe*$^{-/-}$ 78 wks *vs. WT* 6 wks	p. ANOVA
1424032_at	Hvcn1	hydrogen voltage-gated channel 1	74096	48	46	303	43	473	1139	26.71	0.000020
1437540_at	Mcoln3	mucolipin 3	171166	26	9	18	26	287	468	18.26	0.000200
1419463_at	Clca3a2	chloride channel accessory 3A2	80797	24	19	5	30	373	386	12.88	0.000100
1435945_a_at	Kcnn4	potassium intermediate/small conductance calcium-activated channel, subfamily N, member 4	16534	337	460	250	158	692	1501	9.51	0.000080
1459850_x_at	Glrb	glycine receptor, beta subunit	14658	10	52	233	82	120	582	7.13	0.000080
1434653_at	Ptk2b	PTK2 protein tyrosine kinase 2 beta	19229	261	463	424	263	748	1346	5.12	0.000001
1416956_at	Kcnab2	potassium voltage-gated channel, shaker-related subfamily, beta member 2	16498	55	104	109	89	245	420	4.74	0.010000
1424125_at	Kcnk13	potassium channel, subfamily K, member 13	217826	156	152	105	101	231	385	3.82	0.000900
1417297_at	Itpr3	inositol 1,4,5-triphosphate receptor 3	16440	224	280	499	214	476	812	3.79	0.000020
1434500_at	Ttyh2	tweety family member 2	117160	282	386	358	246	725	933	3.79	0.000010
1417611_at	Tmem37	transmembrane protein 37	170706	248	318	232	208	370	600	2.89	0.002000
1425525_a_at	P2rx4	purinergic receptor P2X, ligand-gated ion channel 4	18438	981	1075	1000	992	2007	3273	3.3	0.000005
1431705_a_at	Mcoln2	mucolipin 2	68279	119	143	102	132	177	382	2.89	0.002000
1437226_x_at	Marcksl1	MARCKS-like 1	17357	310	395	405	294	597	810	2.75	0.000300
1433505_a_at	Lrrc8d	leucine rich repeat containing 8D	231549	209	373	287	218	485	580	2.66	0.000300
1417852_x_at	Clca3a1	chloride channel accessory 3A1	12722	164	139	241	169	403	448	2.65	0.000200
1439787_at	P2rx7	purinergic receptor P2X, ligand-gated ion channel, 7	18439	335	463	522	352	719	922	2.62	0.000002
1452527_a_at	P2rx4	purinergic receptor P2X, ligand-gated ion channel 4	18438	795	656	705	788	1380	2060	2.62	0.000020
1415850_at	Rasa3	RAS p21 protein activator 3	19414	693	752	929	688	1048	1778	2.59	0.000040
1455157_a_at	Piezo1	piezo-type mechanosensitive ion channel component 1	234839	559	675	609	604	949	1477	2.44	0.000060
1419853_a_at	P2rx7	purinergic receptor P2X, ligand-gated ion channel, 7	18439	138	186	113	129	250	300	2.33	0.002000
1452702_at	Clcn7	chloride channel, voltage-sensitive 7	26373	584	695	734	579	849	1216	2.1	0.000003
1450148_at	Mcoln3	mucolipin 3	171166	126	148	159	118	236	245	2.07	0.006000

Affymetrix Probe set ID	Gene Symbol	Gene Name	Entrez Gene ID	Mean WT aorta 6 wks	Mean WT aorta 32 wks	Mean WT aorta 78 wks	Mean *Apoe*$^{-/-}$ aorta 6 wks	Mean *Apoe*$^{-/-}$ aorta 32 wks	Mean *Apoe*$^{-/-}$ aorta 78 wks	Fold change *Apoe*$^{-/-}$ 78 wks *vs. WT* 6 wks	p. ANOVA
1456873_at	Clic5	chloride intracellular channel 5	224796	253	465	378	199	416	388	1.95	0.002000
1433506_at	Lrrc8d	leucine rich repeat containing 8D	231549	136	206	136	150	286	285	1.9	0.002000
1417030_at	Pacc1	proton activated chloride channel 1	66950	205	173	124	160	230	279	1.74	0.020000
1438448_at	Otop1	otopetrin 1	21906	81	777	221	136	483	227	1.67	0.001000
1439505_at	Clic5	chloride intracellular channel 5	224796	161	350	237	141	320	232	1.65	0.003000
1441248_at	Clcn3	chloride channel, voltage-sensitive 3	12725	133	79	240	167	115	249	1.49	0.005000
1456741_s_at	Gpm6a	glycoprotein m6a	234267	321	375	691	339	405	372	1.1	0.005000
1436957_at	Gabra3	gamma-aminobutyric acid (GABA) A receptor, subunit alpha 3	14396	1378	2766	2277	1588	2137	1495	-1.06	0.000300
1455514_at	Kcnd1	potassium voltage-gated channel, Shal-related family, member 1	16506	312	222	344	435	217	270	-1.61	0.004000
1430485_at	Trpc2	transient receptor potential cation channel, subfamily C, member 2	22064	269	195	129	257	191	156	-1.65	0.006000
1435730_at	Cacna1c	calcium channel, voltage-dependent, L type, alpha 1C subunit	12288	438	514	485	417	308	233	-1.79	0.002000
1449544_a_at	Kcnh2	potassium voltage-gated channel, subfamily H (eag-related), member 2	16511	1171	1586	2022	1734	1449	956	-1.81	0.002000
1435720_at	Kcnd3	potassium voltage-gated channel, Shal-related family, member 3	56543	1020	1487	1601	1042	1028	561	-1.86	0.000100
1424308_at	Slc24a3	solute carrier family 24 (sodium/potassium/calcium exchanger), member 3	94249	2161	2675	2667	2403	1882	1292	-1.86	0.000300
1416190_a_at	Sec61a1	Sec61 alpha 1 subunit (S. cerevisiae)	53421	754	474	357	684	461	365	-1.88	0.001000
1436043_at	Scn7a	sodium channel, voltage-gated, type VII, alpha	20272	824	1112	671	989	1056	524	-1.89	0.000100
1451840_at	Kcnip4	Kv channel interacting protein 4	80334	341	250	323	305	243	158	-1.93	0.001000
1421453_at	Jph2	junctophilin 2	59091	848	765	632	920	519	459	-2	0.000300
1449999_a_at	Cacna2d1	calcium channel, voltage-dependent, alpha2/delta subunit 1	12293	509	356	283	443	317	221	-2.01	0.000900
1423550_at	Slc1a4	solute carrier family 1 (glutamate/neutral amino acid transporter), member 4	55963	586	212	291	513	186	253	-2.03	0.000020
1421297_a_at	Cacna1c	calcium channel, voltage-dependent, L type, alpha 1C subunit	12288	629	646	550	657	396	317	-2.08	0.000020

Affymetrix Probe set ID	Gene Symbol	Gene Name	Entrez Gene ID	Mean WT aorta 6 wks	Mean WT aorta 32 wks	Mean WT aorta 78 wks	Mean *Apoe*$^{-/-}$ aorta 6 wks	Mean *Apoe*$^{-/-}$ aorta 32 wks	Mean *Apoe*$^{-/-}$ aorta 78 wks	Fold change *Apoe*$^{-/-}$ 78 wks *vs. WT* 6 wks	p. ANOVA
1449433_at	P2rx5	purinergic receptor P2X, ligand-gated ion channel, 5	94045	957	789	664	819	520	393	-2.08	0.000500
1436912_at	Cacnb4	calcium channel, voltage-dependent, beta 4 subunit	12298	188	190	136	206	178	98	-2.1	0.000900
1421198_at	Itgav	integrin alpha V	16410	791	365	315	593	363	282	-2.1	0.000400
1417680_at	Kcna5	potassium voltage-gated channel, shaker-related subfamily, member 5	16493	226	257	191	203	211	96	-2.12	0.002000
1421629_at	Gabre	gamma-aminobutyric acid (GABA) A receptor, subunit epsilon	14404	337	347	271	360	259	169	-2.13	0.009000
1427495_at	Scn7a	sodium channel, voltage-gated, type VII, alpha	20272	317	406	219	385	317	179	-2.15	0.000500
1435721_at	Kcnq4	potassium voltage-gated channel, subfamily Q, member 4	60613	819	826	890	904	626	416	-2.17	0.000050
1435933_at	Scn2a	sodium channel, voltage-gated, type II, alpha	110876	447	462	580	585	392	266	-2.2	0.003000
1455404_at	Jph2	junctophilin 2	59091	3451	4048	4664	4167	2645	1881	-2.22	0.000300
1449677_s_at	Tmem38b	transmembrane protein 38B	52076	2329	1986	1669	2458	1620	1106	-2.22	0.000009
1417279_at	Itpr1	inositol 1,4,5-trisphosphate receptor 1	16438	4139	4007	4177	4481	3246	2015	-2.22	0.000010
1456401_at	Cacnb2	calcium channel, voltage-dependent, beta 2 subunit	12296	897	857	993	941	619	422	-2.23	0.000300
1429246_a_at	Anxa6	annexin A6	11749	2661	2026	1937	2591	1790	1160	-2.23	0.000300
1437631_at	Kcnip4	Kv channel interacting protein 4	80334	388	394	367	309	316	135	-2.3	0.000070
1428948_at	Kcnma1	potassium large conductance calcium-activated channel, subfamily M, alpha member 1	16531	1313	1673	1494	1674	1297	711	-2.36	0.000400
1448083_at	Nalcn	sodium leak channel, non-selective	338370	682	804	673	814	679	332	-2.45	0.000500
1448468_a_at	Kcnab1	potassium voltage-gated channel, shaker-related subfamily, beta member 1	16497	5653	5003	5882	5456	3743	2217	-2.46	0.000020
1425987_a_at	Kcnma1	potassium large conductance calcium-activated channel, subfamily M, alpha member 1	16531	869	718	649	1004	538	406	-2.48	0.000200
1450123_at	Ryr2	ryanodine receptor 2, cardiac	20191	572	746	831	798	452	315	-2.54	0.000020
1449094_at	Gjc1	gap junction protein, gamma 1	14615	1922	1945	1714	1813	1474	687	-2.64	0.000040
1455765_a_at	Abcc8	ATP-binding cassette, sub-family C (CFTR/MRP), member 8	20927	232	251	121	170	233	59	-2.87	0.006000

Affymetrix Probe set ID	Gene Symbol	Gene Name	Entrez Gene ID	Mean WT aorta 6 wks	Mean WT aorta 32 wks	Mean WT aorta 78 wks	Mean *Apoe*$^{-/-}$ aorta 6 wks	Mean *Apoe*$^{-/-}$ aorta 32 wks	Mean *Apoe*$^{-/-}$ aorta 78 wks	Fold change *Apoe*$^{-/-}$ 78 wks *vs. WT* 6 wks	p. ANOVA
1421400_at	Kcnmb1	potassium large conductance calcium-activated channel, subfamily M, beta member 1	16533	3767	3312	3139	3810	2438	1312	-2.9	0.000050
1429794_a_at	P2rx1	purinergic receptor P2X, ligand-gated ion channel, 1	18436	562	467	669	525	501	180	-2.92	0.000600
1460719_a_at	P2rx1	purinergic receptor P2X, ligand-gated ion channel, 1	18436	1108	837	919	1096	787	374	-2.93	0.000001
1418852_at	Chrna1	cholinergic receptor, nicotinic, alpha polypeptide 1 (muscle)	11435	340	234	184	328	187	110	-3	0.005000
1427280_at	Scn2a	sodium channel, voltage-gated, type II, alpha	110876	405	391	294	526	320	165	-3.19	0.001000
1421401_at	Kcnmb1	potassium large conductance calcium-activated channel, subfamily M, beta member 1	16533	1411	1150	997	1603	1003	465	-3.45	0.000500
1454043_a_at	Kcnab1	potassium voltage-gated channel, shaker-related subfamily, beta member 1	16497	2379	1571	1474	2214	1077	512	-4.33	0.000000
1425861_x_at	Cacna2d1	calcium channel, voltage-dependent, alpha2/delta subunit 1	12293	613	269	237	685	338	149	-4.6	0.000030
1447787_x_at	Gjc1	gap junction protein, gamma 1	14615	569	290	297	541	293	79	-6.83	0.010000
1424848_at	Kcnma1	potassium large conductance calcium-activated channel, subfamily M, alpha member 1	16531	198	143	95	211	133	29	-7.2	0.005000
1452476_at	Cacnb2	calcium channel, voltage-dependent, beta 2 subunit	12296	315	253	396	482	262	39	-12.48	0.000800

E. ligand-gated ion channel activity (GO: 0015276)

Affymetrix Probe set ID	Gene Symbol	Gene Name	Entrez Gene ID	Mean WT aorta 6 wks	Mean WT aorta 32 wks	Mean WT aorta 78 wks	Mean *Apoe*$^{-/-}$ aorta 6 wks	Mean *Apoe*$^{-/-}$ aorta 32 wks	Mean *Apoe*$^{-/-}$ aorta 78 wks	Fold change *Apoe*$^{-/-}$ 78 wks *vs.* *WT* 6 wks	p. ANOVA
1437540_at	Mcoln3	mucolipin 3	171166	26	9	18	26	287	468	18.26	0.000200
1459850_x_at	Glrb	glycine receptor, beta subunit	14658	10	52	233	82	120	582	7.13	0.000080
1434653_at	Ptk2b	PTK2 protein tyrosine kinase 2 beta	19229	261	463	424	263	748	1346	5.12	0.000001
1417297_at	Itpr3	inositol 1,4,5-triphosphate receptor 3	16440	224	280	499	214	476	812	3.79	0.000020
1425525_a_at	P2rx4	purinergic receptor P2X, ligand-gated ion channel 4	18438	981	1075	1000	992	2007	3273	3.3	0.000005
1431705_a_at	Mcoln2	mucolipin 2	68279	119	143	102	132	177	382	2.89	0.002000
1439787_at	P2rx7	purinergic receptor P2X, ligand-gated ion channel, 7	18439	335	463	522	352	719	922	2.62	0.000002
1452527_a_at	P2rx4	purinergic receptor P2X, ligand-gated ion channel 4	18438	795	656	705	788	1380	2060	2.62	0.000020
1415850_at	Rasa3	RAS p21 protein activator 3	19414	693	752	929	688	1048	1778	2.59	0.000040
1419853_a_at	P2rx7	purinergic receptor P2X, ligand-gated ion channel, 7	18439	138	186	113	129	250	300	2.33	0.002000
1450148_at	Mcoln3	mucolipin 3	171166	126	148	159	118	236	245	2.07	0.006000
1436957_at	Gabra3	gamma-aminobutyric acid (GABA) A receptor, subunit alpha 3	14396	1378	2766	2277	1588	2137	1495	-1.06	0.000300
1449544_a_at	Kcnh2	potassium voltage-gated channel, subfamily H (eag-related), member 2	16511	1171	1586	2022	1734	1449	956	-1.81	0.002000
1421453_at	Jph2	junctophilin 2	59091	848	765	632	920	519	459	-2	0.000300
1429794_a_at	P2rx1	purinergic receptor P2X, ligand-gated ion channel, 1	18436	562	467	669	525	501	180	-2.92	0.000600
1460719_a_at	P2rx1	purinergic receptor P2X, ligand-gated ion channel, 1	18436	1108	837	919	1096	787	374	-2.93	0.000001
1418852_at	Chrna1	cholinergic receptor, nicotinic, alpha polypeptide 1 (muscle)	11435	340	234	184	328	187	110	-3	0.005000
1424848_at	Kcnma1	potassium large conductance calcium-activated channel, subfamily M, alpha member 1	16531	198	143	95	211	133	29	-7.2	0.005000

Affymetrix Probe set ID	Gene Symbol	Gene Name	Entrez Gene ID	Mean WT aorta 6 wks	Mean WT aorta 32 wks	Mean WT aorta 78 wks	Mean *Apoe*$^{-/-}$ aorta 6 wks	Mean *Apoe*$^{-/-}$ aorta 32 wks	Mean *Apoe*$^{-/-}$ aorta 78 wks	Fold change *Apoe*$^{-/-}$ 78 wks *vs.* *WT* 6 wks	p. ANOVA
1421629_at	Gabre	gamma-aminobutyric acid (GABA) A receptor, subunit epsilon	14404	337	347	271	360	259	169	-2.13	0.009000
1449433_at	P2rx5	purinergic receptor P2X, ligand-gated ion channel, 5	94045	957	789	664	819	520	393	-2.08	0.000500
1455404_at	Jph2	junctophilin 2	59091	3451	4048	4664	4167	2645	1881	-2.22	0.000300
1417279_at	Itpr1	inositol 1,4,5-trisphosphate receptor 1	16438	4139	4007	4177	4481	3246	2015	-2.22	0.000010
1429246_a_at	Anxa6	annexin A6	11749	2661	2026	1937	2591	1790	1160	-2.23	0.000300
1428948_at	Kcnma1	potassium large conductance calcium-activated channel, subfamily M, alpha member 1	16531	1313	1673	1494	1674	1297	711	-2.36	0.000400
1425987_a_at	Kcnma1	potassium large conductance calcium-activated channel, subfamily M, alpha member 1	16531	869	718	649	1004	538	406	-2.48	0.000200
1450123_at	Ryr2	ryanodine receptor 2, cardiac	20191	572	746	831	798	452	315	-2.54	0.000020